

DRAFT

NUREG/CR

PU-NE 94/1

=====
Scientific Design of Purdue University
Multi-dimensional Integral Test
Assembly (PUMA) for GE SBWR
=====

Manuscript completed: February 1994
Revised Manuscript Completed: July 1994

Prepared by:

M. Ishii, S.T. Revankar, R. Dowlati, M.L. Bertodano, I. Babelli,
W. Wang, H. Pokharna, V. H. Ransom and R. Viskanta

School of Nuclear Engineering
Purdue University
West Lafayette, IN 47907

Prepared For
Division of System Research
Office of Nuclear Regulatory Research
U.S. Nuclear Regulatory Commission
Washington, D.C. 20555
Contract No. NRC-04-93-049

9408170024 940809
PDR ADOCK 05200004
B PDR

ABSTRACT

The scientific design of the Purdue University Multi-dimensional Integral Test Assembly (PUMA) has been carried out under the "Confirmatory Integral System Testing for the GF SBWR Design" contract sponsored by the U.S. Nuclear Regulatory Commission. The design is based on a three-level scaling method developed for this task. The first level of scaling, the integral scaling, is based on a well-established approach obtained from the application of integral response function to the thermal-hydraulic system. This level ensures that the steady-state as well as dynamic characteristics of the thermal-hydraulic loops will be similar between SBWR and PUMA. The second scaling level addresses the boundary flow of mass and energy between components, insuring flow and inventory similarity. The third scaling level focuses on the similarity of key local phenomena governed by constitutive relations. The PUMA facility has 1/4 height and 1/100 area ratio scaling. This corresponds to the volume scale of 1/400. The PUMA power scaling based on the integral scaling is 1/200. The present scaling method predicts that PUMA time scale will be one-half that of SBWR. The system pressure for PUMA is full scale, therefore, a prototypic pressure is maintained. However, the facility is designed to simulate relatively low pressure thermal-hydraulic phenomena which occur after the initial blowdown depressurization phase. PUMA is designed to operate at and below 1.03 MPa (150 psi), which allows it to simulate the prototypic SBWR accident conditions below 1.03 MPa (150 psi). The facility includes models for all the major components of SBWR safety and non-safety systems that are important to the transient response to postulated LOCA and other transients. The PUMA component designs and detailed instrumentations are presented in this report.

This page is Blank

TABLE OF CONTENTS

ABSTRACT.....	i
LIST OF FIGURES.....	vii
LIST OF TABLES.....	xi
NOMENCLATURE.....	xiv
1. INTRODUCTION.....	1-1
2. OBJECTIVES.....	2-1
3. PROGRAM REQUIREMENTS.....	3-1
4. DESIGN BASIS FOR INTEGRAL FACILITY.....	4-1
4.1 Systems Characteristics (Safety).....	4-1
4.1.1 Reactor Pressure Vessel (RPV).....	4-1
4.1.2 Containment System.....	4-2
4.1.3 Main Steam Lines.....	4-3
4.1.4 Automatic Depressurization System, (ADS).....	4-4
4.1.5 Gravity Driven Core Cooling System (GDCCS).....	4-4
4.1.6 Passive Containment Cooling System (PCCS).....	4-6
4.1.7 Isolation Condenser System (ICS).....	4-7
4.1.8 Control Rod Drive (CRD) System and Reactor Water Cleanup/Shutdown Cooling (RWCU/SDC) System.....	4-8
4.1.9 Spectrum of Postulated Breaks.....	4-9
4.2 Governing Processes and Phenomena.....	4-9
4.2.1 Processes Following a LOCA or Transient.....	4-9
4.2.2 Phenomena Accompanying LOCA or Transients.....	4-10
4.3 Identification of Important Phenomena.....	4-13
5. SCALING APPROACH.....	5-1

5.1 General Consideration	5-1
5.2 Scaling Approach	5-2
5.3 Global Scaling	5-3
5.3.1 Integral System Scaling (1st Level)	5-3
5.3.2 Mass and Energy Inventory and Boundary Flow Scaling (2nd Level)	5-12
5.3.3 Pressure Scaling	5-15
5.3.4 Basis for Reduced Height Scaling	5-18
5.4 Local Phenomena Scaling	5-20
5.4.1 Reactor Vessel Flow Dynamics and Instability Scaling	5-20
5.4.2 Choked Flow Case	5-21
5.4.3 Un-choked Flow Case	5-24
5.4.4 Relative Velocity and Flow Regime	5-27
5.4.5 Critical Heat Flux Scaling (CHF)	5-29
5.4.6 Flashing in the Chimney	5-31
5.4.7 Condensation in Suppression Pool	5-32
5.4.8 Vent Phenomena in Suppression Pool	5-36
5.4.9 Mixing in Stratified Fluid Volumes	5-40
5.4.10 Natural Circulation	5-44
5.4.11 Heat Source and Sink	5-46
5.4.12 PCCS Venting into Suppression Pool	5-47
5.4.13 Condensation in PCCS Condensers	5-51
5.4.14 Stratification in the Drywell	5-54
5.4.15 Stratification in the Suppression Pool	5-55
6. SCALE OF THE PUMA	6-1
7. DESIGN OF PUMA-SBWR FACILITY AND SCALING BASIS	7-1
7.1 Reactor Pressure Vessel Design	7-1
7.1.1 Pressure vessel	7-2
7.1.2 Lower plenum	7-2
7.1.3 Core plate	7-3
7.1.4 Core	7-3

7.1.5 Shroud design	7-7
7.1.6 Chimney	7-8
7.1.7 Downcomer	7-10
7.1.8 Separator/Dryer Assembly	7-11
7.2 Drywell Design.....	7-14
7.3 Suppression Pool Design.....	7-20
7.4 Gravity Driven Core Cooling System (GDCCS) Design.....	7-23
7.5 Passive Containment Cooling System (PCCS) and Isolation Condenser System (ICS) Design	7-28
7.6 Automatic Depressurization System (ADS) Design	7-35
7.7 Feed Water Line and Auxiliary Reactor Coolant System	7-37
7.7.1 Feed Water Line (FWL)	7-38
7.7.2 Control Rod Drive (CRD) System	7-38
7.7.3 Reactor Water Clean-Up/Shut-Down Cooling (RWCUSDC) Systems	7-39
7.8 Stored Heat, Heat Loss and Insulation Design.....	7-40
7.8.1 Stored Heat in RPV wall	7-40
7.8.2 Containment Heat Sink Design	7-42
7.8.3 Design of Insulation for Heat Loss.....	7-45
7.9 Break Design	7-47
8. INSTRUMENTATION SYSTEM	8-1
8.1 Overview of PUMA Instrumentation	8-1
8.2 Reactor Pressure Vessel Instrumentation	8-2
8.2.1 Temperatures	8-3
8.2.2 Pressures	8-3
8.2.3 Conductivity Probes	8-4
8.2.4 Additional Measurements.....	8-4

8.2.5 Boundary Measurements	8-5
8.3 Containment Instrumentation	8-6
8.3.1 Temperatures	8-6
8.3.2 Pressure.....	8-6
8.3.3 Oxygen Concentrations	8-6
8.3.4 Additional measurements	8-7
8.3.5 Containment Boundary Measurements	8-7
8.4 Data Acquisition System	8-7
9. PUMA SYSTEM DESIGN	9-1
9.1 Scaling of PUMA Facility	9-1
9.2 Preliminary Design.....	9-2
9.3 Overall Instrumentation	9-3
9.4 Initialization of Test	9-4
9.5 Preliminary Test Matrix	9-5
9.6 Scaling Distortion and Potential Impact on Integral Test	9-6
9.6.1 RPV Core.....	9-6
9.6.2 GDCS Lines.....	9-6
9.6.3 PCCS Condensation	9-7
9.6.4 Drywell	9-7
9.6.5 Suppression Pool	9-8
9.6.6 Helium Gas Distribution.....	9-8
10. SUMMARY AND CONCLUSIONS	10-1

LIST OF FIGURES

Figure 4.1 SBWR containment boundary [Ref. 4.1, p. 6.2-113].....	4-16
Figure 4.2 Cross-sectional view of RPV [Ref. 4.1, p. 5.3-22]	4-17
Figure 4.3 Cross-sectional view of RPV with dimensions [4.6]	4-18
Figure 4.4 Horizontal vent module between the drywell and suppression pool [Ref. 4.1, 6.2-117]	4-19
Figure 5.1 The static upstream stagnation pressure ratio as a function of position and the exit static pressure ratio for a smooth converging-diverging nozzle.....	5-57
Figure 5.2 The nondimensional mass flow through the conveying-diverging nozzle as a function of nozzle pressure ratio	5-58
Figure 5.3 The static to upstream stagnation pressure ratio as a function of position and the exit static pressure ratio for an abrupt expansion nozzle	5-59
Figure 5.4 The nondimensional mass flow through the abrupt expansion nozzle as a function of nozzle pressure ratio	5-60
Figure 5.5 Drywell and suppression pool pressure transient schematic.....	5-61
Figure 5.6 Time period Δt to fill PCCS volume as a function of air concentration	5-62
Figure 7.1 Reactor pressure vessel (RPV) and internal components	7-51
Figure 7.2 Flanges, view ports and special instrument parts on PUMA RPV	7-52
Figure 7.3 PUMA core shroud and mounting design.....	7-53
Figure 7.4 PUMA core inlet plate design showing heater and bypass flow area	7-54
Figure 7.5 Decay heat curve fitting for SBWR	7-55

Figure 7.6 Cross-sectional view of PUMA core section	7-56
Figure 7.7 Typical heater design for PUMA RPV	7-57
Figure 7.8 Top of chimney shroud and lower separate plate in PUMA RPV	7-58
Figure 7.9 PUMA chimney shroud and mounting design.....	7-59
Figure 7.10 PUMA cross-sectional view of chimney partition.....	7-60
Figure 7.11 Separator tube layout on lower separator plate in PUMA RPV	7-61
Figure 7.12 Orifice holes on upper separator plate and support structure in PUMA RPV	7-62
Figure 7.13 Mounting of separator section onto PUMA RPV, separator tube, and separator dryer shroud design.....	7-63
Figure 7.14 Design of drywell, suppression pool, connecting vent line and vacuum breaker lines in PUMA	7-64
Figure 7.15 Jet deflector plate	7-65
Figure 7.16 Jet flow regime transition as a function of Froude number	7-66
Figure 7.17 Gravity-driven cooling system (GDCCS) design in PUMA	7-67
Figure 7-18 Design of PUMA GDCCS pool	7-68
Figure 7.19 Design of PUMA ICS/PCCS condenser modules.....	7-69
Figure 7.20 Lower header penetrations of the ICS/PCCS condenser modules in PUMA.....	7-70
Figure 7.21 Design of PUMA passive containment cooling system (PCCS)	7-71
Figure 7.22 Design of PUMA isolation condenser system (ICS)	7-72
Figure 7.23 Design PUMA ICS/PCCS pools	7-73

Figure 7.24 Plan view of automatic depressurization system (ADS) and main steam lines (MSL) in PUMA.....	7-74
Figure 7.25 Schematic of ADS and MSL in PUMA.....	7-75
Figure 7.26 Typical instrumented ADS line in PUMA.....	7-76
Figure 7.27 Reactor water clean-up/shutdown cooling (RWCU/SDC) system and control rod drive (CRD) system design in PUMA.....	7-77
Figure 7.28 Feed water line and sparger in PUMA.....	7-78
Figure 7.29 Estimated RPV wall temperature profile with time elapsed from blowdown for SBWR.....	7-79
Figure 7.30 Estimated RPV wall heat loss with blowdown for SBWR.....	7-80
Figure 7.31 Cross-sectional view of insulation on typical vessel wall.....	7-81
Figure 7.32 Typical break design in PUMA to simulate double-ended pipe break.....	7-82
Figure 8.1 PUMA RPV temperature instrumentation.....	8-22
Figure 8.2 PUMA RPV pressure and void fraction instrumentation.....	8-23
Figure 8.3a Schematic of the conductivity probe.....	8-24
Figure 8.3b Output signal of conductivity probe.....	8-24
Figure 8.4 PUMA RPV boundary measurements.....	8-25
Figure 8.5 Typical instrumented ADS line.....	8-26
Figure 8.6 Capacitance probe schematic.....	8-27
Figure 8.7 PUMA containment temperatures and pressures.....	8-28
Figure 8.8 PUMA containment boundary flow measurement.....	8-29

Figure 8.9 Water level ranges in the SBWR	8-30
Figure 9.1 Overall schematic of PUMA facility	9-24
Figure 9.2 Plan view of main vessels in PUMA	9-25

LIST OF TABLES

Table 4.1	Dimensions of Reactor Pressure Vessel [Ref. 4.1, p. 1.3-5, 5.1-5, 1.3-4]	4-1
Table 4.2	Thermal-hydraulic Parameters for RPV [Ref. 4.1, p.4.4-6,1.3-2]	4-2
Table 4.3	Containment Parameters [Ref. 4.1, p. 6.2-20, 6.2-61]	4-3
Table 4.4	SRV and DPV Parameters, Water Levels, and ADS Actuation Timings [Ref. 4.1, p. 21-39, 6.2-120, 6.2-121 Table 21.5-1-1, 6.3-28]	4-5
Table 4.5	GDCS Parameters and Equalization Line Parameter [Ref. 4.1, p. 6.2-60, 6.3-5, 6.3-6]	4-6
Table 4.6	PCCS Parameters [Ref. 4.2, Appendix 2]	4-7
Table 4.7	IC pool and ICS Parameters [Ref. 4.2 Appendix 2]	4-8
Table 4.8	Postulated Breaks [Ref. 4.1, p. 6.3-20, 6.3-21]	4-9
Table 6.1	Comparisons for Major Components and Dimensions of Different Height Scaling	6-4
Table 6.2	Comparison of Various Parameters and Non-dimensional Numbers Between Prototype and PUMA (at 1.03 MPa or 150 psi operating pressure)	6-5
Table 7.1	Reactor Pressure Vessel Dimensions	7-2
Table 7.2	Coefficients for Decay Heat Polynomial Fit	7-4
Table 7.3	Decay Power in SBWR and PUMA Facilities	7-4
Table 7.4	Core Power Levels at 1.03 MPa (150 psi) Following Blowdown	7-5
Table 7.5	Core Heater Rod Arrangement	7-6
Table 7.6	Core Parameters	7-6

Table 7.7 Core Shroud Design	7-8
Table 7.8 Chimney Design.....	7-10
Table 7.9 Required Separator Tube Numbers and Their Diameters	7-12
Table 7.10 PUMA Drywell Design	7-16
Table 7.11 PUMA Suppression Pool (SP) Design	7-23
Table 7.12 PUMA GDCS Design.....	7-28
Table 7.13 PUMA PCCS/ICS Condenser Design Parameters	7-33
Table 7.14 PUMA PCCS/ICS Pool Design Parameters	7-35
Table 7.15 SRV and DPV Capacities and Sequence of Action for SBWR	7-36
Table 7.16 Automatic Depressurization System (ADS) for PUMA Facility	7-37
Table 7.17 PUMA Feed Water Line: 2 Each	7-38
Table 7.18 PUMA Component Heat Loss Estimation	7-48
Table 7.19 Containment Heat Loss in PUMA with Addition of Fibrous-based Acoustic Tile to Simulate Concrete Heat Sink	7-50
Table 8.1 Mass and Energy Measurement	8-2
Table 8.2 Vessel measurement.....	8-9
Table 8.3 Drywell Measurement	8-13
Table 8.4 Suppression Pool measurement.....	8-14
Table 8.5 PCCS and ICS Measurement	8-15
Table 8.6 GDCS Measurement.....	8-18

Table 8.7 Boundary Flow Measurement	8-19
Table 8.8 Instruments	8-21
Table 9.1 Comparison of Components Dimensions between Prototype and PUMA	9-9
Table 9.2 Controls and Provisions on Various Components of PUMA.....	9-20
Table 9.3 Phase 1 of the Preliminary Test Matrix-Base Case and GE Counterpart Tests.....	9-21
Table 9.4 Phase 2 of the Preliminary Test Matrix-Sensitivity Study and Beyond DBA Tests.....	9-22
Table 9.5 Geometric Distortion in RPV	9-23

NOMENCLATURE

A	Flow area scale
a	Cross-sectional area [m^2]
B_i	Biot number (Eq. 5.19)
C_o	Distribution parameter (Eq. 5.109)
c_o	Concentration of non-condensables
c_p	Specific heat [J/kg-C]
D,d	Diameter [m]
D_b	Bubble diameter [m]
E	Energy [J]
E_g	Vapor latent heat flux [J/m^2]
F	Total pressure loss coefficient
f	Friction factor, friction
f	Frequency [s^{-1}]
G	Mass velocity [$kg\cdot m/s^2$]
Gr	Grashof number (Eq. 5.193)
g	Gravitational acceleration [m/s^2]
j	Superficial velocity [m/s]
Ja	Jakob number (Eq. 5.189)
H	Height [m]
h	Enthalpy [J/kg]
h	Heat transfer coefficient [$W/m^2\cdot C$]
k	Conductivity [$W/m\cdot C$]
K	Minor loss coefficient
L	Axial length scale
l	Length [m]
m,M	Mass [kg]
\dot{m}	Mass flow rate [kg/s]
n,N	Number
N_d	Drift flux number (Eqs. 5.32 and 5.102)
N_{Fr}	Froude number (Eq. 5.31)
N_f	Friction number (Eq. 5.35)
N_{flash}	Flashing phase change number (Eq. 5.112)
N_{nc}	Natural circulation number (Eq. 5.66)
N_o	Orifice number (Eq. 5.36)
N_{pch}	Phase change number (= Zuber number) (Eq. 5.29)

N_q	CHF number (Eq. 5.110)
N_{sub}	Subcooling number (Eq. 5.30)
N_{th}	Thermal inertia ratio (Eq. 5.34)
Nu	Nusselt number (Eq. 5.169)
N_{Zu}	Zuber number (Eq. 5.29)
p, P	Pressure [Pa]
Pr	Prandtl number (Eq. 5.194)
q	Power [W]
q''	Heat flux [W/m^2]
q'''	Volumetric heat generation [W/m^3]
Q	Volumetric gas flow rate [m^3/s]
Q	Transfer function
Q_s	Heat source number (Eq. 5.20)
\dot{Q}_c	Condensation power
R	Richardson number (Eq. 5.1)
R	Universal gas constant [kJ/kgmol-K]
Ra	Rayleigh number ($Gr Pr$)
Re	Reynolds number (Eq. 5.190)
S	Surface area [m^2]
St	Modified Stanton number (Eq. 5.17)
t	Time [s]
T	Temperature [$^{\circ}C$]
T^*	Time ratio number (Eq. 5.33)
u	Velocity [m/s]
u_f	Internal energy of liquid
U	Overall heat transfer coefficient [W/m^2-C]
v, V	Volume [m^3]
V_{gj}	Drift velocity [m/s] (Eq. 5.100)
w	Work [J]
W	Width [m]
W_a	Non-condensable mass fraction
x	Quality
x	Distance [m]
X	Concentration of steam
z, Z	Distance [m]

Greek Symbols

β	Volumetric thermal expansion coefficient [K^{-1}]
δ	Conduction depth [m]
δ	Perturbation
Δ	Difference
Δh_{fg}	Latent heat of vaporization [J/kg]
α	Void fraction
α_s	Thermal diffusivity [m^2/s]
ρ	Density [kg/m^3]
τ	Time Constant [s]
μ	Dynamic viscosity [kg/m-s]
η	Heated perimeter [m]
ν	Kinematic viscosity [m^2/s]
π	Time constant ratio
Θ	Dimensionless temperature
σ	Surface tension [N/m]
Σ	Summation
ξ	Wetted perimeter [m]
Ψ	Parameter

Subscripts

a	Ambient
b	Bulk
b	Bubble
c	Core, critical, containment
cond	Condensation
DW	Drywell
e	Exit
eq	Equivalent
f	Fluid
g	Gas
i	ith component
in	Inlet
j,J	Jet

m	Model
m	Maximum
m	Mean, average
o	Reference point/component
out	Outlet
p	poolside
p	Prototype
pc	PCCS
R	Ratio
s	Surface, solid
sup,sp	Suppression pool
T	Pool water
t	Throat
th	Thermal
v	Vapor
v	Vent, vessel
w,W	Wall
Wa	Non-condensable mass fraction

Superscripts

* Dimensionless quantity

1. INTRODUCTION

The General Electric Nuclear Energy (GE) has developed a new boiling water reactor called the Simplified Boiling Water Reactor (SBWR) [1.1]. Major differences between the current Boiling Water Reactors (BWRs) and the SBWR are in the simplification of the coolant circulation system and the implementation of passive emergency cooling systems. There are no recirculation pumps to drive the coolant in the vessel of the SBWR. The emergency core cooling and containment cooling systems do not have active pump-injected flows.

There are several engineered safety systems and safety-grade systems in the SBWR which are directly related to the relevant issues and objectives of the present program: 1) the Automatic Depressurization System (ADS), 2) the Gravity-Driven Cooling System (GDCCS), 3) the Passive Containment Cooling System (PCCS), 4) the Isolation Condenser Systems (ICS), and 5) the Pressure Suppression Pool (SP). The GDCCS and PCCS are new designs unique to the SBWR and do not exist in operating BWR's. The ICS is similar to those in some operating BWRs. Both the GDCCS and PCCS are designed for low-pressure operation (less than 1.03 MPa or 150 psia), but the ICS is capable of high pressure operation as well (up to 7.58 MPa or 1100 psia).

The ADS system becomes active at a prescribed vessel condition and depressurizes the reactor vessel so that the gravity driven cooling systems can be activated. The goal of these safety systems is to maintain sufficient core cooling by preventing core uncover and dryout of the fuel pins.

The performance of these safety systems under a loss of coolant accident (LOCA) and other important transients is a major concern. Since the emergency cooling systems are driven by the gravitational head, interaction between the ADS, GDCCS, PCCS and other auxiliary systems are important. The emergency cooling systems depend not only on the gravitational head but also on the relative static pressure differences between the vessel, drywell and wetwell (suppression pool). The safety systems and various natural circulation phenomena encountered after the initial vessel depressurization in the SBWR are somewhat different from the systems and phenomena studied by the nuclear community in existing commercial nuclear reactors.

General Electric has performed tests to assess the GDCCS performance in a low pressure full-height GIST facility with a volume scale of 1/508 [1.2]. Results of this study have demonstrated the feasibility of the GDCCS concept. The GIST facility was scaled from an older SBWR design in which the GDCCS pools were combined with the SP. The PCCS was absent in the GIST facility, hence parallel operation of the GDCCS and PCCS was not observed in the GIST experiments. GE has also performed tests to assess the PCCS performance in a low-pressure, full height Toshiba GIRAFFE facility in Japan with a volume scale of 1/400 [1.3]. The GIRAFFE tests provided data to help model the prototypic SBWR PCCS units, and demonstrated the feasibility of the non-condensable venting concept. However, the GIRAFFE facility was scaled from an older

SBWR design, and it did not investigate GDCS injection in the vessel.

A new PANDA facility in Switzerland is a low-pressure, full-height facility with a volume scale of 1/25 [1.4]. The main focus of the PANDA facility is on PCCS performance and containment phenomena in a relatively large-scale facility so that three-dimensional effects can be assessed. Like GIRAFFE, however, the PANDA facility is not designed for assessing GDCS injection into the vessel. Although GE has performed experimental and analytical studies for the PCCS and GDCS systems and associated phenomena, the U.S. Nuclear Regulatory Commission (NRC) has identified a need to develop additional independent confirmatory data from a well-scaled integral test facility built to reproduce major thermal-hydraulic phenomena at relatively low pressure (< 1.03 MPa or 150 psia) [1.5]. Purdue University was awarded a research contract, "Confirmatory Integral System Testing for GE SBWR Design," to design, construct and operate PUMA (Purdue University Multi-dimensional Integral Test Assembly) to obtain integral test data.

The objectives of this program are to build a scaled integral test facility and obtain confirmatory data for the NRC to assess the RELAP5/CONTAIN code. The general guidelines for assessing the code scalability and uncertainty associated with accident predictions have been developed at NRC [1.6]. This report summarizes the details of the scaling method and scientific design of the integral facility, including its instrumentation.

Note: Throughout this report, "prototype" refers to the GE-SBWR and "model" refers to the present PUMA test facility.

References

- 1.1 GE Nuclear Energy, "SBWR Standard Safety Analysis Report 25A5113 Rev. A, August (1992).
- 1.2 Billig, P.F., "Simplified Boiling Water Reactor (SBWR) Program Gravity-Driven Cooling System (GDCS) Integral Systems Test-Final Report," GEFR-00850, October (1989).
- 1.3 Tsunoyama, S., Yokobori, S., Arai, K., "Development of Passive Containment Cooling System," Proc. International Topical Meeting on Advanced Reactor Safety, Hyatt Regency, Pittsburgh, April 17-21 (1994).
- 1.4 Yadigaroglu, G., "Scaling of the SBWR Related Test," Report NEDC -32258, November (1993).
- 1.5 Han, J.T., Bessett, D.E., Shotkin, L.M., "NRC Confirmatory Testing Program for SBWR," Proceedings of the Twenty-First Water Reactor Safety Information Meeting, Bethesda, Maryland, October 25-27 (1993).
- 1.6 NRC Draft Report, "Compendium of ECCS Research for Realistic LOCA Analysis - Draft Report for Comment", NUREG-1290 (1987).

2. OBJECTIVES

The major objectives of the PUMA program are to:

1. provide integral data to NRC for the assessment of the RELAP5/CONTAIN code for SBWR applications,
2. assess the integral performance of GDCS and PCCS, and
3. assess SBWR phenomena important to LOCAs and other transients

The focus of the PUMA integral test program is the reproduction of the important phenomena expected in the SBWR for use in the assessment of the RELAP5/CONTAIN code. The objective of the scaling method is to provide a facility design that will reproduce those phenomena which occur during both the later stages of depressurization of the SBWR pressure vessel and during the functioning of the gravity-driven safety systems. A corollary objective of the scaling will be to preserve, to the extent necessary and possible, the sequence and interrelation method of the key phenomena. In this way, comprehensive data which can be related to prototypical condition will be provided for assessing the code models.

The particular focus of the integral experiments will be to obtain data on the performance and interaction of the GDCS and PCCS, particularly as related to the maintenance of the coolant level in the RPV, containment integrity, maintenance of natural circulation, possible occurrence of two-phase natural circulation instabilities, the effect of non-condensable on PCCS performance and potential impact on coolability of the core. Data will also be obtained regarding system interaction between the GDCS, PCCS and regarding auxiliary cooling systems, and possible water hammer occurrence during GDCS injection, feedwater injection, and ICS condensate draining into the vessel.

The data collected will provide qualitative as well as quantitative tests of the code models and overall predictive capability of RELAP5/CONTAIN. In this way, the uncertainty associated with the calculation of the safety margins predicted to exist for design-basis accidents can be comprehensively assessed by the NRC using the code scaling and uncertainty analysis methodology established several years ago.

3. PROGRAM REQUIREMENTS

The PUMA tests are primarily concerned with: developing a well scaled integral test data base for NRC to assess the ability of RELAP5/CONTAIN code to simulate the effectiveness of the GDCS and PCCS, and assessing the interaction among safety and non-safety systems. It has been found in previous studies that the largest uncertainties in predicting safety system performance are found in the later stages of accident events in which the system pressure is reduced through the automatic depressurization systems or break flow. The stated objective of the Nuclear Regulatory Commission is to obtain confirmatory data from a scaled integral test facility for major thermal-hydraulic phenomena at low pressure after vessel depressurization in the SBWR. In view of this, the test facility should be designed to reproduce the phenomena at 1.03 MPa (150 psia) or below in the plant. This maximum pressure is one of the most important factors affecting the design and cost of the proposed integral test facility.

The data collected will serve as part of the basis in the assessment of the model applicability and code uncertainties associated with the use of the RELAP5/CONTAIN safety analysis code for SBWR applications. The data should confirm the performance of various engineered safety features in simulated accident conditions.

The integral test facility design should be based on a rational scaling method which embodies conservation principles. The scaled-down system design requires that separate considerations be used for the length scale and the flow area scale. The product of these two scales give the overall volume scale. For natural circulation-driven flow, both the driving force and flow resistance simulations are very important, since the natural circulation flow is essentially determined by the balance between these two forces.

In the past, a full-height and reduced-area facility was often justified on the basis of preserving the total driving force. However, this is often not a valid argument because such a scaling approach may lead to a significant distortion of frictional resistance. The magnitude of the frictional resistance is proportional to the length-to-diameter ratio l/d . For a full-height but reduced-area facility, the natural circulation rate may be significantly smaller as a result of much larger values for l/d in the pipe sections. One way to reduce this impact is to enlarge the diameter of piping sections. However, this will lead to significant distortions of the scaled mass and energy inventories, which usually must be conserved. Since the inventory balance between the vessel, the containment, and the suppression pool largely determines the course of events in SBWR accidents and transients, inventory distortion is highly undesirable in the test facility.

The integral test facility scaling method should also provide a rational basis for scaling the integral test facility results up to the prototype conditions. Therefore, it is necessary to have scaling criteria for time, velocity, pressure, void, mass inventory and energy inventory in addition to the geometric scaling criteria. The integral test results should not only qualitatively identify the key thermal-hydraulic phenomena and sequence of events, but also quantify the system

response, phenomena and sensitivity, and the effects of interactions of components and phenomena. However, because of some scaling distortions, data from test facilities, including PUMA, GIRAFFE, and PANDA are not expected to reproduce quantitatively the system response and sensitivity exactly as in SBWR.

The integral tests are primarily concerned with the phenomena encountered after the reactor vessel is depressurized to the level when the GDCS is activated. Therefore, the facility should represent the major vessel internal structures, decay heat in the core, the depressurization systems, GDCS, PCCS, ICS, suppression pool, and non-safety systems. In addition to these, a system for water injection to the feedwater lines is necessary in order to address the interactions of GDCS with the non-safety systems such as the control rod drive system (CRD), Reactor Water Cleanup/Shutdown Cooling System (RWCU/SDCS) and Fuel and Auxiliary Pools Cooling Systems (FAPCS). The latter requires a spray system in the dry well.

The integral test facility should have instrumentation to provide phenomena comprehension, quantification, and evaluation, and also be usable by the NRC in model development and assessment of the RELAP5/CONTAIN code. The instrumentation should measure at least

- pressure at various locations
- ΔP in vessel for void measurements
- mixture level in the vessel
- in-vessel void fraction
- flow in various connecting lines
- non-condensable concentration
- temperatures
- natural circulation rate in the vessel
- water level in the pools
- power input
- heater surface temperature
- heat loss

The scaling method must address the following phenomena and issues:

- 1) in-vessel natural circulation and two-phase flow instability,
- 2) flashing in the chimney,
- 3) inflow or outflow from various components and intercomponent flow,
- 4) initial and boundary conditions,
- 5) important containment phenomena,

- 6) single phase and two-phase natural circulation
- 7) condensation phenomena in the presence of non-condensable gases, and
- 8) system stored energy and decay heat.

Thus, tasks to be performed under the present program are:

- Perform phenomena identification for SBWR LOCAs and transients, to be used for the design of the integral experiments and development of a test plan.
- Develop a well-balanced and justifiable scaling approach for the design of the SBWR integral facility, PUMA.
- Design a well-scaled integral test facility having proper and sufficient instrumentation.
- Construct the scaled integral SBWR test facility.
- Develop boundary and initial conditions for the integral tests based on the scaling method and computer code simulation using RELAP5/CONTAIN.
- Perform the integral tests under strict quality assurance over the experiments, as well as the reporting procedures.
- Report the results in a NUREG/CR document.

4. DESIGN BASIS FOR THE PUMA INTEGRAL FACILITY

4.1 Systems Characteristics (Safety)

In this section, the system characteristics of the SBWR that are relevant to the safety of the reactor are discussed. Some figures and data for the tables presented in the discussion were obtained from the GE Standard Safety Analysis Report (SSAR) [4.1] and the captions for these figures and tables include references to the SSAR page number for immediate reference. All dimensions presented are for nominal size.

In Figure 4.1, the SBWR containment boundary is shown. Within the containment boundary there are the reactor pressure vessel (RPV), drywell, suppression pool (SP), gravity driven-core cooling system (GDCCS) pools, isolation condenser system (ICS) piping, passive containment cooling system (PCCS) piping and the automatic depressurization system (ADS). The condensers and pools for the ICS and pools for the PCCS are located outside the containment boundary.

4.1.1 Reactor Pressure Vessel (RPV)

Figure 4.2 shows the cross-sectional view of the SBWR vessel. The dimensions of the vessel are given in Table 4.1. The thermal-hydraulic parameters of the RPV at the normal full-power operation are given in Table 4.2.

Table 4.1. Dimensions of Reactor Pressure Vessel
(Ref. 4.1, p. 1.3-5, 5.1-5, 1.3-4)

Inside Height	24.612 m
ID	6 m
Wall Thickness	157.175 mm
Coolant Volume	607.3 m ³
Total Volume	669 m ³
Active Fuel Length	2.743 m

In Figure 4.3, the levels of various parts and internals of the RPV are shown. The overall height of the RPV is about 25 m. This permits natural circulation driving forces to produce the required core coolant flow. An increased thermal driving head is provided by a long "chimney" in the space which extends from the top of the core to the entrance of the steam separator assembly. The chimney region has vertical panels for flow partition. The RPV volume provides a large reserve of water above the core. This volume assures a long period of time before core uncovering in the case of feedwater flow interruption or loss of coolant. The large RPV volume also reduces the reactor pressurization rates that develop when the reactor is suddenly isolated

from the normal heat sink.

Table 4.2. Thermal-hydraulic Parameters for RPV
(Ref. 4.1, p. 4.4-6, 1.3-2)

Core Power (100%)	2000 MWth
Core Inlet Flow	27.2×10^6 kg/h
Feedwater Inlet Flow	3.88×10^6 kg/h
Steam Dome Pressure	7.17 MPa
Core Inlet Pressure	7.28 MPa
Core Outlet Pressure	7.23 MPa
Average Core Power Density	41.5 kW/liter
Average Heat Flux	430.58 kW/m ²
Maximum Heat Flux	1225.23 kW/m ²
Core Average Quality	14.3
Feedwater Temperature	215.6°C
Core Inlet Temperature	278.5°C
Core Outlet Temperature	280.3°C

The reactor internals consist of core support structures and other equipment. The core support structures locate and support the fuel assemblies, form partitions within the reactor vessel to sustain pressure differentials across the partitions, and direct the flow of coolant water. The major internal structures consist of a shroud, shroud support, core plate, and integral fuel support and control rod guide tubes (CRGT).

The other reactor internals are the control rods, feedwater spargers, in-core guide tubes, chimney, chimney partitions, chimney head, steam separator assembly, and the steam dryer assembly. The shroud support, shroud and chimney make up a cylindrical stainless steel assembly that partitions the upward flow of coolant through the core from the downward recirculation flow in the downcomer.

4.1.2 Containment System

The SBWR has a low-leakage containment which is divided into the drywell and pressure suppression chamber. The containment is a cylindrical, steel-lined, reinforced concrete structure integrated with the reactor building. The drywell design conditions are 379 kPa (gauge) and 171°C. The suppression chamber design conditions are 379 kPa (gauge) and 121°C. The drywell is divided by the vessel support skirt into a lower drywell (below the skirt) and an upper drywell (above the skirt). There is an open flow area between the lower and upper drywells to allow for pressure equalization. The upper drywell houses the main steam lines and feedwater piping, the SRVs, GDCS pools, main steam drain piping and upper drywell coolers. The

suppression pool is higher in elevation than the top of the core. This provides a gravitational driving head for injecting suppression pool water into the vessel when the vessel is depressurized and the equalizing lines (total of three) between the suppression pool and the vessel are opened.

The gas space above the suppression pool serves as the LOCA blowdown gas reservoir for the upper and lower drywell nitrogen and other noncondensable gases, which pass through the eight drywell-to-suppression chamber vertical vent pipes. Each vent pipe has three horizontal vents located below the suppression pool surface. There are 24 horizontal vents between the drywell and suppression pool. In Figure 4.4, a detailed view of the horizontal vent module is shown. To prevent suppression pool water from flowing into the drywell via the horizontal vents, there is a vacuum breaker system between the suppression chamber and drywell. The vacuum breakers consist of check valves which open when the suppression chamber pressure exceeds the drywell pressure at a preset pressure difference. In Table 4.3 relevant containment parameters are given.

Table 4.3. Containment Parameters
(Ref. 4.1, p. 6.2-60, 6.2-61)

Drywell volume above skirt	4598 m ³
Drywell volume below skirt	892 m ³
Suppression pool gas volume	3819 m ³
Suppression pool water volume	3255 m ³
SP vertical vents area	9 m ²
SP surface area	588 m ²
Vertical vent pipe inside diameter	1.2 m
Vertical vent pipe height	12.7 m
Horizontal vent diameter	0.7 m
Heights of horizontal vents, from pool floor	
Top vent	3.5 m
Middle vent	2.13 m
Bottom vent	0.76 m

4.1.3 Main Steam Lines

Two main steam lines (MSLs) of 711 mm diameter carry steam from the RPV to the turbine main steam systems. Each of the two MSLs has a flow-restricting nozzle built into the RPV exits. In the event of a MSL break accident, the restrictor limits the coolant blowdown rate from the reactor vessel to a choked flow rate equal to or less than 200% of rated steam flow at 7.07

MPa. Each MSL has two steam isolation valves, one inside and one outside the containment. On each MSL, there are four safety relief valves (SRVs) and one depressurization valve (DPV). These SRVs and DPVs are discussed below.

4.1.4 Automatic Depressurization System (ADS)

The function of the automatic depressurization system (ADS) is to systematically depressurize the RPV in the event of LOCA or transient, to allow the GDCS water injection to the vessel, preventing the core uncover and maintaining the core temperature below design limits. The ADS also keeps the reactor depressurized for continued operation of the GDCS after a system accident response, without power. The ADS consists of the eight SRVs, six DPVs and their associated instrumentation and controls. There are four SRVs and one squib-type DPV on each main steam line. Four DPVs are flange-mounted on horizontal stub lines connected to the RPV at about the elevation of the MSLs. The SRVs discharge into the suppression pool through spargers. The DPVs discharge into the upper drywell.

The SRVs and DPVs are actuated in several groups at staggered times as the reactor undergoes a controlled depressurization. This minimizes reactor mixture level swell during the depressurization phase. When the low water level (Level 1) signal persists for at least 10 seconds, then the ADS is activated. First, four SRVs (two from each MSL) open and discharge steam to the SP. The remaining four SRVs open after an additional 10-second time delay. At 55 seconds after ADS actuation, the first group of two DPVs (on MSLs) start to discharge to drywell. Likewise, the second group of two DPVs open after 100 seconds and the third group of two DPVs open after 145 seconds of ADS actuation. In Table 4.4, SRV and DPV parameters, ADS actuation and water level definitions are given.

4.1.5 Gravity Driven Core Cooling System (GDCS)

The emergency core cooling systems (ECCS) of the SBWR are the GDCS and ADS. The ADS described above provides depressurization through the use of safety relief valves (SRVs) and depressurization valves (DPVs). Once the reactor is depressurized, the GDCS provides gravity-driven flow from three separate water pools located within the drywell at an elevation above the active core region. The GDCS initiation signal is related to the confirmed Level 1 signal. Three squib valves are activated. 150 seconds after confirmed Level 1 signal, one in each of the injection lines connecting the GDCS pools to the RPV. The additional water flow from the SP can be injected into the RPV through three equalizing lines to meet long-term post-LOCA core cooling requirements. After 30 minutes and when the RPV coolant level decreases to 1 m above the top of the active fuel (TAF), squib valves are opened in each of three equalization lines. The 30 minute delay and the above criterion ensure that the GDCS pools have had time to drain into the RPV and, that as a result of the blowdown, the initial RPV level collapse does not open the equalizing lines.

Table 4.4. SRV and DPV Parameters, Water Levels, and ADS Actuation Timings
(Ref. 4.1, p. 21-39, 6.2-120, 6.2-121, Table 21.5-1-1, 6.3-28)

SRV Inlet Line Diameter	203.2 mm
SRV Outlet Line Diameter	254 mm
SRV Flow Area	67 cm ²
DPV (MSL) Inlet Line Diameter	304.8 mm
DPV (RPV) Inlet Line Diameter	457.2 mm
DPV Flow Area	248 cm ²
Levels w.r.t. TAF Control Functions	
Normal water Level (NWL)	11767 mm
Level 9 - (L9)	12870 mm
Level 8 - (L8)	12200 mm
Level 3 - (L3)	10840 mm
Level 2 - (L2)	7930 mm
Level 1 - (L1)	3930 mm
Level 0.5 - (L0.5)	1000 mm
TAF w.r.t. Inside Bottom of RPV	6493 mm
BAF w.r.t. Inside Bottom of RPV	3750 mm
Value Actuation Sequence after Level 1* Signal Confirmed	
4 SRVs	0.0 s
4 SRVs	10 s
2 DPVs	55 s
2 DPVs	100 s
2 DPVs	145 s
*Maximum Allowable Time Delay to Confirm Level 1 Signal 10 s	
RPV Water Level	Control Function
L9	Initiate trip feedwater pumps runback.
L8	Trips CRD high pressure make up, scrams reactor, closes main turbine stop valves, and initiates feedwater pumps runback
L3	Runback RWCV pump, Trips leak detection and isolation system (LD & IS), and scrams reactor
L2	Initiates the CRD high pressure makeup mode, Initiates alternate rod intention (ARI), Initiate IC's, and Closes MSIV's, containment isolation valves except IC's
L1	Initiate ADS, GDCS and Trips LD & IS
L0.5	Initiate GDCS Equalizing line

In Table 4.5, the GDCS parameters are given. As shown in Table 4.5, the minimum equalizing line driving head of 1 m is determined by the elevation differential between the top of the first SP horizontal vent and the centerline of the equalizing line RPV nozzle. The 203.2 mm (8 inch) lines from each GDCS pool branch out into the 152.4 mm (6 inch) lines just before they enter RPV.

Table 4.5. GDCS and Equalization Line Parameter
(Ref. 4.1, p. 6.2-60, 6.3-5, 6.3-6)

GDCS Pool Numbers	3
Each GDCS Pool Minimum Drainable Inventory	329 m ³
Minimum Surface Elevation of GDCS Pool above the RPV Nozzle	13.3 m
SP Inventory 1 Meter above TAF	1475 m ³
Minimum Equalizing Line Head	1 m
GDCS Line Size from GDCS Pool (three total)	203.2 mm
GDCS Line Size at RPV (six total)	152.4 mm
RPV-Injection Line Nozzle Size (six total)	76.2 mm
Equalizing Line Nozzle Size (three total)	50.8 mm

4.1.6 Passive Containment Cooling System (PCCS)

The passive containment cooling system (PCCS) is an engineered safety feature and therefore it is a safety-related system. The PCCS removes the core decay heat energy, rejected to the containment after a LOCA, to outside of the containment. It provides containment cooling for a minimum of 72 hours after a LOCA. The PCCS consists of three PCCS condensers. The condenser is sized to maintain the containment within the design pressure limits of 379 kPa (gauge) (55 psig) for design basis accidents (DBAs). The PCCS is designed as a passive system without power actuated valves or other components that must actively during the accident.

Each PCCS condenser is composed of two identical modules. One PCCS condenser assembly is designed for 10 MWt capacity under conditions of saturated steam in tubes at 308 kPa (45 psia) and 134°C and pool water at atmospheric pressure and 101°C. The noncondensable gas

purging system is driven by the pressure difference between the drywell and the suppression chamber.

The PCCS parameters are given in Table 4.6. Each PCCS condenser has two identical bundles of vertical heat-transfer tubes connected to a steam drum above as an inlet plenum and a similar drum below as an outlet plenum. The vent and drain lines from each lower header are routed to the drywell through a single containment penetration. The condensate drains into an annular duct around the vent pipe and then flows into a line which connects to a large common drain line which also receives flow from the other header. The drain line discharges condensate into a GDCS pool. The non-condensibles from the PCCS condenser are vented through the vent pipe into the suppression pool.

4.1.7 Isolation Condenser System (ICS)

The isolation condenser system removes core decay heat from the reactor by natural circulation. It can function with minimum or no loss of coolant inventory from the reactor when the normal heat removal system is unavailable. For example, it can be activated for the following events: 1) sudden reactor isolation from power operating conditions, 2) reactor hot standby mode, and 3) safe shutdown condition.

Table 4.6. PCCS Parameters
(Ref. 4.2, Appendix 2)

Number of Units	3
Modules per Unit	2
Tubes per Module	248
Total Heat Transfer Area Inside/Outside	4(X)/430 m ²
Total Flow Area	2.6 m ²
Condenser Tube	
- Length	1.8 m
- OD	50.8 mm
- ID	47.5 mm
- Material	Stainless Steel
Headers	
- Length	2.4 m
- OD	750 mm
Condenser Tube Bundle Volume	3.2 m ²

The ICS consists of three independent high-pressure loops, each of which contains a steam isolation condenser (IC). The steam is condensed on the tube side and transfers the heat to a large ICS/PCCS pool by evaporating water to the atmosphere. Each IC is designed for 30 MWt capacity and is made of two identical modules.

Each IC is located in a subcompartment of the IC/PCCS pool, and all pool subcompartments communicate at their lower ends for full utilization of the collective water inventory. Steam condenses inside vertical tubes and collects in the lower header. Two pipes from each lower header take the condensate to the common drain line leading to the RPV. Noncondensable gases are purged through vent lines into the SP.

During LOCA transients, the ICS is activated when the reactor water level falls below Level 2. In Table 4.7, the IC/PCCS pool and ICS parameters are given. Note that the 254 mm hot steam inlet line shares a steam line with one of the DPVs.

Table 4.7. IC/PCCS Pool and ICS Parameters
(Ref. 4.2, Appendix 2)

IC Pool	
- Depth	4.4 m
- Air space	1.4 m ³
- Volume above top of tubes	1250 m ³
IC Inlet Line Size (from DPV Stub/Tube)	304.8 mm
IC Condensate Return Line Size	152.4 mm
IC Vent Line (to SP) Size	19.05 mm
Number of Units	3
Modules per Unit	2
Condenser Tube	
- Length	1.8 m
- OD	50.8 mm
- ID	46.6 mm
- Number of Tubes. per module	120

4.1.8 Control Rod Drive (CRD) System and Reactor Water Cleanup/Shutdown Cooling (RWCU/SDC) System

The CRD and RWCU/SDC systems are pump-driven non-safety systems. They can also provide high-pressure water injection into the vessel if the AC power is available. The injection of high-pressure makeup water to the reactor is initiated when the normal makeup supply system

(feedwater) is unable to prevent the reactor water level from falling below reactor water Level 2. This makeup water is supplied to the reactor via a bypass line which connects to the feedwater inlet piping via the RWCU/SDC retaining piping.

The SBWR does not have the BWR's residual heat removal system. For a normal shutdown and cooldown operation, the residual and decay heat are removed by the RWCU/SDC system and its condensers. The RWCU/SDC system provides two basic functions: reactor water cleanup and shutdown cooling. The RWCU/SDC system provides the core cooling one half-hour after control rod insertion.

4.1.9 Spectrum of Postulated Breaks

For the SBWR, breaks can be classified as large breaks, intermediate breaks or small breaks. Table 4.8 gives a list of specific break and the flow area associated with each of them.

Table 4.8 Postulated Breaks
(Ref. 4.1, p. 6.3-20, 6.3-21)

Break	Area (cm ²)	Equivalent Nozzle Size (cm)
Large Break		
- DPV stub tube break	1056	36.61
- MSL break	977	35.22
- FWL break	390	22.77
- RWCU/SDC suction line break	295	19.36
Intermediate Break		
- IC return line break	168	14.62
Small break		
- GDSCS injection line break	45.6	7.38
- Bottom head drain line break	20.3	5.08

4.2 Governing Processes and Phenomena

4.2.1 Processes Following a LOCA or Transient

During a LOCA or transient (e.g. loss of feedwater), the control rod drive system (CRDS) shuts down the reactor. The primary function of the GDSCS is to remove the core decay heat in

order to protect the core from uncovering and melting. The GDCS is designed to inject water into the vessel without relying on any active systems by using the gravitational head difference between the GDCS tanks and the vessel. The reactor is operated at high pressure (1040 psia) which needs to drop to a value closer to the containment pressure in order to gain a driving head difference between the GDCS tanks and the vessel. Therefore, before activating GDCS injections, the vessel is depressurized using SRVs and DPVs.

The steam vented through the SRVs is sent to the suppression pool where it is condensed, but the steam vented through DPVs is added to the drywell, which raises the drywell pressure. To lower containment pressure, the PCCS condenses steam in condensers immersed in the ICS/PCCS pools. A mixture of nitrogen and steam is drawn from the containment atmosphere and is passed through condensers. The condensate is drained into the GDCS pools, and the non-condensable gases are purged into the suppression pool.

The SBWR containment is filled with nitrogen in order to prevent the combustion of hydrogen that can form during core uncover by the high-temperature interactions of steam and zirconium in the core. Therefore, the non-condensibles expected to be present in the containment are nitrogen and possibly hydrogen. Purging non-condensibles into the suppression pool serves a dual purpose. First, the suppression pool water removes radioactive contaminants in gases. Second, the PCCS condenser performance deteriorates rapidly with the accumulation of non-condensibles in the tubes, thus purging will restore it to near pure steam environment.

The driving force for the steam and gas mixture through the PCCS is provided mainly by the condensation-induced pressure gradient. There is a pressure gradient between the drywell and suppression pool due to water level difference.

Long term core decay heat is removed in three steps. First, the GDCS injects water into the vessel, thus it removes core energy by boiling and venting into the drywell through DPVs, which remain open once activated. Heat is removed from the core by natural circulation flow within the vessel. Second, the PCCS transfers energy from the drywell to the PCCS/ICS pools by condensing steam from the drywell in the PCCS condensers. Third, the PCCS/ICS pools transfer their energy to the atmosphere outside the containment by vaporizing pool water and venting it. The PCCS also supports the heat removal process by feeding condensate to GDCS pools and by passing noncondensibles to the suppression pools which enhances condensation in the PCCS.

4.2.2 Phenomena Accompanying LOCA or Transients

Inside the RPV, the steady state natural circulation mode can be significantly altered by a break flow which leads to inventory loss and a large pressure gradient within the vessel. At the same time, as the vessel depressurization occurs, the liquid is superheated and flashing can occur in the chimney section as well as in the downcomer.

During this early stage, in-vessel flow instabilities, such as manometric, geysering and density wave instabilities, can occur due to the increased void fraction. The basic density wave instability analyses, carried out in the early seventies, indicate that the two-phase flow is much more unstable at lower pressure and higher void fraction. Hence, significant transient flow instabilities, including the parallel channel flow instabilities, may be encountered.

Outside the reactor vessel, several phenomena are important. These are the steam mixing and condensation in the containment atmosphere, and the condensation of steam in the suppression pool. One important non-equilibrium phase change phenomena is the condensation of steam by the subcooled GDCS water in the reactor vessel. This may lead to the condensation-induced water hammer phenomena or condensation flow instabilities.

Counter current flow limitation (CCFL) phenomena may occur within the reactor vessel. This can lead to the voiding of some subassemblies while others are flooded. Since the natural circulation mode is relatively unstable due to the coupling of the flow and heat transfer (or voiding), the occurrence of the instabilities such as density wave instability and CCFL are possible. The other potential instabilities are manometer-type oscillations and geysering or flashing. The natural circulation instability studies by Ishii et al. [4.3-4.5] indicate that these instabilities can lead to very large amplitude oscillations or cyclic phenomena. Hence, their effects on the GDCS performance can be significant.

The following important governing processes and phenomena should be considered in the model facility:

Time-Dependent Vessel Water Level: The vessel water level in the downcomer dropping below the set limits actuates the ECCS (ADS and GDCS). During the operation of the ECCS, the core natural circulation heat removal depends on the collapsed liquid level difference between the vessel and the downcomer.

Flow Rates of GDCS Water Draining and PCCS Condensate Draining: The difference between the draining rates of GDCS water into the vessel and PCCS condensate into the GDCS pools gives the net rate of emptying GDCS pools. This difference determines the effectiveness of the GDCS at the later stage.

Thermodynamic State of Non-Condensibles: Presence of non-condensibles in the drywell degrades the performance of PCCS condensers. Therefore, the PCCS vents are designed to remove non-condensibles from the drywell into the suppression pool. The measurements of the pressure, temperature, and concentration of non-condensibles are useful to evaluate the condenser performance. The concentration of non-condensibles may vary depending on the location in the drywell.

RPV Inventory with GDCS Flow: Since the GDCS flow will not be initiated until the RPV pressure is low, the steam flow is reduced significantly by the time GDCS injection begins. However, it is possible that the GDCS water can be flashed into steam by contact with hot metal in the injection region. This may adversely affect the GDCS injection flow rate at the initial stage. The GDCS injection flow, break flow and the DPV and SRV flow are the critical parameters in determining the vessel inventory.

GDCS Equalization Flow to the Vessel: The water inventory of the GDCS pools is slowly replenished with condensate draining from the PCCS. However, an effective long-term operation of the GDCS is not possible because only condensed steam from PCCS can replenish GDCS inventory. Due to core boiling, the water level in the vessel will decrease. When the vessel water level reaches 1 m above TAF, the GDCS equalization line will open and water injection from SP to the RPV will begin. Because the driving head difference is small (0.91 m), it is important to know the core cooling capability with the GDCS equalization flow.

Containment Integrity during a LOCA or Transient: During a LOCA or transient, SBWR safety systems operate continuously to remove decay heat from the core to the SP and outside of the containment through the PCCS. Steam is released from the vessel into the containment. The PCCS condenses steam and mitigates the containment over pressurization. The non-condensibles from PCCS condensers are purged into the suppression pool. The effectiveness of PCCS strongly depends on the proper functioning of this purging mechanism.

Thermodynamic and Thermal-Hydraulic Conditions: Pressure and temperature of the drywell atmosphere are the main factors in determining containment integrity. The performance of PCCS condensers depends on the concentration of non-condensibles in the drywell. Water level and temperature in the suppression pool are important in determining the effectiveness of the GDCS equalization flow for core cooling in the event of GDCS pool water depletion that could occur in a long-term operation.

Impact of Non-Condensibles on the Performance of PCCS and ICS: The presence of non-condensable gases is considered in the scaling because it can adversely affect the performance of devices dependent upon condensation heat transfer. When vapor condenses on a heat transfer surface, the concentration of non-condensibles increases. This layer of non-condensibles may insulate the surface from the vapor. In PCCS or ICS more global accumulation of non-condensibles occur. Therefore, it is necessary to continuously remove the non-condensibles and allow vapor to contact the heat transfer surface. PCCS venting into the SP is designed to serve this purpose. Situations which inhibit the removal of non-condensibles by interfering with the PCCS vent flow to the suppression pool will also be studied. This includes the failure of the vacuum breakers to close.

Impact of Drywell Spray: Vacuum breakers will open when drywell pressure drops below the SP gas space pressure. Their flow and opening characteristics are considered in the scaling. Drywell pressure can be reduced due to an operation of the drywell spray which condenses a significant amount of steam from the drywell atmosphere. Thus, the drywell spray may lead to opening of the vacuum breakers.

A number of potential system interactions were identified by the NRC staff in their review of the SBWR testing program proposed by General Electric Nuclear Energy. These interactions include the connection of the DPVs and ICS pipes to a common stub tube, a situation which could allow some blowdown flow through the IC. The test facility will include this feature and will also be designed to allow the study of the combined injection from the GDSCS and suppression pools.

4.3 Identification of Important Phenomena

For a scaled integral test facility, it is necessary to reproduce major thermal-hydraulic phenomena of interest related to engineered safety features. This will ensure that the data can be used to assess the performance of the engineered safety features and to assess the model and code applicabilities for the SBWR safety analysis. For the present facility, the focus is on the phenomena expected to occur in the SBWR at a pressure of 150 psia or less after various accident initiations.

In identifying the key phenomena which should be reproduced in the test facility, two factors should be considered simultaneously. These are the importance of a phenomenon to an accident and the level of understanding of that particular phenomenon. Phenomena identification and ranking should address these factors. The scaling should focus on the highly-ranked phenomena that are the least understood. Such phenomena may not be quantitatively scaled because of the lack of understanding. However, it is necessary that the test facility be able to reproduce and retain the qualitative aspects of these phenomena.

Since not all phenomena can be simulated in the test facility, the data from this test facility can first be used to assess the models in a code at test conditions. When the model can be validated against data under integral test conditions, the scaling effect of that particular phenomena should be re-evaluated in view of the reliable data and validated model. Thus, careful model evaluations and the safety analysis code fills the gap between the integral test data and the prototype conditions.

In this section, a brief summary of the major phenomena of importance to SBWR safety is given. A preliminary BNL PIRT analysis performed for NRC as well as other PIRT analyses performed for GE, have been used together with in-house Purdue assessment of the phenomena.

Flow Instability in RPV: Due to depressurization, significant void fraction is generated in the

RPV. With increased void fraction, flow instability may occur. The natural circulation and break flow can be significantly affected by flow instability. The flow instabilities that are observed in such two-phase natural circulation flow systems are manometric oscillations, density wave oscillations, and flashing induced cyclic flow phenomena [4.7]. At low pressure and low flow conditions, phenomena such as flooding, channel-to-channel oscillation and geysering will also contribute to the oscillatory phenomena. The factors which can affect such oscillatory phenomena are density distribution in the downcomer, void distribution in the core, rate of removal of steam from the vessel and recirculating flow patterns in the core/bypass and chimney. Simulation of void distribution and void propagation is the key to investigating these phenomena.

Blowdown Process: The blowdown process involves critical and subcritical flow of steam, water-steam mixture or water from the RPV. The critical and subcritical flow phenomena are well-known both for single-phase and two-phase. However, the fluid and energy inventory in the RPV depends on the blowdown process. The position of the water level in the RPV triggers the activation of emergency core cooling systems (the GDCS and ADS). The blowdown process thus determines the boundary flow in various components of the SBWR and has the most significant impact on the mass and energy balance in the system. It also governs the pressure transient in the RPV, drywell and wetwell of the SBWR.

GDCS Flow: The GDCS flow into the RPV begins when the RPV pressure is reduced enough so that there is a net higher head in the GDCS water. The draining of the GDCS water into the RPV at later stages of operation when the GDCS pools are replenished with condensate draining from the PCCS is also important. If the RPV level is reduced to the level L0.5, then the GDCS equalization line will open and injection of water from the suppression pool occurs. As the driving head difference is small, the flow from the suppression pool is susceptible to manometric oscillations.

PCCS Condensation: The PCCS is the ultimate heat sink for the containment, and in the long run PCCS performance determines the containment pressure. PCCS condensation efficiency is dependent on the drywell steam non-condensable concentration. The type of non-condensable gases present is also important. If hydrogen is present in the drywell steam then its distribution in drywell, PCCS accumulation and purging process may be different compared to that of nitrogen.

Suppression Pool: The suppression pool is one of the two major heat sinks in the SBWR system. It also works as the retaining tank for the non-condensables gases. The PCCS performance depends on the effective purging of the non-condensable gases into the SP. The heat and mass transfer from the steam and non-condensable gases determine the SP pressure. Condensation of

steam with non-condensibles in the form of jet flow or bubbly flow in the SP is an important phenomenon in determining the containment pressure.

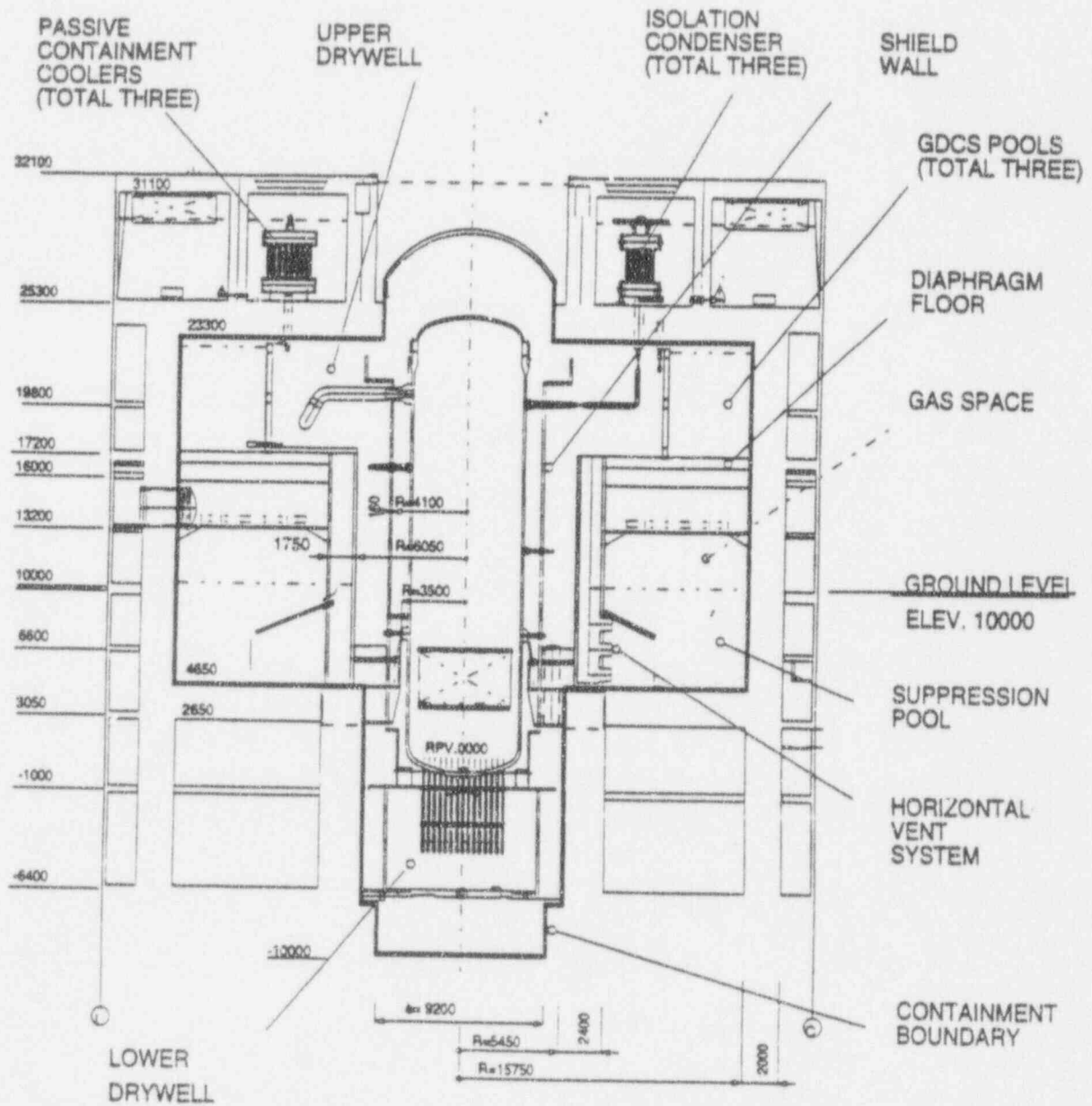


Figure 4.1 SBWR containment boundary [Ref. 4.1, p. 6.2-113]

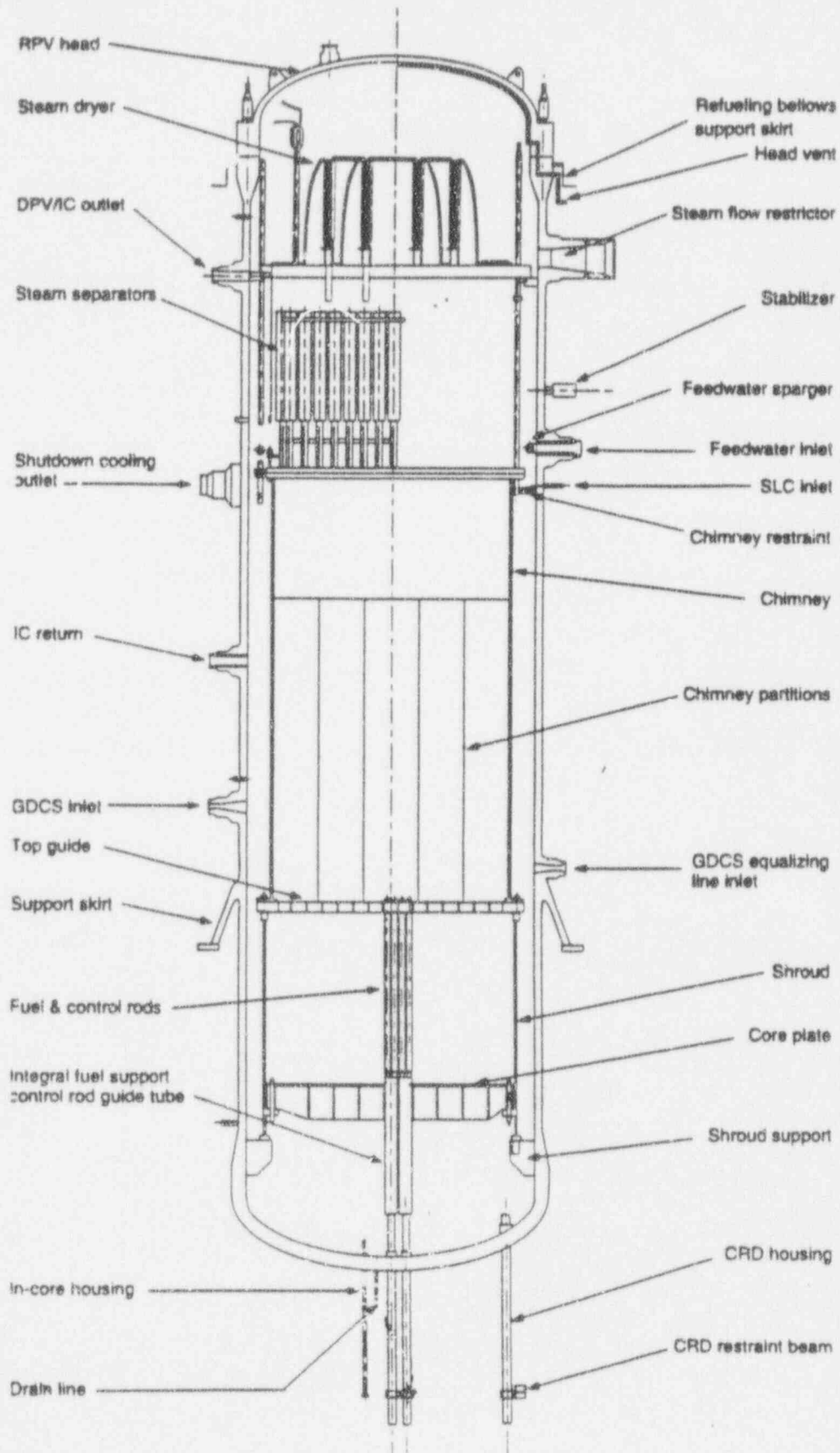


Figure 4.2 Cross-sectional view of RPV [Ref. 4.1, p. 5.3-22]

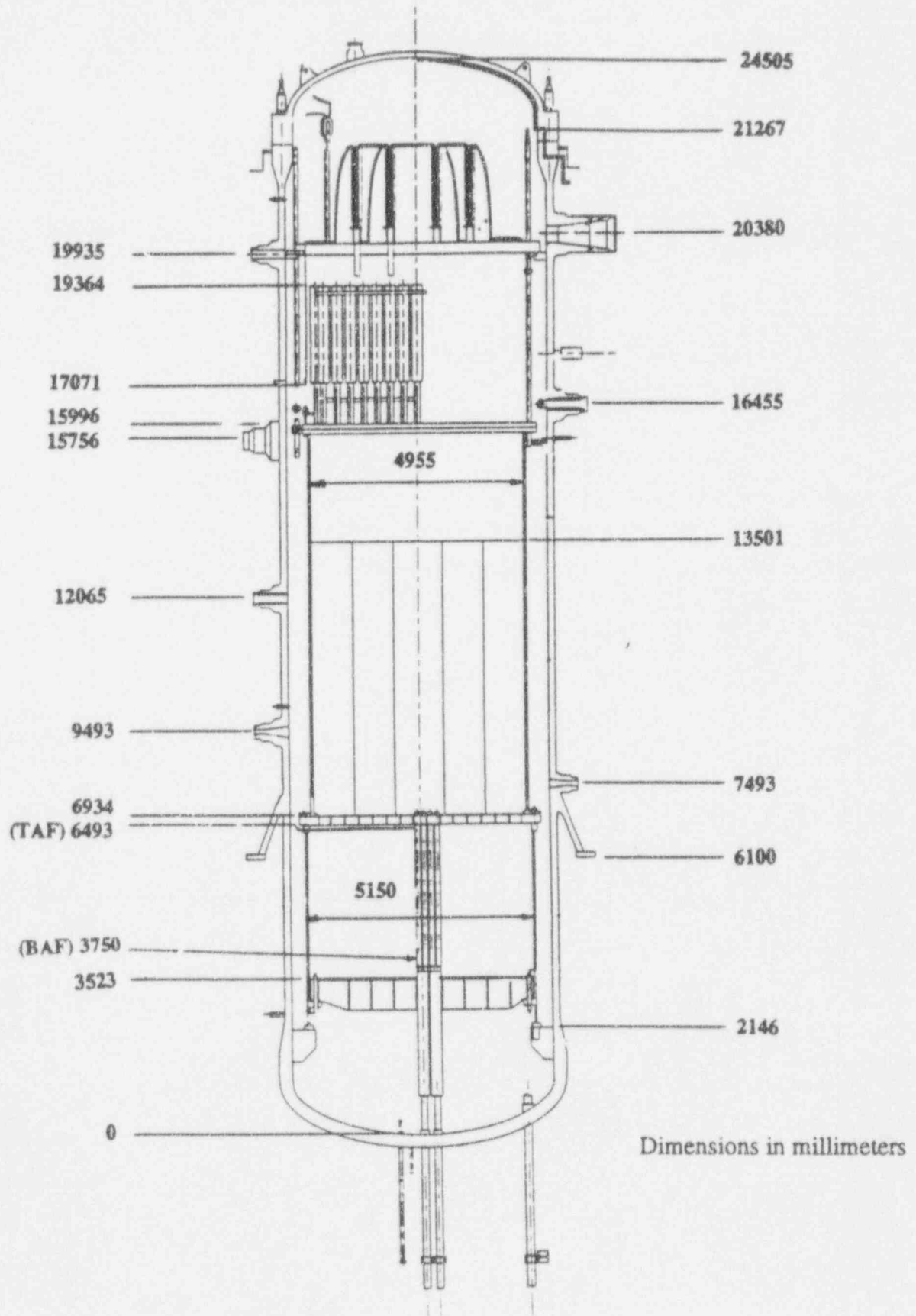
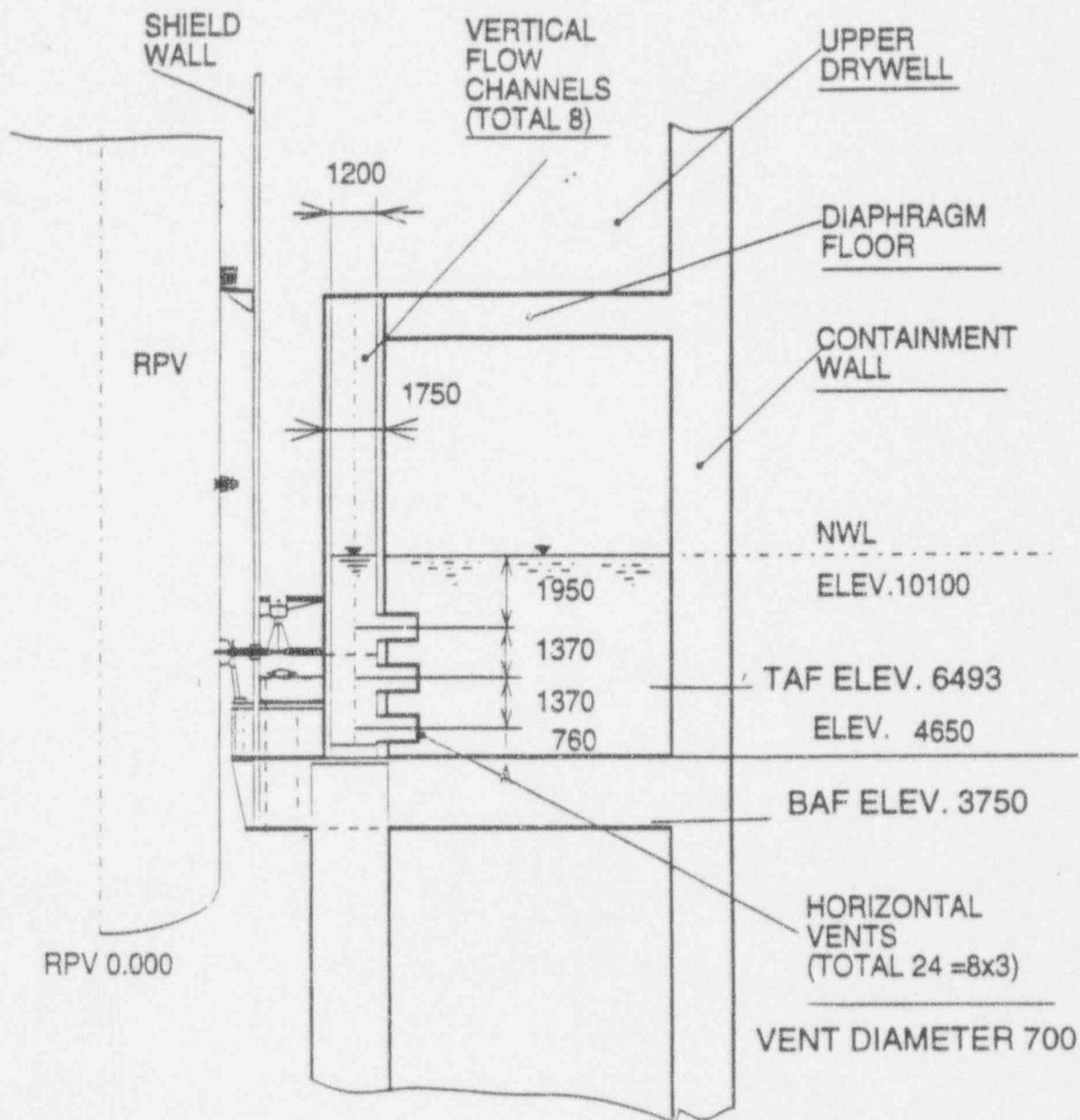


Figure 4.3 Cross-sectional view of RPV with dimensions



Note: Dimensions are in millimeters. Elevations relative to RPV invert EL. 0.000

Figure 4.4 Horizontal vent module between the drywell and suppression pool [Ref. 4.1, 6.2-117]

References

- 4.1 GE Nuclear Energy, "SBWR Standard Safety Analysis Report," 25A5113 Rev. A, August (1992).
- 4.2 U.S. NRC, "Request for Proposal", Requisition No. RS-RES-93-049, U.S. Nuclear Regulatory Commission, Div. of Contracts and Property Mgmt. (1992).
- 4.3 Lee, S.Y. and Ishii, M., "Thermally Induced Flow Oscillation in Vertical Two-phase Natural Circulation Loop", *Nucl. Engr. & Design*, vol. 122, 119-132 (1990).
- 4.4 Lee, S.Y. and Ishii, M., "Characteristics of Two-phase Natural Circulation in Freon-113 Boiling Loop", *Nucl. Eng. and Design*, vol. 121, 69-89 (1990).
- 4.5 Lee, S.Y. and Ishii, M., "Simulation Experiments on Two-phase Natural Circulation in a Freon-113 Flow Visualization Loop", NUREG/CR-5082, ANL-88 (1988).
- 4.6 GE Nuclear Energy "Response to NRC RAI for SBWR Design", MFN No. 077-94, Docket No. STN 52-004, May (1994).
- 4.7 J.-T. Hsu and M. Ishii, "Experimental Study on Two-Phase Natural Circulation and Flow Termination in a Loop", NUREG/CR-4682, ANL-86-32, (1986).

5. SCALING APPROACH

5.1 General Considerations

An important part of the design of the SBWR integral test facility is the development of a well-balanced and justifiable scaling approach. For this task, a three-level scaling approach is used: integral scaling, boundary flow scaling, and local phenomena scaling. The integral scaling is derived from the integral response functions for major variables in single and two-phase flow. This scaling ensures that both the steady-state and dynamic conditions are simulated. It also determines the geometric requirements and time scale. The integral scaling results in the simulation of all the major thermal-hydraulic parameters. The boundary flow scaling simulates the mass and energy inventory of each component and flow of these between components. The third level scaling ensures that key local phenomena can be simulated reasonably well. This is done by examining the constitutive relations, flow regimes and applicable correlations.

Once the test facility scaling is determined from the integral and boundary flow scaling, then the scaling for the local phenomena is considered. It is possible to encounter some distortions in local phenomena while simultaneously satisfying the first two levels of scaling. Since the first two levels of scaling must be satisfied for a correctly scaled facility, the local phenomena should be scaled as accurately as possible while remaining within the constraints imposed by the first two scaling levels. The local phenomena relevant to the SBWR facility are: flashing, choking (blowdown), bypass flow in the reactor core, circulation patterns (forced or natural), slip and phase distribution (flow regime), critical heat flux, condensation, mixing, stratification, stored energy and heat loss.

Once the integral system scaling is complete, the scientific design of the system can be performed. In this stage, various practical considerations, including the instrumentation, should be considered. The scientific design at the optimum conditions should then be translated into an engineering design which meets requirements such as state and local licensing codes, manufacturability, operation and servicing of the test facility.

A well-scaled integral test facility will produce valuable integral experimental data that reproduces all the major phenomena of interest. However, neither the scientific design nor the engineering design can completely satisfy all the scaling requirements. Thus, some scale distortions are inevitable, particularly in the third level of scaling. Distortions are encountered for two major reasons: difficulty in matching the local scaling criteria and lack of understanding of a local phenomenon itself. Therefore, the direct extrapolation of the experimental data to the prototypic conditions is often quite difficult or impossible.

In analyzing data to obtain the corresponding prototypic conditions, the use of a computer code such as RELAP5/CONTAIN can be of great importance. The method that has been devised for using the transient simulation code as a part of the scaling process is a useful approach,

and that will produce greater insight into the RELAP5/CONTAIN transient simulation capabilities and limitations. The method is based on the use of three separate analytical models: the prototype SBWR system model, the "ideal" scaled SBWR model, and the actual PUMA system model. The prototype SBWR model is based on the guidelines developed for applying RELAP5/CONTAIN in order to obtain the best estimate simulation. The "ideal" scaled model is based on the application of all the scaling factors developed for the well-scaled SBWR experiment, again using the RELAP5/CONTAIN application guidelines. The third model is the application of RELAP5/CONTAIN to the actual experimental system and includes all the atypical conditions necessary or unique to the experiment. Some of the atypicalities that can be accounted for between the two scaled models will be: 1) the lack of thermal interaction between components caused by the use of a separated vessel rather than a concentric vessel integrated design for drywell, 2) the difference in the core design necessitated by the minimum heater rod diameter and the cost of providing access to individual heater rods, 3) the differences in the heat sinks of the vessel and piping walls, and 4) any difference caused by initiating the experiment at 1.03 MPa (150 psia) rather than starting from 7.16 MPa (1040 psia). Other minor differences can also be accounted for, such as any difference in boundary conditions, control systems, or differences caused by the instrumentation systems.

The advantage of this three-model system is that differences related to scaling issues can be separated from differences resulting from experimental compromises. These comparisons establish that the experiments capture the qualitative behavior of the SBWR, and give some measure of how closely the phenomena are simulated. The comparisons also assure that the experimental compromises do not qualitatively change the nature of the system response, and that the data can be used to assess the uncertainty in the ability of RELAP5/CONTAIN to predict the actual response of the SBWR system.

The final data analysis compares the PUMA data to the RELAP5/CONTAIN simulations of the PUMA experiments. Such an analysis should be supported by the basic modeling study addressing the true physical mechanisms at the local level. From this, the scalability of the local phenomena in the code can be established. This establishes the ability of RELAP5/CONTAIN to simulate physical phenomena of this type. This ability may need to be increased or decreased based on the differences in response predicted to exist between the PUMA, the "ideal" scaled facility and the actual experiment, and the differences between the full-scale SBWR model and the "ideal" scaled model. As the code scaling and uncertainty analysis methodology [1.6] indicates, the code scalability critically depends on the two-phase flow models and scalability of constitutive models in the absence of near full scale experiments.

5.2 Scaling Approach

The scaling criteria for a natural circulation loop under single-phase and two-phase flow conditions were developed by Ishii, et al. [5.1, 5.2, 5.3]. The criteria include the effects of fluid

properties, so one can also use them for reduced-pressure system scaling.

For a single-phase flow, continuity, integral momentum and the energy equations in one-dimensional area averaged forms are used. First, relevant scales for the basic parameters are determined, then the similarity groups are obtained from the conservation equations and boundary conditions. The heat transfer between the fluid and structure can be included in the analysis by using the energy equation for the structure. From these considerations, the geometrical similarity groups, friction number, Richardson number, characteristic time constant ratio, Biot number and heat source number are obtained. It should be noted that the simulation of a long, large pipe section by a small scale model may encounter some difficulties if the prototype system does not have a reasonably large loss coefficient in addition to the wall frictional loss.

For a two-phase natural circulation system, similarity groups have been developed from a perturbation analysis based on the one-dimensional drift flux model. The set of mass, momentum and energy equations are integrated along the loop, and the transfer functions between the inlet perturbation and various variables are obtained. The scaling parameters are developed from the integral transfer functions, represent the whole-system similarity conditions, and are applicable to transient thermal-hydraulic phenomena.

The scaling approach that has been used for the design of many existing NRC thermal-hydraulic research facilities is summarized in an NRC NUREG Report prepared by Condie, et al. [5.4]. The so-called "full pressure full-height method" was used for most of these facilities. The scaling approach recommended by the NRC, based on the experience accumulated from extensive LOCA studies in scaled integral test facilities, is summarized in a comprehensive paper by Boucher, et al. [5.5]. The present scaling method is an extension of the previously developed scaling approach by Ishii, et al. [5.1, 5.2, 5.3] and consists of three levels of scaling detail. First, integral scaling methods are applied to the system circulation paths. Second, component boundary flow scaling considerations are applied in order to preserve integral mass and energy inventory. Third, scaling criteria are developed that preserve the similarity of local phenomena such as choking, condensation and bubble rise time. These levels of scaling detail are described in the following section.

5.3 Global Scaling

5.3.1 Integral System Scaling (1st Level)

It is imperative to have the single-phase flow similarity requirements as a ready reference, as they are needed to simulate the single-phase to two-phase flow transition. The system consists of a thermal energy source, energy sink and connecting piping system between components. For a natural circulation loop under single-phase flow condition the similarity parameters are obtained from the integral effects of the local balance equations (continuity momentum and

energy) along the entire loop.

The fluid continuity, integral momentum, and energy equations in one-dimensional, area-averaged forms are used along with the appropriate boundary conditions and the solid energy equation. From the non-dimensional forms of these equations, important dimensionless groups characterizing geometric, kinematic, dynamic and energetic similarity parameters are derived. They are given as follows:

$$\text{Richardson Number, } R \equiv \frac{g\beta\Delta T_o l_o}{u_o^2} \quad (5.1)$$

$$\text{Friction Number, } F_i \equiv \left[\frac{f}{d} + K \right]_i \quad (5.2)$$

$$\text{Modified Stanton Number, } St_i \equiv \left[\frac{4h/o'}{\rho_f c_{pf} u_o d} \right]_i \quad (5.3)$$

$$\text{Time Ratio Number, } T_i^* \equiv \left[\frac{l_o/u_o}{\delta^2/\alpha_s} \right]_i \quad (5.4)$$

$$\text{Heat Source Number, } Q_{si} \equiv \left[\frac{q_s''' l_o}{\rho_s c_{ps} u_o \Delta t_o} \right]_i \quad (5.5)$$

where subscripts i , f and s identify the i th component of the loop, fluid and solid, and u_o , ΔT_o and l_o and, temperature difference and equivalent length, respectively (for PUMA, l_o is heated length and ΔT is temperature rise across core). The symbols appearing in the above set of equations conform to standard nomenclature.

In addition to the physical similarity groups defined above, several geometric similarity groups are obtained. These are:

$$\text{Axial Length Scale: } L_i \equiv l_i/l_o \quad (5.6)$$

$$\text{Flow Area Scale: } A_i \equiv a_i/a_o \quad (5.7)$$

It is noted here that the hydraulic diameter of the i th section, d_i , and the conduction depth, δ_i , are defined by

$$d_i \equiv 4 a_i/\xi_i \quad (5.8)$$

and

$$\delta_i \equiv a_{si}/\xi_i \quad (5.9)$$

where a_i , a_{si} and ξ_i are the flow cross sectional area, solid structure cross sectional area and wetted perimeter of the i th section. Hence, d_i and δ_i are related by

$$d_i = 4(a/a_s)_i \delta_i \quad (5.10)$$

The reference velocity, u_o , and temperature difference, ΔT_o are obtained from the steady-state solution. If the heated section is taken as the representative section, these characteristic parameters are expressed as follows:

$$u_o = \left[\frac{4 \beta g \left(\frac{q_o''' l_o}{\rho_f c_{pf}} \right) \left(\frac{a_{so}}{a_o} \right) l_h}{\sum_i \left(F_i/A_i^2 \right)} \right]^{1/3} \quad (5.11)$$

and

$$\Delta T_o = \left(\frac{q_o''' l_o}{\rho_f c_{pf} u_o} \right) \left(\frac{a_{so}}{a_o} \right) \quad (5.12)$$

where the subscript o here denotes the heated section.

Eqs. (5.1) through (5.5) represent relationships between the dimensionless parameters and the generalized variables characterizing the system under consideration. The similarity criteria between different systems can be obtained through detailed consideration of the similarity groups listed above, together with the necessary closure conditions. If similarity is to be achieved between processes observed in the prototype and in a model, it is necessary to satisfy the following requirements:

$$A_{iR} = (a_i/a_o)_R = 1 \quad (5.13)$$

$$L_{iR} = (l_i/l_o)_R = 1 \quad (5.14)$$

$$\left[\sum_i F_i/A_i^2 \right]_R = \left[\sum_i \left[f_i \frac{l_i}{d_i} + K_i \right] / (a_i/a_o)^2 \right]_R = 1 \quad (5.15)$$

$$R_R = (\beta \Delta T_o l_o / u_o^2)_R = 1 \quad (5.16)$$

$$St_{iR} = (h l_o / \rho_f c_{pf} u_o d_i)_R = 1 \quad (5.17)$$

$$T_{iR}^* = [(l_o / u_o) / (\delta^2 / \alpha_s)_i]_R = 1 \quad (5.18)$$

$$B_{iR} = (h \delta / k_s)_{iR} = 1 \quad (5.19)$$

$$Q_{siR} = (q_s''' l_o / \rho_s c_{ps} u_o \Delta T_o)_{iR} \quad (5.20)$$

where subscript i designates a particular component and R denotes the ratio of the value of a model to that of the prototype, i.e.,

$$\Psi_R \equiv \frac{\Psi_m}{\Psi_p} = \frac{\psi \text{ for model}}{\psi \text{ for prototype}} \quad (5.21)$$

As discussed in detail in [5.1-5.3], the frictional similarity requirement, Eq. (5.15), can be satisfied independently of the remaining scaling requirements. Hence, from the remaining scaling requirements, it can be shown that the following conditions should be satisfied for a complete simulation:

$$(u_o)_R = \left[\frac{\beta q_o''' l_o^2}{\rho_s c_{ps}} \right]_R^{1/3} \quad (5.22)$$

$$(\Delta T_o)_R = \left[\frac{q_o''' l_o}{\rho_s c_{ps} u_o} \right]_R \quad (5.23)$$

$$(\delta_i)_R = (\delta)_R = \left[\frac{\alpha_s l_o}{u_o} \right]_R^{1/2} \quad (5.24)$$

$$(d_i)_R = (d)_R = \left[\frac{\rho_s c_{ps}}{\rho_f c_{pf}} \right]_R \left[\frac{\alpha_s l_o}{u_o} \right]_R^{1/2} \quad (5.25)$$

$$(h_i)_R = (h)_R = (k_s)_R \left[\frac{u_o}{l_o \alpha_s} \right]_R^{1/2} \quad (5.26)$$

where the parameters without the component subscript, *i*, denote universal values that must be satisfied in all components. In addition to the above, the geometric similarity requirements dictate that

$$\left[\frac{l_i}{l_o} \right]_R = 1 \quad \text{and} \quad \left[\frac{\dot{u}_i}{\dot{u}_o} \right]_R = 1 \quad (5.27)$$

must also be met.

With these conditions, Eqs. (5.22-5.27) and Eq. (5.15), the effects of each term in the conservation equations are preserved in the model and prototype without any distortions. If some of these requirements are not satisfied, then the effects of some of the processes observed in the

model and prototype will be distorted.

At this point, a few comments are appropriate regarding the practical implications of the similarity requirements:

1. The friction similarity may be difficult to satisfy, except in components having a subchannel geometry. Often, friction similarity imposes the most significant limit on the size of a scaled-down model [5.1-5.3].
2. The conduction depth ratio and hydraulic diameter ratio should satisfy certain criteria. However, satisfying those criteria over the entire loop may be difficult. It is considered that they are important mainly at the major heat transfer components where these conditions can be easily satisfied. However, the distortions in these criteria over a loop may lead to an overall scale-distortion in terms of structural heat losses. This should be carefully evaluated and compensated.
3. In contrast to the design parameters, the heat transfer coefficient cannot be independent of the flow field. Therefore, there may be some difficulties in meeting the constraint imposed by Eq. (5.26). Satisfying this condition depends on the flow regime. However, relaxation of this similarity requirement influences only the boundary layer temperature drop simulation. When the heat transfer mechanism is not completely simulated, the system will adjust to a different temperature drop in the boundary layer. The overall flow and energy distribution will not be strongly affected by the slow transients typical of a natural circulation system.
4. It is important to note that the above set of requirements does not put constraints on the power density ratio, \dot{q}_{oR} . However, they do put a restriction on the time scale as follows:

$$\tau_R \equiv \left[\frac{l_o}{u_o} \right]_R = \frac{l_{oR}}{[(\beta q_o''' l_o^2)_R / (\rho_s c_{ps})_R]^{1/3}} \quad (5.28)$$

The small perturbation technique and integral response function have been used by Ishii and Kataoka [5.1] to develop similarity criteria for two-phase flow systems. The important dimensionless groups that characterize the kinematic, dynamic and energetic fields are given as follows:

$$\text{Phase Change No. } N_{pch} \equiv \left[\frac{4q_o''' \delta l_o}{du_o \rho_f \Delta h_{fg}} \right] \left[\frac{\Delta \rho}{\rho_g} \right] = N_{Zu} \quad (5.29)$$

This phase change number has been renamed as the Zuber number, N_{Zu} recently in recognition of Zuber's significant contribution to the field.

$$\text{Subcooling No.} \quad N_{sub} \equiv \left[\frac{\Delta h_{sub}}{\Delta h_{fg}} \right] \left[\frac{\Delta \rho}{\rho_f} \right] \quad (5.30)$$

$$\text{Froude No.} \quad N_{Fr} \equiv \left[\frac{u_o^2}{g l_o \alpha_o} \right] \left[\frac{\rho_f}{\Delta \rho} \right] \quad (5.31)$$

$$\text{Drift-Flux No.} \quad N_{di} \equiv \left[\frac{V_{gj}}{u_o} \right]_i \quad (\text{or Void-Quality Relation}) \quad (5.32)$$

$$\text{Time Ratio No.} \quad T_i^* \equiv \left[\frac{l_o/u_o}{\delta^2/\alpha_s} \right]_i \quad (5.33)$$

$$\text{Thermal Inertia Ratio } N_{thi} \equiv \left[\frac{\rho_s c_{ps} \delta}{\rho_f c_{pf} d} \right]_i \quad (5.34)$$

$$\text{Friction No.} \quad N_{fi} \equiv \left[\frac{fl}{d} \right]_i \left[\frac{1 + x(\Delta \rho/\rho_f)}{(1 + x\Delta \mu/\mu_f)^{0.25}} \right] \left[\frac{a_o}{a_i} \right]^2 \quad (5.35)$$

$$\text{Orifice No.} \quad N_{oi} \equiv K_i [1 + x^{3/2} (\Delta \rho/\rho_f)] \left[\frac{a_o}{a_i} \right]^2 \quad (5.36)$$

where V_{gj} , Δh_{fg} , Δh_{sub} , and x are the drift velocity of the vapor phase, heat of evaporation, subcooling and quality, respectively. In addition to the above-defined physical similarity groups, several geometric similarity groups such as (l_i/l_o) and (a_i/a_o) are obtained.

The Froude, friction and orifice numbers, together with the time ratio and thermal inertia groups, have their standard significance. Subcooling, Zuber and drift-flux numbers are associated with the two-phase flow systems. Their physical significance is discussed in

detail elsewhere [5.1-5.3].

Eqs. (5.29) through (5.36) represent relationships between the dimensionless groups and the generalized variables of a two-phase flow system. The dimensionless groups must be equal in the prototype and model if the similarity requirements are to be satisfied. Hence, the following conditions result:

$$(N_{Zu})_R = 1, (N_{sub})_R = 1, (N_{Fr})_R = 1, (N_{di})_R = 1$$

$$(T_i^*)_R = 1, (N_{thi})_R = 1, (N_{fi})_R = 1, \text{ and } (N_{oi})_R = 1 \quad (5.37)$$

It can be shown from the steady-state energy balance over the heated section that N_{Zu} and N_{sub} are related by

$$N_{Zu} - N_{sub} = x_e \left[\frac{\Delta\rho}{\rho_g} \right] \quad (5.38)$$

where x_e is the quality at the exit of the heated section. Therefore, the similarity of the Zuber and subcooling numbers yields

$$(x_e)_R \left[\frac{\Delta\rho}{\rho_g} \right]_R = 1 \quad (5.39)$$

This indicates that the vapor quality should be scaled by the density ratio. When combined with Eqs. (5.35) and (5.36), Eq. (5.39) shows that the friction similarity in terms of N_{fi} and N_{oi} can be approximated by dropping the terms related to the two-phase friction multiplier. Furthermore, by definition it can be shown that $N_d = (\Delta\rho/\rho_g x) [\rho_g/\Delta\rho\alpha - 1] - 1$. Therefore, similarity of the drift-flux number requires void fraction similarity

$$(\alpha_e)_R \left[\frac{\Delta\rho}{\rho_f} \right]_R = 1 \quad \text{or } (\alpha_e)_R = 1 \quad (5.40)$$

Excluding the friction, orifice and drift-flux number similarities from the set of similarity requirements, Eq. (5.37), and solving the remaining equations, one obtains the

following similarity requirements:

$$(u_o)_R = (l_o)_R^{1/2} \quad (5.41)$$

$$(\Delta h_{\text{sub}})_R = \left[\frac{\Delta h_{fg} \rho_g}{\Delta \rho} \right]_R \quad (5.42)$$

$$(q_o)''''_R = \left[\frac{\rho_f \rho_g \Delta h_{fg}}{\Delta \rho} \right]_R \left(\frac{d}{\delta} \right)_R (l_o)_R^{-1/2} \quad (5.43)$$

$$\delta_R = (l_o)_R^{1/4} (\alpha_s)_R^{1/2} \quad (5.44)$$

$$d_R = \left[\frac{\rho_s c_{ps}}{\rho_f c_{pf}} \right]_R (l_o)_R^{1/4} (\alpha_s)_R^{1/2} \quad (5.45)$$

The velocity scale shows that, in contrast to the case of single-phase flow scaling, the time scale for a two-phase flow is not an independent parameter. From Eq. (5.41), the time scale in two-phase flow is uniquely established. Thus,

$$\tau_R = \left[\frac{l_o}{u_o} \right]_R = (l_o)_R^{1/2} \quad (5.46)$$

This implies that if the axial length is reduced in the model, then the time scale is shifted in the two-phase flow natural circulation loops. In such a case, the time events are accelerated (or shortened) in the scaled-down model by a factor of $(l_o)_R^{1/2}$ over the prototype.

It is important to note that when the two-phase flow velocity scale, Eq. (5.41), is used in the single-phase flow geometric scale requirements, the geometric similarity requirements in both cases become the same. Hence, the same geometric scale can be used for single-phase and two-phase flows. However, using the time scale indicated by the two-phase flow scaling, namely $\tau_R = \sqrt{l_o}_R$, the single-phase time events are also scaled by the same criterion. This leads to the very important conclusion that for systems involving

both single and two-phase flow in a reduced length model, real-time scaling is not appropriate.

5.3.2 Mass and Energy Inventory and Boundary Flow Scaling (2nd Level)

The scaled mass and energy inventory histories must be preserved for integral similarity to be achieved. The integral system response scaling methods assure this similarity when friction-dominated loop flow is considered. However, when vessel or system discharges occur that are dominated by non-frictional momentum effects, such as at a point of choked flow or any nozzle flow in which the pressure drop-flow relation is dominated by kinetic loss or by cavitation effects, then additional constraints apply. At such discharge points the fluid velocity depends upon the local pressure ratio across the device, which is preserved in a full-pressure scaled system such as the PUMA facility. In nonfrictional momentum-dominated flows, the fluid velocity is the same in the model as in the prototype. Therefore, the flow area at such discharge points must be scaled to preserve mass and energy inventory rather than loop kinematics. The purpose of this section is to develop the appropriate scaling relations to be applied at such points. This is particularly important for the SBWR experiment, since choked or momentum-dominated flows occur at the reactor vessel steamline discharge and at the safety and depressurization valve openings. It is particularly important that similarity of these phenomena is preserved, since the timing of the SBWR safety systems is a strong function of the system pressure, and the depressurization system is activated based on the preset levels of the vessel coolant inventory. Furthermore, the ECCS flows begin only after near-equalization of the pressures in the reactor vessel and the containment. Thus, an overall criterion for similar behavior between the prototype and the model is that the depressurization histories be the same when compared in the respective (scaled) time frames, i.e.,

$$P_m(t_m) = P_p(t_p) \quad (5.47)$$

This integral condition will be satisfied if the differential pressure change is the same at corresponding times, i.e.,

$$\frac{dP_m}{dt_m} = \frac{dP_p}{dt_p} \quad (5.48)$$

The scaling criteria for similarity of the friction-dominated natural circulation flows yields the result that the time scale of the model, or laboratory time, is related to the prototype time, by

$$t_m = (1/2)t_p = \tau_R t_p \quad (5.49)$$

and the depressurization rates of the model and the prototype are related by

$$\frac{dp_m}{dt_m} = (1/\tau_R) \frac{dp_p}{dt_p} = (2) \frac{dp_p}{dt_p} \quad (5.50)$$

This condition will be satisfied if the corresponding component vessel inventories are similar, i.e.,

$$\left[\frac{M_m}{V_m} \right]_{t_m} = \left[\frac{M_p}{V_p} \right]_{t_p} \quad (5.51)$$

where M_p and M_m are the prototype and model vessel inventory masses, and V_p and V_m are the respective prototype and model vessel volumes. This relation must hold for each component as well as for the overall system if complete similarity is to be ensured.

Mass Inventory and Mass Flow Scaling

For integral experiments, accurate simulation of the mass and energy inventory is essential. This requires a separate scaling criteria for the system boundary flows such as the break flow and various ECCS injection flows. The scaling criteria, stated in Eq. (5.51), are obtained from the overall control volume balance equations.

For the coolant mass inventory, the total mass for a particular component is given by

$$\frac{d}{dt} M = \Sigma m_{in} - \Sigma m_{out} \quad (5.52)$$

By denoting the total volume by V and the mean density by $\langle \rho \rangle$, the balance equation can be written in a non-dimensional form that applies to both the model and the prototype system as

$$\frac{d}{dt^*} \langle \rho^* \rangle = \Sigma m_{in}^* - \Sigma m_{out}^* \quad (5.53)$$

where

$$t^* \equiv t/(l_o/u_o) \quad (5.54)$$

and

$$m_{in}^* \equiv \frac{m_{in} \tau_o}{\rho V} - \frac{\rho_{in}}{\rho} \left[\frac{a_{in}}{a_o} \right] \left[\frac{u_{in}}{u_o} \right] \quad (5.55)$$

where $\tau_o = (l_o/u_o)$ for either the prototype or the model. The definition for m_{out}^* can be given similarly. For equal model and prototype pressure simulation, $(\rho_{out}^*)_R = (\rho_{out}/\rho)_R$ is simply unity. Hence, the simulation of the boundary flow requires

$$\left[\frac{a_{out}}{a_o} \frac{u_{out}}{u_o} \right]_R = 1 \quad (5.56)$$

This is a similarity condition for the flow area and velocity combined. Therefore, it is not necessary at discharge points to satisfy the independent conditions for area and flow given by Eqs. (5.27) and (5.41), which must be satisfied by the other components of the loop. The form of the discharge scaling criterion given by Eq. (5.56) is very convenient from the standpoint of practical implementation.

For example, the break flow velocity, u_{out} , can not be independently controlled if choking occurs. In the case of choking, Mach number similarity is maintained. Thus, for a equal-pressure system the break flow is prototypic in the sense that $(u_{out})_R = 1$, whereas the basic scaling $(u_o)_R = (l_o)_R^{1/2}$ and the criterion given in Eq. (5.56) predict that the break flow area should be scaled according to

$$\left[\frac{a_{in}}{a_o} \right]_R = (l_o)_R^{1/2} \quad (5.57)$$

which would result in a reduction of the break flow area beyond the geometrical scale used for the loop flows.

For the case of ECCS injection flows, the breakflow scaling criterion is also very useful. If the injection lines are scaled according to the geometrical scaling condition, Eq. (5.27), the line diameters become very small and the frictional resistance can be very

large. This will result in mismatched ECCS injection flow, which is unacceptable. Fortunately, the boundary flow scaling criterion, Eq. (5.56), permits an enlarged flow area to obtain the correct volumetric or mass flow rate.

Energy Inventory and Energy Flow Scaling

For the energy inventory, E , the control volume balance is given by

$$\frac{dE}{dt} = q - w + \sum m_{in} h_{in} - \sum m_{out} h_{out} \quad (5.58)$$

By non-dimensionalizing the above equation, it can be shown that the scaling criteria obtained for the natural circulation satisfies the similarity requirement for the heat input, q . The non-dimensional form of the above equation is given by

$$\frac{dE^*}{dt^*} = q^* - w^* + \sum m_{in}^* h_{in}^* - \sum m_{out}^* h_{out}^* \quad (5.59)$$

where

$$m_{in}^* h_{in}^* = m_{in} h_{in} \frac{\tau_0}{\rho V h_0} - \left(\frac{\rho_{in}}{\rho} \right) \left(\frac{u_{in}}{u_0} \right) \left(\frac{u_{in}}{u_0} \right) \left(\frac{h_{in}}{h_0} \right) \quad (5.60)$$

In view of Eq. (5.56), for a full pressure simulation, i.e. $(h_0)_R = 1$, it is necessary to require

$$(h_{in})_R = 1 \quad (5.61)$$

This physically implies that the inflow or outflow should have a prototypic enthalpy. The above non-dimensional energy equation also shows that the initial energy inventory should be scaled by the volume ratio.

5.3.3 Pressure Scaling

The work scope and program objectives of the PUMA are focused on the low-pressure region of operation following the initial depressurization of the vessel. This implies that the prototype pressure maximum is about 150 psi (or 1 MPA). In considering the pressure

scaling of the integral test facility, two effects should be evaluated separately. These are:

1. System pressure level, which affects all the thermal-hydraulic properties of the liquid, vapor and phase changes.
2. Individual component or inter-component pressure distributions.

Considering the pressure scaling in these two separate effects is somewhat analogous to the well-known Boussinesq assumption.

As indicated in the report on pressure scaling by Kocamustafaogullari and Ishii [5.3], the reduced-system pressure scaling or fluid-to-fluid scaling introduces large uncertainties and scaling distortions due to the difficulties in matching all the non-dimensional groups under changing system pressure conditions. For transients involving system pressure changes, the adoption of the prototypic system pressure for a scaled model is the best and simplest approach. This guarantees that all the thermal-hydraulic properties are essentially prototypic, so that the system scaling criteria can be significantly simplified.

Since the experimental focus is on the various low pressure phenomena associated with the emergency cooling systems and vessel depressurization systems, the adoption of the prototypic pressure for the model integral test facility significantly increases the confidence level of the scaling approach and design of the scaled integral facility, as well as the usefulness of integral test data. Furthermore, the maximum pressure of 1.03 MPa (150 psia) is low enough that its impact on the overall cost of the project is small compared to a reduced-pressure model. The detailed scaling study carried out by Ishii, et al. [5.1-5.3] indicates that the reduced-pressure simulation is possible for a narrow window of pressure transients. However, it is very difficult to simulate all transients.

In view of the above, the prototypic pressure is taken as the system pressure scaling base. Hence, the system pressure and all other fluid properties are considered to be prototypic. This will greatly simplify the scaling procedures. Thus, we have the global pressure scaling given by

$$p_R = 1 \quad (5.62)$$

Under the above prototypic system pressure scaling, the thermodynamic and transport properties at every component are considered prototypic. However, the pressure distribution in each component may not be prototypic. It should be noted that the pressure distribution within a component or between components can be the controlling factor in determining the flow by forced convection or natural circulation. This aspect of the pressure

effect in a reduced-height system should be considered separately. At the initial blow-down phase of a LOCA or other transient, the major intercomponent flow occurs due to the initial pressure difference between the reactor pressure vessel and the containment. For this initial phase, the pressure difference between these two components should be prototypic at the same elevation. Thus,

$$(\Delta P_{ij})_R = 1 \quad \text{at } Z_R = l_R \quad (5.63)$$

where the notation i and j stand for the reactor vessel and containment, respectively.

However, in the case of natural circulation-dominated flow, such as the reactor vessel internal circulation, GDCS injection or PCCS venting, the hydrostatic head is the essential driving force. For this case, the differential pressure is scaled by the reduced height scaling. Hence,

$$(\Delta P)_R = l_R \quad (\text{at } \Delta Z_R = l_R), \quad (5.64)$$

For all components where the flow is governed by the pressure difference due to hydrostatic head, the latter pressure scaling criterion should be used. This criterion is consistent with the hydrostatic pressure distribution within each component, and guarantees the proper intercomponent flows driven by the gravitational head. A significant deviation or distortion from this differential pressure scaling at any component may lead to inconsistent flow among components and may destroy overall scaling of integral phenomena of interest.

For the PUMA, the initial differential pressure scaling is set by the initialization process with isolated components. At the later stages of accident simulation, most of the significant liquid flows between components are driven by the hydrostatic head. These flows are accurately simulated by using proper height scaling of all major elements and components based on

$$\Delta Z_R = l_R \quad (5.65)$$

which implies the complete axial geometrical similarity. This condition, together with the void distribution simulation based on the integral scaling, insures that the differential pressure is scaled by the reduced height scaling.

5.3.4 Basis for Reduced Height Scaling

Under the prototypic pressure simulation, the system geometry can be determined from the integral system scaling and the boundary flow scaling discussed above. The dynamic scaling requirements for a two-phase flow system are given by Eqs. (5.29-5.36). In general it is difficult to match all these similarity criteria for a scaled down system, so a careful evaluation of each of these requirements should be made.

Based on the original scaling study [5.1-5.3] it is evident that the Froude number and Friction number scale the gravitational driving force and frictional resistance against the inertia term. The Zuber (phase change) number and subcooling number scale the energy transfer for a boiling process. It is essential that these latter numbers are satisfied for the energy and kinematic similarities. As indicated by Eqs. (5.38-5.40), these two similarity criteria give the simulation of the void fraction and the steam quality under the prototypic pressure simulation.

In considering the dynamics of the system, two conditions should be considered separately. The first is on the quasi-steady flow simulation and the second is the dynamic response of the system, including the inertia effect. It is clear that the Froude number and friction number scale the dynamic response. When the inertia forces are not important, only the balance between the frictional resistance and gravitational force should be considered. This can be achieved by taking the product of these two numbers. Thus, natural circulation number is defined as

$$N_{nc} = N_f N_{Fr} = \left[\frac{\text{friction}}{\text{inertia}} \right] \left[\frac{\text{inertia}}{\text{gravity head}} \right] \quad (5.66)$$

This equation can be extended to include the minor loss coefficient as

$$N_{nc} = (N_f + N_o)N_{Fr} \quad (5.67)$$

In general, the requirement of

$$(N_{nc})_R = 1 \quad \text{or} \quad \left\{ (N_f + N_o)N_{Fr} \right\}_R = 1 \quad (5.68)$$

is less restrictive than $(N_f)_R = (N_o)_R = (N_{Fr})_R = 1$.

However, the energy and kinematic similarities require that the velocity be scaled by Eq. (5.41) and the void fraction by Eq. (5.40). Under these conditions, it can be shown that

$$(N_{Fr})_R = \left[\frac{u^2}{gl\alpha} \frac{\rho_f}{\Delta\rho} \right]_R = 1 \quad (5.69)$$

Hence Eq. (5.68) can be reduced to

$$(N_f + N_o)_R = 1 \quad (5.70)$$

Combining the above equation with Froude number similarity, it is seen that these two also constitute an approximate dynamic similarity between the inertia term, gravitational term and flow resistance.

The advantage of Eq. (5.70) relative to the two independent requirements of $(N_f)_R = 1$ and $(N_o)_R = 1$ is significant. Under a homogeneous flow assumption, the requirement given by Eq. (5.70) can be approximated by

$$(N_f + N_o)_R \approx \left[\frac{fl}{d} + K \right]_R \left[\frac{a_o}{a_i} \right]_R^2 = 1 \quad (5.71)$$

By using the geometrical similarity criteria,

$$\left[\frac{fl}{d} + K \right]_R = 1 \quad (5.72)$$

A careful analysis of Eq. (5.72) clearly indicates the great advantage of using the reduced-height system for a given volume scale in satisfying the dynamic similarity criteria. By reducing the flow area, the hydraulic diameter is reduced by $d_R = \sqrt{a_i}$, except at bundle sections such as the core. For most small integral test facilities, it is necessary to have $l_R > d_R$ in order to maintain a reasonably large axial height so that the naturally existing two-phase level fluctuations do not adversely affect various transient phenomena. In general, the ratio of the first friction term itself is always larger than unity. However, by reducing the height of a facility, this ratio can be made closer to unity by increasing d_R for a fixed value of v_R . The second significant point is that the minor loss coefficient is an

easy parameter to adjust through small design modifications in such a way that $K_R < 1$ to compensate for increased friction. Hence by properly modifying the K value, Eq. (5.72) can be achieved.

In view of the above and the cost consideration, the volume scale of 1/4(0) and the height scale of 1/4 appear to be most desirable for the Purdue integral test facility. This implies the general area ratio of 1/100. A more detailed discussion of the system geometry and other considerations is given in Chapter 6 and 7. However, for the subsequent local scaling phenomena analysis, these geometrical scales are used as reference conditions.

5.4 Local Phenomena Scaling (3rd Level)

5.4.1 Reactor Vessel Flow Dynamics and Instability Scaling

The dynamic behavior and stability of a boiling flow system can be analyzed by using a one-dimensional drift flux model [5.6] and a small perturbation method [5.7-5.9]. A perturbation of inlet flow is introduced, given by

$$\delta v(t) = \epsilon e^{st} \quad (5.73)$$

where $s = a + j\omega$. Thus, s is a complex number; the real part gives the amplification coefficient and the imaginary part represents the angular frequency, ω .

By formally integrating the four differential balance equations in the one-dimensional drift flux model, various transfer functions between major variables, such as the velocity, void fraction, density, enthalpy, pressure drop and inlet velocity, can be obtained. These can be expressed symbolically by

$$\delta f(s, z, t) = Q(s, z) \delta v(s, t) \quad (5.74)$$

where Q represents the transfer function and δf is the perturbed part of the variable, f , at location z . It has been shown that both the dynamic and transient response of the system are governed by the transfer function between the internal pressure drop over the system and the inlet flow [5.7-5.9]. Thus, the most important relation is given by

$$\delta \Delta P(s, t) = Q(s) \delta v(s, t) \quad (5.75)$$

In a real physical system, the perturbation comes from the boundary condition on the pressure which induces flow change. Thus,

$$\delta v = \frac{1}{Q(s)} \delta \Delta P \quad (5.76)$$

The dynamic response depends on the form of the transfer function, $1/Q(s)$, whereas the linear stability of the system depends on the root of the characteristic equation given by

$$Q(s) = 0 \quad (5.77)$$

The characteristic function, $Q(s)$ can be nondimensionalized by introducing proper scales for various variables [5.7-5.9]. Thus

$$Q^*(s^*) = Q^*(s^* \cdot N_1, N_2, \dots, N_m) \quad (5.78)$$

where N_1, \dots, N_m are the same non-dimensional groups listed in Section 5.3. This indicates that the dynamics of the system can be simulated if the scaling parameters, $N_1 \dots N_m$, are identical between two systems. The disappearance of z in Q is due to the formal integration of the momentum equation over the entire system length.

Since our general scaling is based on these non-dimensional groups, as discussed in Section 5.3, it is assured that the dynamic behavior and instability characteristics can be well-simulated in the reactor pressure vessel of the integral test facility if the flow can be considered close to one-dimensional. The SBWR reactor pressure vessel has a relatively large l/d , which causes it to be dominated by the axial flow. Furthermore, the present reduced height system has the aspect ratio reasonably close to the prototype at $(l/d)_R = 2.5$. This number, which is a good scale of the three dimensionality of the facility, is better matched than most of the full-height integral test facilities for similar purposes.

5.4.2 Choked Flow Case

The RPV is depressurized by the discharge of steam or water from a break and by the SRV and DPV flows when these systems are activated. In the early phase of the depressurization, the upstream pressure is sufficient to cause sonic velocity at the minimum-area section of the steam line venturi, or at the throat of the SRV or DPV, and at the break location. A bottom drain line break (BDLB) also results in choked flow when cavitation occurs at the throat or minimum area in the break line. For these cases, the velocity at the

break or the throat will be the same in the model as in the prototype since the pressures and thermodynamic conditions are the same. The flow in short nozzles and valve contraction sections can be considered to be nearly frictionless and adiabatic so that an isentropic model of the flow process is a good approximation. The prototype-to-model ratio of velocity multiplied by the area should equal 200 in order to satisfy the conditions for similarity of the mass and energy inventories as previously discussed. In the choked flow case, no additional restrictions on the geometry or loss mechanisms are required. However, as we shall see, additional restrictions will result from the need to preserve the pressure or pressure ratio at which the transition from choked flow to unchoked flow will occur.

Two quite different nozzle geometries are found in the SBWR system. First, the steamline contains a converging-diverging de Laval-type nozzle that is designed to limit the steam discharge rate in the case of a main streamline break, yet result in little pressure loss under normal operation. The low pressure loss under normal operation is achieved by the use of a low-angle conical diffuser downstream of the nozzle throat so that flow separation is avoided and good pressure recovery is achieved. This type of nozzle will become choked only when a modest drop in the discharge pressure occurs as a result of a break or other decrease in the downstream flow resistance. The flow will remain choked until the upstream pressure drops to near the downstream value. This process is illustrated in Figures 5.1 and 5.2 for the case of isentropic flow through a converging-diverging nozzle. Figure 5.1 is a surface plot of the static pressure ratio (ratio of static pressure to isentropic stagnation pressure) throughout the nozzle for a range of the exit pressure ratio. Notice that the throat pressure ratio drops as the downstream pressure ratio is lowered, until sonic flow is reached at the throat. From that point on, the upstream pressure distribution is constant independent of the downstream pressure (choked). The pressures in the downstream, or diverging section of the nozzle have a rather complex behavior due to the possibility of a normal shock (the discontinuous rise in pressure shown in Figure 5.1). The flow velocity changes from supersonic to subsonic across the normal shock. Note that subsonic diffusion downstream of the normal shock results in an increase in the static pressure as the flow velocity decreases. At a sufficiently low discharge pressure, the normal shock will occur downstream of the nozzle exit. Thus, we see that it is possible for such a nozzle to be choked under a wide range of pressure ratios. This is more clearly illustrated in Figure 5.2, where the nondimensional mass flow parameter is plotted as a function of the ratio of the nozzle exit pressure to the upstream stagnation pressure. Note that the mass flow rate is constant up to a pressure ratio of approximately 0.98.

The SRV and DPV systems have a different nozzle geometry that consists of a smooth contraction down to the throat followed by an abrupt increase in the flow area. This type of nozzle has quite a different flow characteristic. The abrupt increase in flow area downstream of the throat results in large pressure losses due to the irreversibility associated

with turbulence downstream of the abrupt increase in area. The static pressure ratios through such a nozzle are illustrated in Figure 5.3 as a function of the downstream pressure ratio. Compare Figure 5.3 with 5.1 and note the considerable drop in the discharge pressure that occurs prior to reaching the choked condition, indicated by the constancy on the upstream pressures. In this case, the downstream pressure losses have been modeled using the Bourda-Carnot loss model for an abrupt area change. The dramatic difference in the flow characteristic between this nozzle and the converging-diverging nozzle previously discussed can be seen by comparing the non-dimensional mass flow as a function of pressure ratio (compare Figure 5.4 with Figure 5.2). In this case, choked flow is maintained only up to a pressure ratio of 0.56, which is characteristic of an orifice or any discharge point having an abrupt area change.

In order to maintain similarity in the scaled mass and energy inventories it is necessary to scale the throat area between the model and the prototype by the ratio $1/2(K)$. However, in order to assure correct transition to subsonic or unchoked flow, it will also be necessary to preserve the diffusion characteristics of the downstream section of the nozzle. This requires that geometric similarity be maintained, and to a lesser degree that Reynolds similarity be maintained. Thus, the nozzle contour and especially the diverging section cone angle must be geometrically similar in the model and the prototype.

For a break of flow area, a_{out} , with break flow velocity, u_{out} , the boundary flow scaling requirement is given by

$$(a_{out} u_{out})_R = (a_o u_o)_R = (a_o)_R (u_o)_R = 1/2(K) \quad (5.79)$$

For critical flow, the ratio of velocity at the throat is given by $(u_t)_R = 1$. From boundary flow scaling, $(a_t u_t)_R = 1/2(K)$. Since the model has prototypic pressure, the density ratio $\rho_R = 1$. Thus, the area ratio is

$$(a_t)_R = 1/2(K) \quad (5.80)$$

This shows that the throat area where choking occurs should be scaled differently from loop sections in which $(a_o)_R = 1/1(K)$. This can be accomplished by using a nozzle of throat area ratio $(a_t)_R = 1/2(K)$.

One additional case needs to be considered, and that is the case of a cavitating venturi such as would occur at a bottom drain line break (BDLB). This case is more complex than the ideal gas case just discussed. However, the considerations are very similar and the resulting conditions for similarity are the same. The reason for this is that even though the choking phenomena is due to the onset of vaporization caused by the lowering of the static

pressure to less than the saturation pressure, the pressure behavior is primarily governed by the same inviscid, or in this case Bernoulli, flow phenomena. The pressure recovery/loss mechanism that occurs downstream of an abrupt area change is more complex than the single-phase flow case, but it too is mainly governed by the geometry and is thus is approximately simulated by preserving geometric similarity.

5.4.3 Unchoked Flow Case

For non-critical flow, the size of the connection line is determined by the loss coefficients and the total pressure difference between the ends of the line. The actual requirement can be obtained by the total loss coefficient of the line. Thus,

$$\Delta p_m = K_m \frac{\rho u_m^2}{2} \quad (5.81)$$

and

$$\Delta p_p = K_p \frac{\rho u_p^2}{2} \quad (5.82)$$

From pressure scaling $\Delta p_R = 1$, or the inter-component pressure difference is prototypic. Thus,

$$\frac{K_m}{K_p} = \left[\frac{u_p}{u_m} \right]^2 = \frac{1}{u_R^2} = [2(K)(a_t)_R]^2 \quad (5.83)$$

With a nozzle of throat area, a_t , the total loss coefficient, K , is given by

$$K = K_{out} + K_t \left[\frac{a_{out}}{a_t} \right]^2 \quad (5.84)$$

Therefore,

$$\left[\frac{K_m}{K_p} \right] = \frac{\left[K_{out} + K_t \left(\frac{a_{out}}{a_t} \right)^2 \right]_m}{\left[K_{out} + K_t \left(\frac{a_{out}}{a_t} \right)^2 \right]_p} \quad (5.85)$$

In general, $(K_{out})_p < 1$ and $(K_t)_p \approx 2$. For the model $(K_{out})_m = 10$, the typical diameter ratio is $1/10$, and $(K_t)_m \approx 2$.

This requires that

$$\left[\frac{a_{out}}{a_t} \right]_m^2 \gg \left[\frac{a_{out}}{a_t} \right]_p^2 \quad (5.86)$$

Since $(a_t)_R = 1/2(0)$, the above requirement can be satisfied if $(a_{out})_R = 1/1(0)$. In fact, this is in agreement with the geometrical scaling. In conclusion, for the break flow or for the flow in ADS lines, the pipe size area is scaled as

$$(a_{out})_R = 1/1(0) \quad (5.87)$$

and the nozzle where choking occurs is scaled with throat area ratio $(a_t)_R = 1/2(0)$.

The flow in the GDCS injection lines is essentially single phase liquid. A simple momentum integral equation for these lines is given by

$$\rho \frac{du}{dt} l + \frac{\rho u^2}{2} \left[\frac{l}{d} + K \right] + (p_v - p_c) = \rho g H \quad (5.88)$$

where l , H and d are the line length, driving head and hydraulic diameter, respectively. Eq. (5.88) shows that the liquid hydrostatic head controls the GDCS flow against the liquid inertia, friction and pressure difference between the vessel and containment.

For the fully depressurized case under quasi-steady state condition, the flow is determined by the balance between friction and gravity. Thus, the velocity scale ratio is given by

$$u_R = \left[\frac{H}{f/l/d + K} \right]_R^{1/2} \quad (5.89)$$

Furthermore, the mass inventory scaling requires that

$$\left[\frac{a_g}{a_o} \frac{u}{u_o} \right]_R = 1 \quad (5.90)$$

where a_g is the line flow area. By combining these two requirements, the line size can be obtained:

$$a_{gR} = \frac{a_{oR} l_{oR}^{1/2}}{\left[\frac{H}{f/l/d + K} \right]_R^{1/2}} \quad (5.91)$$

which clearly indicates that the GDCS line flow area scale ratio, a_{gR} , should be increased to compensate for the increased friction number. This increase in the flow area beyond the geometrical scale, a_{oR} , guarantees that the mass flow rate is scaled to preserve the mass inventory. A similar criterion applies to the PCCS draining lines.

Similar scaling calculations can be made for PCCS venting by considering the hydrostatic driving head at the suppression pool (the liquid level difference between the vent exit and the vertical flow channels). If this height, h , is scaled according to the basic geometrical scale, then $H_R = l_{oR}$. Thus, the single phase gas flow scaling requires that

$$a_{vR} = a_{oR} \left[\frac{f/l}{d} + K \right]_R \quad (5.92)$$

This relation shows that the venting line flow area should be increased to compensate for the increased friction for a scaled model.

The drywell/wetwell venting depends on the pressure difference between the suppression pool and containment, as well as the water height above the vents, H . Hence,

$$p_c - p_{sup} \geq H \rho g \quad (5.93)$$

For a reduced height system there are several approaches for setting this pressure difference. However, the best way to scale this Δp is according to the height scale as discussed in Section 5.3.3, thus

$$(p_c - p_{sup})_R = l_{oR} = 1/2 \quad (5.94)$$

because for most components such as the vessel, suppression pool and GDCCS, the pressure distribution is close to the hydrostatic. By scaling the pressure difference using l_{oR} , all the component pressure balances in the containment can be easily preserved. It follows that

$$H_R = l_{oR} \quad (5.95)$$

The size of the opening can be determined by a scaling criterion similar to that of the PCCS venting.

5.4.4 Relative Velocity and Flow Regime

The present scaling method, based on the integral response function, implies that the parameter given by the following expressions are correctly scaled:

$$\Delta \rho x / \rho_f = N_{Zu} - N_{sub} \quad (5.96)$$

and

$$\left[\Delta \rho x / \rho_f \right]_R = 1 \quad (5.97)$$

For the full pressure scaling, this leads to the similarity of vapor quality given by

$$(x)_R = 1 \quad (5.98)$$

The two-phase flow regimes depend on geometry, vapor quality and relative velocity. The effect of the relative velocity is scaled by the drift flux number given by

$$N_d = \frac{V_{gj}}{u_o} \quad (5.99)$$

In the drift flux formulation, the drift velocity is given in the form [5.6],

$$V_{gj} = [C_o - 1]j + \langle\langle V_{gj} \rangle\rangle \quad (5.100)$$

where the total volumetric flux is

$$j = u_o \left[1 + \Delta\rho x / \rho_g \right] \quad (5.101)$$

Hence, the drift flux number becomes

$$N_d = (C_o - 1) \left(1 + \Delta\rho x / \rho_g \right) + \frac{\langle\langle V_{gj} \rangle\rangle}{u_o} \quad (5.102)$$

The right-hand-side terms represent the slip due to void and velocity profile and the local slip between phases, respectively.

Since the distribution parameter, C_o , is a weak function of the density ratio [5.6], the first term is completely scaled. The local drift velocity depends on the two-phase flow regimes and the hydraulic diameter [5.10]. The major effect of the local slip is mostly limited to the chimney section of the RPV. For a relatively large-diameter channel, the local drift velocity [5.10] is approximately given by

$$\langle\langle V_{gj} \rangle\rangle = 0.54 \sqrt{gd} \quad \text{for} \quad d < 30 \sqrt{\frac{\sigma}{g\Delta\rho}} \quad (5.103)$$

and

$$\langle\langle V_{gj} \rangle\rangle = 3 \left[\frac{\sigma g \Delta\rho}{\rho_l^2} \right]^{1/4} \quad \text{for} \quad d > 30 \sqrt{\frac{\sigma}{g\Delta\rho}}$$

The former applies to slug flow and the latter to cap bubbly flow. This shows that for a channel having d smaller than $30\sqrt{(\sigma/g\Delta\rho)}$, the bubbly flow becomes slug flow at a higher gas flux, whereas for a larger channel the bubbly flow becomes cap bubbly flow.

Therefore, for a chimney section of an integral facility it is necessary to have

$$(d)_{\text{chim}} > 30 \sqrt{\frac{\sigma}{g\Delta\rho}} \quad (5.104)$$

in order to simulate the two-phase flow regimes. A hydraulic diameter smaller than above leads to a formation of slug flow accompanied by a cyclic flow behavior which is a characteristic of small channels.

However, the simulation of the two-phase flow regime in the chimney section leads to some distortion of the drift flux number. This is due to the fact that the reference inlet velocity is scaled by $u_{oR} = l_{oR}^{1/2}$, but the local relative velocity itself remains prototypic. This will lead to some distortion in the void fraction also, because it can be expressed as

$$\alpha = \frac{j_g}{C_{0j} + \langle\langle V_{gj} \rangle\rangle} \quad (5.105)$$

where $j_g = u_o(\Delta\rho x/\rho_g)$. However, it can be seen that the effect of $\langle\langle V_{gj} \rangle\rangle$ is small if j is large. Comparison of Eqs. (5.89) and (5.92) indicates that the impact of distortion in $\langle\langle V_{gj} \rangle\rangle / u_o$ is much smaller for the void fraction than for the drift flux number.

5.4.5 Critical Heat Flux Scaling (CHF)

The CHF condition at low flow has been reviewed by Leung [5.11], Katto [5.12], and Mishima and Ishii [5.13] among others. The modified Zuber correlation [5.10] for low flow is given by

$$q_c'' = 0.14(1-\alpha) \rho_g \Delta h_{fg} \left[\frac{\sigma g \Delta \rho}{\rho_g^2} \right]^{1/4} \quad (5.106)$$

Based on the limited data on blowdown experiments, the above correlation is recommended for the mass velocity range of -24 (down flow) to 10 g/cm² s [5.13]. It is evident that this correlation is based on a pool boiling CHF mechanism and has been developed for LOCA studies.

Katto's correlation [5.12] for low flow is given by

$$q_c'' = \frac{1}{4} \Delta h_{fg} G \frac{d_o}{l_o} \left[\left(\frac{\sigma \rho}{G^2 l_o} \right)^{0.043} + \frac{\Delta h_{sub}}{\Delta h_{fg}} \right] \quad (5.107)$$

which implies that the critical quality is $x_c = (\sigma \rho / G^2 l_o)^{0.043}$. Here G and Δh_{sub} are the mass velocity and inlet subcooling. The typical value of x_c is 0.5 to 0.8, so the underlying mechanism should be the annular flow film dryout. This correlation can be applied to most slow transient situations at low flow, except very low flow near flow stagnation.

However, there is a possibility that the CHF may occur at much lower exit quality than given above, due to a change in two-phase flow regimes [5.14]. In a natural circulation system with very small flow fluctuations, the occurrences of CHF have been observed at the transition between the churn-turbulent to annular flows. Beyond this transition, the lack of large disturbance waves eliminated the pre-existing rewetting of dry patches. This leads to the formation of permanent dry patches and CHF. The criteria developed by Mishima and Ishii [5.13] for this case is given by

$$q_c'' = \frac{d_o}{4l_o} \left\{ \left[\frac{1}{C_o} - 1 \right] \Delta h_{fg} \sqrt{\rho_g \Delta \rho g d_o} + G \Delta h_{sub} \right\} \quad (5.108)$$

Here, C_o is the distribution parameter for the drift-flux model, given by

$$C_o = 1.2 - 0.2 \sqrt{\rho_g / \rho} \quad (5.109)$$

These CHF criteria should be used to develop a similarity criterion for the fluid-solid boundary instead of the heat transfer coefficient. This ensures that the CHF occurs under similar conditions in a simulated system. The CHF number is given by

$$N_q = \frac{q_c''}{q_o''} \quad (5.110)$$

For proper scaling of the CHF it is necessary to have

$$(N_q)_R = 1 \quad \text{or} \quad \frac{q_{cR}}{q_R} = 1 \quad (5.111)$$

The substitution of a particular CHF correlation yields the actual value of the CHF number ratio. Thus, by using the scaling parameters obtained from the integral response function approach,

$$(N_q)_R = \frac{1}{q_R} = l_R^{1/2} \quad (\text{Zuber Modified})$$

$$(N_q)_R = \frac{v_R d_R}{q_R l_R} = d_R \quad (\text{Katto})$$

$$(N_q)_R = \left[\frac{d_R^{3/2}}{l_R^{1/2}} - d_R \right] \quad (\text{Mishima})$$

The above expressions show that it is difficult to satisfy the CHF number scaling criteria for a model which does not have a prototypic bundle geometry (i.e., $l_R = 1$ and $d_R = 1$).

However, for most of the transients and accidents of importance in SBWR safety, the reactor power is scrammed and it stays at the decay heat level. The focus of the present integral tests is on the latter part of the RPV depressurization and subsequent natural circulation stages for various emergency cooling systems. At this level, the dryout in the prototype is mainly caused by the uncovering of the core due to the drop of the mixture level to the top of the core. This type of CHF may be approximately predicted by the modified Zuber correlation. The CHF number for this correlation indicates the dependence on the length ratio, l_R . However, in reality it is dominated by the change in the liquid concentration ($1-\alpha$) between the liquid-continuous to vapor-continuous regimes (see Eq. (5.100)). Hence, this type of CHF can be correctly scaled if the void fraction is properly scaled. The Katto and Mishima correlations show that by using a larger hydraulic diameter in the core section, the premature CHF by other mechanisms can be avoided in a model.

5.4.6 Flashing in the Chimney

The above scaling criteria for a two-phase natural circulation loop were obtained by considering the phase change (or boiling) due to the heat addition in the heater section. This effect is represented by the standard phase change number (or Zuber number) given by Eq. (5.29). However, in the SBWR geometry, significant flashing or vaporization due to depressurization of two-phase mixture in the chimney section is possible because of the

decreasing hydrostatic head along the axial elevation. Hence, it is necessary to introduce the second phase change number based on the depressurization superheat.

By denoting the pressures at the bottom and top of the chimney section as p_1 and p_2 , the corresponding saturation temperatures are given by $T_1 = T_{\text{sat}}(p_1)$ and $T_2 = T_{\text{sat}}(p_2)$, where $T = T_{\text{sat}}(p)$ is the saturation relation. The flashing phase change number is given by

$$N_{\text{flash}} = \frac{c_{\text{pl}} (T_1 - T_2)}{\Delta h_{\text{fg}}} \frac{\Delta p}{\rho_g} (1 - \alpha) \quad (5.112)$$

This number represents the non-dimensional scale for the magnitude of the vapor volume generation due to flashing. The superheating $(T_1 - T_2)$ is directly related to the hydrostatic pressure decrease $(p_1 - p_2)$ through the Clausius-Clapeyron equation. For a reduced-height scale model, the length of the chimney section is smaller than the prototype system. Hence, the magnitude of the flashing is also smaller in the reduced-height model at full-pressure simulation. It is noted, however, that the impact of the flashing can be completely simulated if an appropriate reduced pressure level is used in the experiments, due to the density ratio factor in the above N_{flash} expression. By using a reduced-pressure, the ratio $\Delta p/\rho_g$ can be made larger in a model than in a prototype to compensate for the reduction in $(T_1 - T_2)$ or $(p_1 - p_2)$.

The above option is considered as a part of the test matrix. The preliminary calculations show that about a fifty percent reduction in the absolute pressure causes the flashing phase change number to be matched.

5.4.7 Condensation in Suppression Pool

The scaling of the condensation phenomena in the suppression pool can be divided into two sections: one related to the injection from the SRV spargers and the other related to the injection from the vertical vent pipes. The essential parameters important for the condensation phenomena scaling are the condensation power and the vapor latent heat energy flux given by

$$\dot{Q}_c = a_i h_{\text{cond}} (T_{\text{sat}} - T_{\text{pool}}) \quad (5.113)$$

and

$$E_g = \rho_g Q_g \Delta h_{fg} \quad (5.114)$$

where a_i , h_{cond} and Q_g are the total interfacial area, condensation heat transfer coefficient and total vapor volumetric flow rate, respectively.

For most cases, h_{cond} , $(T_{\text{sat}} - T_{\text{pool}})$ and Δh_{fg} can be considered approximately prototypic. Hence, for the proper scaling of the condensation phenomena, it is required that

$$\left[\frac{\dot{Q}_c}{E_g} \right]_R = \frac{a_{iR}}{Q_{gR}} = 1 \quad (5.115)$$

where $Q_{gR} = (a_{in} u_{in})_R$. The product of the area and velocity ratios is determined by the integral scaling method discussed in the previous sections. Thus,

$$Q_{gR} = (a_{in} u_{in})_R = a_{oR} \sqrt{l_{oR}} \quad (5.116)$$

This requires that

$$a_{iR} = a_{oR} \sqrt{l_{oR}} \quad (5.117)$$

For the sparger in the suppression pool, the total bubble interfacial area can be scaled by

$$a_i = \pi n N D_b^2 \quad (5.118)$$

where n , N and D_b are the total number of sparger holes, the number of bubbles which can exist in the vertical line above each hole and the bubble diameter. By using the frequency of the bubble generation at a hole, f ,

$$N = \frac{l_T f}{u_b} \quad (5.119)$$

where l_T is the pool depth and u_b is the bubble rise velocity. The frequency is given by

$$f = \frac{Q_g}{n V_b} = \frac{6Q_g}{\pi n D_b^3} \quad (5.120)$$

Here V_b is the volume of a bubble and Q_g/n is the volumetric flow rate at each hole. Substituting Eqs. (5.113) and (5.114) into Eq. (5.118) yields,

$$a_1 = \frac{6 l_T Q_g}{u_b D_b} \quad (5.121)$$

Thus,

$$\frac{\dot{Q}_{cR}}{E_{gR}} = \frac{l_{TR}}{(u_b)_k (D_b)_k} \quad (5.122)$$

For the evaluation of condensation phenomena scaling, u_b and D_b should be given. The relation between the D_b and the volumetric flow rate is given by a simple model,

$$D_b = 1.5 \left[\left[\frac{Q_g}{n} \right]^2 \frac{1}{g} \right]^{1/5} \quad (5.123)$$

where a cap bubble rise velocity and the maximum frequency has been used. The rise velocity of a bubble is given by

$$u_b = 0.71 \sqrt{g D_b} \quad (5.124)$$

where D_b is the volume equivalent or drag diameter of a cap bubble. Thus,

$$\frac{\dot{Q}_{cR}}{E_{gR}} = \frac{l_{TR}}{D_{bR}^{1.5}} = 1 \quad (5.125)$$

By substituting the expression for D_{hR} from Eq. (5.123) into Eq. (5.125),

$$n_R = Q_{gR} l_{TR}^{-1.67} \quad (5.126)$$

The above correlation gives the correct number of sparger holes for a model. For the present model, $Q_{gR} = 1/200$ and $l_{TR} = 1/4$. Thus,

$$n_R = \frac{n_m}{n_p} = \frac{1}{20} \quad (5.127)$$

This relatively large number of holes compensates for the reduced height of the suppression pool.

Little information is available in the literature on condensation in pools in the presence of noncondensibles. What information is available, is considered proprietary. Recently, results from an experimental study on condensation in the presence of noncondensibles under chugging conditions have become available [5.15]. Based on a *transient conduction-diffusion model*, a transition criteria for the onset of chugging with the effects of noncondensable gases has been presented as follows:

$$0.06 \left[1 + \frac{k_w}{k_d} \frac{Ja}{2} \frac{\delta_s}{\delta_d} \sqrt{\frac{D_{sa}}{\alpha_w}} x_n \right]^{0.5} Re_f^{0.5} Pr^{0.5} Ja^{-1} \leq 1.0 \quad (5.128)$$

where D_{sa} is the mass diffusion coefficient of steam through air.

Nearly all the parameters in the above criterion are property-dependent and can be considered to be prototypic in the model. Only the steam Reynolds number contains scalable velocity and length parameters. The velocity is based on the steam velocity at the exit of a vent opening, and the length scale is simply the vent opening diameter. Hence, the model-to-prototype ratio of the above criteria is given by

$$\left[Re_f \right]_R^{0.5} = \left[U_s D_j \right]_R^{0.5} = \left[\frac{1}{20} \right]^{0.5}$$

The above result indicates that the transition criteria for the onset of chugging in the

presence of noncondensibles may not be properly scaled.

Liang and Griffith [5.15] have also presented a criteria to determine the critical air content in steam mixture condensation required for the diffusion resistance mode of condensation, which would begin to dominate outside conduction resistance due the heated thermal layer:

$$x_n \geq \frac{k_a^d}{k_w} \frac{2}{Ja} \frac{\delta_a}{\delta_s} \sqrt{\frac{\alpha_f}{D_{sa}}} \quad (5.129)$$

It should be emphasized that the transition criteria given above are the only ones available in the literature, and the validity of transition criteria Eq. (5.129) under various test conditions has yet to be established.

5.4.8 Vent Phenomena in Suppression Pool

In the initial blowdown stage, the total gas flow through the vertical flow channels and horizontal vents into the suppression pool is expected to be very large. Under this condition, the vent flow forms a horizontal jet at the exit of the horizontal vents. The axial extent of this jet depends on the condensation rate, concentration of non-condensable gas and jet instability. For the scaling of the condensation phenomena for this horizontal jet, the first criterion to be satisfied is the one given by Eq. (5.115), which scales the global interfacial area for condensation.

By denoting the width and height of the horizontal vents by W_{in} and l_{in} , respectively, the total exit flow area is given by

$$a_{in} = n_{in}(W_{in}l_{in}) \quad (5.130)$$

From the boundary flow scaling, the gas volumetric flow rate should satisfy

$$Q_{gR} = (a_{in}u_{in})_R = a_{oR} \sqrt{l_{oR}} \quad (5.131)$$

Hence, for PUMA one has $Q_{gR} = 1/2(0)$.

For the prototype system having circular vents of a diameter D_{tp} , the interfacial area is

$$a_{ip} = (n\pi D_j l_j)_p \quad (5.132)$$

For the model system, interfacial area is given by

$$a_{im} = \{2n(W_{in} + l_{in})l_j\}_m \quad (5.133)$$

However, scaling the inlet velocity by $(u_{in})_R = \sqrt{l_{oR}}$,

$$a_{oR} = \frac{(nW_{in}l_{in})_m}{(n\frac{\pi}{4}D_j^2)_p} = \frac{1}{1(K)} \quad (5.134)$$

Thus, it is required that

$$\left[\frac{\dot{Q}_c}{E_g} \right]_R = \frac{a_{iR}}{Q_{gR}} = \frac{2}{\pi} n_R \left[\frac{(W_{in} + l_{in})_m}{D_{op}} \right] \frac{l_{jR}}{Q_{gR}} = 1 \quad (5.138)$$

The height scaling of the vents implies

$$\frac{l_{in}}{D_{op}} = l_{oR} = \frac{1}{4} \quad (5.136)$$

The axial extent of the horizontal jet l_j is scaled by the pool size. Thus,

$$l_{jR} = \sqrt{a_{oR}} = \frac{1}{10} \quad (5.137)$$

Using Eqs. (5.122), (5.130) and (5.131), the condensation scaling criterion reduces to

$$\frac{2(K)}{\pi} n_R \left[\frac{1}{4} + \frac{W_{in m}}{D_{op}} \right] = 1 \quad (5.138)$$

This can be approximated by

$$n_R \leq \frac{\pi}{5} \quad (5.139)$$

This implies that n_R is between 1/2 and 1. Since the prototype number of the vertical flow channels in the prototype is eight, four to eight sets of the horizontal vents are required. With the prototypic n for the model, the relative condensation rate is about twice that of the prototype.

For the intermediate gas flow rates in the vertical channel, it is possible to form a vertical gas jet at the exit of the horizontal vents. There is great uncertainty in estimating the diameter of this gas jet in a pool of water. However, a good scaling reference for this vertical gas jet is the width of the horizontal vents. Using a similar formulation as the one explained above, the relative condensation rate is scaled by

$$\left[\frac{\dot{Q}_c}{E_f} \right]_R = \frac{(u_i)_R}{Q_{fR}} = \frac{n_R l_{TR} D_{JR}}{Q_{fR}} \quad (5.140)$$

where l_T is the depth of water and D_J is the jet diameter. The boundary flow scaling with $(u_{in})_R = 1/2$ implies

$$(u_{in})_R = (nW_{in}l_{in})_R = 1/100 \quad (5.141)$$

Since $(l_{in})_R = l_{oR} = 1/4$, one obtains

$$(nW_{in})_R = 1/25 \quad (5.142)$$

Thus, by using the approximation

$$D_J = W_{in} \quad (5.143)$$

one obtains

$$\left[\frac{\dot{Q}_c}{E_g} \right]_R = \frac{1}{Q_{gR}} l_{TR} (nW_{in})_R = 2 \quad (5.144)$$

This implies that the relative condensation rate for this case is about twice as high in the model as in the prototype. It is noted that the result is independent of the vent width or the number of the vents.

The above results for horizontal and vertical jets show that the condensation rates are somewhat higher in the model than in the prototype system. However, their orders of magnitude are similar. These results apply before the jet disintegrates into smaller bubbles. The disintegration is expected when the condensation rate is insufficiently high or there is a significant amount of non-condensable gas in the gas mixture.

When the vertical or horizontal jet disintegrates, the most probable flow regime in the pool is the maximum size cap bubble regime. In this case, a model similar to the one used for the sparger should be used to evaluate the relative condensation rate.

In the later stages of an accident after the initial blowdown, the gas flow through the vertical channel is considerably reduced. In this case, the formation of multiple bubbles at the exit of the horizontal vents is expected. As explained in the sparger scaling, there are two regimes in terms of the bubble size: the flow-rate dependent bubble size regime and the maximum size cap bubble regime.

Considering very large diameter of the horizontal vents, the prototype system should be in the maximum size cap bubble regime. For the initial scaling estimate, the model vent size is about 2 cm x 17 cm, which is also a large orifice. Thus, the bubble size in the model is the maximum or slightly below it.

Both the jet disintegration case and the bubbling case may be modeled as the maximum size cap bubbly flow. The relative condensation rate scaling is given by Eq. (5.116). Thus,

$$\left[\frac{\dot{Q}_c}{E_g} \right]_R = \frac{l_{TR}}{(u_h)_R (D_{hk})} \quad (5.145)$$

For the maximum size cap bubble regime,

$$(u_b)_R = 1 \quad \text{and} \quad (D_b)_R = 1 \quad (5.146)$$

Then

$$\left[\frac{\dot{Q}_c}{E_g} \right]_R = l_{TR} = \frac{1}{4} \quad (5.147)$$

This shows that in the bubbly flow regime, the relative condensation rate is considerably smaller in the model than in the prototype. However, this is a conservative estimate because the bubble size in the model can be much smaller than the maximum cap bubble size given by

$$D_b = 30 \sqrt{\frac{\sigma}{g\Delta\rho}} \quad (5.148)$$

In the flow-rate dependent bubble size regime, the bubble size is given by Eq. (5.123). This equation indicates that the bubble size decreases with decreasing gas flow rate and increasing number of horizontal vents. In the preliminary design of the horizontal vents, the relative condensation rate is increased in the early stage and decreased in the later stages of accident simulation in the model. In the intermediate region where both the jets and bubbles exit, the scaling should have a compensating effect between these two flow regimes so that the total condensation can be well simulated. Furthermore, if the condensation rate is high enough such that either the bubbles or the entire jet can condense before they reach the top of the water pool, the rate itself has little impact on the overall simulation. For SBWR or PUMA this is expected in the bubbly flow due to the large subcooling and considerable pool depth.

5.4.9 Mixing in Stratified Fluid Volumes

Mixing and stratification are multidimensional effects. Scaling these phenomena requires considerations beyond the one-dimensional integral scaling criteria. The additional criteria were obtained from Peterson and his co-workers [5.16, 5.17]. The model that has been developed [5.16] is a buoyant jet pointed upwards in a square cavity with a stratified fluid. The jet is assumed to be cylindrical, although a conical jet would produce similar results. The objective is to model the amount of mixing that occurs as the jet ascends into the stratified layer at the top. This mixing process then determines the level

of stratification.

In the model for inertia-dominated jets (i.e., the inertia of the jet is much greater than the buoyancy), four time constants are identified:

1) The transport time of the jet,

$$\tau_{jt} = \frac{n_j \frac{\pi}{4} d_j^2 H}{Q_0} \quad (5.149)$$

where n_j is the number of jets, d_j is the diameter of the jets, H is the height of the cavity and Q_0 is the volumetric flow at the inlet.

2) The entrainment time constant, which is the time it takes for the jets to entrain a volume of surrounding fluid equal to their own volume,

$$\tau_{je} = \frac{n_j \frac{\pi}{4} d_j^2 H}{n_j u \pi d_j H} \quad (5.150)$$

where u is the average velocity of the surrounding fluid into the jet. The entrainment volumetric flow into the jet is given by

$$n_j u \pi d_j H = \alpha 4\sqrt{2} \frac{H}{d_j} Q_0 \quad (5.151)$$

where α is Taylor's jet entrainment constant so that

$$\tau_{je} = \frac{n_j \frac{\pi}{4} d_j^3}{4\sqrt{2} \alpha Q_0} \quad (5.152)$$

3) The transport time of the surrounding fluid,

$$\tau_{st} = \frac{V}{Q_0} \quad (5.153)$$

where V is the volume of the cavity.

4) Entrainment time of the surrounding fluid,

$$\tau_{se} = \frac{V}{n_j u \pi d_j H} \quad (5.154)$$

However, this last time constant can be obtained from the previous three:

$$\tau_{se} = \frac{\tau_{st} \tau_{je}}{\tau_{jt}} \quad (5.155)$$

So, in effect, there are only three independent time constants. Two independent non-dimensional groups can be formed out of these three by taking ratios. Peterson, et al. [5.16] chose the following two:

$$\pi_1 = \frac{\tau_{jt}}{\tau_{je}} = 4\sqrt{2} \alpha \frac{H}{d_j} \quad (5.156)$$

and

$$\pi_2 = \frac{\tau_{jt}}{\tau_{st}} = \frac{n_j \frac{\pi}{4} d_j^2 H}{V} \quad (5.157)$$

These non-dimensional groups could have been obtained from the Buckingham- π theorem as well. The second non-dimensional number may be expressed as

$$\pi_2 = n_j \frac{d_j^2}{D^2} \quad (5.158)$$

The ratio $\pi_{s \text{ experiment}}/\pi_{s \text{ prototype}} = 1$ means that

$$n_{jR} d_{jR}^2 = D_R^2 = a_R \quad (5.159)$$

which is already satisfied by area ratio scaling. Dividing the above equation by H^2 results in

$$n_{jR} \left(\frac{d_j}{H} \right)_R^2 = \left(\frac{D}{H} \right)^2 \quad (5.160)$$

But, preservation of π_j imposes

$$\left(\frac{d_j}{H} \right)_R = 1 \quad (5.161)$$

which means that

$$n_{jR} = \frac{1}{(H/D)_R^2} \quad (5.162)$$

To obtain similar mixing in the experiment, it is necessary that the number of jets be reduced by a factor that is inversely proportional to the ratio of the vessel aspect ratios squared. However, this imposes a very restrictive limitation on the number of jets; since the ratio of the aspect ratios is 2.5 this means that the number of jets would be reduced by a factor of 6 in the PUMA facility.

Peterson, et al. [5.16] then developed another model for buoyant plumes where buoyancy is dominant over inertia. The entrainment process is governed according to List's model,

$$n_j u \pi d_j H = \frac{5}{3} k_u \left[g \frac{\Delta \rho}{\rho} Q_0 \right]^{1/3} Z H \quad (5.163)$$

where Z is the vertical position and k_u is an entrainment constant. The jet scaling criterion

becomes

$$\pi_j = \left[\frac{\pi}{4} \right]^{2/3} \frac{5}{3} k_u Ri_j^{1/3} \left[\frac{H}{d_j} \right]^{5/3} \quad (5.164)$$

Not only is it necessary to preserve the aspect ratio of the jets but also each jet's Richardson number Ri_j . However, the Richardson number is already preserved by the integral scaling criteria, so this additional constraint is automatically satisfied.

In the case of the discharge through the suppression pool and PCCS vents that occurs during long-term decay heat removal, the rising plumes are formed by condensed steam and noncondensable bubbles. The buoyancy in the plume is caused primarily by the noncondensable bubbles. The Richardson number for two-phase flow is given by

$$Ri_{2\phi} = \frac{gH\alpha}{u^2} = \frac{\pi^2}{16} g\alpha \frac{d_j^5}{x^2 Q_0^2} \frac{H}{d_j} \quad (5.165)$$

where α is the void fraction in the plume and x is the molar concentration of noncondensibles in the nitrogen-steam mixture coming through the vent. Assuming this is the same for model and prototype,

$$[Ri_{2\phi}]_R = \alpha_R \quad (5.166)$$

It is difficult to predict the value of the void fraction. However, since this is the only difference, $Ri_{2\phi}$ should be similar in both cases. The condition for similarity is given by Eq. (5.155) for single-phase buoyant jets and plumes, assuming Eqs. (5.151) and (5.156) are valid for two-phase bubbly jets and plumes.

5.4.10 Natural Circulation

For natural circulation turbulent single-phase convective heat transfer in the walls of the containment, the correlation by Tokuhiro[5.18-5.19] may be used:

$$\frac{Nu}{(1 + Nu s)^{2.5}} = Ra^{1/3} \quad (5.167)$$

where $Ra = Gr \cdot Pr$ is the Rayleigh number and

$$s = \frac{T_{\text{top}} - T_{\text{bottom}}}{T_w - T_{\infty}} \quad (5.168)$$

is the stratification number. For small values of s ,

$$\text{Nu} = \frac{h H}{k} = \text{Ra}^{1/3} = H \quad (5.169)$$

so that h is not a function of H . However, at a high level of stratification, the heat transfer coefficient increases as the height is reduced.

A more significant effect on the containment heat transfer is the increased surface-to-volume ratio in the reduced-volume system. This ratio is scaled by

$$\left[\frac{S}{V} \right]_R = \frac{1}{D_R} \quad (5.170)$$

which indicates that the reduction in the facility's cross-sectional area has a major impact on the available heat transfer area. As the cross-sectional area decreases, the surface-to-volume ratio increases. Hence, the taller the facility, the more distortion in the heat transfer area. This is one of the important factors to be considered in determining the height and area ratios, l_R and a_R . In general, a tall and thin system has overwhelming heat transfer to the structure, which has been the major shortcoming of most of the integral test facilities built in the U.S. and other countries. For the proposed facility, the height is reduced to 1/4 to accommodate a relatively large cross-sectional area. As pointed out, the proposed facility has the smallest aspect ratio among existing and under-construction of test facilities for the SBWR. This is one of the significant advantages of the proposed design.

For the effect of mixing at the wall boundary layers produced by natural circulation, Peterson, et al., [5.16] recommended the following scaling criterion:

$$\pi_{\text{bl}R} = \frac{P_{\text{bl}R}^1 H_R^{7/10}}{\tau_R \sqrt{V_R}} \quad (5.171)$$

where P_{bl}^1 compares the actual perimeter to the perimeter of a cylindrical vessel with equal

volume and height. This scaling criterion does not account for condensation or other more complicated phenomena.

5.4.11 Heat Source and Sink

It is important to account various heat sources and sinks in the integral facility following a transient, so that energy balance is satisfied. The thermal transients after the initial depressurization are relatively slow processes. Hence, the thermal energy stored is more important than the instantaneous heat transfer to or from the structure.

For the structure, the thermal penetration depth is given by

$$d_{th} = \sqrt{\pi \alpha_s t} \quad (5.172)$$

From this, the characteristic time constant for conduction heat transfer in the wall can be calculated. For the reactor pressure vessel wall, the characteristic time is about 500 s. For the SBWR blowdown process, the time required is about 500-700 s. It is necessary to estimate the energy stored in the vessel wall. This can be done by solving the one-dimensional transient conduction heat transfer equation to get the temperature profile. Integrating the temperature profile over the period of time, the stored energy can be calculated. During and following the blowdown process, the stored energy is released into the vessel liquid. Since the vessel in the present model is designed for 1.03 MPa (150 psig) rather than 7.16 MPa (1040 psi) as in the prototype, the wall thickness is thinner. Hence, an additional heat source which is 1/200, should be provided for the model vessel, to simulate the heat energy released from the prototype vessel wall.

In the containment, the thick concrete wall has a large conduction time constant. However, in this case the containment wall is at a lower temperature, and the discharged steam acts as a energy source to the wall. Since the characteristic time constant of the transient for concrete is much longer than the blowdown period, a lumped parameter model is appropriate for the containment wall, which acts as heat sink following transient.

Hence,

$$a_s \rho_s c_{ps} \frac{dT}{dt} = \eta_{in} q''_{in} - \eta_{out} q''_{out} \quad (5.173)$$

where a_s is the cross-sectional area of the structure. The heat flux, q'' and heated perimeter, η couple this equation to the fluid energy equation. The important scaling parameter for the structural heat transfer is the thermal inertia ratio given by

$$N_{th} = \frac{a_s \rho_s c_{ps}}{a \rho c_p} \quad (5.174)$$

The similarity between the model and prototype is satisfied by $(N_{th})_R = 1$. For very thick materials, the cross-sectional area is given by

$$a_s = \eta_{in} d_{th} \quad (5.175)$$

where d_{th} is the maximum penetration depth calculated from the end of the transient. Thus by substitution Eq. (5.175) into Eq. (5.174) the scaling requirement reduces to

$$(k_s \rho_s c_{ps})_R^{1/2} = \frac{a_R}{\eta_{in} \sqrt{t_R}} = \frac{1}{5\sqrt{2}} \quad (5.176)$$

For concrete, the thermal diffusivity is small. This indicates that for most transients, only the region near the inner wall participates in the energy transfer. For example, about 5 hours are required, for 15 cm (6 inch) thermal penetration. The thermal inertia of this thickness can be simulated by 1.5 cm (0.6 in.) thick equivalent insulation material.

5.4.12 PCCS Venting into Suppression Pool

Here, we consider the mechanism of PCCS venting into the suppression pool. Most of the steam flow rate into the drywell from the RPV is proportional to the decay heat of the core. The steam is condensed by the PCCS condensers at later stages of the blowdown following a LOCA. Since the drywell steam is mixed with air, this steam-air mixture enters the PCCS condensers and condenses, leaving air to accumulate in the lower header of the PCCS condenser. After sufficient accumulation of air in the PCCS condenser, the condensation becomes ineffective. This leads to an increase in the drywell pressure. There is a water head pressure difference between drywell and the suppression pool. When the drywell pressure exceeds this head, the gas from the PCCS is vented into the suppression pool. This venting process decreases the non-condensable concentration in the PCCS condenser, and the PCCS condenser begins condensing steam again, which will decrease or stabilize the drywell pressure.

The schematic of the PCCS venting process is shown in Figure 5.5. At time $t=t_0$, the PCCS has just vented gas into the suppression pool. After $t=t_0$, condensation in the PCCS is very efficient and the drywell pressure decreases and will reach a point where steam flow rate from the RPV is equal to the condensation rate. As the condensation proceeds,

the non-condensable gas accumulates in the PCCS enclosure. This will decrease PCCS efficiency. At $t=t_1$, the condenser is filled with non-condensable gas. Then, the pressure in the drywell rises due to steam flow from the RPV. At $t=t_2$, the pressure in the drywell is such that $P_{DW} - P_{sp} \geq P_{Head}$, and the PCCS vents into the suppression pool. After this, the cycle continues. For each cycle, the minimum pressure difference ΔP_{min} decreases as the SP pressure increases due to the non-condensable gas vented into it. Eventually, suppression pool pressure exceeds the drywell pressure after a number of vent cycles. When the suppression pool pressure is higher than that of the drywell by 3.45 kPa (0.5 psi), gas passes through the vacuum breakers. When the vacuum breakers are opened, the drywell and suppression pool pressure equalize. The time period required for each venting is $\Delta t_1 + \Delta t_2$. The time period Δt_1 is almost constant and independent of P_{DW} . However, Δt_2 is dependent on ΔP_{min} . If the $\Delta P_{min} = 0$, that is $P_{DW} = P_{sp}$, then Δt_2 becomes longest. For the scaling of the venting phenomena, the time periods Δt_1 and Δt_2 need to be evaluated.

First, we derive the time period Δt_1 . At the end of this period the PCCS condenser is filled with non-condensibles and condensation is totally stopped. If V_{pc} is the volume of the condenser tubes, then V_{pc} is the maximum volume of air required to fill the condenser tubes so that condensation is totally stopped. In the PCCS condenser, the flow near the tube inlet is like forced convection and near the tube end the flow is stagnant. The air accumulates at the bottom of the condenser tube. For simplicity and conservatism, it is assumed that the air begins to accumulate from the bottom of the condenser tube, and the condensation stops when the air has occupied the whole tube length. For each fraction of the air filled, the condensation area is decreased by that amount.

For the first filling of the condenser with steam containing c_0 fraction of air, the volume occupied by the air is $V_{pc}c_0$. This leaves $V_{pc}(1-c_0)$ of volume for the next filling. After the second filling the remaining volume in the PCCS condenser is $V_{pc}(1-c_0)^2$. Similarly, after the third filling, the volume left is $V_{pc}(1-c_0)^3$. Thus, after n fillings, the volume left is $V_{pc}(1-c_0)^n$.

Thus, the accumulated air after n fillings is given by

$$V_{pc}[1-(1-c_0)^n] \quad (5.177)$$

Let t_{c1} be the time for single filling of the condenser, then for n fillings the required time is approximately given by

$$t_{cn} = t_{c1}(1-c_0)^{n-1} \quad (5.178)$$

Thus the total time required to fill the condenser by non-condensibles is

$$\Delta t = \sum_{n=1}^{\infty} t_{cn} = t_{c1} \sum_{n=1}^{\infty} (1-c_0)^{n-1} = \frac{t_{c1}}{c_0} \quad (1.179)$$

The characteristic time for a single filling of PCCS condenser volume by steam/air mixture is given by

$$t_{c1} = t = \frac{v_{pc} \rho}{\dot{m}} \quad (5.180)$$

Here, ρ is the density of the vapor mixture entering the PCCS condenser. The rate of steam produced in the drywell, \dot{m} , is given by

$$\dot{m} = \frac{q}{\Delta h_{fg}} \quad (5.181)$$

Where q is the decay heat rate of the RPV core. From Eqs. (5.180) and (5.181) the time constant for the prototype is $t_p = 0.3168$ s, and for the model $t_m = 0.158$ s. Thus, the time constant for the model is half that of the prototype. This is consistent with the scaling of time for the model chosen.

In Figure 5.6, the time period Δt required to fill the PCCS condenser with non-condensibles as the function of non-condensibles concentration is shown. For 10% of air concentration in steam, the time period Δt , for the prototype is $t_p \times 10 = 3.16$ s. For 1% of air concentration, this time period is 31.6 s. For the PUMA, $\Delta t_{lm} = 1.58$ s for $c_0 = 0.1$ and at $c_0 = 0.01$ (1%), $\Delta t_{lm} = 15.8$ s.

After the condensation has totally stopped, the pressure in the drywell increases due to the addition of steam. Now we evaluate Δt_2 , the time period at which the drywell pressure exceeds the suppression pool pressure by an amount greater than the water head, P_{Head} , that exists between SP and drywell. If SP and DW are at the same pressure, then from the ideal gas law we have

$$P_{Head} = \frac{T}{V_{DW}} R_2 \left[\frac{q}{\Delta h_{fg}} \right] \Delta t_2 \quad (5.182)$$

Thus,

$$\Delta t_2 = \frac{P_{\text{Head}} V_{\text{DW}}}{T R_2 (q/\Delta h_{fg})} \quad (5.183)$$

where T is the absolute temperature of steam, R_2 is the gas constant for steam and V_{DW} is the drywell volume.

Now we take the prototype-to-model time period ratio:

$$(\Delta t_2)_R = \left[\frac{P_{\text{Head}} V_{\text{DW}}}{T R_2 (q/h_{fg})} \right]_R \quad (5.184)$$

When the fluids used and the pressure condition are same for the prototype and model, then $(TR_2)_R = 1$. For 1/4 height, 1/4(0) volume and 1/2(0) mean flow rate scaled model, one obtains

$$(\Delta t_2)_R = \frac{1}{8} \quad (5.185)$$

This indicates that the time period for the model is shorter than for the prototype. Typical time period for the prototype at 206 kPa (30 psi) drywell pressure can be calculated from Eq. (5.183). At a decay power level of 40 MW, it can be shown that $\Delta t_{2p} = 12.63$ s. The corresponding time period for the model is $\Delta t_{2m} = 1.6$ s.

The above time period was estimated assuming both the DW and SP were initially at the same pressure level. However, as shown in Figure 5.5, the pressure difference between the DW and SP could be anywhere from Δp_{Head} to 0. The Δt_{2p} given in Eq. (5.176) gives the maximum time required for the vent to open when the PCCS condenser stops condensation due to accumulated non-condensibles.

It can be assumed that the time period required to vent the non-condensable gas from the PCCS is negligible. Hence, for each venting cycle, the time period is $\Delta t_1 + \Delta t_2$. The time period (Δt_1) is higher (~ 30 s) for PCCS performance when the air concentration in the drywell is reduced. For most cases, Δt_2 is smaller than 12.63 s for the reason mentioned above. Hence, the vent cycle period is largely determined by the (Δt_1) time period, which is well-scaled in the model. However, during the initial phase of the decay heat cooling, when the air concentration in the drywell is higher, the time period ($\Delta t_1 + \Delta t_2$) for

the model will be shorter than in the prototype, so frequent venting is expected in the model. However, as the drywell air concentration is reduced, the time period required for PCCS venting in the model will be close to the correct by scaled time period of the prototype. It is expected that for the long time transients, the model PCCS venting will perform as required applying the current scaling methodology.

5.4.13 Condensation in PCCS Condensers

The PCCS condensers provide decay heat removal by condensing steam from the drywell and supplying condensate water to the RPV through the GDSC tanks. The scaling of the heat transfer rate through the condenser is given by

$$\dot{Q}_{\text{PCCS}} = N_{\text{tubes}} N_{\text{units}} U_h A_i (T_g - T_p) \quad (5.186)$$

where N_{tubes} is the number of PCCS condenser tubes, N_{units} is the number of PCCS units, U_h is the overall heat transfer coefficient, A_i is the inner surface area of a condenser tube, and T_g and T_p are the steam and PCCS pool temperatures. The overall heat transfer coefficient is given by

$$U_h = \left[\frac{1}{h_c A_i} + \frac{\ln(D_o/D_i)}{2\pi k_w L} + \frac{1}{h_p A_o} \right]^{-1} \quad (5.187)$$

In the RHS of Eq. (5.187), the first term corresponds to the tube side condensation heat transfer coefficient, the second term corresponds to the tube wall conduction heat transfer coefficient, and the third term corresponds to the outside tube pool heat transfer coefficient.

The condensation heat transfer coefficient is for the condensation of steam and air or nitrogen mixture in a vertical tube. Siddique, et al. [5.20] have studied the condensation heat transfer coefficient for steam-air mixture in the tube. The condensation heat transfer Nusselt number given by them is

$$Nu_c = \frac{h_c D_i}{k_g} = 6.213 Re^{0.223} \left[\frac{W_{a,w} - W_{a,h}}{W_{a,h}} \right]^{1.44} Ja^{-1.253} \quad (5.188)$$

where

$$Ja = \frac{c_p (T_b - T_w)}{\Delta h_{fg}} \quad (\text{Jacob number}) \quad (5.189)$$

$$Re = \frac{\rho_m v_m D_i}{\mu_m} \quad (\text{Reynolds number}) \quad (5.190)$$

$$W_a = \frac{\dot{m}_a}{\dot{m}_a + \dot{m}_v} \quad \left[\begin{array}{l} \text{Non-condensable} \\ \text{mass fraction} \end{array} \right] \quad (5.191)$$

The pool side heat transfer coefficient, h_p , depends on whether pool side transfer is due to boiling or natural convection. For natural convection, the heat transfer Nusselt number is given by

$$Nu_p = \frac{h_p L_{\text{tube}}}{k_p} = 0.021(GrPr)^{0.4} \quad (5.192)$$

where

$$Gr = \frac{g\beta (T_w - T_p)L_{\text{tube}}^3}{\nu^2} \quad (\text{Grashof number}) \quad (5.193)$$

$$Pr = \frac{\nu}{\alpha} \quad (\text{Prandtl number}) \quad (5.194)$$

For the correct scaling of heat removal by the PCCS condensers we should have

$$\frac{\left[\dot{Q}_{\text{PCCS}} / \dot{m} \Delta h_{fg} \right]_m}{\left[\dot{Q}_{\text{PCCS}} / \dot{m} \Delta h_{fg} \right]_p} = 1 \quad (5.195)$$

where \dot{m} is the inlet steam mass flow rate to the PCCS condenser. From Eqs. (5.186) and (5.191), the scaling requirement for PCCS condenser heat removal rate is given as

$$\left[N_{\text{tubes}} N_{\text{units}} U_h A_i (T_h - T_p) / \dot{m} \Delta h_{fg} \right]_R = 1 \quad (5.196)$$

If the prototype and model have the same operating pressure condition and use the same operating fluid (water), then the temperature difference can be preserved. From Eqs. (5.195) and (5.196) we have

$$\frac{\left[\dot{Q}_{\text{PCCS}} / \dot{m} \Delta h_{fg} \right]_m}{\left[\dot{Q}_{\text{PCCS}} / \dot{m} \Delta h_{fg} \right]_p} = \left[\frac{N_m}{N_p} \right]_{\text{tubes}} \left[\frac{N_m}{N_p} \right]_{\text{units}} \left[\frac{U_m}{U_p} \right]_h \left[\frac{A_m}{A_p} \right]_i \left\{ \frac{(T_h - T_p)_m}{(T_h - T_p)_p} \right\} \left[\frac{\dot{m}_p}{\dot{m}_m} \right] \left[\frac{\Delta h_{fgp}}{\Delta h_{fgm}} \right] \quad (5.197)$$

First, we evaluate $\left[\frac{U_m}{U_p} \right]_h$ or $(U_h)_R$.

From Siddique, et al. [5.20], the average Reynolds number for the prototype PCCS condenser tube is approximately given by $\bar{Re}_p = (13000 + 10000)/2 = 7000$. This is for a prototype condenser tube length of 18 m. For the model, with the present choice of 1/4 length scale and 1/400 volume scale, the condenser tube length is 0.45 m. If the model tube diameter is the same as that of the prototype, then the results of the Siddique, et al. [5.20] can be directly applied. For the model, the average Reynolds number is $\bar{Re}_m = (13000 + 8000)/2 = 10500$. The corresponding condensation heat transfer coefficients for the prototype and model are $\bar{h}_{cm} = 4000 \text{ W/m}^2 \text{ } ^\circ\text{K}$ and $\bar{h}_{cp} = 2500 \text{ W/m}^2 \text{ } ^\circ\text{K}$. The pool side heat transfer coefficient is available from SSAR [5.21] as $h_p = 4500 \text{ W/m}^2 \text{ } ^\circ\text{K}$. For the prototype tube material, stainless steel with OD = 50.8 mm and ID = 47.5 mm, the ratio $(U_h)_R$ is calculated from Eq. (5.187) as

$$(U_h)_R = 1.442 \quad (5.198)$$

In the present scaling, we have heat transfer area scaling of 1/200 and boundary mass flow rate scaling of 1/200. Hence,

$$\left(\frac{N_m}{N_p}\right)_{\text{tube}} \left(\frac{N_m}{N_p}\right)_{\text{units}} \left(\frac{A_m}{A_p}\right)_i = \frac{1}{2(\lambda)} \quad (5.199)$$

and

$$\left(\frac{\dot{m}_p}{\dot{m}_m}\right) = \frac{1}{2(\lambda)} \quad (5.200)$$

Since temperature differences are preserved in the model we have from Eq. (5.197) through (5.200),

$$\frac{\left[Q_{\text{pccs}}/\dot{m}\Delta h_{fg}\right]_m}{\left[Q_{\text{pccs}}/\dot{m}\Delta h_{fg}\right]_p} = 1.442 \quad (5.201)$$

This indicates that the present model condenser removes about 44% more heat than the correct scaled model. Apparently, this is a distortion of the heat removal rate of the PCCS condensers. It is proposed that certain portions of the PCCS condenser tube's outer surface be covered with insulating material like Teflon™ sheet, so that smaller areas of the PCCS condenser tube is exposed to the pool side. This will effectively reduce the heat transfer rate of the condenser. The insulator will be snugly wrapped around the condenser tube to cover 30% of the tube's outer surface. The reduction in the condensibles total surface will result in satisfying the correct scaling criteria for the PCCS condensers given by Eq. (5.195).

5.4.14 Stratification in the Drywell

The stratification in the drywell will affect the operation of the PCCS. If the steam stratifies above the nitrogen, the amount of non-condensable gas entering the PCCS will be reduced. During the blowdown stage, the drywell is at a higher pressure than the suppression pool, and the steam coming out of the reactor vessel will mix with the steam and nitrogen in the drywell and vent into the suppression pool chamber. A simple calculation shows that at the end of blowdown, the amount of nitrogen left in the drywell is almost negligibly small.

The steam jets coming out of the drywell during blowdown carry a lot of momentum. Therefore, mixing is expected to be good. The Richardson number for these jets is approximately 1×10^{-4} . The amount of steam produced during the vessel depressurization is given by

$$\frac{M_{\text{steam}}}{M_{\text{initial}}} = \frac{u_{f \text{ initial}} - u_{f \text{ final}} + Q/M_{\text{initial}}}{\bar{h}_g - u_{f \text{ final}}} \quad (5.202)$$

where \bar{h}_g is the mean enthalpy of the steam coming out of the vessel, M_{initial} is the initial mass of coolant in the vessel, u_f is the internal energy of the coolant and Q is the amount of decay heat during depressurization. The steam mass produced is approximately 100 tons, which corresponds to a volume of $60,000 \text{ m}^3$ at 3 atm. This is twelve times the volume of the drywell. Assuming perfect mixing, the concentration of steam at the end of blowdown is

$$X_{\text{steam}} = 1 - e^{-12} = 0.999994 \quad (5.196)$$

so the amount of non-condensibles left in the drywell accounts only for 0.005% of the mixture mass. After blowdown, the vacuum breakers discharge the nitrogen from the suppression pool back into the drywell. In this case, the Richardson number is 0.002, so again, these jets are inertia-dominated and will reach the top of the drywell and deflect along the containment walls, resulting in good mixing.

The steam coming out of the reactor vessel during decay heat removal carries relatively little momentum. The Richardson number for these plumes is 0.2. The possibility of stratification in this case is greater.

Because the Richardson number is part of the integral scaling criteria, these phenomena should be similar in the SBWR and in PUMA. However, because the number of jets in PUMA is greater than Eq. (5.162) specifies, the amount of mixing will be greater. This implies that in case of the steam plumes during decay heat removal, the amount of stratification will be reduced.

5.4.15 Stratification in the Suppression Pool

The stratification of the pressure suppression pool affects the pressure in the containment system. The pressure in the pressure suppression pool chamber is the sum of the pressure of the non-condensable gases and the saturation pressure of the steam at the temperature of the pressure suppression pool surface.

During vessel blowdown, the jets coming out of the drywell vents and the SRV spargers are well mixed. The question that remains is the effect of the PCCS vents discharge during non-condensable venting on the pool stratification.

The PCCS vents are very shallow, 200 mm in the PUMA design and 800 mm in the SBWR. While a full fluid dynamic evaluation of stratification may be very complicated in this case, a simple argument shows that PCCS venting effect is negligible. Assuming that the period of non-condensable discharge from the PCCS is 15 seconds and that each discharge corresponds to the whole volume of the PCCS, it may be shown that this is equivalent to a heat source of 1100 Watts in PUMA. With this heat input, a layer of 200 mm thick on top of the suppression pool would heat up at a rate of approximately 1°C per hour. The reason for this layer will heat up uniformly is that, the bubbles will entrain water from the vicinity of the discharge so there is an induced liquid flow that is of the same order as the bubble volumetric flow. Therefore, the liquid layer above the discharge is constantly getting mixed. The worst case to assume is that there is no mixing with the rest of the pool and to neglect evaporation at the surface, conduction to the walls and conduction to the rest of the pool. Then the liquid layer above the discharge heats up adiabatically at the rate previously mentioned.

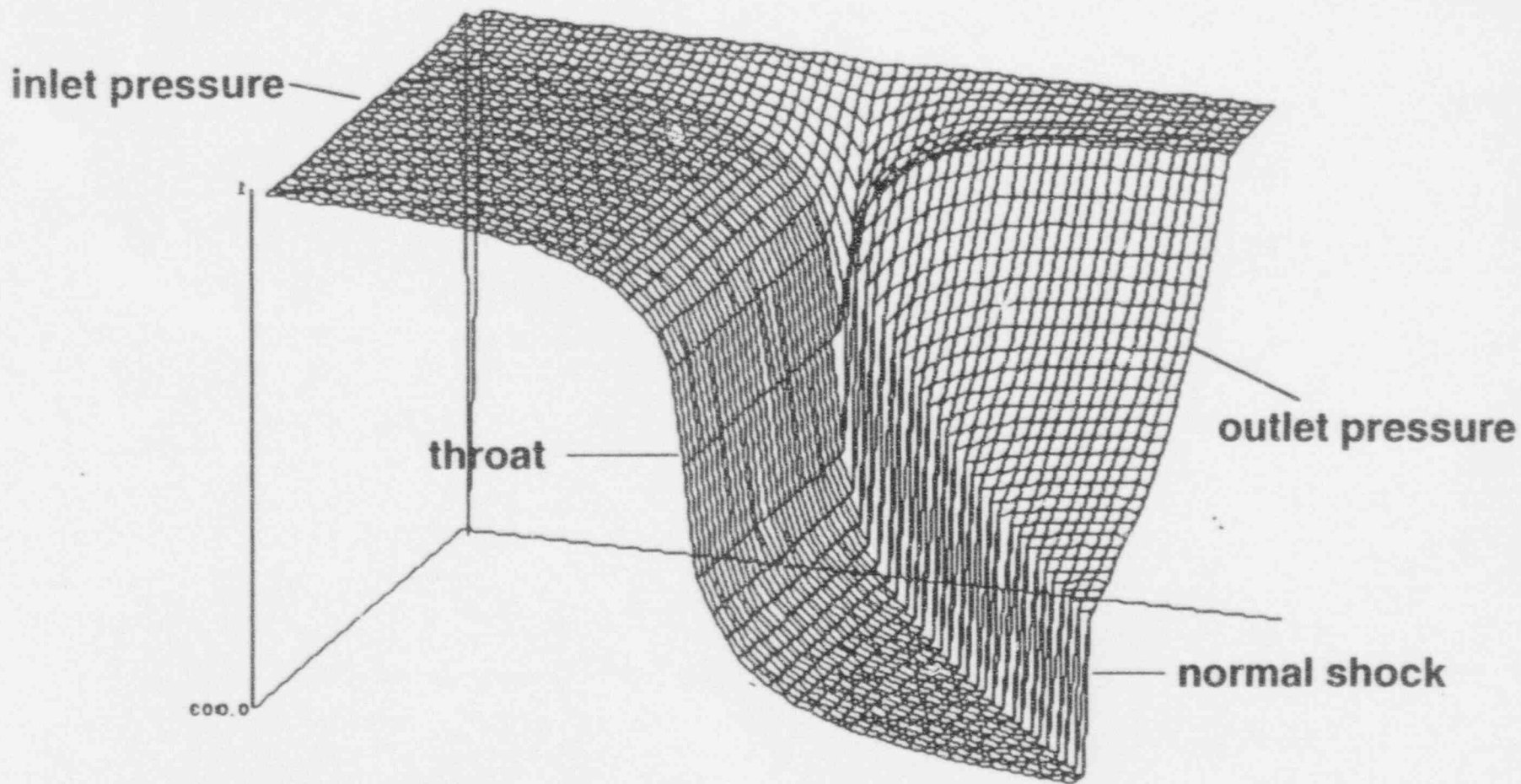


Figure 5.1 The Static to Upstream Stagnation Pressure Ratio as a Function of Position and the Exit Static Pressure Ratio for a Converging-Diverging Nozzle

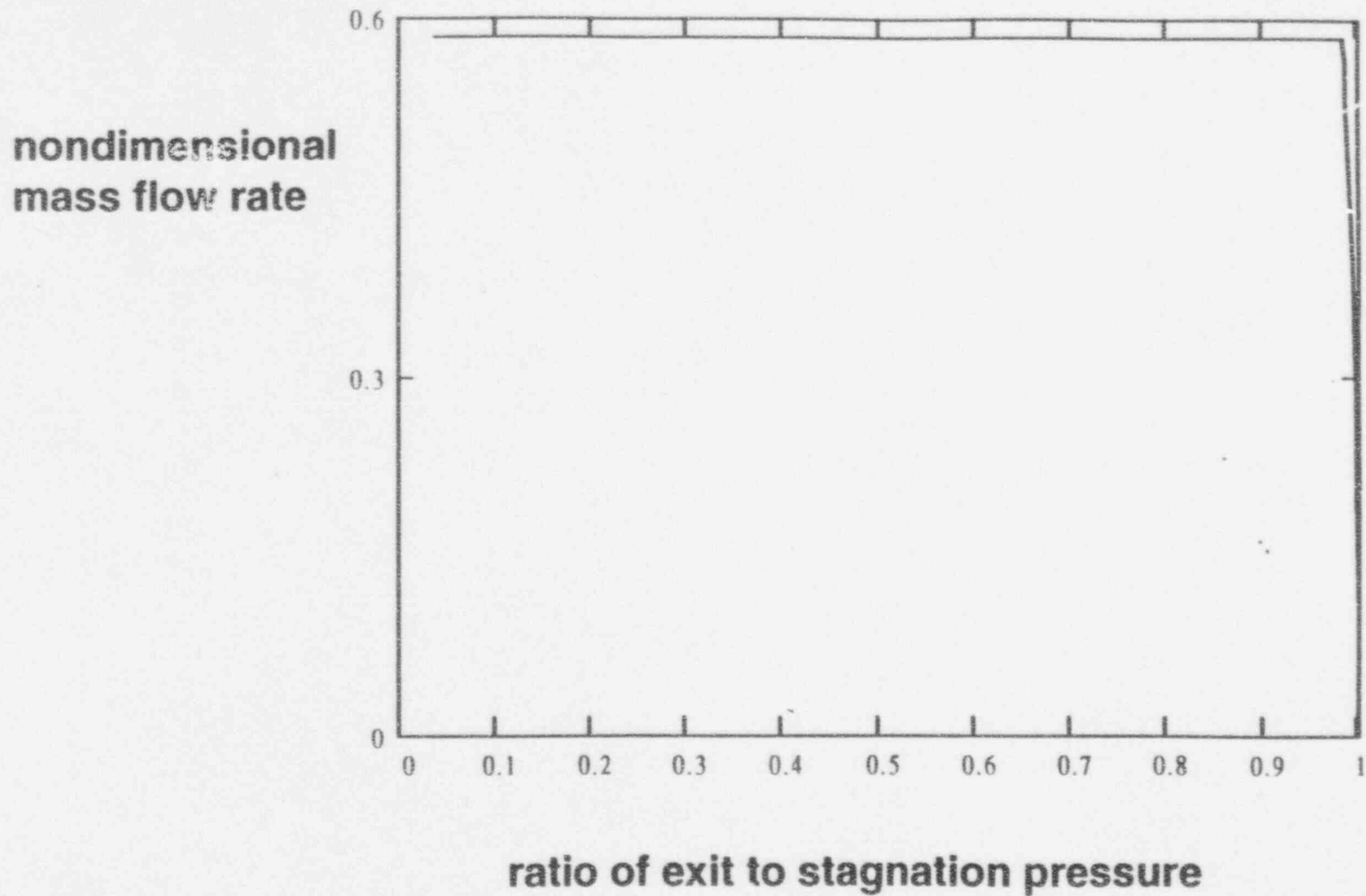


Figure 5.2 The Nondiemenstional Massflow Through the Converging-Diverging Nozzle as a Function of Nozzle Pressure Ratio

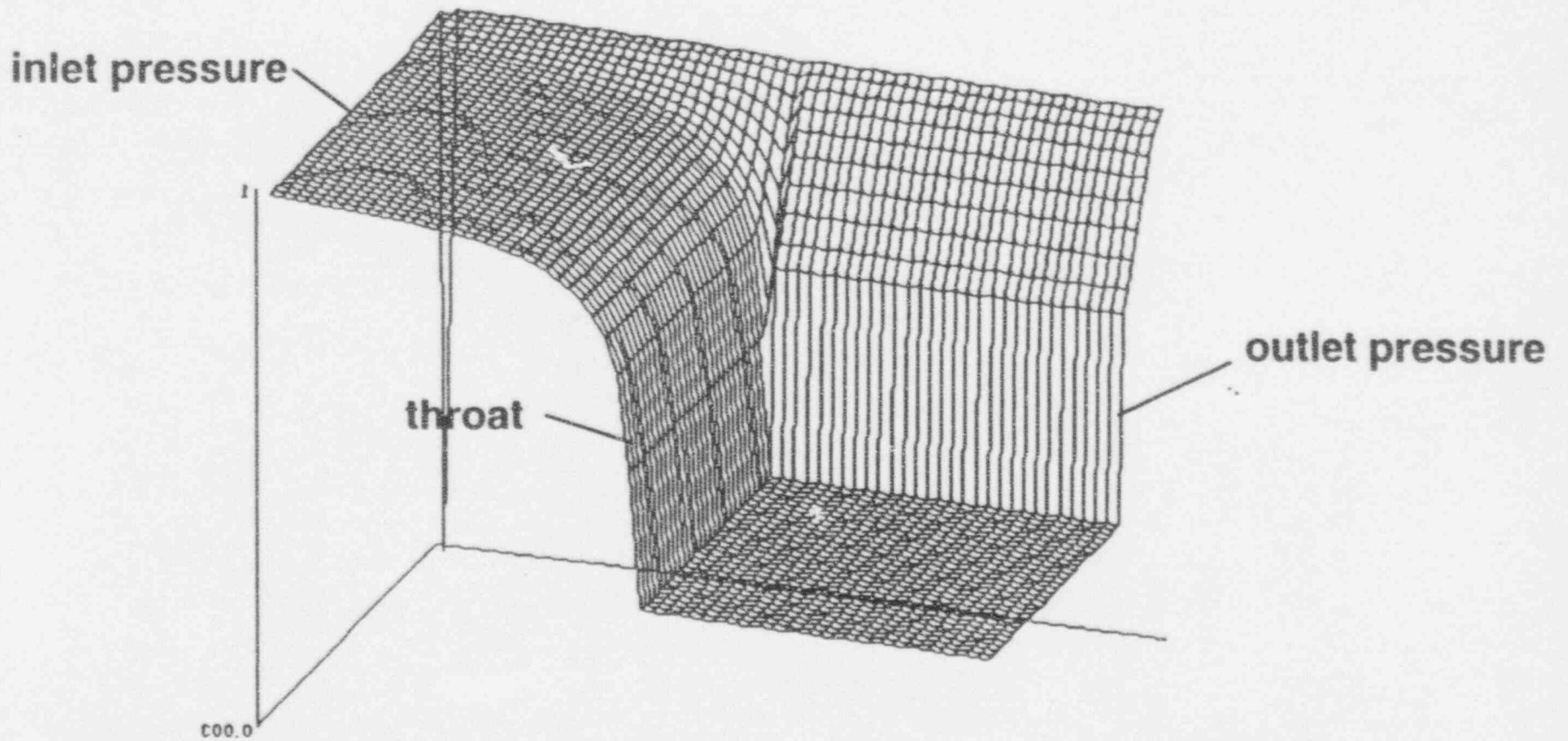
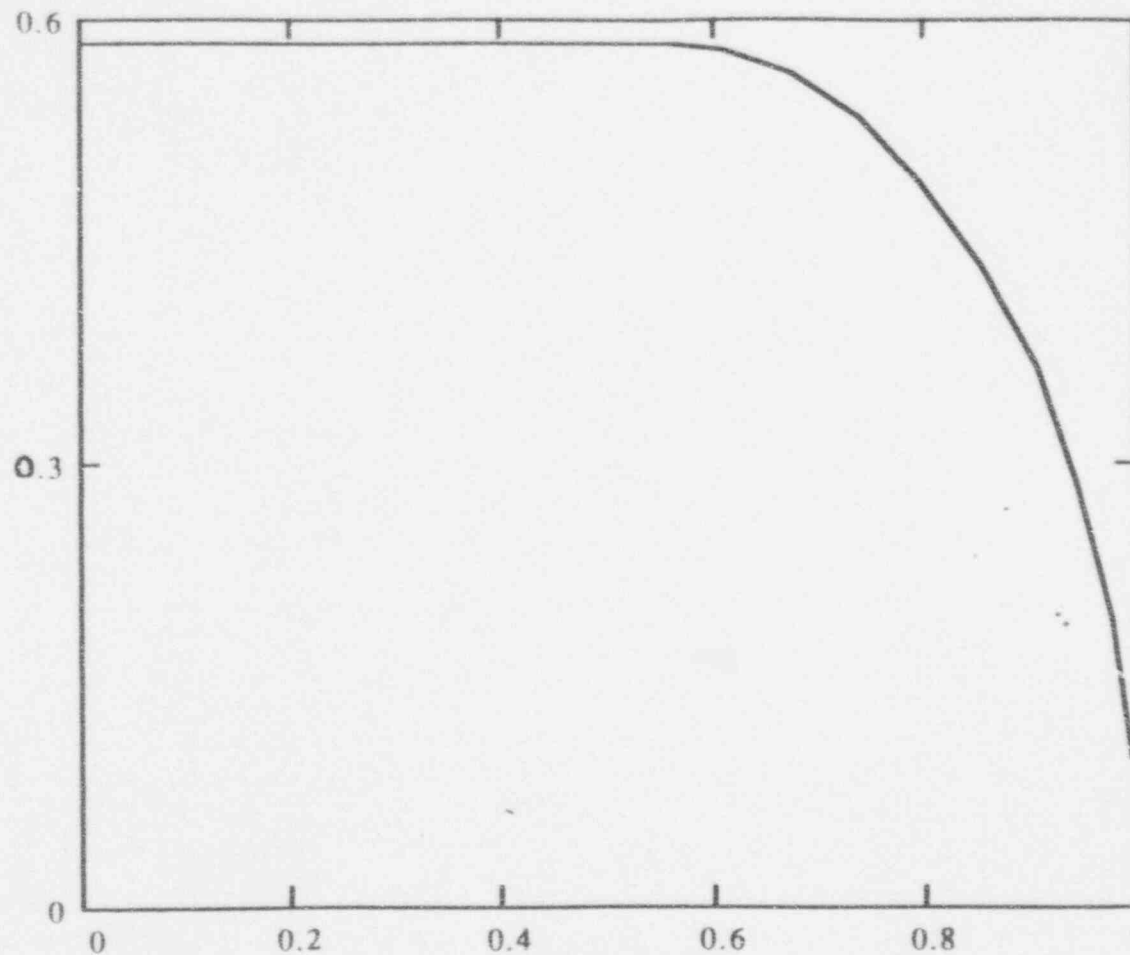


Figure 5.3 The Static to Upstream Stagnation Pressure Ratio as a Function of Position and the Exit Static Pressure Ratio for an Abrupt Expansion Nozzle

nondimensional
mass flow rate



ratio of exit to stagnation pressure

Figure 5.4 The Nondimensional Massflow Through the Abrupt Expansion Nozzle as a Function of Nozzle Pressure Ratio

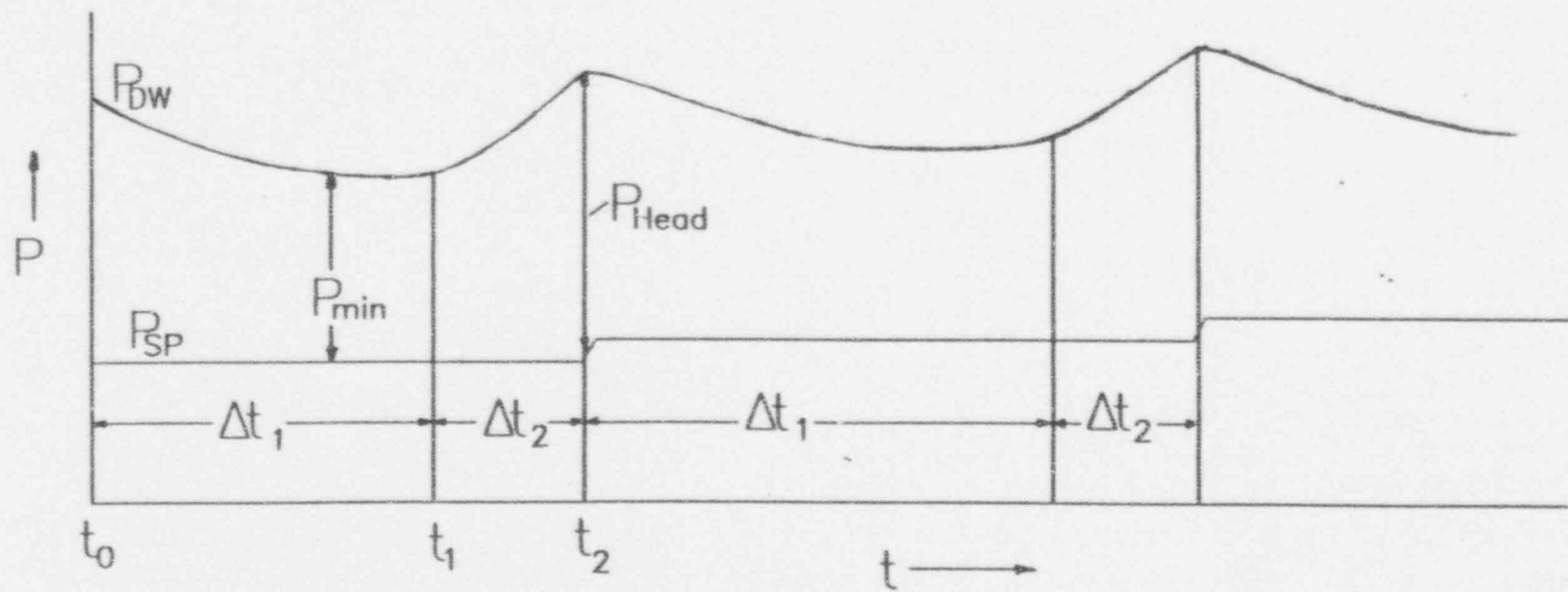


Figure 5.5 Drywell and suppression pool pressure transient schematic

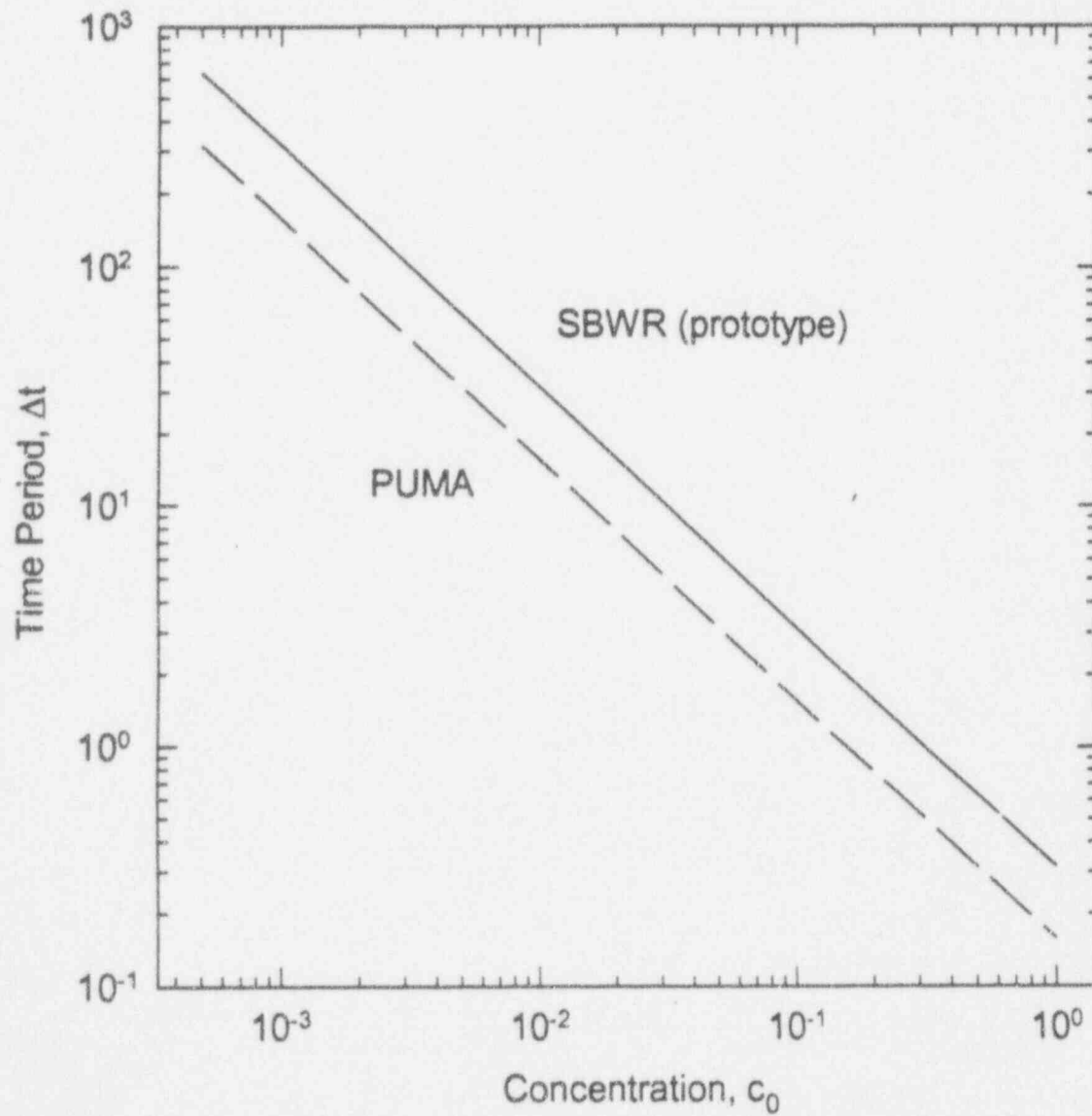


Figure 5.6 Time period Δt to fill PCCS volume as a function of air concentration

References

- 5.1 Ishii, M., Kataoka, I., "Similarity Analysis and Scaling Criteria for LWRs under Single Phase and Two-Phase Natural Circulation", NUREG/CR-3267, ANL-83-32 (1983).
- 5.2 Kocamustafaogullari, G., Ishii, M., "Scaling Criteria for Two-Phase Flow Natural and Forced Convection Loop and their Application to Conceptual 2x4 Simulation Loop Design", ANL-83-61, NUREG/CR-3420 (1983).
- 5.3 Kocamustafaogullari, G., Ishii, M., "Reduced Pressure and Fluid to Fluid Scaling Laws for Two-Phase Flow Loop", NUREG/CR-4584, ANL-86-19 (1986).
- 5.4 Condie, K.G., Larson, T.K., Davis, C.B., McCreery, G.E., "Evaluation of Integral Continuing Experimental Capability (CEC) Concepts for Light Water Reactor Research-PWR Scaling Concepts", NUREG/CR-4824, EG&G 2494 (1987).
- 5.5 Boucher, T.J., DiMarzo, M., Shotton, L.M., "Scaling Issues for a Thermal-Hydraulic Integral Test Facility", NPC Paper.
- 5.6 Ishii, M., "One-Dimensional Drift-Flux Model and Constitutive Equations for Relative Motion Between Phases in Various Flow Regimes", Argonne National Laboratory Report, ANL-77-47 (1977).
- 5.7 Ishii, M. and Zuber, N., "Thermally Induced Flow Instabilities in Two-Phase Mixtures," 4th International Heat Transfer Conference, Paris, Paper No. B5.11 (1970).
- 5.8 Ishii, M., "Study on Flow Instabilities in Two-Phase Mixtures," Argonne National Laboratory Report, ANL-76-23 (1976).
- 5.9 Ishii, M., "Thermally Induced Flow Instabilities in Two-Phase Mixtures in Thermal Equilibrium," Ph.D. Thesis, Georgia Institute of Technology (1971).
- 5.10 Kataoka, I. and Ishii, M., "Drift Flux Model for Large Diameter Pipe and New Correlation for Pool Void Fraction", *Intl. J. Heat Mass Transfer*, vol. 30, 1927-1939 (1987).
- 5.11 Leung, J.C.M., "Occurrence of Critical Heat Flux during Blowdown with Flow Reversal", Argonne National Laboratory Report, ANL-77-4 (1977).
- 5.12 Katto, Y., "A Generalized Correlation of Critical Heat Flux for Forced Convection Boiling in Vertical Uniformly Heated Round Tube", *Intl. J. Heat Mass Transfer*, vol. 21, p.1527 (1978).
- 5.13 Mishima, K. and Ishii, M., "Critical Heat Flux Experiments under Low Flow Conditions in a Vertical Annulus", NUREG/CR-2647, ANL-82-6 (1982).

- 5.14 Griffith, P., Pearson, J.F., and Lepkowski, R.J., "Critical Heat Flux During a Loss-of-Coolant Accident", *Nuclear Safety*, 18(3), p. 298 (1977).
- 5.15 Liang, K.S. and Griffith, P. "Experimental and Analytical Study of Direct Contact Condensation of Steam in Water," *Nucl. Engr. and Design*, 147 pp. 475-435 (1994).
- 5.16 Peterson, P.F., Schrock, V.E. and Greif, R., "Scaling for Integral Simulation of Mixing in Large, Stratified Volumes", NURETH-6, October 5-8, 1993, Grenoble, France.
- 5.17 Peterson, P.F., "Scaling and Analysis of Mixing in Large Stratified Volumes," *Intl. J. Heat Mass Transfer*, 37, 97-106 (1994).
- 5.18 Tokuhiko, A.T., Lykoudis, P.S., "Natural Convection Heat Transfer from a Vertical Plate - 1. Enhancement with Gas Injection", *Intl. J. Heat Mass Transfer*, 37(6), 997-1003 (1994).
- 5.19 Tokuhiko, A.T., Lykoudis, P.S., "Natural Convection Heat Transfer from a Vertical Plate - 2. With Gas Injection and Transverse Magnetic Field", *Intl. J. Heat Mass Transfer*, 37(6) 1005-1012 (1994).
- 5.20 Siddique, M, Golay, M.W., Kazimi, M.S., "Local Heat Transfer Coefficient for Forced Convection Condensation of Steam in a Vertical Tube in the Presence of Air," *Nuclear Technology*, Vol. 106, No. 2, pp. 202-215 (1994).
- 5.21 G.E. Nuclear Energy, "SBWR Standard Safety Analysis Report," 25A5113, Rev. A., August (1992).

6. SCALE OF THE PUMA

At the prototypic pressure simulation, the following relations are obtained from the integral system scaling and the boundary flow scaling results given in Chapter 5:

$$p_R = 1 \quad (6.1)$$

$$A_{iR} = \left[\frac{a_i}{a_0} \right]_R = 1 \quad (6.2)$$

$$L_{iR} = \left[\frac{l_i}{l_0} \right]_R = 1 \quad (6.3)$$

$$u_R = l_R^{1/2} \quad (6.4)$$

$$q_R = 1/l_R^{1/2} \quad (6.4)$$

At the major heat transfer sections, such as at the core and heat exchanges, it may be possible to make

$$d_R = 1 \quad (6.6)$$

which implies that the heater or heat exchanger sections should have a prototypic hydraulic diameter.

According to Eqs. (6.2 and 6.3), the major geometric configurations of the scaled model are determined by $A_{iR} = 1$ and $L_{iR} = 1$. This leaves some freedom in choosing on the height ratio, l_R , and area ratio, a_R . The overall cost of the facility is reflected in the volume ratio, $V_R = l_R a_R$ and height ratio, l_R . In determining the overall size of the proposed facility, it is necessary to consider four essential factors:

- 1) the need to consider scale relations to the existing facility,
- 2) the need to compensate for the shortcomings of existing facilities or complement the overall data base,
- 3) the need for justifiable rationale for the chosen values of a_R and l_R , and

- 4) the overall impact on the total cost.

For the PUMA, the above factors have been examined in detail. Based on these considerations, a 1/4 height and 1/400 volume scale have been chosen as the optimum design.

The existing or under-construction integral facilities for the SBWR are all full height. The GE's GIST facility is a low pressure, full-height facility with $l_R = 1$ and $a_R = 1/508$. The GIRAFFE facility in Japan has $l_R = 1$ and $a_R = 1/400$. The planned PANDA facility has $l_R = 1$ and $a_R = 1/25$. The aspect ratio l_R/d_R , for these facilities are 22.5, 20 and 5, respectively. In view of the overall cost, the volume scale of these facilities, friction and structural heat similarities, a new facility at the volume scale of about 1/400 appears to be optimum. This will match the mass and inventory of the GIST and GIRAFFE facilities also.

Since the existing facilities are all full height, the impact of the actual total height on various phenomena can be evaluated sufficiently. However, the existing facilities fall into the category of thin and tall systems, which have some major shortcomings. In Table 6.1, the dimensions of various components of the SBWR are compared between prototype and full-height, 1/4-height and 1/8-height scaled model for a 1/400 volume scaled facility. As seen in Table 6.1 for a full-height scaled model, the flow area is reduced substantially. The reduction in flow area increases the frictional resistance significantly. This effect can be quantified by the friction number, or more specifically by a factor f/d , where f is the friction factor. For most nuclear reactor systems, the major flow resistances are located at the bundle sections such as the core or steam generators. These sections can be made quite prototypic by taking the similar bundle cross-sectional geometry, so that the reduction of the flow area, up to a certain level, does not strongly affect the overall frictional resistance. However, a flow area ratio of less than 1/200 can have a significant impact on the total frictional resistance. Since the friction number has a factor f/d , a reduction in l can significantly help to scale flow resistances. At the same time, d_R can be increased by decreasing l_R for a fixed volume scale. Hence, the reduction in height can effectively eliminate the significant problem in the simulation of the friction number.

The complete scaling analysis presented in Chapter 5 indicates that the reduction in the height does not necessarily distort the natural circulation phenomena because the circulation rate is determined by the balance between the driving head and the loop frictional resistance. In order to preserve the kinematic and energy similarity, the system velocity and time scales should be reduced by the specified factors in a reduced height system. Under these conditions the driving head and loop frictional resistance can be matched. In contrast, a thin and tall facility may significantly distort the natural circulation by increasing one of these two balancing forces.

The second advantage of using the reduced-height system is that the aspect ratio becomes much closer to the prototype system. Thus, it is a much better system to simulate the two- or three-dimensional phenomena expected in the SBWR core, chimney, downcomer and

containment. As shown in Table 6.1, the 1/8-height scaled model is close to a linearly scaled model. It has very fat vessels, especially the upper drywell and suppression pool. For 1/8 height scale, the required core power is also large. The 1/4 height and $a_R = 1/100$ scaled facility has moderate power requirement and makes the aspect scaling ratio factor to be only 1/2.5, which is very close to the prototype system.

The present quarter-height system with a volume scale of 1/4(0) has the advantage of well-matched gravitational and frictional forces. Furthermore, due to relatively large cross-sectional areas, the important phenomena of two- or three-dimensional voiding patterns and flow regimes in the core and chimney can be simulated well. This is particularly important for assessing the effects of various instabilities such as the manometer oscillation, density wave instability, geysering and flashing-induced cyclic phenomena in the natural circulation cooling and stability of the GDCS. Even in comparison with the PANDA facility, the present system has a smaller aspect ratio, and therefore a significant advantage for simulating certain phenomena.

The present facility, which simulates the 2-D and 3-D phenomena very well because of its smaller aspect ratio, is called the Purdue University Multi-dimensional Integral Test Assembly (PUMA). In Table 6.2, the important non-dimensional numbers, derived from scaling considerations, are compared between the prototype and PUMA. These numbers are calculated for 1.03 MPa (150 psi) operating pressure condition. From this table, the numbers for PUMA match the prototype dimensionless numbers, except N_{flash} . The N_{di} in PUMA is also smaller than in the prototype due to a large contribution of local slip to the total slip. The chimney N_{fi} in PUMA is smaller than in the prototype. However, the frictional pressure drop in chimney is not important, as it is very small compared to the gravitational pressure drop.

One of the possible shortcomings of the reduced height system is the reduction in the flashing phenomena in the chimney. The superheating due to the reduction in the hydrostatic head as the two-phase mixture rises in the chimney section is essentially related to the height of the chimney. Hence, by reducing the height, the flashing is somewhat reduced.

Since flashing can be one of the important local phenomena of interest, it is necessary to focus some of the experiments on this flashing phenomena distortion. The vapor generation due to flashing can be simulated by reducing the system pressure by about 45% relative to the prototype system. By reducing the pressure, the vapor density can be made significantly smaller. This will lead to similar vapor volume generation and void fraction as in the prototype. This type of experiment, focused essentially on the impact of the flashing phenomena, will comprise a small portion of the preliminary test matrix.

**TABLE 6.1 COMPARISONS FOR MAJOR COMPONENTS
AND DIMENSIONS OF DIFFERENT HEIGHT SCALING***

<u>COMPONENT</u>	<u>PROTOTYPE</u>	<u>1/1 HEIGHT</u>	<u>1/4 HEIGHT (PUMA)</u>	<u>1/8 HEIGHT (LINEAR)</u>
<u>REACTOR PRESSURE VESSEL</u>				
Total height (mm)	24600	24600	6150	3075
I.D. (mm)	6000	300	600	848.7
Total volume (m ³)	669	1.67	1.67	1.67
<u>CORE</u>				
Rod material	Zr clad	S.S alloy	S.S alloy	S.S alloy
Active length (mm)	2743	2743	685	342.9
Total power	45 mW	112.5W	225 kW	318.2 kW
Core shroud I.D (mm)	5150	257.5	515	728.4
<u>CHIMNEY SECTION</u>				
Total height (mm)	9000	9000	2250	1125
Partition height	6500	6500	1625	812.5
# of divided areas	25	9	9	9
I.D. of shroud (mm)	4955	247.75	495.5	700.8
<u>CONTAINMENT</u>				
Wall material	Concrete/steel	S.S	S.S	S.S
Upper head volume(m ³)	3770	9.4	9.4	9.4
Upper head height (mm)	6100	6100	1525	762.5
Upper head dia.(mm)	28050	1402.5	2800	3967.5
Lower head volume (m ³)	1696.5	4.24	4.24	4.24
Lower head height (mm)	27200	27200	6800	3400
Lower head dia. (mm)	8911	445.55	891.1	1260.4
<u>SUPPRESSION POOL</u>				
Initial water volume (m ³)	3255	8.13	8.13	8.13
Initial gas space (m ³)	3819	9.55	9.55	9.55
Height (mm)	11950	11950	2987	1493
Diameter (mm)	27450	1372.5	2800	3882.6
<u>GDCS POOL (1 OF 3)</u>				
Diameter (mm)	Not circular	450	900	1273
Height (mm)	6100	6100	1525	762.5
Volume (m ³)	348	0.87	0.87	0.87

*Note: The volume scaling ratio is kept as 1/400 for all different height scaling.

**TABLE 6.2 COMPARISON OF VARIOUS PARAMETERS &
NON-DIMENSIONAL NUMBERS BETWEEN PROTOTYPE & PUMA**
(at 1.03 MPa or 150 psi operating pressure)

QUANTITY / NUMBERS	PROTOTYPE	PUMA
CORE EXIT QUALITY	4.3×10^{-3}	4.166×10^{-3}
CORE EXIT VOID FRACTION	0.4	0.41
$N_{pch}(\text{core})$.72	.694
$N_{flash}(\text{chimney})$	0.298	0.074
N_d	0.85	0.46
N_f		
-core support plate and core	4.4	4.2
-chimney	3.4×10^{-3}	1×10^{-3}
-separator	1.19	0.91

Losses for major lines in both PROTOTYPE and PUMA

Component	PROTOTYPE		PUMA	
	K	f / D	K	f / D
MSL	6.6	0.4	34.8	2.1
SRV	5.8	1.4	56.6	13.7
DPV (MSL)	101.8	0.14	526.6	0.5
DPV (RPV)	14.7	0.1	113.4	0.8
IC supply line	6.5	1.0	131.6	20
IC condensate line	3.4	1.4	26.2	10.8
IC vent line	10.2	32.9	20148.2	64987.8
PCCS supply line	4.6	0.5	23.3	2.5
PCCS vent line	3.3	1.3	16.7	6.1
PCCS condensate	5.5	1.2	42.4	9.3
GDCS equalization line	40.5	1.1	19.5	0.5
GDCS line	12.4	1.2	121.1	11.7
FWL	6.2	1.1	8.2	1.5

- SRV losses were estimated since Purdue did not receive its isometric drawing from GE.

- Losses were estimated using the Crane Paper.

7.0 DESIGN OF PUMA-SBWR FACILITY AND SCALING BASIS

7.1 Reactor Pressure Vessel Design

The Reactor Pressure Vessel (RPV) is the most vital component in the scaling, design and experimentation of the Simplified Boiling Water Reactor (SBWR) system. This observation is based on the fact that nearly all SBWR safety systems are designed to prevent core uncover, and that the RPV is the main source of steam/energy inventory in the integral facility. Of the components that make up the RPV, the most significant are:

- Pressure vessel
- Lower plenum
- Core plate
- Core
- Chimney
- Steam separators
- Steam dryers
- Downcomer.

The issues of scaling and design of these RPV components are discussed in later subsections of this chapter.

Proper scaling of the RPV requires careful scaling of the vessel geometry. The core power is properly scaled next, followed by the pressure drop across each component. Even though the geometrical scaling is straightforward, it may be restricted in more than one component by other considerations, such as core power and core heat flux.

The core power scaling is derived from the heat source number, Eq. (5.5), where the volumetric heat generation is given by

$$q''' = \frac{u_0}{l_0} = \frac{1}{\sqrt{l_0}} \quad (7.1)$$

From the integral and boundary flow scaling of the reactor system, the area ratio, a_R , and length ratio, l_R , are given by

$$a_R = \frac{1}{l(x)} \quad \text{and} \quad l_R = \frac{1}{4} \quad (7.2)$$

which results in the following value for the core power scale:

$$q_R = \frac{1}{2(\kappa)} \quad (7.3)$$

7.1.1 Pressure Vessel

The pressure vessel scaling is purely geometrical. The choices of vessel material and structural design are dictated by factors such as vessel integrity and operating conditions, which are independent of scaling issues. The PUMA pressure vessel dimensions are given in Table 7.1.

In Figure 7.1, a schematic of the pressure vessel is shown with the major internal components and their corresponding heights. As shown in Figure 7.2, the vessel has three parts separated by flange connections, which allow access to the internals during assembly and maintenance.

Table 7.1 Reactor Pressure Vessel Dimensions.

Component	SBWR	PUMA	Scale
Total Height (mm)	24505	6126	1/4
ID (mm)	6040	604	1/10
Area (m ²)	28.65	0.2865	1/100
Volume (m ³)	669	1.755	1/400
Wall Material	Carbon Steel	Stainless Steel	

7.1.2 Lower Plenum

The SBWR lower plenum houses the Control Rod Drive (CRD) mechanisms and other internal structures, whereas the PUMA lower plenum houses the non-heated length of the fuel-simulated electrical heater rods. The SBWR internal structures in the lower plenum are not considered in this scaling analysis. This leads to distortion in the flow area and volume scaling in the lower plenum approximately 26% greater than the volume scaling criteria of 1/400. Such a distortion will affect pressure drop and vessel inventory. In order to minimize this distortion, a volume filler piece is added to the lower plenum, as shown in Figure 7.3, to reduce the volume distortion to 16.4%. The tentative design of the filler pieces calls for a sealed block made of thin stainless steel sheets, which will have a negligible effect on stored heat.

7.1.3 Core Plate

In order to obtain a properly-scaled nominal flow rate through the core, the core plate in PUMA is designed considering the total pressure drop across the core. The distortion in the oversized PUMA core flow area leads to a distortion in the core flow rate and core pressure drop. Hence, the core plate in PUMA is designed not only to match the scaled pressure drop across the core plate, but also to account for the area distortion in the core. As shown in Figure 7.4, the PUMA core plate is designed to house two orifice groups:

i. Bypass orifice group

- 1 x 10 mm I.D. at core plate center
- 12 x 10 mm I.D. equally spaced at a radius of 179 mm from core plate center

ii. Core heaters orifice group

- 38 x 34 mm I.D. giving an annular geometry for heater orifices

7.1.4 Core

a. Core Heater Rods

Adopting the scaling approach of Kocamustafaogullari and Ishii [7.1], the appropriate scaling of the core fuel rods results in use of 439 heater rods, 12.27 mm O.D., capable of providing 455.6 W of power per rod. The cross-sectional area of the 439 heater rods, in addition to the flow area around each rod, consumes the total core area. This is clearly unacceptable as the core area must also include the bypass area and several instrumentation penetrations into the core. An alternative configuration, therefore, would be a reduced number of enlarged heaters.

Other important considerations in the heater design are the need for a variable power profile and the need to over-design the heater power. These provisions are necessary to compensate for the unexpected power failure of individual heaters and to accommodate over-power tests where 10% over-power is used.

SBWR realistic decay heat data [7.2] were fitted with a tenth order polynomial. The decay power is given by

$$y = \sum_{n=0}^{10} b_n x^n \quad (7.4)$$

Here, $y = \log p/p_0$, p is decay power at time t , $p_0 = 2000$ MWt, $x = \log t$, and the coefficients b_n are given in Table 7.2.

Table 7.2 Coefficients for Decay Heat Polynomial Fit

b_0	-0.45865
b_1	-1.20325
b_2	-0.5128
b_3	1.140821
b_4	0.35704
b_5	-0.91525
b_6	0.126003
b_7	0.289916
b_8	-0.16738
b_9	0.035941
b_{10}	-0.0028

In Figure 7.5, the polynomial fit is shown with decay heat data. In Table 7.3, SBWR time and decay power are compared with PUMA time and power scaled values 600 seconds following scram.

Table 7.3 Decay Power in SBWR and PUMA Facilities

SBWR Time	SBWR Power (kW)	PUMA Time	PUMA Power (kW)
600 s	4.50×10^4	300 s	225
1 h	2.65×10^4	0.5 h	
2 h	2.15×10^4	1 h	108
3 h	1.91×10^4	1.5 h	
4 h	1.75×10^4	2 h	88
8 h	1.43×10^4	4 h	71

The experiments on PUMA are designed to start at a blowdown condition of 1034 kPa (150 psi). Table 7.4 lists the power levels in both the SBWR and PUMA facilities at 1034 kPa (150 psi) for various postulated break transients with one DPV failure. Table 7.4 is derived from the information given in Figures 6.3-10 and 6.3-80 in [7.3]. PUMA core power levels are based on the core

power scaling criteria of 1/200.

Table 7.4 Core Power Levels at 1034 kPa (150 psi) Following Blowdown

Break Location	1 GDCS Valve Failure (s)	1 DPV Failure (s)	SBWR Power (MW)	PUMA Power (kW)
STB	290		51.8	259
Inside SLB		270	52.49	262.45
FWLB		230	53.87	269.35
RWCU/SDC Break		370	49.53	247.65
IC Return LB		600	44.1	220.5
GDCS Injection		310	51.12	255.6
BDLB		500	46.06	230.3

STB - Stub Tube Break

BDLB - Bottom Drain Line Break

From Table 7.4, it can be seen that the highest scaled decay power level (269.35 kW) is for the feedwater line break (FWLB) at 1034 kPa (150 psi) following blowdown. Hence, a total of approximately 300 kW is needed for the core power of the PUMA facility to accommodate all possible blowdown conditions.

A number of design iterations were performed to determine the PUMA core heater rod layout each taking into consideration PUMA total power requirement, accommodation of bypass flow area, provision for variable power profile, commercial availability, and practical design and assembly considerations. The resultant design includes thirty-eight heater rods, each one 25.4 mm (1 inch) in diameter, placed in three concentric rings as shown in Figure 7.6. The layout of the heaters allows sufficient space for instrument probe penetrations into the core through the core plate. The three-ring design allows for a non-uniform power profile by separately controlling the power to each ring.

Typical radial power profiles from the SSAR, Chapter 4.1 [7.3], were studied. Relative to the inner ring of heaters, the PUMA middle ring power level per heater rod is designed to be greater by a factor of 1.2, whereas the outer ring power level per heater rod is lesser by a factor of 0.8. Table 7.5 lists the arrangement of the heater rods for a maximum core power of 400 kW.

Table 7.5 Core Heater Rod Arrangement

Circle radius (mm)	No. of rods	Max. rod power (kW)	Operating power (kW)	Maximum heat flux (kW/m ²)
Inner ring				
70	6	11.0	5.5	201.0
Middle ring				
145	12	13.5	6.6	246.7
Outer ring				
240	20	9.0	4.4	164.5

A typical heater rod is shown in Figure 7.7. The heated length of the heater rod is based on the scaled length of the SBWR active fuel length. For assembly and access purposes, the heater rods penetrate from the bottom of the RPV and extend up to the inlet of the chimney section. Heater rods are manufactured from commercially available Inconel or stainless steel with commercially prepared surfaces.

b. Bypass

Constructing the PUMA core as three rings of variable-power heater rods suggests using the central area of the core as one bypass area and the annular space between the second and third heater rods rings as the second bypass area.

The core parameters for PUMA are compared with prototype in Table 7.6.

Table 7.6 Core Parameters

Component	SBWR	PUMA	Scale
Number of Rods	43920	38	
Rod Diameter (mm)	12.27	25.4	
Rod Material	Zr Clad	SS Alloy Clad	
Rod Active Length (mm)	2743	686	1/4
Flow Area-Fuel (m ²)	7.4	0.1255	distorted
Flow Area-Bypass (m ²)	5.6	0.02491	distorted
Mass Flow Rate (kg/s)	7555.6	37.8	1/200
Pressure Drop (Pa)	48200	12050	1/4

Based on the pressure drop across the core and inlet plate and the flow area for bypass and fuel channels, the following design was chosen for PUMA:

- Central bypass pipe with I.D. of 54.0 mm
- Annular area with a smaller diameter of 340 mm and a larger diameter of 380 mm.

Figure 7.4 shows the bypass regions and the inlet holes at the core plate.

From the design we see that the available area for the flow in the core is 0.15041 m^2 , which is larger than the flow area of the appropriately scaled PUMA core by approximately 15.7%. This enlargement will result in a distortion in the scaled velocity in the PUMA core of approximately 15.7% as well. Therefore, the velocity ratio in the core for the enlarged area is $(V_{\text{core}})_R = 1/3.6$.

The pressure drop is similarly distorted. To compensate for the decrease in pressure drop across the core due to the enlargement of the flow area, the core plate orifice area is substantially decreased, as discussed above.

7.1.5 Shroud design

The core shroud acts as a thermal shield, preventing heat from directly reaching the vessel wall. It also separates the core from the downcomer section of the RPV. The core shroud can be modeled as a cylindrical wall placed around the core.

Dimensions of the core shroud are summarized in Table 7.7. The core shroud extends from the top of the fuel to a certain distance below the core plate. The height and diameter of the core shroud are scaled using the geometrical scaling criteria of length and area.

The PUMA core shroud consists of a single cylinder surrounding the core assembly extending from above the heaters to the bottom of the RPV, as shown in Figure 7.3. The lower portion of the core shroud is perforated with large holes to simulate the open flow area in the lower plenum. These perforations begin at the correct scaled height location in the core shroud (i.e., 536.5 mm from the bottom of the RPV) in order to preserve the flow pattern in the downcomer and the region below the core plate. The perforations extend to the bottom of the RPV.

The shroud is welded to the bottom flange of the RPV. This single-shroud design provides the rigid structure needed for precise positioning of the electrical heaters. Removal of the core assembly for maintenance is also made simpler with the single-shroud design.

To prevent bypass leakage between the inside of the core shroud and the outer perimeter of the core inlet plate, an O-ring is placed on the core inlet plate, as shown in Figures 7.3 and 7.4.

The core inlet plate is supported by bolting the core shroud to the plate with angle supports welded onto the outer rim of the core inlet plate, as shown in Figures 7.3 and 7.4.

Table 7.7 Core Shroud Design

Component	SBWR	PUMA	Scale
Shroud Height (mm)	4788	1197	1/4
Core Shroud OD (mm)	5250	525	1/10
Core Hydraulic Diam. (mm)	19.7	62	distorted
Core Flow Area (m ²)	7.4	0.1255	distorted

7.1.6 Chimney

The chimney extends from the top of the core to the bottom of the steam separator assembly. The chimney shroud creates an annulus with the vessel wall, providing the downcomer flow area. Following an interruption in feedwater line or a LOCA, the large reserve of water in the shroud above the core allows for an extended period of time in which core uncovering can be prevented. The height of the chimney which contains a two-phase mixture provides the natural buoyancy driving force that circulates water to the core through the downcomer.

Vertical partitions placed in the chimney shroud extend from the bottom of the chimney to about 75% of the chimney height. The partitions act as a deterrent to any lateral flow disturbances due to non-uniform void fraction profiles, and prevent flow redistribution. Such disturbances may cause two-phase flow dynamic instability in the chimney section. The instabilities, if no partitions are present, may then lead to local circulation of the two-phase mixture in the chimney region, thus decreasing the overall natural circulation flow in the RPV. Therefore, it is important that partitions also be simulated in PUMA, not only to prevent any dynamic instability, but also to preserve the inherent two-dimensionality of the two-phase flow mixture.

A mixing plenum is present at the exit of the chimney partition and extends to the top of the chimney shroud, immediately preceding the entrance to the steam separator. The mixing plenum is an open area which allows the two-phase mixture exiting the partitions to mix and form a more homogeneous mixture, avoiding channeling effects in the separator. Table 7.8 summarizes the geometrical dimensions of the chimney. The height and diameter of the chimney are scaled using the geometrical scaling criteria of length and area. Figure 7.1 shows the location of the PUMA chimney in the RPV.

Figures 7.8 and 7.9 show a general schematic of the chimney shroud mounting and assembly. The bottom of the chimney shroud is connected to the top of the core shroud by a double slip joint (Figure 7.9). The slip joint serves a number of purposes. During initial assembly, the slip joint allows for proper centering/positioning of the chimney shroud. During normal operation, the slip joint prevents any flow leakage between the downcomer and core region at the location where the core shroud ends and the chimney shroud begins. Finally, during RPV maintenance, the slip joint allows the bottom portion of the vessel housing the heater rods to be readily disengaged. This is accomplished by simply unbolting the lower flange connection, and removing the bottom portion of the vessel with a minimum lowering clearance. The weight of the chimney shroud is supported by bolting the top of the chimney shroud wall to a cylindrical ring welded to the bottom of the lower steam separator plate (Figure 7.8). This design also allows for minimizing the number of devices needed to support the shroud, which would have otherwise created more obstacles in the downcomer flow area.

As mentioned earlier, the SBWR chimney shroud contains 25 square partitions. Each square partition covers approximately the cross-sectional flow area of 9 fuel cells (3 X 3). In PUMA design, it is not necessary to geometrically scale the partitions or to use partitions of similar configurations, since the SBWR chimney partition configuration is based mainly on the square layout of the fuel assemblies.

A number of criteria were set in order to determine the PUMA chimney partition configuration. The first was the need to preserve two radial flow areas that coincide with the ring-like layout of the PUMA heaters. The second criteria called for approximately equal cross-sectional flow area through each of the partitions. Also, the hydraulic diameter of each partition would need to be larger than the expected slug size, which is discussed below.

After a number of iterations, the PUMA chimney partition was designed to have five cylindrical tubes, 165 mm I.D. each, with one tube placed in the center of the shroud and the remaining four symmetrically positioned around the center in each quadrant. This design results in nine partitioned flow areas and is unique in that each partition has the same cross-sectional flow area. A cross-sectional schematic of the PUMA chimney partitions is shown in Figure 7.10.

The partitions need to preserve the two-dimensionality of the two-phase flow mixture through the chimney. The duct size should be larger than the expected maximum slug bubble size, D , which is given by the following correlation [7.4]:

$$D_h = 40 \sqrt{\frac{\sigma}{g\Delta\rho}} \quad (7.5)$$

For steam-water mixture, the maximum slug size, which is equal to 108.4 mm, is calculated from this correlation. It is clear that the PUMA partition duct size is larger than the minimum set by the size of slug bubble formation.

7.1.7 Downcomer

The RPV downcomer area extends from the top of the chimney to the lower plenum. In the SBWR, the width of the downcomer in the chimney section is slightly larger than that in the core region, due to the difference in the outer diameters of the chimney and core shrouds. The width of the downcomer in each region of the RPV is scaled in PUMA using the geometric scaling criteria of 1/10. This results in downcomer widths of 47.3 and 37.5 mm for the PUMA chimney and core regions, respectively. A schematic of the PUMA RPV indicating the downcomer width is shown in Figure 7.3.

In the previous section, the choice of the partition dimension in the chimney region was based on the requirement to support the maximum bubble slug size. In the PUMA downcomer region, similar consideration is made. It is clear that the PUMA downcomer width is smaller than the largest bubble slug size predicted by Eq. (7.5). However, the annular geometry of the downcomer region has two length scales: namely, the width of the annulus and its perimeter. The maximum bubble size depends on these two length scales. Since the perimeter is much larger than the maximum slug bubble size calculated from Eq. (7.5), it is expected that the bubble shape will be distorted, having a thickness of approximately the gap size and a width given by Eq. (7.5). Such a bubble is expected to rise with a velocity corresponding to the spherical cap bubble having a diameter equal to that of a critical size bubble. Therefore, the relative velocity in the PUMA downcomer section is well-simulated.

Table 7.8 Chimney Design

Component	SBWR	PUMA	Scale
Chimney Height (mm)	9060	2266	1/4
Nominal ID (mm)	4955	496	1/10
Partition Height (mm)	6570	1642	1/4
No. of Partitions	25	9	--
Average Coolant Flow Area (m ²)	18.55	0.185	1/100
N_{flash}	0.554	0.128	

7.1.8 Separator/Dryer Assembly

The steam separator assembly located directly above the chimney shroud is designed to efficiently remove entrained water from the steam-water mixture entering the separators. This provides moist steam to the dryer assembly, which then undergoes additional separation to provide dry steam for the turbine generators. Information provided by GE on the steam separator performance under normal operating conditions allows for approximate pressure drop scaling of the separator for use in PUMA. Scaling the pressure drop across the separator would simulate the effective flow resistance in PUMA during vessel operation.

The proprietary SBWR separator consists of a large array of standpipes welded to the top of the separator plate. Each standpipe contains internal vanes to create a centrifugal force on the steam-water mixture, pushing the water against the inner walls of the standpipe. At different elevations, pick-off rings are located in the standpipes. The pick-off rings remove the water flowing along the inner wall and divert it outside of the standpipe through openings in the pipe wall adjacent to the rings. Water separated in the standpipe flows back into the downcomer region.

The elevation of the pick-off rings (and their adjacent openings in the standpipe wall) are designed to be above the normal operating water level. During a LOCA, however, there may be sufficient swell in the two-phase mixture level to reach the openings in the standpipe wall. This can potentially create a problem as water can flow back down into the chimney region by entering the standpipes through the openings.

Total pressure drop across the SBWR separator under normal operating conditions is given as 26.3 kPa [7.5, Attachment B, p. 9]. The gravitational pressure drop needs to be subtracted from the total pressure drop in order to obtain the frictional component, which is then scaled by 1/4 to obtain a proper scaling of the pressure drop. Based on typical operating conditions of 14% flow quality at 7.23 MPa (i.e. $\rho_m = 231 \text{ kg/m}^3$), and using the SBWR separator height [7.6], the gravitational pressure drop is calculated to be approximately 7.65 kPa. Therefore, the prototype frictional pressure drop under these operating conditions is estimated to be 18.65 kPa. Scaling this value by the pressure drop scaling of 1/4, PUMA frictional pressure drop is given as 4.66 kPa.

In order for the PUMA separator to provide this pressure drop, the mass flow rate through the separator must also be scaled to obtain the correct flow area and determine the number of separator tubes. Typical SBWR mass flow rate in the core is estimated to be 7,690 kg/s [7.3, p. 1.3-2]. When scaled by the flow scaling criteria of 1/200, the PUMA mass flow rate in the core is found to be 38.5 kg/s. Setting the minor loss coefficient, K-value, across an opened tube to 1.5, which corresponds to one sudden expansion and one sudden contraction in a short open-ended pipe, the

velocity of the mixture for a pressure drop of 4.66 kPa is calculated to be 5.18 m/s from the following relation:

$$\Delta P = n \frac{K \rho V^2}{2} \quad (7.6)$$

Assuming n separator tubes, atypical flow condition of 14% flow quality at 7.23 MPa (i.e. $\rho_m = 231 \text{ kg/m}^3$) and a mass flow rate of 38.5 kg/s, the flow area can be calculated from

$$\rho a V = \frac{38.5}{n} \quad (7.7)$$

Solving for the flow area, a , the following condition is obtained:

$$a = \frac{0.032}{n} \quad (7.8)$$

A list of tube diameters and the equivalent number of tubes satisfying the above condition is given in Table 7.9.

Table 7.9 Required Number of Separator Tubes Number and Diameters

n	Diameter (mm)
10	63.8
13	56.0
16	50.8
17	49.0
63	25.4

From this table, commercially available tube sizes and a reasonable number of tubes, a value of sixteen for n was chosen, with a pipe size of 50.8 mm (2 inch) diameter. The length of these tubes and the mounting mechanism of the lower steam separator plate will be discussed later in this section. The proposed layout of the tubes in the separator plate is given in Figure 7.11.

In order to provide an additional mechanism to separate entrained liquid from the steam, an upper steam separator plate containing a similar number and size of holes as the lower plate (described above) will be placed above the separator tubes. This upper steam separator plate

will contain short open-ended tubes placed directly above the holes in the plate. The tube lengths will be discussed later in this section. The openings are positioned so they are not directly above the separator pipes, causing a change in the steam-water mixture flow path. Any entrained liquid not separated in the first stage will exit the separator tubes with the steam, impact on the top separator plate and fall back down without flowing directly into the top separator tubes. The proposed layout of the tubes in the upper separator plate is given in Figure 7.12. Elevation of the upper steam separator plate and its mounting mechanism will be discussed later in this section.

Since the PUMA steam separator design is not based on geometrical similarity with the SBWR separator assembly, the choice of separator tube length and upper steam separator plate is somewhat arbitrary. The only device in the SBWR steam separator which needs to be properly scaled in PUMA using the length scale criteria is the elevation of the first level of pick-off ring openings in the SBWR stand pipes. As mentioned above, in the case of sufficient water inventory swell in the downcomer region these openings will be the first access points for water flow back into the standpipes and down into the chimney region. Hence, four symmetrically positioned holes are made in the PUMA separator tube walls, as shown in Figure 7.13. The elevation of these holes is based on 1/4 length scale of the elevation given at the lowest level of pick-off ring openings in the SBWR standpipes [7.5].

Allowing a sufficient clearance from the side holes in the separator tubes, the determination of the length of the open-ended tube, shown in Figure 7.13, is complete. A sufficient gap is allowed between the top of the separator tubes and the upper steam separator plate to allow the steam-water mixture to separate as the mixture impinges on the upper plate. Hence, the steam separator tubes extend from the lower steam separator plate to 60 mm below the upper steam separator plate, as shown in Figure 7.13.

The SBWR dryer consists of vertical perforated plates placed in a parallel configuration. Several flow path changes through the vertical channels cause moisture from the wet steam to collect on the plates and fall into horizontal collecting trays located at the bottom of the dryer plates. The trays then feed into a vertical duct which acts as a skimmer and returns the water to the downcomer region beneath the normal water level. This prevents the collected water from being entrained back into the upflowing steam mixture.

In order to simulate the skimmer duct, a single vertical tube is connected beneath the upper steam separator plate, as shown in Figure 7.13. The length of the tube is based on the 1/4 length scale to properly position scale its bottom end in respect to the normal water level.

In order for water collected on the upper steam separator plate to drain back down through the skimmer tube, only short tubes (76.2 mm) are needed above the separator plate, as shown in Figure 7.13.

As shown in Figure 7.13, the lower steam separator plate, the separator tubes and chimney shroud are all supported by a ring which is, in turn, anchor bolted to the inside of the vessel at several locations. This support ring does not exist in the SBWR, so it is perforated to allow for communication across the ring wall.

The support ring extends approximately 50.8 mm below the lower steam separator plate. This lower portion of the support ring is not perforated and serves several purposes. First, it allows the chimney shroud to be properly positioned during installation procedures by guiding the shroud to fit closely against the support ring. Also, the weight of the chimney shroud and partitions are supported by bolting the top of the shroud to the inside of the ring, as shown in Figures 7.8 and 7.13. Finally, the close fit between the chimney shroud and supporting ring minimizes the possibility of steam rising from the chimney and escaping into the downcomer region.

In the SBWR, the outer periphery of the steam dryer forms a wall-like barrier, preventing the separated dry steam from directly entering the downcomer area. As shown in Figure 7.2, the steam rises toward the top of the vessel, then reverses direction as it travels into the downcomer region. This steam flow redirection is simulated in PUMA using a cylindrical ring called the dryer skirt. The height of this skirt is scaled by 1/4 height scaling. The bottom of the skirt extends down into the separator region similar to the SBWR barrier around the separator region. The bottom elevation corresponds to the point where the skimmer tubes return water to the downcomer region. This elevation is also scaled by 1/4 height scaling. The main purposes of this shroud-like barrier are to direct steam leaving the separator standpipes into the dryer region and to prevent steam from escaping into the downcomer region.

The weight of the upper steam separator plate, short tubes and dryer skirt is supported by anchor bolting the bottom of the skirt to the inside the vessel. A vessel flange connection is placed at a specified location in the steam separator assembly to allow access to the support structures, as shown in Figure 7.2.

7.2 Drywell Design

The SBWR containment, as shown in Figure 4.1, is a reinforced concrete cylindrical structure which houses the RPV, GDCS, SP, ADS and their related components. The containment wall is designed to provide a leak-tight containment boundary. The containment is divided into a drywell (DW) region and a suppression pool (SP) chamber region (or wetwell) which are interconnected through vent lines.

The drywell region is designed to provide a leak-tight gas space and boundary against the release of radioactive fission products, steam and/or water released during a LOCA. It is also

designed to withstand the pressure and temperature loading associated with a break in any of the main system pipes inside the drywell and to withstand the negative differential pressures associated with a depressurization event. The drywell structure is designed for maximum temperature and pressure conditions of 171°C and 483 kPa (70 psia). The drywell directs nearly all the steam released during a LOCA into the suppression pool through the DW/SP vent system.

The prototype drywell consists of an upper drywell volume and a lower drywell volume, which are divided by the vessel support skirt and connected by an open flow area to allow for pressure equalization. The upper drywell surrounds the upper portion of the RPV and houses the ADS, PCCS/ICS piping, GDCS and other related systems. The lower drywell houses the portion of the RPV below the vessel support skirt, the control rod drive system and other vessel-bottom piping. It also acts as a sump, to collecting any water that enters the containment.

In integral systems, the mass flow from one component to another is an important parameter in measuring the system's accurate mass conservation and in explicitly studying flow behavior. In order to allow for such measurements in the drywell and the RPV, the drywell is designed as separate from the RPV, though they are connected by piping. This simplification in design facilitates construction of the vessels, instrumentation and flow visualization.

From the geometrical scaling criteria, the volume of the drywell is scaled by $1/4(X)$ and the height is scaled by $1/4$. The resultant model will have an appropriately-scaled cross-sectional area. In Table 7.10, the dimensions of the PUMA drywell are given along with information on the piping connected to the drywell.

In the present model, the annular geometry of the drywell around the RPV is modeled as a single cylinder. The reasons for this are two-fold. First, if the annular geometry of the drywell were to be scaled as an annulus, the width of the annulus would be scaled by $1/10$ due to geometric scaling considerations. This would substantially increase frictional losses due to the reduced hydraulic diameter. Second, construction of a single cylinder would be simpler compared to an annulus. Figure 7.14 shows a schematic of the PUMA drywell design.

The top portion of the upper drywell is shown in Figure 7.14. The scaled volume of the upper dome in the prototype drywell has been added to the upper head volume in PUMA. This is due to the fact that the dome volume contributes only 5% of the total drywell volume, and its presence does not significantly affect the mixing or flow distribution in the upper drywell. This approach also simplifies construction of the PUMA drywell.

Table 7.10 PUMA Drywell Design

• Number of Units:	1		
• Upper Drywell Height:	1525 mm		
• Upper Drywell Diameter:	2750 mm		
• Annular Section Diameter:	850 mm		
• Annular Section Height:	4300 mm		
• Lower Drywell Height:	6800 mm		
• Lower Drywell Diameter:	890 mm		
• Connecting Lines:			
Line Function	Line From	Line To	Pipe I.D. (mm/inch)
MSL	RPV	Drywell	76.2/3
MSL (To DPV)	RPV	Drywell	76.2/3
DPV Line	RPV	Drywell	76.2/3
FWL Break	RPV	Drywell	38.1/1.5
GDCS Line Break	GDCS Line	Drywell	50.8/2
PCCS Supply Line	Drywell	PCCS Tank	38.1/1.5
Drywell Vent	Drywell	SP	407/16
Vacuum Breaker	SP	Drywell	50.8/2
Vacuum Breaker Leak	Vac, Break Line	Drywell	6.35/0.25
RWCU/SDS Break	RWCU/SDS Line	Drywell	6.35/0.25

A brief analysis is given here to compare important safety phenomena between the SBWR and PUMA in the containment following LOCA behavior. An important phenomena expected to occur in the drywell region of the containment is mixing and stratification of steam and non-condensable gases. The degree of mixing/stratification in the drywell affects a number of other processes in the SBWR. For example, the performance of the PCCS, whose inlet is drawn from the upper region of the drywell, will be affected by the level of mixing/stratification of steam and non-condensable gases in the drywell. As the main driving force for the flow of steam and non-condensibles into the PCC condensers is based on the condensation-induced pressure difference between the drywell and suppression pool, pressure in the drywell will also be affected by mixing/stratification. In turn, the mixing/stratification phenomena will also be affected by the rate of steam condensation on the walls of the drywell.

As the PUMA containment is initially filled with air, the main source of steam into the containment will come from DPVs or breaks in the steam lines. Steam flow out of the RPV may also include some hydrogen from radiolysis of water within the core. The behavior of the

steam/hydrogen flow through DPVs or breaks into the drywell will initially be characterized as turbulent buoyant jets. As the density and velocity of the jet diminish, gravitational forces begin to affect the jet's motion. The jet will enter into an intermediate region, and eventually buoyancy forces will dominate the jet's motion [7.7]. One of the important dimensionless parameters used when the inertia and buoyancy forces are coupled, which can also be used for scaling purposes, is the modified Froude number defined as

$$Fr_j = \frac{u_j^2}{g d_j (\rho_a - \rho_j) / \rho_j} \quad (7.9)$$

where u_j , d_j and ρ_j are the jet exit velocity, jet diameter at the source and jet density at exit, and ρ_a is defined as the containment mixture density.

Based on a large experimental database for round jets discharging into an infinite volume of fluid of uniform density, Rodi [7.7] provided empirical relationships for predicting the axial decay of the maximum (centerline) jet velocity away from the jet source and the excess density for three different flow regimes. The empirical correlations for each flow regime are given below.

(a) Non-buoyant region:

$$\frac{u_m}{u_j} = 6.2 \left[\frac{\rho_j}{\rho_a} \right]^{1/2} \left[\frac{x}{d_j} \right]^{-1} \quad (7.10)$$

$$\left[\frac{\rho_a - \rho_m}{\rho_a - \rho_j} \right] = 5.0 \left[\frac{\rho_j}{\rho_a} \right]^{1/2} \left[\frac{x}{d_j} \right]^{-1} \quad (7.11)$$

(b) Intermediate region:

$$\frac{u_m}{u_j} = 7.26 Fr_j^{-1/10} \left[\frac{\rho_j}{\rho_a} \right]^{9/20} \left[\frac{x}{d_j} \right]^{-4/5} \quad (7.12)$$

$$\left[\frac{\rho_a - \rho_m}{\rho_a - \rho_j} \right] = 0.44 Fr_j^{1/8} \left[\frac{\rho_j}{\rho_a} \right]^{-7/16} \left[\frac{x}{d_j} \right]^{-5/4} \quad (7.13)$$

(c) Plume region:

$$\frac{u_m}{u_j} = 3.50 Fr_j^{-1/3} \left[\frac{\rho_j}{\rho_a} \right]^{1/3} \left[\frac{x}{d_j} \right]^{-1/3} \quad (7.14)$$

$$\left[\frac{\rho_a - \rho_m}{\rho_a - \rho_j} \right] = 9.35 Fr_j^{1/3} \left[\frac{\rho_j}{\rho_a} \right]^{-1/3} \left[\frac{x}{d_j} \right]^{-5/3} \quad (7.15)$$

where the subscript m refers to the jet centerline, and x is the coordinate in the normal direction. A dimensionless group incorporating the modified Froude number is used to set the criteria for transition from one flow regime to the next.

$$Fr_j^{-1/2} \left[\frac{\rho_j}{\rho_a} \right]^{-1/4} \frac{x}{d_j} \begin{cases} < 0.5 & \text{non-buoyant} \\ 0.5 \leq \text{and} \leq 5 & \text{intermediate} \\ > 5 & \text{plume} \end{cases} \quad (7.16)$$

Consider the steam flow from a DPV stub valve after the ADS has been activated. Although the orientation of the DPV opening provides for a horizontally-directed jet flow, the SBWR design includes a deflector plate located directly in front of the flow path. The main function of this plate is to prevent internal damage to the containment due to direct impact of the steam. The tentative SBWR design of this deflector resembles a semi-circular pipe, vertically oriented. Acting as thrust-reversers, the deflector plates can be considered to divide the mass flow into two approximately equal vertical streams, as shown in Figure 7.15. Therefore, the effective jet diameter may be taken as

$$d_j = \sqrt{2} d_{j0} \quad (7.17)$$

The empirical correlations of Rodi [7.7] have been applied to a single-source steam jet for the SBWR and PUMA drywells at the same velocities. Figure 7.16 shows the results of the calculations for a range of Froude numbers. The range of Froude numbers covered here corresponds to the steam velocities at the jet source from initial blowdown to long-term decay heat vaporization from the core. The value of x/d_j indicated for each drywell corresponds to the top of the drywell, where d_j is based on the effective jet diameter. The top of the drywell is the most important location to consider when determining the dominant flow regime, since it is at this point where the jet impacts the containment wall and determines the degree of mixing/stratification and condensation.

The results indicate that all three flow regimes can be expected in the PUMA drywell, similar to the SBWR. As the Froude number (i.e., jet velocity) reaches low values, buoyancy effects become dominant and the jet behaves as a buoyant plume. Hence, possible flow stratification in the drywell may be expected in the long-term behavior of the drywell after blowdown. The Froude number at which transition occurs from one flow regime to another, however, is slightly shifted to higher Froude numbers in PUMA. This implies that for the same jet velocity, the transition from non-buoyant to intermediate to plume flow regimes may occur sooner in the PUMA drywell than in the SBWR drywell.

It should be emphasized, however, that the Rodi correlations are strictly valid for round, vertical jets in an infinite volume of fluid of uniform density. They do not include any interactions such as condensation, the effects of internal structures or walls, or mixing due to shear, all of which can affect the degree of mixing/stratification and condensation. There is currently no database for the dynamic behavior of jets in finite volumes of fluids, enclosed by boundaries. Hence, the above analysis provides for approximate results and comparison between drywell behavior in SBWR and PUMA.

It is also interesting to compare the PUMA-to-SBWR dimensionless numbers considered here. Assuming similar fluid properties, the modified Froude number ratio for both critical and subcritical flow velocities is given as

$$\left[Fr_j \right]_R = \left[\frac{u_j^2}{gd_j \Delta \rho / \rho_j} \right]_R = \left[\frac{u_j^2}{d_j} \right]_R \begin{cases} 14 \text{ critical flow} \\ 2.5 \text{ subcritical flow} \end{cases} \quad (7.18)$$

The PUMA-to-SBWR ratio of the dimensionless group used by Rodi [7.7], Eq. (7.16), for determining flow regime transition is also determined here for the critical and subcritical flow velocity conditions,

$$\left[Fr^{-1/2} \left(\frac{\rho_j}{\rho_a} \right)^{-1/4} \frac{x}{d_j} \right]_R = \left[\frac{x}{u_j \sqrt{d_j}} \right]_R \begin{cases} 0.94 \text{ critical flow} \\ 1.6 \text{ subcritical flow} \end{cases} \quad (7.19)$$

The previous discussion centered on the comparison of the jet flow regime in the drywells of the SBWR and PUMA. We now apply the scaling criteria discussed in Section 5.4.7, where additional scaling issues introduced by Peterson, et al. [7.8] regarding mixing and stratification were presented. The final analysis of that study resulted in a dimensionless number representing the number of jets in a given volume,

$$n_{jR} = \frac{1}{(H/D)^2_R} \quad (7.20)$$

where H/D is the aspect ratio. The PUMA to SBWR ratio of H/D is given by

$$(H/D)_R = 2.5 \quad (7.21)$$

Therefore, from Eq. (7.20) the ratio of the number of jets is approximately 1/6.

Based on the Peterson, et al. argument, preserving this ratio would result in a proper scaling of the degree of mixing and stratification. However, this ratio is clearly not preserved in PUMA, as the PUMA-to-SBWR ratio of potential jet sources in the drywell is 0.66 (4 DPVs in PUMA, 6 DPVs in SBWR). It can be expected that, for given jet conditions, a higher level of mixing is expected in PUMA.

7.3 Suppression Pool Design

As discussed in Section 7.2, the containment is divided into a drywell region and a suppression chamber region (or wetwell), which are connected by vent lines. The suppression chamber consists of the suppression pool and the gas space located above the pool. The suppression pool is a large reservoir of water capable of absorbing a large amount of energy by condensing the steam discharged from the safety relief valves (SRV) in case of pipe break accidents a LOCA. The water serves as an additional source of reactor water makeup and as a reactor heat sink through the GDCS equalization line that connects the suppression pool to the RPV.

The gas space above the suppression pool is designed to be leak-tight, as it serves to collect and retain any non-condensable drywell gas following a LOCA blowdown without exceeding the design pressure of the containment. The design temperature and pressure of the suppression chamber are given as 121°C and 483 kPa (70 psia), respectively.

The suppression pool is connected to the drywell through the drywell/suppression pool (DW/SP) vent system, which is comprised of eight vertical/horizontal vent modules. Each module consists of a vertical flow channel extending into the suppression pool water with three horizontal vent pipes opening into the pool, as shown in Figure 4.1. In the event of a LOCA or pipe break within the drywell, the increased pressure inside the drywell forces a mixture of steam, water and non-condensable gases through the DW/SP vent system. The steam quickly condenses in the pool, and the noncondensable gases rise and collect in the gas space volume of the suppression chamber. Hence, the suppression pool also acts as a means of preventing over-pressurization of the drywell.

The SRVs also discharge steam into the suppression pool through discharge piping connected to spargers near the bottom of the pool. Similarly, the noncondensable gas vent lines from the PCCS and ICS are routed through the suppression pool and vented into the pool water. The gas rises to the top of the water level and collects in the gas space volume.

In the event that the pressure in the gas space exceeds the pressure in the drywell, vacuum breakers located on top of the suppression chamber open to the drywell region. Each of the three vacuum breakers are equipped with check valves designed to begin opening when the pressure in the suppression chamber rises to 3.45 kPa (0.5 psi) above the pressure in the drywell. The vacuum breakers become fully open when the pressure in the suppression chamber rises to 13.8 kPa (2 psi) above the pressure in the drywell. The vacuum breakers prevent the overpressurization of the suppression chamber, which can only operate properly when its pressure is below that of the drywell under these conditions, the DW/SP vent system and PCCS remain operational.

Based on the previously discussed geometrical scaling criteria for the PUMA model, the volume of the SBWR suppression pool is scaled by $1/4(X)$, and the height is scaled by $1/4$. This scaling approach ensures that the cross-sectional area is also properly scaled. The configuration of the SBWR suppression pool resembles an annular pool nearly surrounding the RPV. However, a simplification is made in the PUMA model and the pool is designed as a single cylindrical vessel, as shown in Figure 7.14.

To model the eight vertical vent modules connecting the drywell to the suppression pool, a single vent line, scaled by the total prototype vent flow area using the boundary flow scaling criteria, is used, as shown in Figure 7.14. The single vent line is centered in the suppression pool with multiple openings on the perimeter of the submerged line, simulating eight prototype vents

opening into the suppression pool. Table 7.11 lists the suppression pool design parameters.

A number of issues need to be considered when scaling the horizontal portion of the vent lines opening directly into the suppression pool. As discussed in Section 5.4.7, different scaling criteria apply to the vent openings depending on whether the steam/non-condensable gas mixture exiting the suppression pool is in the jet or bubble flow regime. Applying the general boundary flow scaling to determine the PUMA vent size may lead to over-condensation in the horizontal and vertical jet flow regimes. The condensation may be under-rated in the bubbly flow regime. Therefore, different vent sized openings may lead to different rates of condensation in the suppression pool.

Scaling the height of the vents also needs to be considered. This approach is more straightforward. As 1/4 height scaling has been implemented throughout the PUMA facility, we maintain the 1/4 height scaling for consistency. Hence, the location of the three rows of vent openings in the single vertical vent pipe is determined using 1/4 height scaling.

Because of the difficulty in scaling the vent sizes to maintain similar condensation rates under all possible flow regimes, the driving factor in the PUMA design is flexibility of use. This requires designing the vent size in such a fashion which the openings can be adjusted depending on the local conditions, so as to maintain similar rates of condensation. This approach will also allow separate tests to be performed on the condensation phenomena in the suppression pool.

The PUMA design calls for three rectangular-shaped slots at each of the three row elevations on the vertical vent line, as shown in Figure 7.14. The size of each opening is oversized, due to the general boundary flow scaling criteria, to measure 200 mm in width and 175 mm in height.

Bolt holes are placed around the periphery of each opening. The bolt holes will allow plates of various sizes and configurations to be connected to the openings in order to adjust the number and size of vent openings.

The three vacuum breakers located at the top of the SBWR suppression chamber, opening into the drywell, are also scaled in PUMA. Each of the three lines is scaled by the boundary flow scaling criteria. Therefore, the flow area of the PUMA vacuum breakers is scaled by 1/100 of that in the SBWR. Each vacuum breaker line in PUMA is equipped with a check valve which is designed to open when the pressure in the suppression chamber rises to 862 Pa (0.125 psi) above the pressure in the drywell. This value is obtained by applying the 1/4 differential head scaling criteria to the prototype value of 3.45 kPa (0.5 psi).

Once the pressure in the suppression chamber equals that in the drywell, the vacuum breakers are expected to shut to a leak-tight position. This is essential for the suppression

pool/chamber and PCCS to perform properly. However, in the case of a malfunction where a leak path remains in the vacuum breakers, this will have a negative affect on the long-term safety system of the SBWR. In order to simulate this scenario, a separate, smaller line is connected between the suppression chamber and the drywell, as shown in Figure 7.14. This line is to be equipped with an operator-actuated solenoid valve. During a test where the vacuum breaker leak condition is to be included, the solenoid will open to simulate a leak in the vacuum breakers.

Table 7.11 PUMA Suppression Pool (SP) Design

• Number of Units:	1		
• Tank Height:	2838 mm		
• Tank Diameter:	2817 mm		
• Connecting Lines:			
Line Function	Line From	Line To	Pipe ID (mm/inch)
SRV Line	MSL	SP	50.8/2
GDCS EQ Line	SP	RPV	12.7/0.5
PCCS Non-Cond Vent	PCCS Tank	SP	38.1/1.5
ICS Non-Cond Vent	ICS Tank	SP	12.7/0.5
SP Vent	Drywell	SP	356/14
SP Feed/Drain	SP	Drain	25.4/1
Vacuum Breaker	Drywell	SP	50.8/2

7.4 Gravity Driven Core Cooling System (GDCS) Design

As part of the Emergency Core Cooling System (ECCS), the Gravity Driven Core Cooling System (GDCS) plays a major role in the SBWR safety mechanisms. The GDCS can be considered as two separate systems: a short-term safety system and long-term safety system.

The former is designed to provide short-term water makeup to the reactor vessel for maintaining fuel cladding temperatures below safety limits. Three separate water pools, located within the upper drywell at an elevation above the active core region, provide gravity-driven water makeup to the reactor vessel. A 203 mm (8 inch) drain pipe from each of the GDCS pools passes through a loop seal, then branches into two 152 mm (6 inch) lines which feed into the downcomer annulus region of the reactor vessel through flow-restricting nozzles. Squib valves located on the GDCS drain lines are actuated 150 seconds after Level 1 is reached in the reactor vessel.

The long-term GDCS safety system is designed to provide long-term vessel cooling by keeping the core region covered with water, again through gravity-driven flow. This is accomplished

through three GDCS equalization lines connecting the suppression pool to the reactor vessel. Each line is independent and designed to open when the water level in the reactor vessel reaches 1 m above the top of the active fuel (TAF).

For PUMA, the volume and elevation of each of the GDCS pools is scaled using volumetric (1/400) and height (1/4) scaling. Due to the reduced diameter and height of the PUMA reactor vessel, it is also necessary to reduce the number of GDCS penetrations into the vessel in order to maintain some similarity to the SBWR in the degree of mixing occurring in the downcomer region by each GDCS penetration's plume. A reduction in the number of penetrations into the PUMA reactor vessel is also consistent with the overall PUMA aspect ratio of 2.5. Hence, the two 152 mm (6 inch) lines branching from the main 203 mm (8 inch) drain line are combined and scaled into one line for PUMA. As shown in Figure 7.17, this two-line-into-one combination is performed for 2 of the 3 PUMA GDCS pools.

In order to simulate a malfunction or break in one of the 6 inch SBWR penetration lines, it is also necessary for PUMA to maintain a scaled, branched line for the third GDCS pool. Therefore, the total number of GDCS drain penetrations into the PUMA reactor vessel is reduced from six to four. Loop seals in each GDCS drain line are also scaled in PUMA using height scaling criteria.

In the SBWR, the GDCS drain line from each GDCS pool is elevated from the bottom of the pool, leaving a small volume of water at the bottom of the pool once the pools are drained. The elevation of this drain line penetration is designed to prevent water flowing out of the reactor vessel through the DPV lines, once all GDCS water is drained into the vessel. The elevation of this penetration into the GDCS pool is also simulated in PUMA using 1/4 height scaling, as shown in Figure 7.17.

Each GDCS drain line in PUMA is equipped with a fast-acting, electric-actuated, full-port ball-valve. Analog signals are used to activate the valves. The logic timing governing the analog signals and the opening of the valves is similar to that used for the SBWR GDCS drain line activation.

Each of the three GDCS equalization lines used for long-term cooling of the reactor core is simulated in PUMA, as shown in Figure 7.17. The penetration elevation of each line between the suppression pool and reactor vessel is scaled using 1/4 height scaling, and the pipe size is chosen using boundary flow scaling criteria.

Each PUMA GDCS equalization line is equipped with a fast-acting electric actuator mounted on a full-port ball valve. The actuator will receive an analog signal from the main relay control board to determine the appropriate time for the valve to open. As described earlier in this

section, the GDCS equalization line is designed to open when the water level in the RPV drops to a pre-specified level. Since the water level in the RPV will be continuously measured during the tests, a set point representing the specified level in the RPV can be programmed into the data acquisition software that will send a signal to the relay control board to activate the electric actuator to open the ball valve. An electronic flow switch mounted on the electric actuator will send a signal back to the operator indicating that the valve has fully opened.

Boundary flow scaling criteria are used to properly scale the flow area for gravity-driven flow lines such as the GDCS drain lines and GDCS equalization lines. This approach is common to all piping in the PUMA facility. The methodology for applying the boundary flow scaling criteria to piping is given in detail here.

In boundary flow scaling, the approach is to apply the continuity equation and derive the area and velocity scaling relation as discussed previously in Chapter 5. From the boundary flow scaling criteria we have

$$\left[\frac{au}{a_0 u_0} \right]_R = 1 \quad (7.22)$$

Since, $[a]_R = 1/100$ and $[u]_R = 1/2$, the boundary mass flow rate requirement becomes

$$\dot{m}_R = 1/2(00) \quad (7.23)$$

Using the momentum equation, a relationship between the area ratio and the loss coefficient ratio can be obtained from the momentum equation

$$\Delta p = \frac{1}{2} \rho u^2 K = \frac{1}{2} \frac{\dot{m}^2}{\rho a^2} K \quad (7.24)$$

Here, K is the total loss coefficient, including the friction and the minor losses, a is the cross-sectional flow area of the pipe and Δp is the pressure drop across the pipe for the mass flow rate, \dot{m} . Hence, the ratio of Δp for prototype to model becomes

$$\left[\Delta p \right]_R = \frac{\dot{m}_R^2}{a_R^2} K_R \quad (7.25)$$

Substituting $\dot{m}_R = \frac{1}{2(\lambda)}$ in the above equation, we obtain

$$\frac{a_R}{\sqrt{K_R}} = \frac{1}{2(\lambda)\sqrt{\Delta p_R}} \quad (7.26)$$

From pressure scaling, it is known that if the flow is mainly gravity-driven, then the pressure drop ratio becomes equivalent to the height ratio, i.e., 1/4. Water flow in pipelines such as the GDCS drain lines, GDCS equalization lines, PCCS/ICS condensate lines and PCCS supply lines can all be considered to be gravity-driven, and the scaling criteria of $(\Delta P)_R = 1/4$ applies to these lines. However, flow in lines such as the steam lines, DPV lines and SRV lines are mainly determined by the pressure difference between two components or vessels. In these cases, the pressure scaling given by $(\Delta P)_R = 1$ is applied. From Eq. (7.26), since the prototype loss coefficients and the diameters of the pipes are known, the PUMA pipe size can be determined by an iterative process. For practical purposes, it is necessary to choose commercially available pipe sizes and adjust the pipe loss coefficient of PUMA by placing an orifice in over-sized pipes.

As described earlier, each SBWR GDCS pool has one 203 mm (8 inch) pipe that branches into two 152 mm (6 inch) lines before connecting to the RPV. In the PUMA facility, the two branch lines are replaced by a single drain line for two of the three GDCS pools. From the momentum equation applied to the prototype drain pipe we have

$$\Delta p = \frac{1}{2} \rho u_1^2 K_1 + \frac{1}{2} \rho u_2^2 K_2 \quad (7.27)$$

where subscript 1 refers to the 203 mm (8 inch) line and subscript 2 refers to the 152 mm (6 inch) line. From the continuity equation we have

$$a_1 u_1 = 2a_2 u_2 \quad (7.28)$$

The factor 2 on the right hand side of Eq. (7.28) is due to the two 152 mm (6 inch) lines

branching from the 203 mm (8 inch) lines. From Eqs. (7.27) and (7.28) we have

$$\Delta p = \frac{1}{2} \rho K_{eq} u_2^2 \quad (7.29)$$

where K_{eq} is defined as the equivalent loss coefficient given by

$$K_{eq} = \frac{4a_2^2}{a_1^2} K_1 + K_2 \quad (7.30)$$

As the flow is driven by gravity for the GDCS drain lines, the pressure drop scaling is given by $(\Delta p)_R = 1/4$. Hence, Eq. (7.26) can be written as

$$\frac{d_m^2/d_p^2}{\sqrt{K_m/K_p}} = \frac{1}{100} \quad (7.31)$$

The PUMA drain pipe replaces two 152 mm (6 inch) lines with a single line. Therefore, an equivalent diameter for this single line can be calculated by combining the flow area for each 152 mm (6 inch) line, which is given by $d_{p,eq} = 215.7$ mm (8.49 inch). Using the loss coefficients for 203 mm (8 inch) and 152 mm (6 inch) lines from information given in [7.3], K_{eq} for the prototype can be calculated from equation (7.30) as $K_{p,eq} = 13.59$. From Eq. (7.31), the scaled PUMA pipe diameter can be determined if K_m is known. However, K_m cannot be determined until the pipe size is known. A pipe size has to be assumed for which equation (7.31) can be satisfied. For 25.4 mm (1 inch) pipe, the total K_m was calculated as 33.69 for the PUMA facility. Substituting these values $K_{p,eq} = 13.59$, $K_m = 3$, $d_{p,eq} = 215.7$ mm (8.49 inch), $d_m = 25.4$ mm (1 inch) into Eq. (7.31) we have

$$\frac{(d_m/d_p)^2}{\sqrt{K_m/K_p}} = \frac{1}{113.4} \quad (7.32)$$

This is slightly less than the scaled requirement of 1/100 as given in Eq. (7.31). Next,

considering a 38.1 mm (1.5 inch) pipe, the corresponding loss coefficient is 131.75. Then the left-hand side of Eq. (7.31) is calculated to be 1/99.75, which is nearly the same as the scaled requirement. Hence, 38.1 mm (1.5 inch) pipe is the appropriate choice for the GDCS drain line where 2 branched lines are combined into one.

In order to conserve space and simplify construction procedures, the three PUMA GDCS pools are designed to fit into a single cylindrical tank. As shown in Figure 7.18, the tank is vertically partitioned into three independent pools isolating each of the three GDCS pools. The tank is sized so that the liquid volume in each of the three partitioned pools corresponds to the 1/4(0) volume scaling of the SBWR GDCS pool. The top of the partition is designed to be above the normal water level, though it does not extend to the top cover of the tank. This allows for a common gas space above the pools. The GDCS pools in the SBWR are open to the containment at the top, allowing for pressure equalization. In PUMA, a single line connects the common gas space at the top of the GDCS tank to the upper drywell. Table 7.12 summarizes the PUMA GDCS design parameters.

Table 7.12 PUMA GDCS Design

• Number of Tanks:	1		
• Tank Height:	1525 mm		
• Tank Diameter:	1540 mm		
• No. of Partitions	3		
• Connecting Lines:			
Line Function	Line From	Line To	Pipe I.D. (mm/inch)
GDCS Drain	GDCS Tank	RPV	38.1/1.5
GDCS Line Break	GDCS Line	Drywell	50.8/2
GDCS Air Supply	Drywell	GDCS Tank	50.8/2

7.5 Passive Containment Cooling System (PCCS) and Isolation Condenser System (ICS) Design.

The Passive Containment Cooling System (PCCS) is designed to remove the core decay heat that has been rejected to the containment after a LOCA, whereas the Isolation Condenser System (ICS) has been designed to remove decay heat from the RPV after any reactor isolation following interruption in normal reactor operation.

In the SBWR, a total of three PCCS condensers and three ICS condensers are submerged in a large, interconnected ICS pool of water, which is located outside and above the containment. Each PCCS and ICS condenser is designed to dissipate a maximum of 10 MWt and 30 MWt energy, respectively. The volume of water in the ICS pool is sufficient to provide decay heat removal for 72 hours following a LOCA without replenishment. Boil-off from the pool is vented to the ambient.

Each PCCS condenser consists of two identical modules with 248 tubes per module [7.6]. The tubes are 1800 mm in length, with 50.8 and 47.5 mm O.D. and I.D. respectively. Each PCCS condenser is connected to a 254 mm (10 inch) line that vents the non-condensibles to the suppression pool, and a 152 mm (6 inch) line that returns the condensed water to the GDCCS pool. The inlet supply to the PCCS condenser is a 254 mm (10 inch) line. This inlet is always open to the drywell to allow free flow of steam/gas from the drywell to the PCCS condenser tubes. The vertical condenser tubes of the PCCS modules are connected between two drums acting as the inlet and outlet plenum. The driving head of the PCCS is provided by the pressure difference between the drywell and the suppression pool. There are no valves, pumps or fans in the PCCS, which makes it a passive system by design. The PCCS is a unique design of the SBWR, which does not exist in any operating BWRs. On the other hand, the non-condensable vent from the ICS is not a fully passive system like the PCCS. The vent lines from the ICS are equipped with manually-operated solenoid valves.

Each ICS condenser also consists of two identical modules, but with 120 tubes per module [7.6]. The tubes are 1800 mm in length, with 50.8 and 46.6 mm O.D. and I.D., respectively. Each ICS condenser is connected to a 254 mm (10 inch) inlet line that receives steam from the RPV and a 152 mm (6 inch) line that returns the condensate to the vessel. Any non-condensibles in the ICS condenser are vented to the suppression pool via a 19.05 mm (0.75 inch) line. The 254 mm (10 inch) steam supply line shares the same stub line with a squib-type depressurization valve (DPV) which is part of the ADS system.

In scaling the PCCS and ICS for PUMA, first the PCCS condenser tubes will be considered. This will be followed by the ICS condenser tubes, then the PCCS and ICS headers, and finally the pool sizes.

Since the basic function of the PCCS is the removal of decay heat, the condenser tubes are scaled using power scaling. For a 1/4 height scaled system, the power density is scaled by

$$q_R''' = \frac{1}{\sqrt{l_R}} = 2 \quad (7.33)$$

For the reactor core, the total power is scaled using the power ratio

$$[\text{power}]_R = q_R'' V_R = \frac{1}{2(\lambda)} \quad (7.34)$$

Therefore, the condensation capacity of the PCCS is scaled by a factor of $1/2(\lambda)$. Since the condensation capacity is proportional to the tube inner surface area, the tube surface area is also scaled by $1/200$. The underlying assumption is that negligible condensation is occurring in the PCCS headers. The surface area ratio is then given by

$$S_R = [\text{power}]_R = n_R(\pi d)_R H_R \quad (7.35)$$

where n is the number of tubes, d is the tube diameter, and H is the tube height.

Maintaining a tube diameter similar to that in the SBWR, and applying the $1/4$ height scaling criteria to the tube length, the PCCS tube number scaling criteria is given by

$$n_R = \frac{1}{5(\lambda)} \quad (7.36)$$

As noted earlier, each of the three SBWR PCCS units consists of two modules, with 248 condenser tubes per module. The approach taken in PUMA is to combine two modules into one. Applying the criteria given by Eq. (7.36), this results in approximately 10 condenser tubes for each of the three PUMA PCCS condenser units.

Volume scaling of the PCCS condenser tubes is not considered here, since the tubes do not store an initial water inventory as the ICS condenser tubes do, and the volume scaling in the PCCS tubes is considered to be a secondary effect in comparison to the heat transfer area scaling preserved as described above. The volume of steam in the PCCS condenser tubes (assuming tubes full of steam) represent a relatively negligible volume of water in comparison to the RPV inventory.

In scaling the ICS condenser tubes, a similar method to that described for heat transfer scaling in the PCCS is also applied. However, in addition to heat transfer scaling, volume scaling in the ICS condenser tubes must also be considered. Since the steam supply from the RPV to the ICS is always open, and the condensate drain line returning to the RPV is closed until activated, condensate is expected to fill the condenser tubes and headers in the ICS. By applying the volume scaling to the ICS condenser tubes, this initial volume of condensate will also be

properly scaled. Volume scaling of the headers will be discussed later in this section.

The volume in the ICS condenser tubes is scaled by the volume ratio given by

$$V_R = n_R(\pi d_R^2)H_R = 1/4(0) \quad (7.37)$$

In applying Eqs. (7.35) and (7.37) to the ICS condenser tubes, it is clear that by maintaining 1/4 height scaling in the tube lengths and prototypical tube diameter, both equations cannot be satisfied with a single tube number ratio. Hence, we need to allow the PUMA tube diameter to differ from that of the prototype, while maintaining 1/4 height scaling on the tube lengths.

Dividing Eq. (7.37) by Eq. (7.35), we obtain a scaling criteria for the ICS condenser tube diameter:

$$\frac{V_R}{S_R} = d_R = \frac{1}{2} \quad (7.38)$$

Substituting Eq. (7.38) in either of Eqs. (7.35) or (7.37), the ICS tube number scaling is given by

$$n_R = \frac{1}{25} \quad (7.39)$$

As noted earlier, each of the three SBWR ICS units consists of two modules with 120 condenser tubes per module. Similar to the PUMA PCCS modeling, the approach taken here is to combine two ICS modules into one. Therefore, based on the criteria given by Eq. (7.39), the PUMA ICS is designed with 10 condenser tubes for each of the three condenser units. As well, application of Eq. (7.38) determines the PUMA ICS condenser tube diameters as being 1/2 the prototype diameter. Hence, the PUMA ICS tubes are chosen to be 25.4 mm (1 inch).

As noted above, the reduction of the SBWR ICS tube condenser diameter from 50.8 mm (2 inch) to 25.4 mm (1 inch) in the PUMA ICS is primarily based on the need to maintain volumetric scaling in the ICS at 1/4(0). Since the ICS tubes are initially filled with water, any distortion in the volume scaling will affect the inventory of the system as the water drains into the RPV during the isolation stage. The reduction in condenser tube diameter is not expected to cause any appreciable distortion to phenomena occurring in PUMA. First, the role of the ICS in the SBWR safety system is appreciably reduced after the ADS system has been activated, which is the time scale with which the PUMA facility is primarily concerned. It can be shown from

Dukler's analysis of condensation in vertical tubes that a reduction in tube diameter from 50.8 mm (2 inch) to 25.4 (1 inch) will not appreciably affect the overall rate of condensation. The analysis of Dukler is outlined in [7.9]. Working from the definition of eddy viscosity and using the Deissler equation for its variation near a solid boundary, Dukler found that the velocity distribution curve in the liquid film was dependent on the interfacial shear and film thickness. Assuming that the ratio of the eddy thermal diffusivity to the eddy viscosity was unity and that the viscosity was unity and that the physical properties of fluid do not change in the direction of heat transfer, equivalent temperature profiles were constructed. Integrating the velocity and temperature profiles, the liquid film thickness and point heat transfer coefficients were computed. The results are displayed in [7.9] as a function of the Reynolds and Prandtl numbers with the interfacial shear as a parameter.

For the present analysis, we assume that the interfacial shear is proportional to the steam/non-condensable gas velocity, which is, in turn, related to the flow area.

Compared to the general flow scaling of the condenser tubes, where $n_R=1/50$ and the tube diameter remains prototypic, the adjusted scaling approach of the ICS condenser tubes ($n_R=1/25$ and $d_R=1/2$) results in a doubling of the steam/non-condensable gas velocity through the tubes for a fixed mass flow rate. Based on the above assumption, the interfacial shear can also be expected to increase by approximately a factor of 2. Using Dukler's analysis for the appropriate Prandtl number, an incremental increase of the interfacial shear of this magnitude results in only an incremental increase in the condensation rate. Hence, a reduction of the ICS condenser tube from the prototypic value of 50.8 mm (2 inch) to 25.4 (1 inch) is not expected to add any appreciable distortion to the condensation rate in the tubes.

Next, we consider scaling the PCCS and ICS headers. In each case, the SBWR headers are designed as horizontal cylinders. In scaling the headers for PUMA, we impose two scaling criteria, namely 1/4 height and 1/4(X) volume scaling.

Each SBWR PCCS header has a volume of 0.779 m^3 with height of 600 mm. Applying the height and volume scaling criteria to these dimensions and noting that in PUMA two module headers are combined into one, the PUMA PCCS header dimensions are given as $3.895 \times 10^{-3} \text{ m}^3$ in volume and 165 mm in height. Considering only vertical cylinders, this results in a cylinder diameter of approximately 174 mm.

Based on a cylinder of this diameter, it was found that it is impossible to accommodate all of ten PCCS condenser tubes, with 50.8 mm (2 inch) tube diameter each. After several iterations, still it was decided that in order to best accommodate the condenser tubes and maintain the header volume and height scaling, the PUMA PCCS headers would be designed by connecting two cylinders of different diameters, as shown in Figure 7.19.

The diameter of the cylinder was chosen in order to accommodate the condenser tubes. Once a practical height was chosen for this portion of the header, the dimensions of the smaller cylinder were chosen in order to satisfy the volume and height scaling. Hence, even though the PUMA PCCS header is designed as two sections, the combined dimensions are chosen in such a way as to maintain proper volume and height scaling. As shown in Figure 7.19 the inlet and outlet PCCS headers are designed to be similar, as is the case in the SBWR.

The PUMA ICS headers are also scaled using the 1/4 height and 1/4(8) volume scaling, similar to the PCCS headers. The dimensions of the ICS headers are given in [7.10]. Applying the height and volume scaling criteria to these dimensions and noting that in PUMA two module headers are combined into one, the PUMA ICS header dimensions are given as $4.978 \times 10^{-3} \text{ m}^3$ in volume and 170 mm in height. Again, considering a vertical cylindrical geometry, this results in a cylinder diameter of approximately 193 mm.

Unlike the difficulty that was encountered with accommodating the PCCS condenser tubes with the scaled dimension of the cylinder base, the ten PUMA ICS condenser tubes can be readily positioned in a cylinder base of 193 mm in diameter. This is primarily due to the fact that the PUMA ICS tube diameters are half of those in the PCCS. This implies that a single cylindrical header can be designed for each PUMA ICS unit.

However, in order to maintain consistent geometries between the PUMA ICS and PCCS headers, the ICS headers are also designed as two combined cylinders with different diameters, as shown in Figure 7.19. The diameter of the larger cylinder is chosen to accommodate the condenser tubes. Once a practical height is chosen for this portion of the header, the dimensions of the smaller cylindrical section are determined in order to satisfy the volume and height scaling using the combined dimensions of both sections. Again, the inlet and outlet header in the PUMA ICS are designed to be similar, as is the case in the SBWR. The PUMA PCCS/ICS condenser design parameters are given Table 7.13.

Table 7.13 PUMA PCCS/ICS Condenser Design Parameters

• No. of IC Condenser Units:	1
• No. of IC Condenser Tubes:	10
• IC Condenser Tube Diameter:	23.3 mm
• No. of PCCS Condenser Units:	1
• No. of PCCS Condenser Tubes:	10
• PCCS Condenser Tube Diameter:	47.5 mm
• IC/PCCS Condenser Tube Length:	450 mm

A simple design is adopted for both the PUMA PCCS and ICS headers in order to allow the efficient separation of non-condensibles from condensate in the outlet headers. As shown in Figure 7.20, a single condensate drain pipe is positioned at the lowest elevation in each of the outlet headers. Condensate collecting on the bottom cylinder head will readily drain through the drain pipe. The diameter of the PUMA PCCS and ICS condensate lines is determined based on boundary flow scaling.

Also shown in Figure 7.20, the non-condensable gas is removed from the PCCS and ICS headers at a higher elevation in the lower headers than the condensate drain. Penetration of the non-condensable vent line into the larger cylindrical portion of the outlet header prevents any condensate collecting in the bottom header from entering the vent line. Also, in order to prevent any condensate from flowing directly into the vent line from the condenser tubes above the vent opening, a hood-like device is positioned on top of the vent opening. The diameter of the PUMA PCCS and ICS vent lines is determined based on boundary flow scaling.

In the SBWR, each ICS/PCCS condenser is located in a subcompartment of the ICS pool. The subcompartments are formed by vertical baffles. All pool subcompartments communicate through openings beneath the baffles to the larger ICS reservoir, enabling full use of the water inventory independent of the operational status of any given ICS/PCCS loop.

Pool water can heat up to about 101°C, forming steam. This produces a slight positive pressure relative to ambient forcing the steam from the space above each ICS/PCCS condenser to be released to the atmosphere through discharge vents.

Applying the volume scaling criteria (1/400) to the SBWR ICS/PCCS initial total water inventory [7.11, Doc.25A5044, Sh.30] results in a relatively large volume, which from a cost and design point of view would be difficult to accommodate in PUMA, as the ICS/PCCS are located at the highest elevation in the facility. The important issue to consider in the scaling of the ICS/PCCS pool sizes in PUMA is maintaining 1/4 height scaling of the water, thereby maintaining the submerged level of the condenser units.

To maintain this scaling criteria, and avoid the difficulty of dealing with large water inventory, the width (or diameter) of the PUMA pools are chosen in such a way as to allow a practical and sufficient volume of water to be stored at a high elevation. To this effect, the ICS and PCCS pools in PUMA are separated into two smaller pools. The diameter of each pool is designed so that it is large enough to accommodate all three ICS condensers or all three PCCS condensers. For simplicity, the dimension of the PUMA ICS and PCCS pools are kept similar. Each pool is partitioned into three pie-shaped sections (similar to the PUMA GDCS pool), with an opening at the bottom of the partitions to allow for communication.

The height of the pools is determined by the need to accommodate the 1/4 scale water height. The water level is controlled by a system which can supply water from a storage tank located at the ground level. The water is fed independently into the bottom of the pool. The dimension of the PUMA PCCS and ICS pools is given in Table 7.14. For simplicity, the dimension of the PUMA ICS and PCCS pools are kept the same.

A schematic of the PUMA PCCS system is shown in Figure 7.21. The inlet for each PCCS condenser is connected to the upper drywell. In order to simulate the effect of the steam/non-condensate distribution in upper drywell on the PCCS condenser performance, three sets of steam feedlines are provided with manual valves. These steam feedlines can selectively supply to the PCCS condenser from the center, middle or wall locations of the upper drywell. The diameter of the PCCS steam supply lines is determined by boundary flow scaling.

A schematic of the PUMA ICS system is shown in Figure 7.22. The inlet for each ICS is connected to the RPV via the DPV lines. Since there are two DPV lines in PUMA, one line from the DPV is branched into two lines to allow for a total of three ICS supply lines. The diameter of the ICS steam supply lines is determined by boundary flow scaling. A summary of the PUMA ICS and PCCS line sizes are given in Table 7.14.

Table 7.14 PUMA PCCS/ICS Pool Design Parameters

• Number of Pools:	2 (3 condensers each)		
• Tank Height:	1450 mm		
• Tank Diameter:	1225 mm		
• Connecting Lines:			
Line Function	Line From	Line To	Pipe ID (mm/inch)
PCCS Supply	Drywell	PCCS Tank	38.1/1.5
PCCS Non-Cond Vent	PCCS Tank	SP	38.1/1.5
PCCS Condensate Drain	PCCS Tank	GDCS Tank	25.4/1
ICS Supply	DPV Line	ICS Tank	38.1/1.5
ICS Condensate Drain	ICS Tank	RPV	25.4/1
ICS Non-Cond Vent	ICS Tank	SP	12.7/0.5

7.6 Automatic Depressurization System (ADS) Design

The ADS is part of the SBWR emergency core cooling system (ECCS). Its function is to depressurize the reactor so that the gravity-driven GDCS water can be injected into the reactor.

The ADS consists of eight safety relief valves (SRVs) and six depressurization valves (DPVs) and their associated instrumentation and control.

The SRVs are mounted vertically on top of the main steam lines (MSLs) in the drywell. Each SRV discharges steam through a discharge line to a point below the minimum water level in the suppression pool. Four DPVs are horizontally mounted on horizontal stub tubes connected to the RPV at about the same elevation as the MSLs. The two remaining DPVs are horizontally mounted on lines branching from each MSL. The SRVs are spring-loaded valves and can be operated in safety (steam pressure) mode and relief (power-actuated) mode. Each SRV is equipped with a pneumatic accumulator and a check valve for safety mode and manual opening functions. The DPVs are straight-through, squib-actuated, non-reclosing valves with a metal diaphragm seals. The DPV is closed with a cap covering the inlet chamber. The cap will readily shear off when pushed by a valve plunger actuated by an explosive initiator-booster. The DPV size provides about twice the depressurization capacity of an SRV.

The ADS automatically actuates on a water level (Level 1) signal that persists for at least 10 seconds. For the PUMA facility, Level 1 is defined as 900 mm above the Top Active Fuel (TAF). The SRVs and DPVs are actuated in groups of two or four valves at staggered times as the reactor undergoes relatively slow depressurization. In Table 7.15, the SRV and DPV capacity and their opening sequence are given.

Table 7.15 SRV and DPV Capacities and Sequence of Action for SBWR

Total Max. DPV Flow Capacity at Vessel Pressure	6.35 x 10 ⁶ kg/h. 7.481 MPa
Total Max. SRV Flow Capacity at Vessel	4.084 x 10 ⁶ kg/h.
Initiating Signal (Level 1)	3600 mm (above TAF)
Max. Allowable Time Delay to Confirm Level 1 Signal	10 s
Valve Actuation Sequence after Level 1 Signal Confirmed:	
4 SRVs	0.0 s
4 SRVs	10 s
2 DPVs	55 s
2 DPVs	100 s
2 DPVs	145 s

For the PUMA facility, the four SRVs on each MSL are replaced by one SRV line. From boundary flow scaling, the size of the SRV line is scaled by 1/10. Thus four 203 mm (8 inch) SRV lines are replaced by a 50.8 mm (2 inch) SRV line. For the discharge nozzle, the nozzle size is scaled by $1/(10 \times \sqrt{2})$, according to break flow scaling criteria. In PUMA, the four DPVs on the RPV are replaced by two DPVs, and each DPV on a MSL is replaced by one DPV each. In Table 7.16, the sizes of DPVs and SRVs in the PUMA facility are compared to the prototype SBWR system.

The plan view of the ADS is shown in Figure 7.24. On one of the MSLs, the DPV is treated as a MSL break for MSL break simulation. The front view of the ADS is shown in Figure 7.25. This figure indicates the DPV and SRV lines leading to the upper drywell and suppression pool. Full-port ball valves with electrical actuators are used for the opening and closing of the SRVs and DPVs. These ball valves have response times of 2 to 5 seconds. Each of the SRVs and DPVs are instrumented with flow, temperature and pressure measurement devices. A typical ADS line is shown in Figure 7.26. The ball valve is followed by pressure and temperature sensors, then a capacitance meter and a magnetic flow meter. At the end of the line a flow nozzle of appropriate size is used for measuring flow with DP transducers. The opening and closing of the ball valve is controlled by a logic circuit which is monitored from the computer control network.

Table 7.16 Automatic Depressurization System (ADS) for PUMA Facility

Component	SBWR (mm/inch)	PUMA (mm/inch)	Area Scale
SRV line	203/8 (4 each)	50.8/2 (1 each)	1/100
SRV Nozzle	203/8 (4 each)	29/1.13 (1 each)	1/200
DPV (MSL) line	305/12	76.2/3	1/100
DPV (MSL) Nozzle	305/12	21.6/0.85	1/200
DPV (RPV) line	457/18 (4 each)	76.2/3 (2 each)	1/100
DPV (RPV) Nozzle	457/18 (4 each)	30.5/1.2 (2 each)	1/200

7.7 Feed Water Line (FWL) and Auxiliary Reactor Coolant System

Main components of the Feed Water Line (FWL) and auxiliary reactor cooling system are shown in Table 7.17.

Table 7.17 PUMA Feed Water Line: 2 Each

Auxiliary Systems			
● Components: 1) CRD, 2) RWCU/SDCS			
● Connecting Lines			
Line Function	Line From	Line To	Pipe I.D. (mm/inch)
RWCU/SDC Line	RPV Bottom	Aux. Tank	12.7/0.5
RWCU/SDC Line	Aux. Tank	RPV Side	25.4/1
CRD Line	Aux. Tank	RPV Bottom	25.4/1
RWCU/SDC & CRD Break	RPV Bottom	Drywell	50.8/2

7.7.1 Feed Water Line (FWL)

The SBWR FWL is designed to supply water to the RPV over the full range of reactor power operation. The two FWLs are vented from the turbine building and carry condensate the feed water lines (FWLs) consist of two 355.6 mm (14 inch) diameter lines connected to RPV nozzles. Each line branches into two lines which then connect to the RPV at an elevation near the top of the chimney section. The use of two lines minimizes the number of containment penetrations while providing two separate flow paths. Each of the four penetrations into the RPV connect to spargers located on the inside wall of the vessel. This design allows for proper feed water flow distribution in the downcomer region. The Control Rod Drive (CRD) system provides makeup water via the Reactor Water Clean-Up/Shut-Down Cooling (RWCU/SDC) system piping to the core any time the feed water flow is not available. The CRD and RWCU/SDC system are described in the following sections.

In the PUMA facility, the FWL is scaled by boundary flow scaling and two lines are combined into one. The PUMA FWL then branches into two lines symmetrically penetrate the RPV, as shown in Figure 7.27. Each FWL penetration then connects to a sparger as shown in Figure 7.28. The sparger flow area is scaled by the total sparger flow area in the SBWR. The choked area is sealed from the FWL nozzle area.

7.7.2 Control Rod Drive (CRD) System

The CRD system is designed to operate only when on-site AC power is available. As such, it is considered a non-safety system. The system is composed of three major components: Electro-hydraulic Fine Motion Control Rod Drive (FMCRD) mechanisms, Hydraulic Control

Units (HCU), and the Control Rod Drive Hydraulic Subsystem (CRDHS). The FMCRDs provide electric-motor-driven positioning for normal insertion and withdrawal of the control rods and hydraulic-powered rapid insertion (scram) of control rods during abnormal operation conditions. The hydraulic power required for scram is provided by high pressure water stored in the HCUs. Each HCU contains a nitrogen-water accumulator charged to high pressure and the necessary valves and components necessary to scram two FMCRDs. The CRDHS supplies demineralized water to provide charging of the HCU scram accumulators and purge water flow to the FMCRDs during normal operation. The CRDGS is the source of pressurized water for purging the RWCU/SDC system pumps. The primary task of the CRDHS is to provide high pressure make-up water to the reactor during events, such as LOCA, in which the feed water system is unable to maintain reactor water level. This makeup water is supplied to the reactor via a bypass line off the CRD pump discharge header which connects to the feed water inlet piping via the RWCU/SDC return piping.

In the PUMA facility, the following function of the CRD system is important, as it occurs during a reactor LOCA event: The CRD system supplies high pressure makeup water to the reactor when the normal makeup supply system (feed water) is unable to prevent reactor water level from falling below reactor water Level 2. In the PUMA facility the CRD system is simulated for the above function, as shown in Figure 7.28. The water is taken from the auxiliary tank and pumped to the CRD line. Part of it is bypassed to the feed water line through RWCU/SD system return lines. Here a break on the CRD line is also shown. The pipe sizes of the CRD lines are scaled by the boundary flow scaling method. The CRD lines are only on the "B" feed water line.

7.7.3 Reactor Water Clean-Up/Shut-Down Cooling (RWCU/SDC) Systems

The RWCU/SDC system is designed to operate only when on-site AC power is available. Hence, similar to the CRD system, it is also considered as a non-safety system. The RWCU/SDC system performs two basic functions: reactor cleanup and shutdown cooling functions. The important functions of RWCU/SDC that apply to PUMA facility are the control of reactor water level during shutdown and shutdown checking. The RWCU/SDC system is composed of two independent pump-and-purification equipment systems. During normal plant operation, the system continuously recirculates water taken from the mid-RPV level and from the reactor bottom and returns it via the feed water line to the RPV.

In the case of the loss of preferred off-site AC power, the RWCU/SDC system brings the plant to cold shutdown in 36 hours in conjunction with the ICS. Following a transient, the RWCU/SDC system has the capacity of removing the core decay heat, plus compensate the CRD purge flow, one-half hour following scram. One of the possible LOCA events is the break

of the RWCU/SDC line near reactor bottom. This break has the potential of draining reactor coolant coming from both RWCU/SDC lines, one near mid-section of reactor and the other at the bottom, through the break. In Figure 7.28, the RWCU/SDC system for PUMA facility is shown with the break location.

7.8 Stored Heat, Heat Loss and Insulation Design

7.8.1 Stored heat in RPV wall

The relatively thick wall (154 mm) of the reactor pressure vessel (RPV) has a very large heat capacity and will act as an important source of stored energy during the reactor blowdown process. In addition to the core decay heat, stored energy from the vessel wall will be released into the reactor, adding to the fluid enthalpy. This additional source of heat needs to be properly scaled in order to balance the total energy of the system.

The stored energy in the prototype vessel wall cannot be readily physically scaled in PUMA, due to its relatively thin walls. An alternative would be to install electric heaters on the outer perimeter of the PUMA RPV in order to match the scaled stored energy. This procedure is also difficult to implement, since the electric heaters need to be distributed in such a way as to provide uniform heat to the wall in order to avoid localized heating. In addition, adequate insulation needs to be added to prevent heat loss from the electric heaters to the surrounding ambient environment.

The approach taken here is to quantify the amount of stored energy in the SBWR vessel wall, and then scale this energy to the PUMA model. The scaled energy can then be compared to the core decay energy in order to gauge its magnitude to the overall energy. This would determine how the additional energy can be added to the system through the core heaters. The stored heat from the vessel wall can also be calculated as a function of time to observe the importance of the heat release as it decreases with time.

The one-dimensional, transient heat conduction equation for a wall can be written as

$$\frac{\partial^2 T}{\partial x^2} = \frac{1}{\alpha} \frac{\partial T}{\partial t} \quad (7.40)$$

The initial and boundary conditions for the RPV wall are

$$\begin{aligned}
 T(x,0) &= T_i \\
 T(0,t) &= T_S = f(t) \\
 \frac{\partial T}{\partial x} \Big|_{x=L} &= 0
 \end{aligned}
 \tag{7.41}$$

The information needed to evaluate $f(t)$ is obtained from SBWR vessel blowdown curves, where TRACG has been used to predict vessel pressure as a function of time. The saturation temperature is then correlated in terms of pressure in order to obtain the inside vessel wall temperature as a function of time.

Solving Eq. (7.40) for a constant surface temperature, using the initial and boundary conditions listed above, the approximate solution given a semi-infinite slab assumption

$$\frac{T_x - T_i}{T_s - T_i} = 1 - \operatorname{erf} \frac{x}{2\sqrt{\alpha_s t}}
 \tag{7.42}$$

In order to calculate T_i and obtain the wall temperature profile, the following iteration scheme was implemented:

$$T_i |_{t=j+1} = T_i(x=L) |_{t=j}
 \tag{7.43}$$

Figure 7.29 shows the temperature profile for several time steps beginning from 600 seconds, which is the time at which the RPV is at 1.034 MPa (150 psi) following a loss of feedwater break. The calculations show that within one hour of the initial blowdown, a nearly uniform temperature profile exists across the RPV wall. Hence, shortly after one hour from the initial blowdown, the RPV wall no longer acts as an important heat source and no additional measures need to be taken into account in PUMA for scaling purposes.

The total amount of heat released to the inside of the vessel from the RPV wall can then be estimated by

$$q = \rho c_p V \Delta T_m
 \tag{7.44}$$

where the mean wall temperature difference, ΔT_m , from 600 seconds to 5 hours after blowdown, can be estimated from Figure 7.29 to be approximately 84°C. The total amount of heat released to the inside of the vessel within this time period is then calculated to be approximately 0.6948 MJ. Scaling this value by the power scaling criteria of 1/200, results in the PUMA heat loss equivalent of 3.474 kJ. This amount of additional heat needed to properly scale the RPV wall heat loss can be readily compensated by increasing the PUMA core electrical heaters. Hence, there is no need to install additional electrical heaters on the outer surface of the PUMA RPV to simulate the heat loss.

Finally, Figure 7.30 illustrates the heat transfer calculated for the SBWR RPV wall as a function of time, following blowdown and using the calculation procedures described above. The curve shows an initial sudden rise in heat transfer, which is due to the fact that after the initial blowdown there is a sudden depressurization taking place in the vessel, resulting in lower saturation temperatures inside the vessel. This creates a steep temperature gradient between the inside of the vessel and the vessel wall, which still maintains a large amount of stored heat. The rate of heat transfer reaches a peak at about 800 seconds and then begins to decrease as the thermal penetration depth extends further into the vessel wall, thus reducing the thermal gradient.

The heat transfer profile of the vessel wall can also be simulated in PUMA when the power to the electrical heaters is increased to compensate for the vessel wall. This may be accomplished by inputting a time function to the designated power controllers to follow a similar profile as that in the prototype.

7.8.2 Containment heat sink design

Due to the massive concrete wall structure of the SBWR containment, the concrete has the potential to serve as an important heat sink during the reactor blowdown process. As steam comes into contact with the containment wall, condensation will occur due to the cold surface of the wall. This rate of heat removal needs to be properly scaled in order to match the boundary flow of energy.

To properly scale the containment heat sink in PUMA, it is necessary to evaluate the temperature penetration and the thermal inertia of the concrete wall structure to obtain appropriate scaling parameters.

Treating the wall as a semi-infinite slab, the one-dimensional transient heat conduction equation is given by Eq. (7.40). By using the thermal diffusivity of the containment wall α_c and the following initial and boundary conditions

$$\begin{aligned} T(x, 0) &= T_i \\ T(0, t) &= T_o \\ T(\infty, t) &= T_i \end{aligned}$$

the solution of the temperature profile for the above equation can be expressed in terms of the heat flux at the surface ($x=0$):

$$q'' \Big|_{x=0} = \frac{k_s (T_o - T_i)}{\sqrt{\pi \alpha_s t}} q'' \Big|_{x=0} = k_s \frac{\partial T}{\partial x} \Big|_{x=0} \quad (7.45)$$

Equation (7.45) shows that the thermal penetration depth, d_{th} , can be given by

$$d_{th} = \sqrt{\pi \alpha_s t} \quad (7.46)$$

Proper scaling of the penetration depth would result in the correct temperature profile in the containment wall structure. Since the time scaling in PUMA is half that of the SBWR, the thermal penetration ratio can be written as

$$(d_{th})_R = \sqrt{\frac{(\alpha_s)_R}{2}} \quad (7.47)$$

In order to obtain an appropriate scaling parameter for the thermal inertia of the wall structure, an energy balance needs to be considered. The lumped parameter energy equation for the wall structure is

$$a_s \rho_s c_{ps} \frac{dT}{dt} = (\xi q'')_{in} - (\xi q'')_{out} \quad (7.48)$$

By non-dimensionalizing the above equation and performing several manipulations, an appropriate scaling parameter, the thermal inertia ratio, N_{th} , can be defined as

$$N_{th} = \left[\frac{a_s \rho_s c_{ps}}{a_f \rho_f c_{pf}} \right]_R \quad (7.49)$$

In order to properly scale the heat sink, as well as the heat transfer, the value of N_{th} should be unity. By defining the effective solid cross-sectional area, a_s , as the product of the inner circumference and the penetration depth, one obtains

$$a_s = \pi d d_{th} \quad (7.50)$$

Substituting Eqs. (7.46) and (7.50) into Eq. (7.49) and noting that $(a_f)_R = 1/100$, $d_R = 1/10$, and similar fluid properties, the thermal inertia ratio reduces to

$$N_{th} = \frac{10}{\sqrt{2}} (\sqrt{k_s \rho_s c_{ps}})_R \quad (7.51)$$

Substituting the properties of concrete into Eq. (7.51), the PUMA requirement necessary to satisfy proper scaling of the heat sink is obtained:

$$(k_s \rho_s c_{ps})_m = 20900 \quad (7.52)$$

This product has units of $J^2/s-m^4-K^2$. It is noted that this requirement only depends on the solid material properties. Based on commercially available material, with sufficient flexibility to be installed around cylindrical vessels it was found that fibrous-based acoustic tiles, ($\rho = 290 \text{ kg/m}^3$, $k = 0.058 \text{ w/m-K}$, $c_p = 1340 \text{ J/kg-K}$) which are commonly used in office buildings would best match the above criteria:

$$(k_s \rho_s c_{ps})_{\text{acoustic tile}} = 23000 \quad (7.53)$$

Hence, the concrete surrounding the containment in the prototype can be scaled very closely by using the fibrous-based acoustic tile as a source of heat sink in PUMA.

In order to evaluate the necessary thickness of the PUMA heat sink, the penetration depth in the SBWR needs to be estimated. Considering a time of 10 hours after the initial blowdown, Eq.

(7.46) can be used to calculate a penetration depth of 23.6 mm in the SBWR. Scaling the depth by a length scale of 1/10, the PUMA heat sink thickness is estimated to be 23.6 mm.

7.8.3 Design of insulation for heat loss

It is important to estimate the rate of heat loss from the PUMA components in order to quantify the amount of heat that needs to be added to the system to compensate for the losses. The estimated rate of heat loss in the system can be compensated for by increasing the power input to the system and preventing heat loss from distorting the thermodynamic equilibrium in the system.

The rate of heat loss from each of the components can be estimated by a simple one-dimensional heat conduction equation:

$$q'' = U\Delta T \quad (7.54)$$

where ΔT is the overall temperature difference. Since all major components in PUMA have a cylindrical geometry, the heat conduction equation can be expressed in cylindrical coordinates. The overall heat transfer coefficient, U , expressed in terms of the inside surface area for a cylinder with one layer of insulation and of unit length (Figure 7.31) is given by

$$U_1 = \left[\frac{r_1}{k_A} \ln \frac{r_2}{r_1} + \frac{r_1}{k_B} \ln \frac{r_3}{r_2} + \frac{r_1}{r_3} \frac{1}{h_o} \right]^{-1} \quad (7.55)$$

The outside heat transfer coefficient, h_o , can be determined from empirical free convection correlations. For vertical cylinders of height, L , satisfying the criterion given by,

$$\frac{d}{l} \geq \frac{35}{Gr_l^{1/4}} \quad (7.56)$$

the following correlation [7.12] is recommended to calculate the average heat transfer coefficient for both constant heat flux and constant surface temperature conditions over the entire range of Rayleigh number, Ra_l , under both laminar and turbulent conditions:

$$\bar{h} = \frac{k}{l} \left\{ 0.825 + \frac{0.387 Ra_l^{1/6}}{\left[1 + (0.492/Pr)^{9/16} \right]^{8/27}} \right\}^2 \quad (7.57)$$

where Gr_l and Ra_l are defined as,

$$Gr_l = \frac{g\beta\Delta TL^2}{\nu^2} \quad (7.58)$$

$$Ra_l = \frac{g\beta\Delta TL^3}{\nu\alpha} \quad (7.59)$$

In order to calculate the heat transfer coefficient from pipes, the following correlation [7.13] recommended for long horizontal cylinders over a wide Rayleigh number range can be used:

$$\bar{h} = \frac{k}{l} \left\{ 0.60 + \frac{0.387 Ra_d^{1/6}}{\left[1 + (0.559/Pr)^{9/16} \right]^{8/27}} \right\}^2 \quad (7.60)$$

In order to calculate the Rayleigh number, Ra , in the above equations, a wall temperature (T_w) of 35°C and ambient temperature (T_∞) of 24°C are assumed as being typical of normal operating conditions. For the major components, the calculated value of Ra ranges from 10^9 to 10^{11} , with an average free convection heat transfer coefficient calculated to be approximately 4 W/m²K. For pipe diameters ranging from 25.4 to 76.2 mm, which are typical of the pipe sizes in PUMA, Rayleigh number calculations range from 10^4 to 10^5 , with an average free convection coefficient calculated to be approximately 5 W/in²K.

Table 7.18 lists the estimated heat loss calculations for the PUMA RPV and the suppression pool, including three different pipe diameter sizes. Various insulation thickness are shown in order to choose an appropriate thickness for the insulation material. Each table specifies an assumed inside wall temperature for the specified component, which is based on the maximum temperature expected during the initial stage of each experiment. As this temperature decreases with time, the heat loss will also decrease. Calculations shown in these tables are maximum values and will decrease as the blowdown process continues. Considering 76.2 mm (3 inch)

insulation for the components listed, the overall heat loss is seen to be relatively small.

Similar calculations are also performed to estimate the heat loss from the PUMA containment. However, since a large portion of the containment surface area is covered by heat sink material (see Section 7.8.2 concerning scaling heat-sink material), this additional layer will also act as insulation and needs to be accounted for in heat loss calculations. Table 7.19 lists the estimated heat loss calculations for the PUMA containment with 31.75 mm (1.25 inch) thick heat sink material (fibrous acoustic tile) for various insulation thickness. Again, considering 76.2 mm (3 inch) insulation, the overall heat loss is seen to be relatively small.

The sum of all heat loss from the PUMA components and piping is estimated to be under 5 kW over the duration of the experiments. This amount of heat can be readily compensated by increasing the core electrical power.

7.9 Break Design

The double-ended pipe breaks on lines such as the GDCS drain, GDCS equalization, ICS condensate drain, RPV bottom drain, RWCU/SDC, and FWL are simulated in PUMA, as shown in Figure 7.31. The break sizes for the prototype are listed in Table 4.8. As seen in this table, the largest break size in this category is that of the FWL break (area 390 cm²). In PUMA, the break area is scaled by 1/200. The equivalent nozzle cross sectional area for the FWL break in PUMA is 1.95 cm². The break receiver tee shown in Figure 7.31 is 50.8 mm (2 inch) in diameter (cross sectional area 20.26 cm²). Thus, the flow area of the receiving pipe is about 10 times larger than the FWL break area. For choked flow through the break, the downstream conditions do not effect the flow through the break. For non-choked flow, the receiving tee is large enough such that there is no significant pressure loss in the drain side of this tee section. Also, as the receiving side of the tee has a large flow area compared to the break, the flow from the break and the top side of the tee are not affected, since there is no pressure build-up in the tee section. This break simulation requires a single instrument set to measure the total break flow coming out of the double-ended pipe break.

Table 7.18 PUMA component heat loss estimation

RPV		
insulation thickness (mm/inch)	heat flux (W/m ²)	heat loss (W)
0	500.20	6219.02
12.7/0.5	230.98	2871.79
25.4/1	152.21	1892.38
50.8/2	92.52	1150.29
76.2/3	67.75	842.35
101.6/4	54.17	673.49
127/5	45.58	566.68

SUPPRESSION POOL		
insulation thickness (mm/inch)	heat flux (W/m ²)	heat loss (W)
0	323.35	12337.83
12.7/0.5	143.62	5480.08
25.4/1	92.60	3533.29
50.8/2	54.43	2076.77
76.2/3	38.73	1477.86
101.6/4	30.17	1151.35
127/5	24.79	945.81

GDCS		
insulation thickness (mm/inch)	heat flux (W/m ²)	heat loss (W)
0	527.16	9603.88
12.7/0.5	173.32	3157.54
25.4/1	104.37	1901.46
50.8/2	58.73	1069.93
76.2/3	41.24	751.26
101.6/4	31.99	582.75
127/5	26.26	478.47

Table 7.18 continued...

3 INCH PIPELINE		
insulation thickness (mm/inch)	heat flux (W/m ²)	heat loss (W/m)
0	710.98	174.06
12.7/0.5	305.45	74.78
25.4/1	207.66	50.84
50.8/2	137.61	33.69
76.2/3	108.94	26.67
101.6/4	93.06	22.78
127/5	82.83	20.28

2 INCH PIPELINE		
insulation thickness (mm/inch)	heat flux (W/m ²)	heat loss (W/m)
0	716.36	118.16
12.7/0.5	360.42	59.45
25.4/1	258.16	42.58
50.8/2	179.99	29.69
76.2/3	146.56	24.17
101.6/4	127.57	21.04
127/5	115.13	18.99

1 INCH PIPELINE		
insulation thickness (mm/inch)	heat flux (W/m ²)	heat loss (W/m)
0	976.87	81.77
12.7/0.5	488.88	40.92
25.4/1	357.22	29.90
50.8/2	258.51	21.64
76.2/3	216.18	18.10
101.6/4	191.88	16.06
127/5	175.76	14.71

Table 7.19 Containment heat loss in PUMA with addition of fibrous-based acoustic tile to simulate concrete heat sink

TOP OF UPPER DRYWELL		
insulation thickness (mm/inch)	heat flux (W/m ²)	heat loss (W)
0	117.54	3015.73
0.5	81.14	2081.75
1	62.08	1592.80
2	42.42	1088.25
3	32.34	829.87
4	26.22	672.81
5	22.11	567.23

ANNULAR SECTION		
insulation thickness (mm/inch)	heat flux (W/m ²)	heat loss (W)
0	118.88	1385.40
12.7/0.5	91.44	1065.85
25.4/1	74.65	869.99
50.8/2	55.15	642.66
76.2/3	44.15	514.52
101.6/4	37.09	432.21
127/5	32.16	374.81

BOTTOM OF LOWER DRYWELL		
insulation thickness (mm/inch)	heat flux (W/m ²)	heat loss (W)
0	115.67	880.74
12.7/0.5	88.39	672.97
25.4/1	71.72	546.10
50.8/2	52.41	399.01
76.2/3	41.54	316.29
101.6/4	34.57	263.24
127/5	29.72	226.33

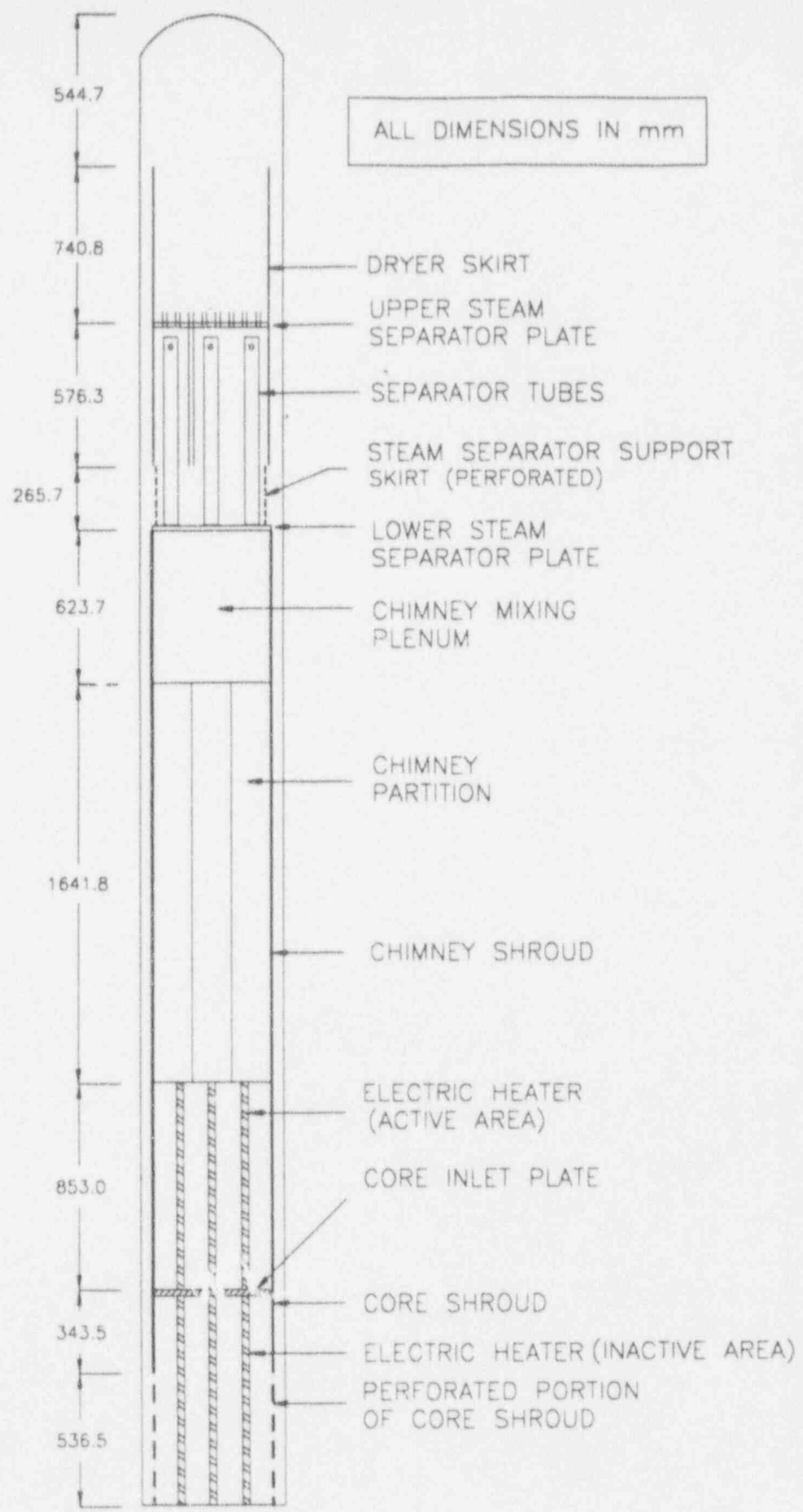


Figure 7.1 Reactor pressure vessel (RPV) and internal components

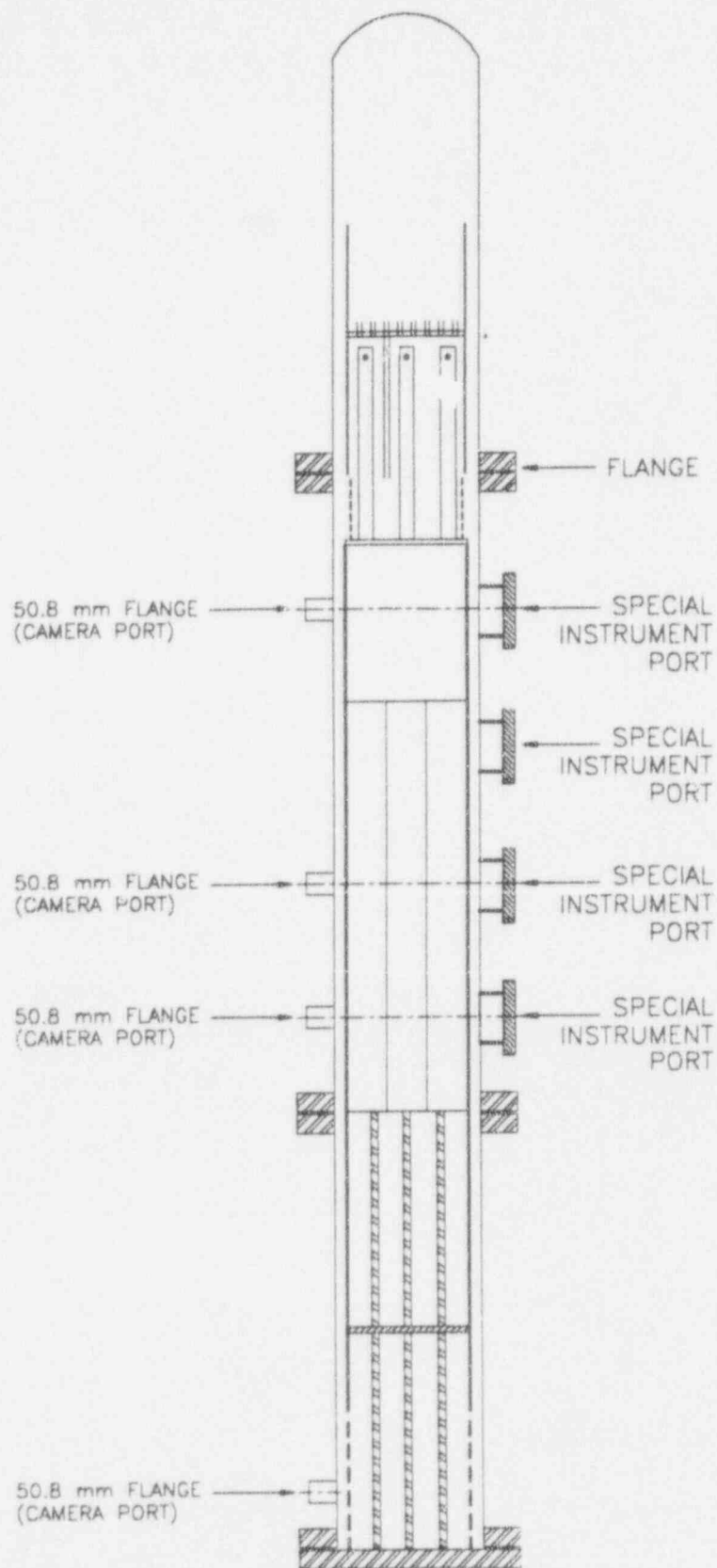


Figure 7.2 Flanges, view ports and special instrument parts on PUMA RPV

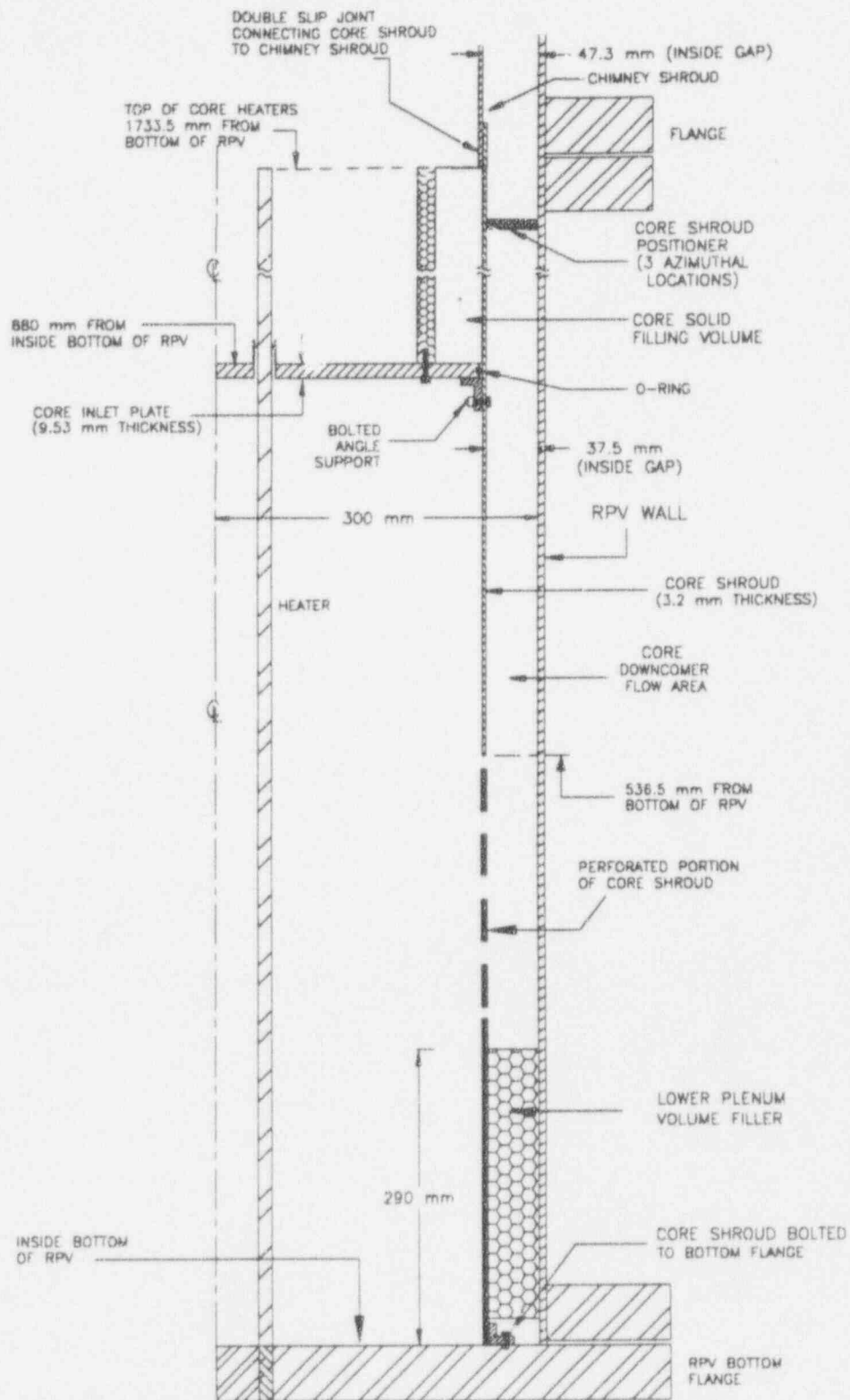


Figure 7.3 PUMA core shroud and mounting design

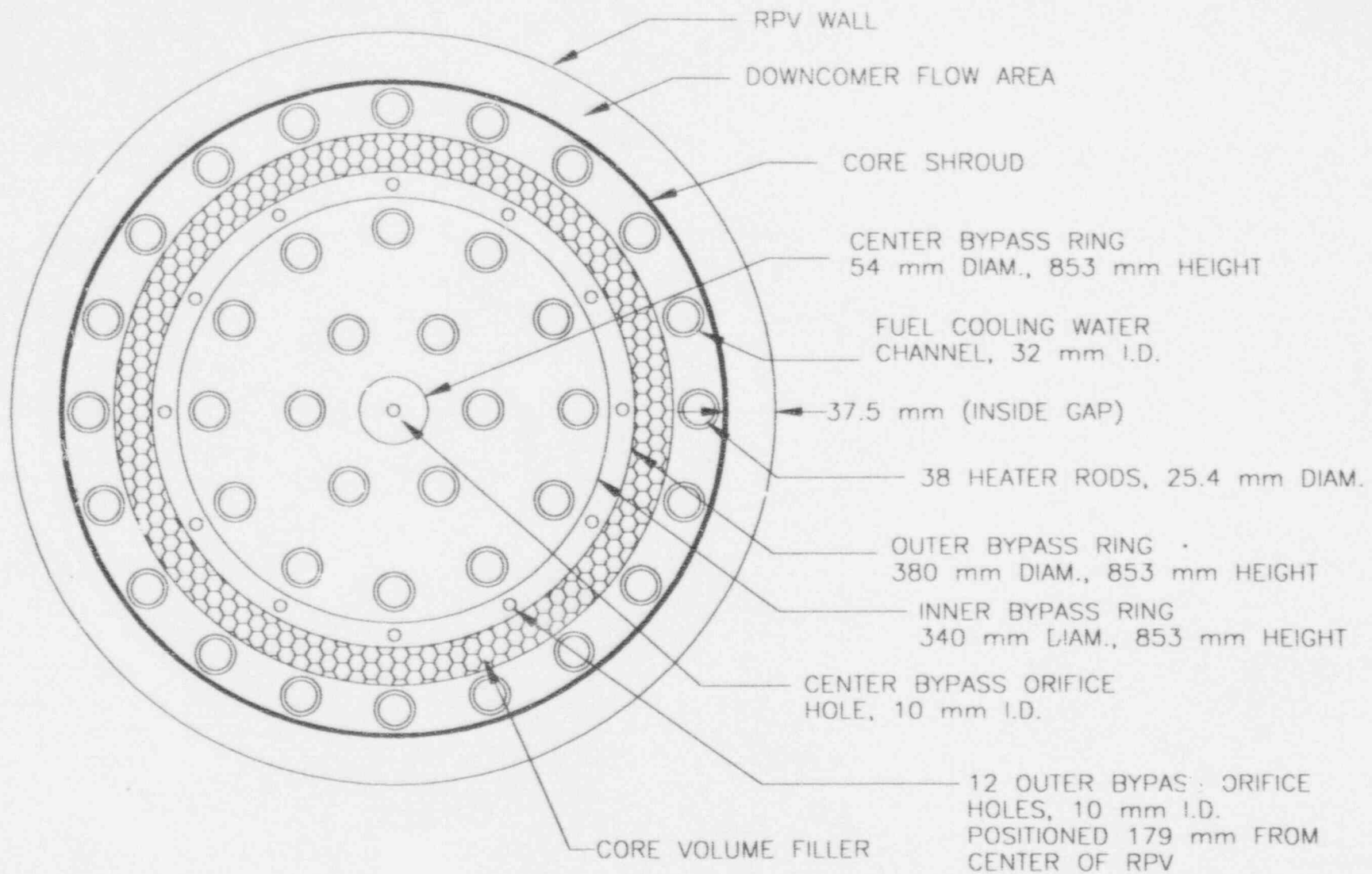


Figure 7.4 PUMA core inlet plate design showing heater and bypass flow area

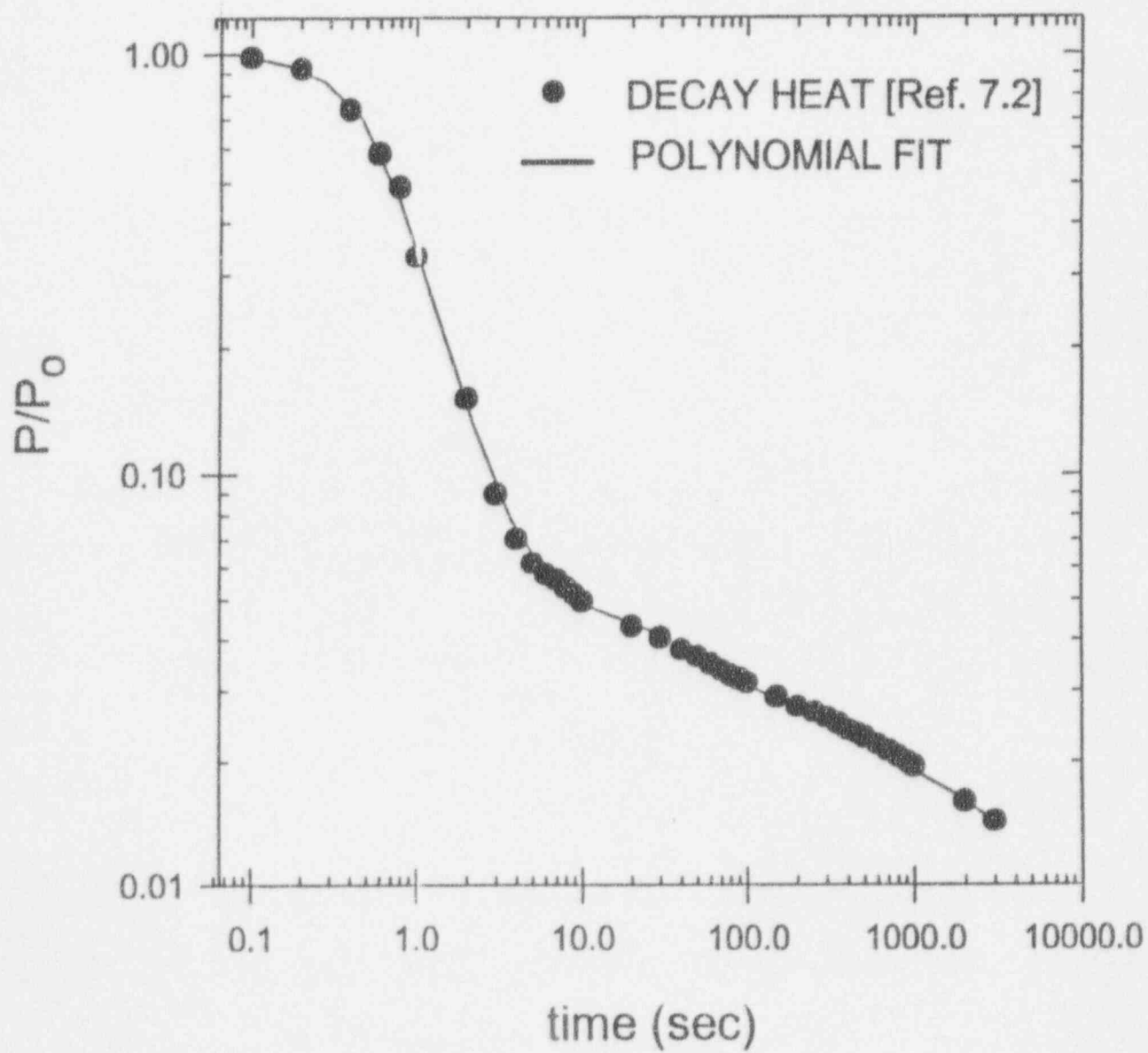


Figure 7.5 Decay heat curve fitting for SBWR

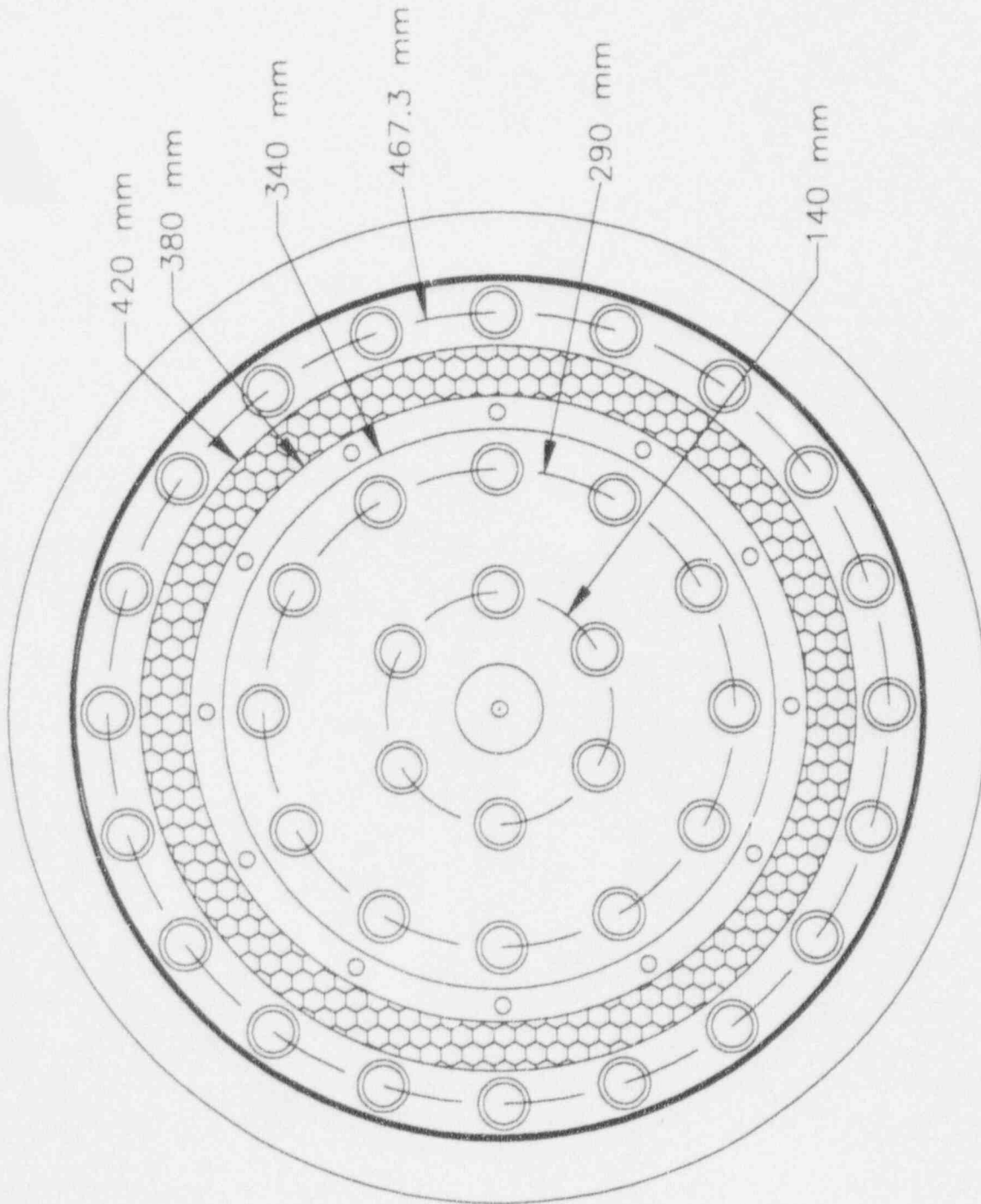


Figure 7.6 Cross-sectional view of PUMA core section

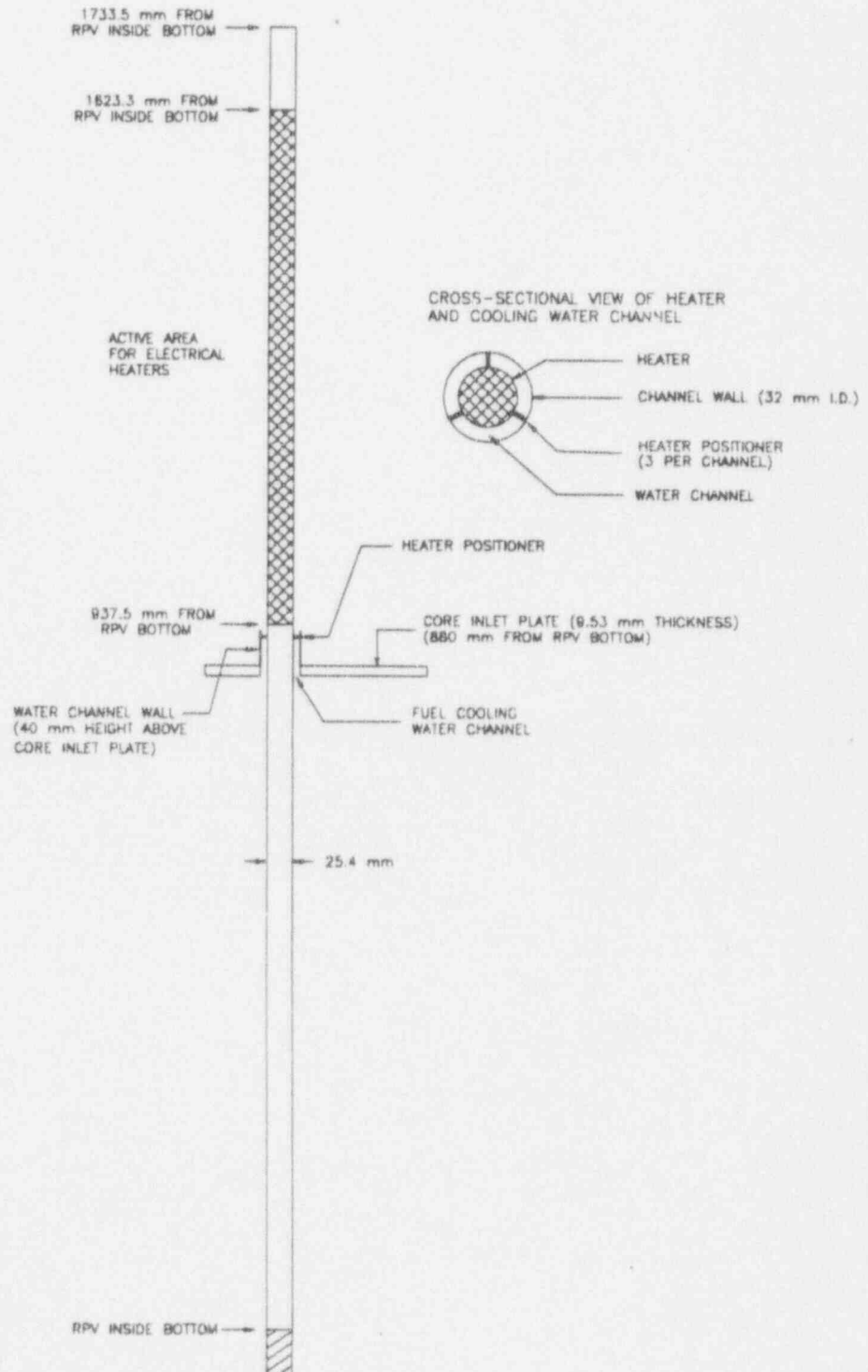


Figure 7.7 Typical heater design for RPV

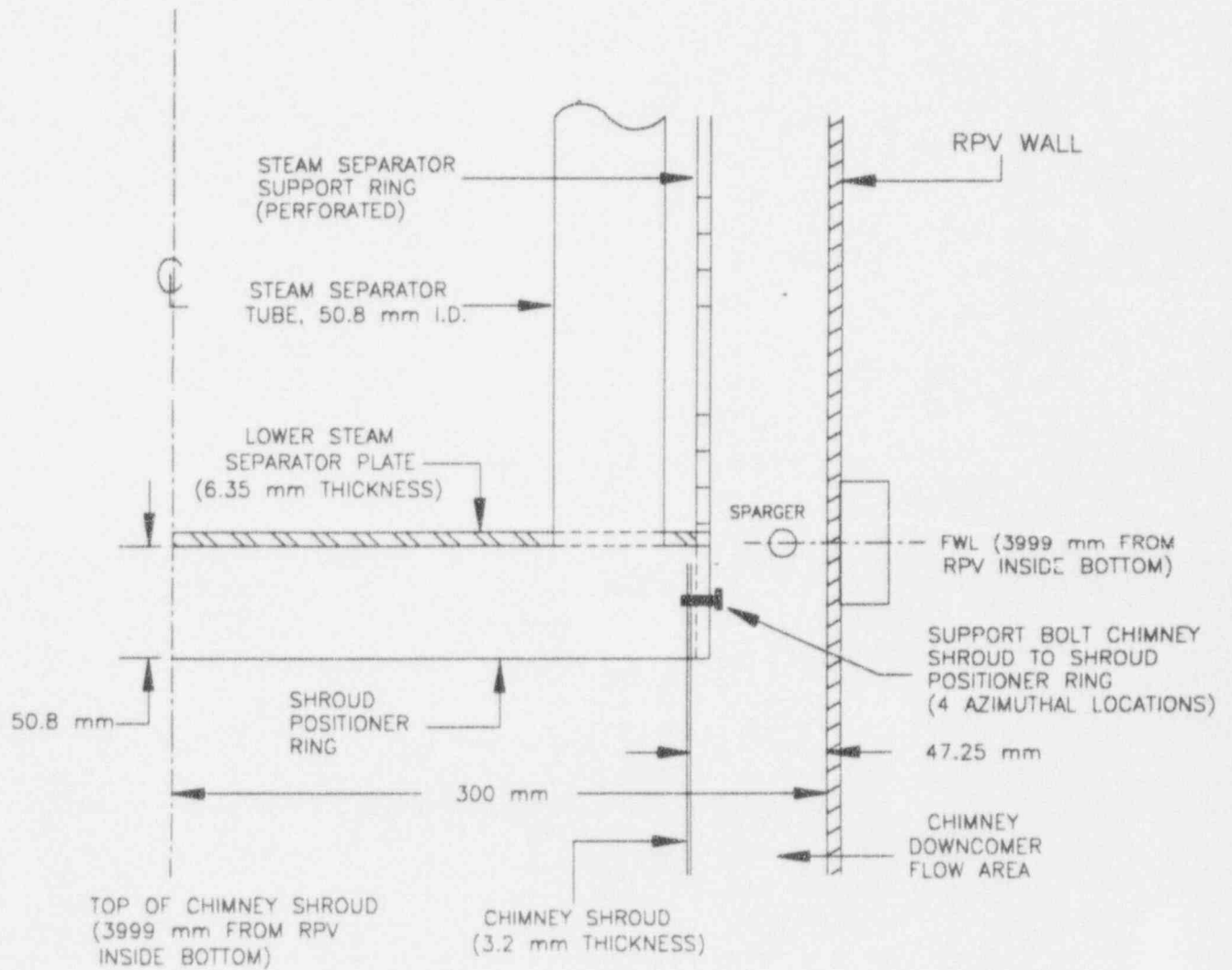


Figure 7.8 Top of chimney shroud and lower separate plate in PUMA RPV

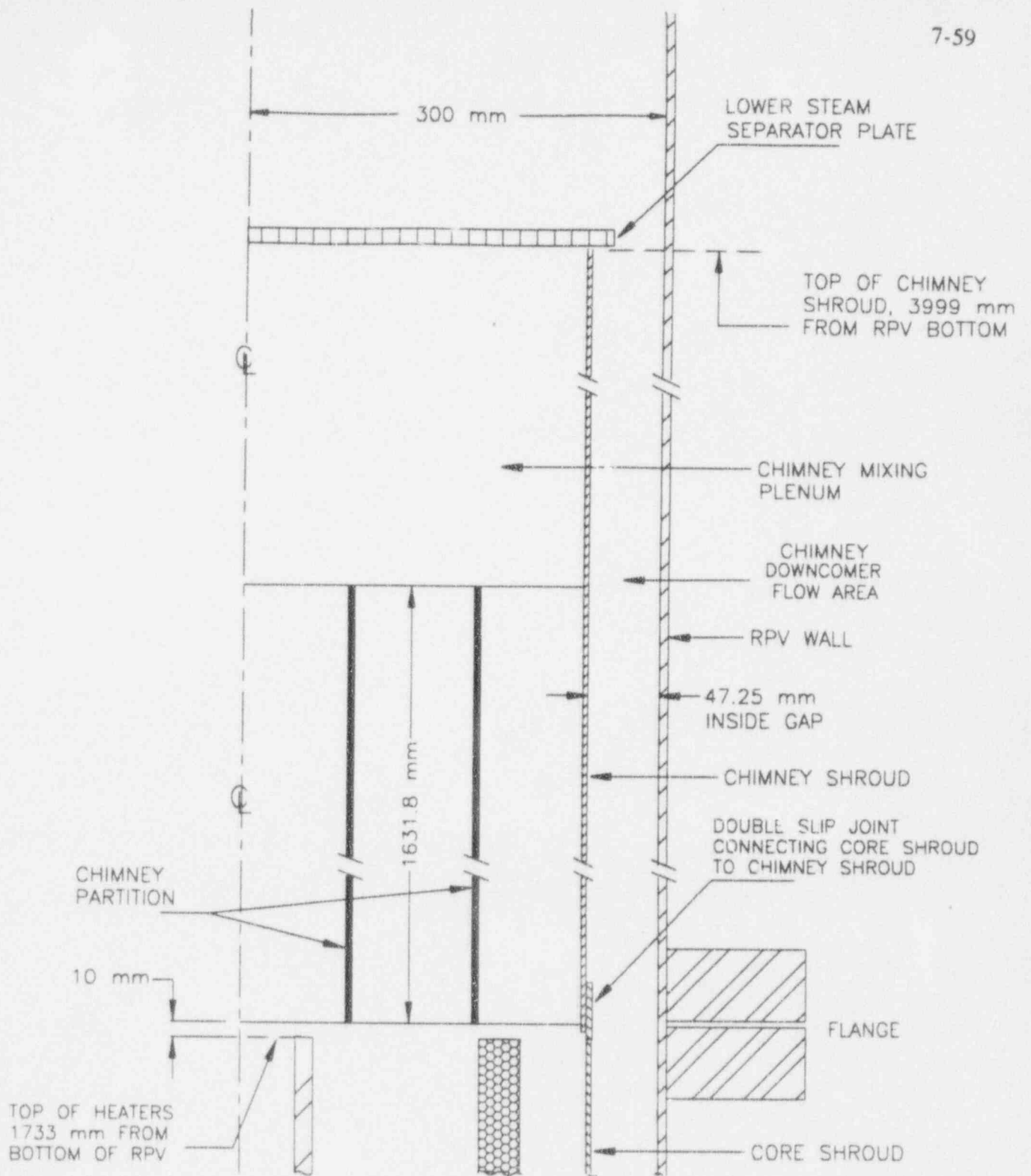


Figure 7.9 Chimney shroud and mounting design

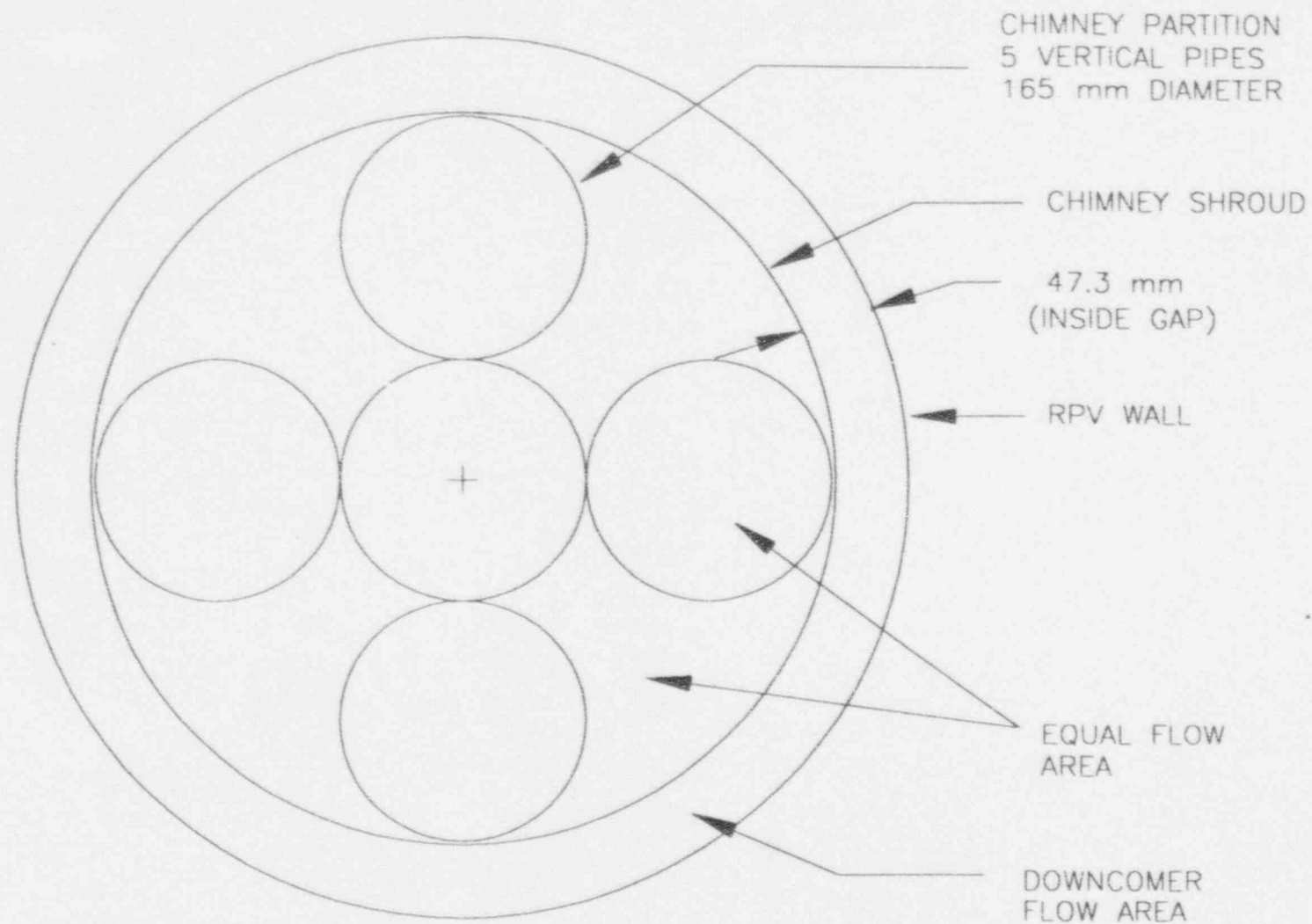


Figure 7.10 PUMA cross-sectional view of chimney partition

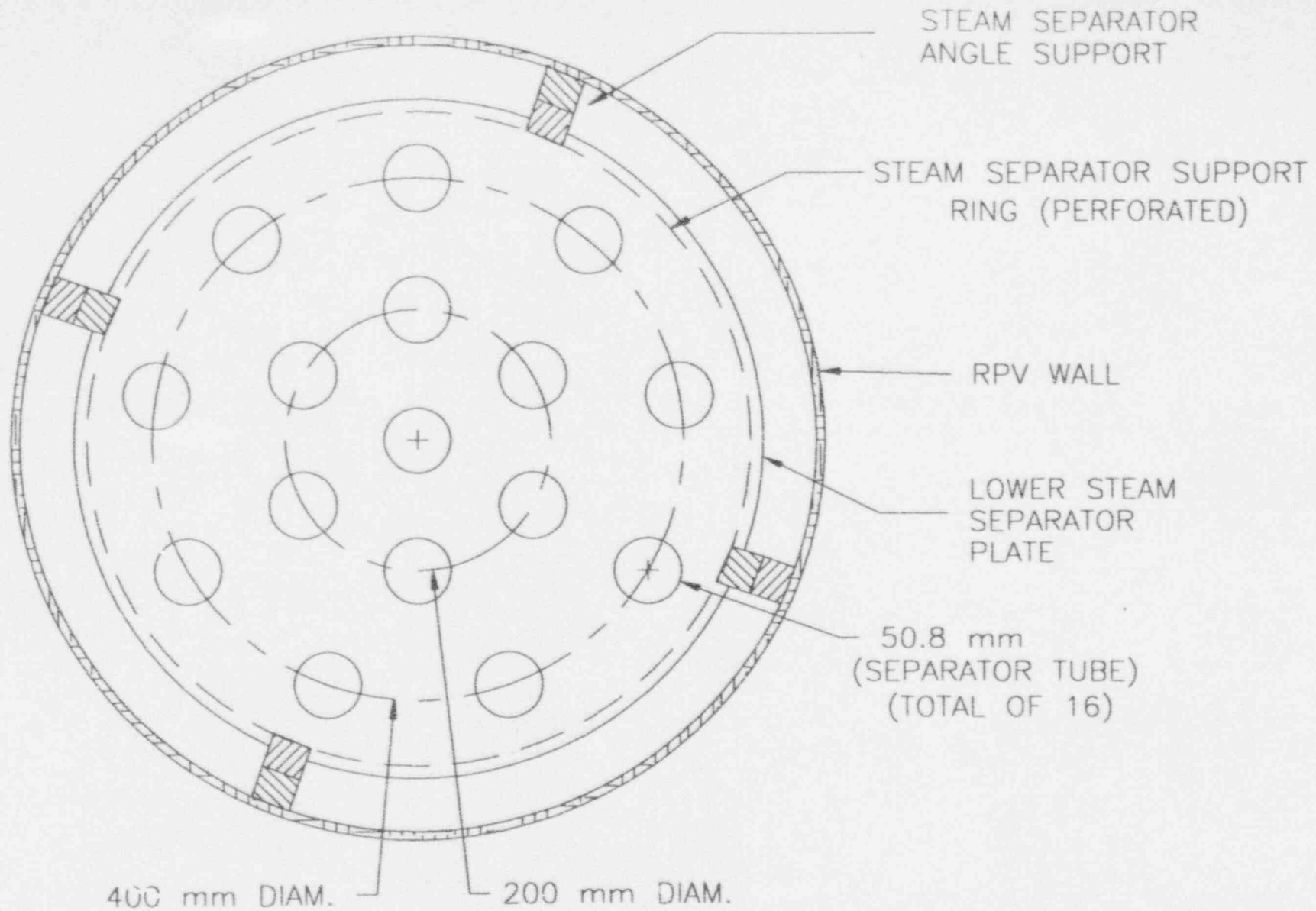


Figure 7.11 Separator tube layout on lower separator plate

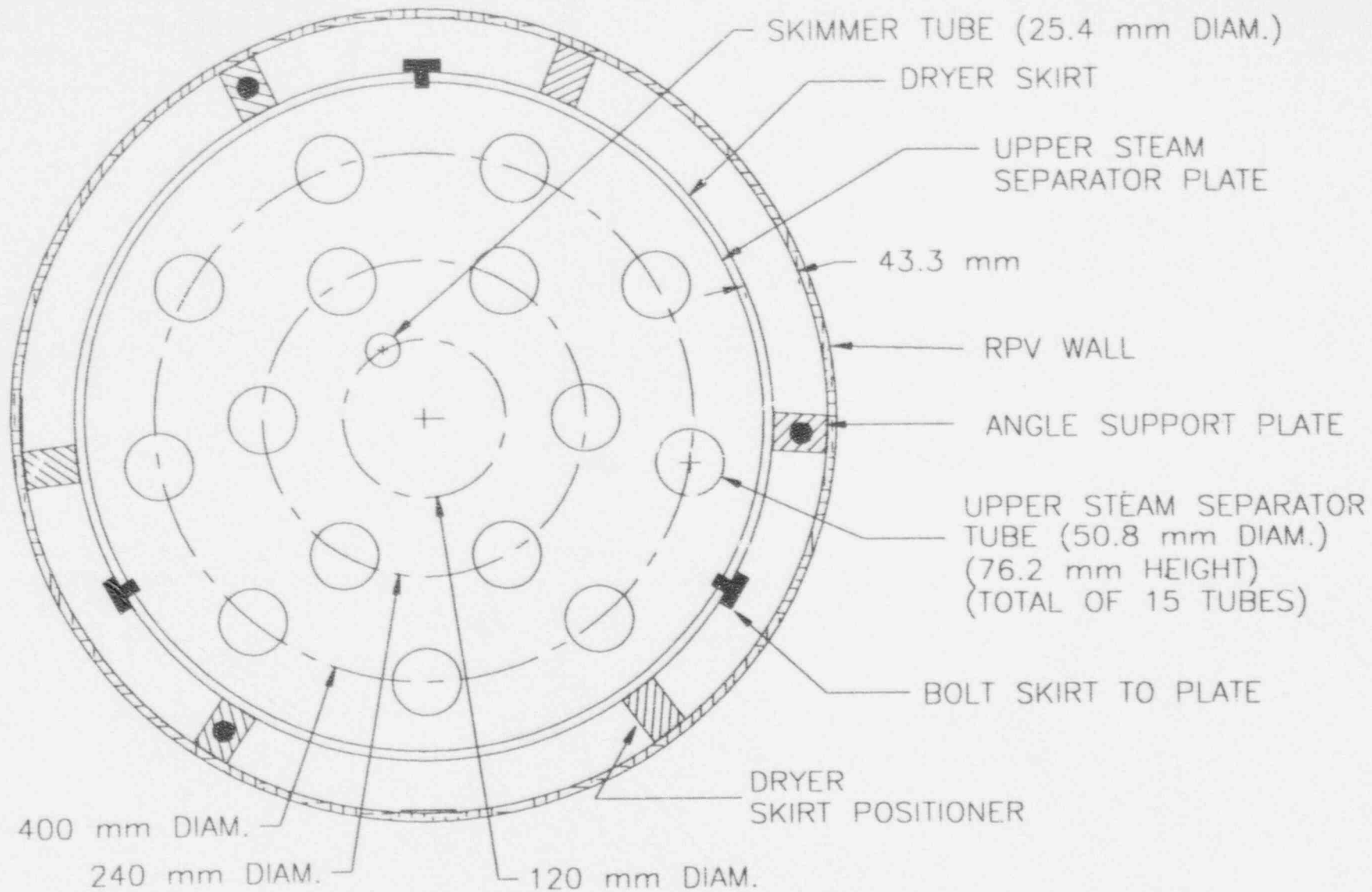


Figure 7.12 Orifice holes on upper separator plate and support structure on RPV

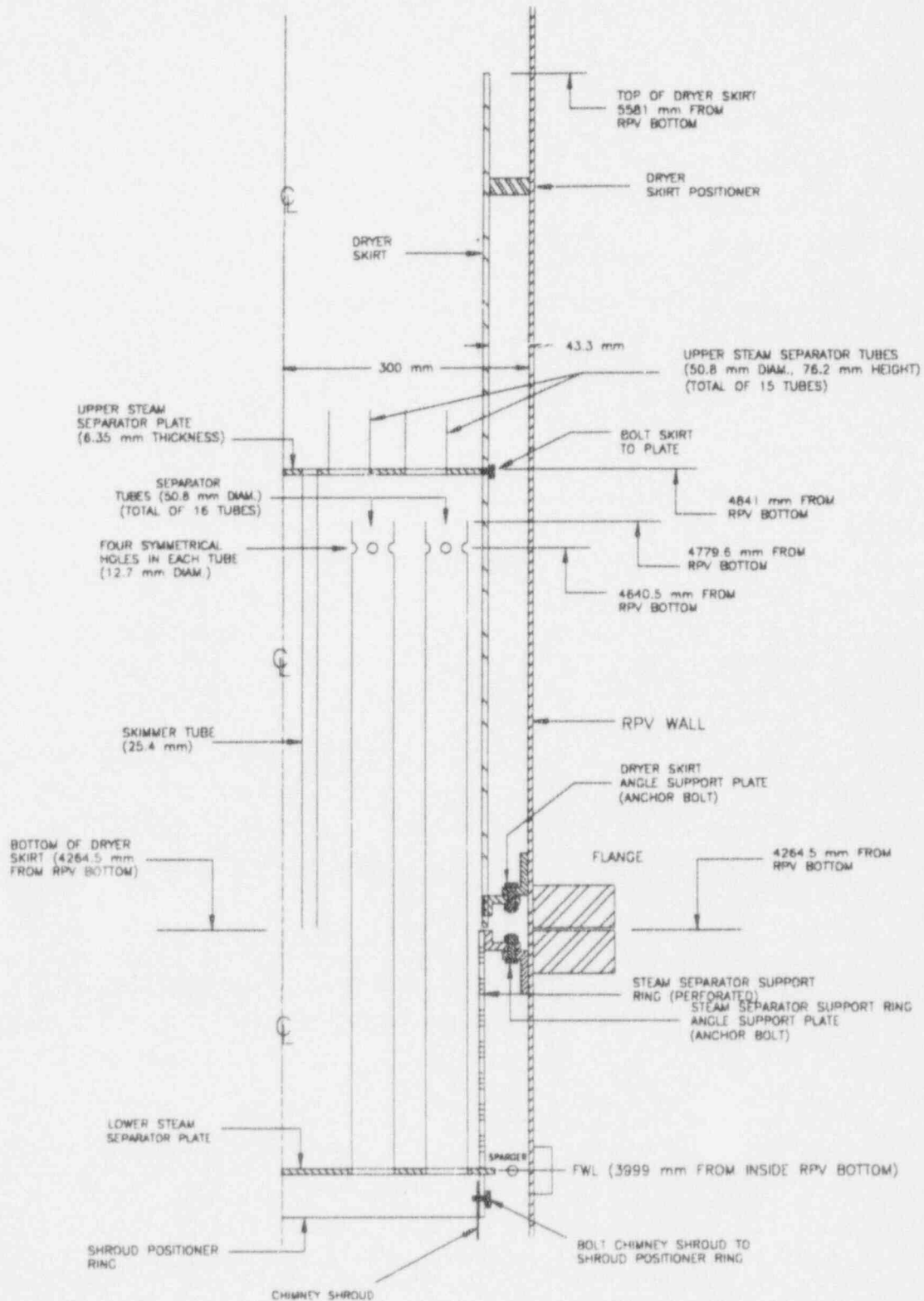


Figure 7.13 Mounting of separator section onto PUMA RPV, separator tube, and separator dryer shroud design

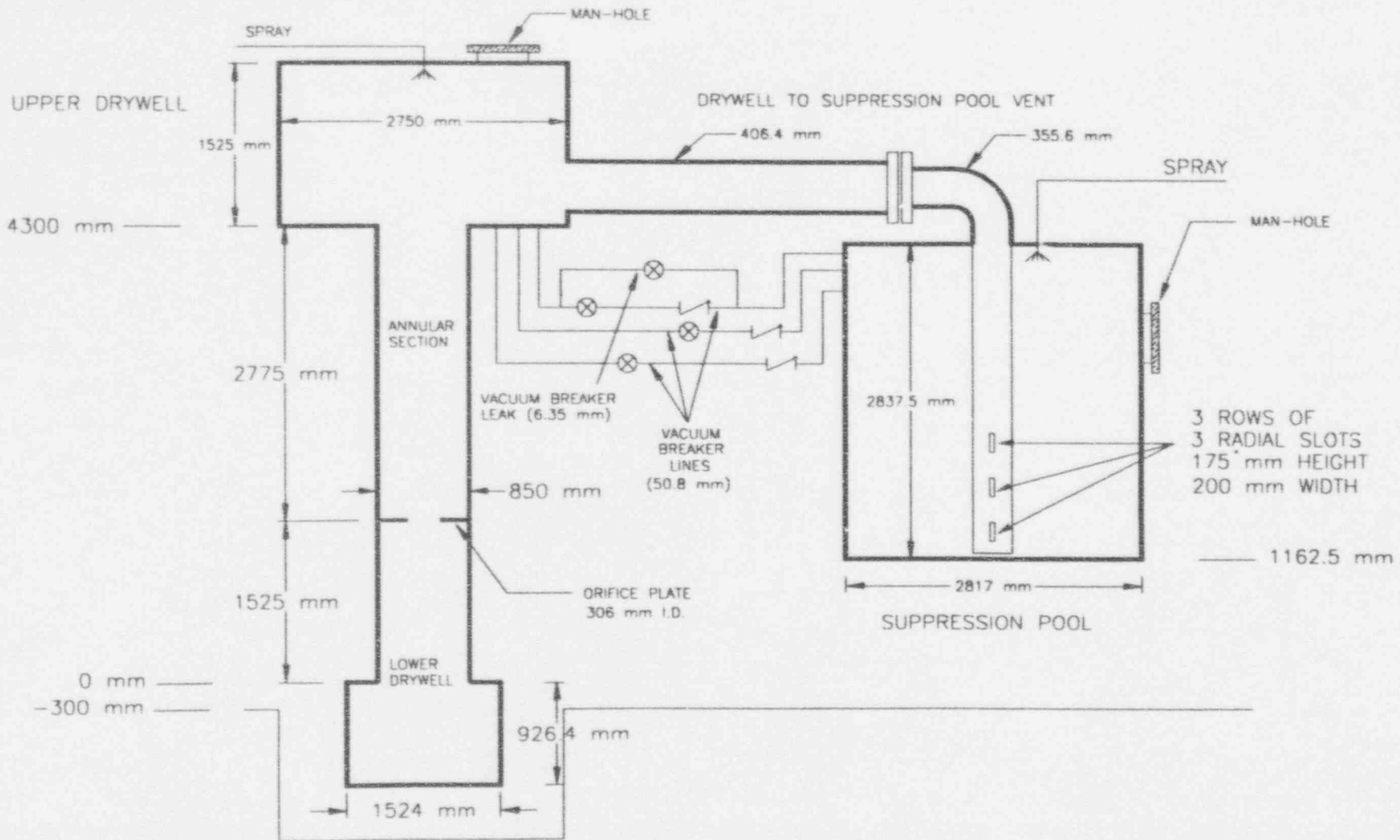


Figure 7.14 Design of drywell vessel, suppression pool vessel, connecting vent line and vacuum breaker lines

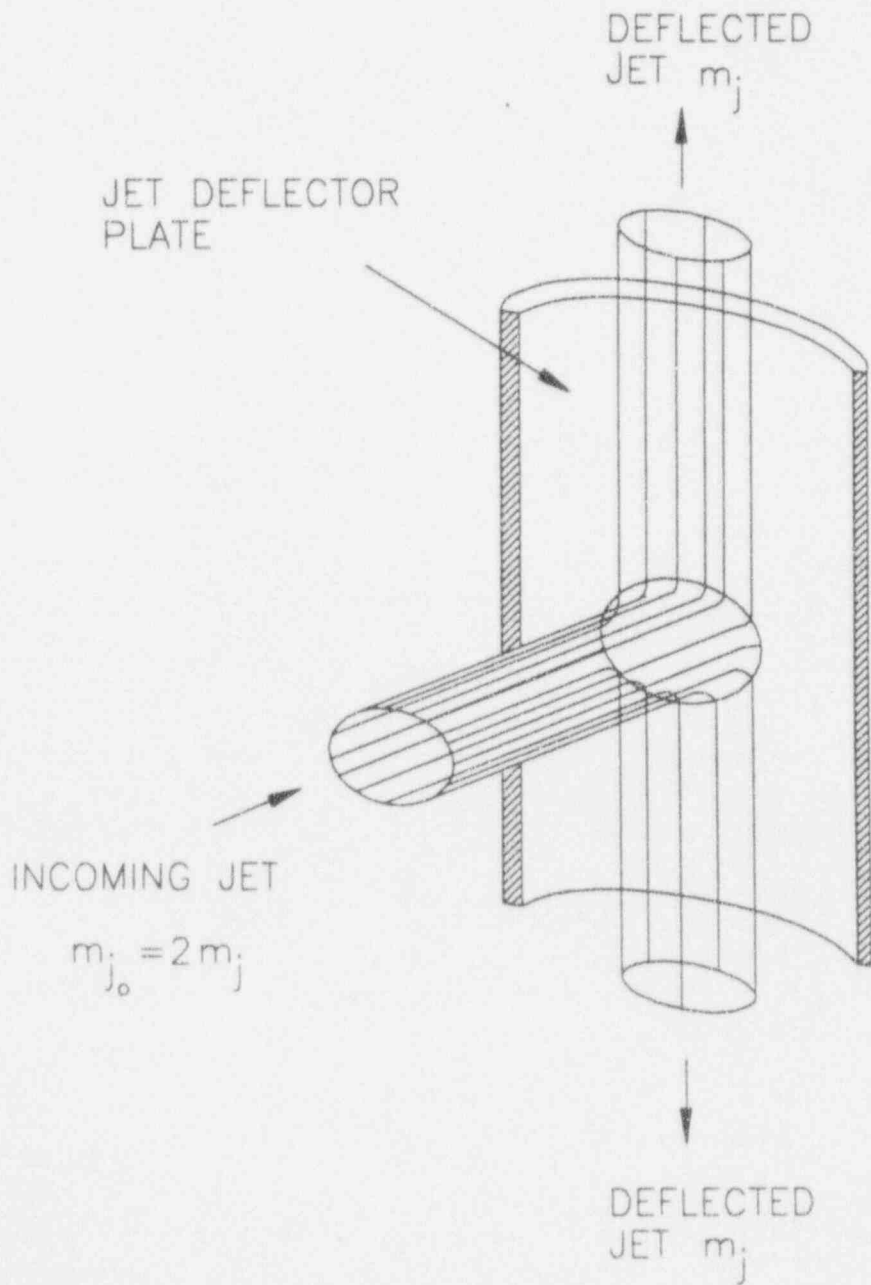


Figure 7.15 Jet deflector plate

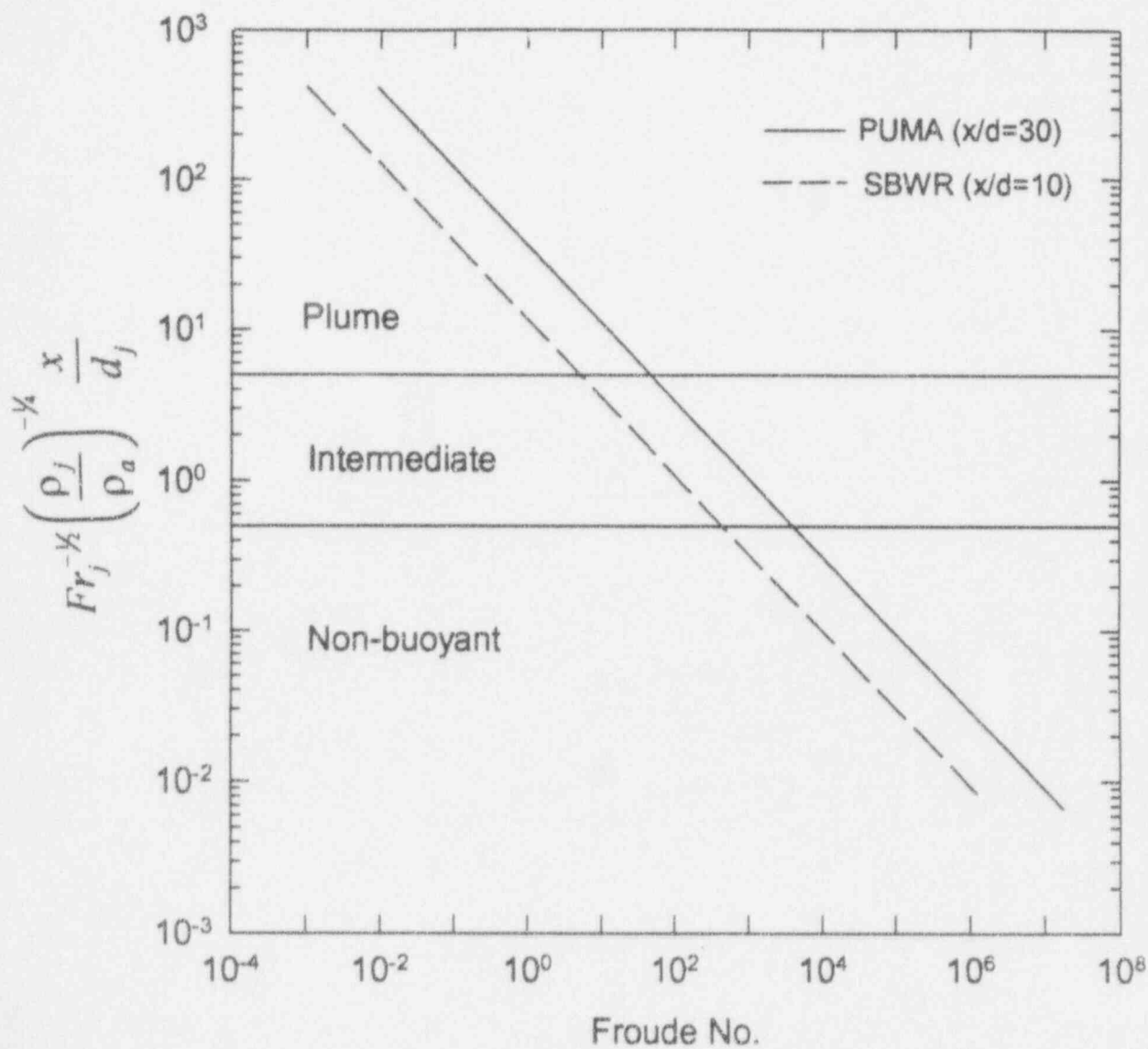


Figure 7.16 Jet flow regime transition as a function of Froude number

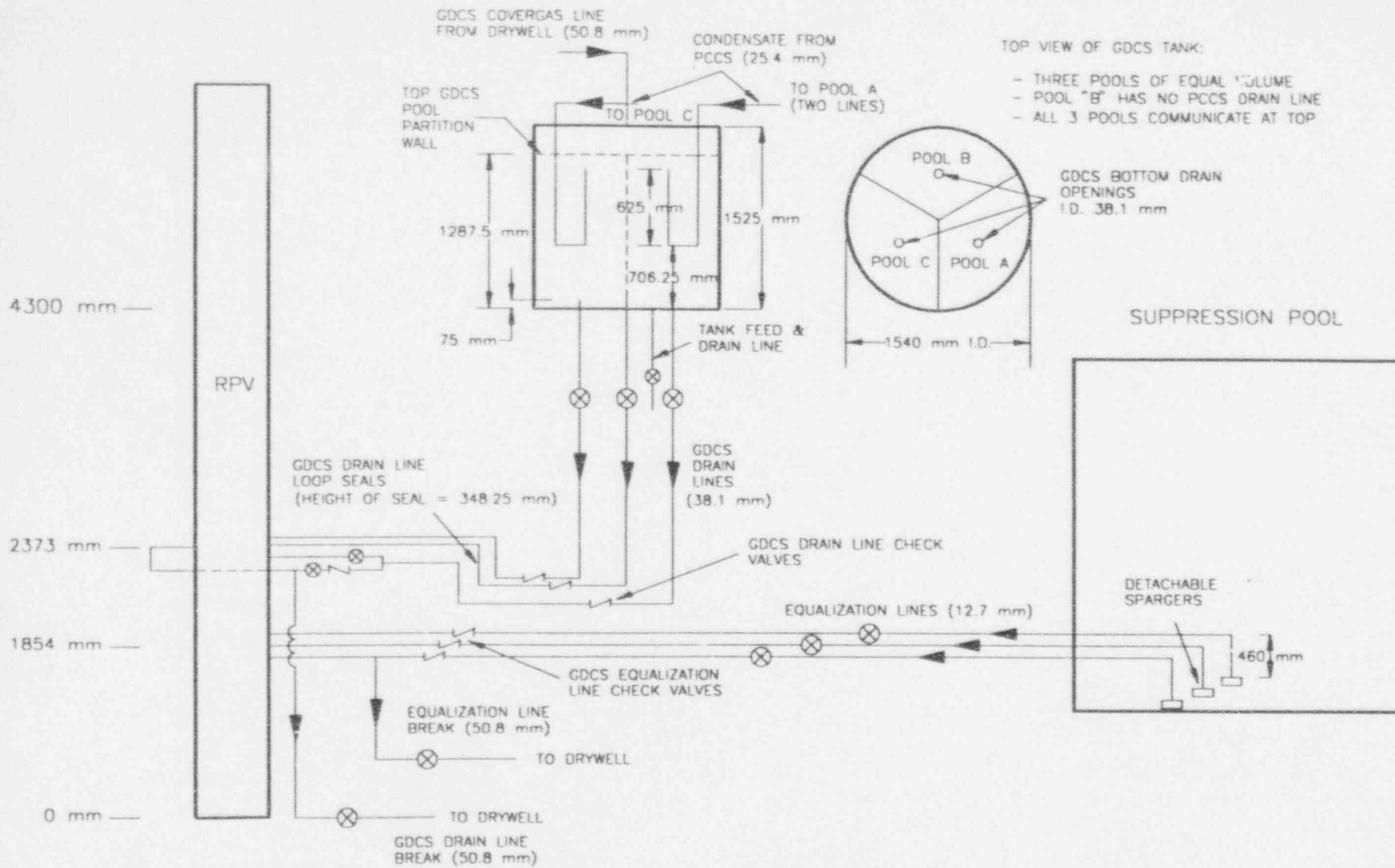
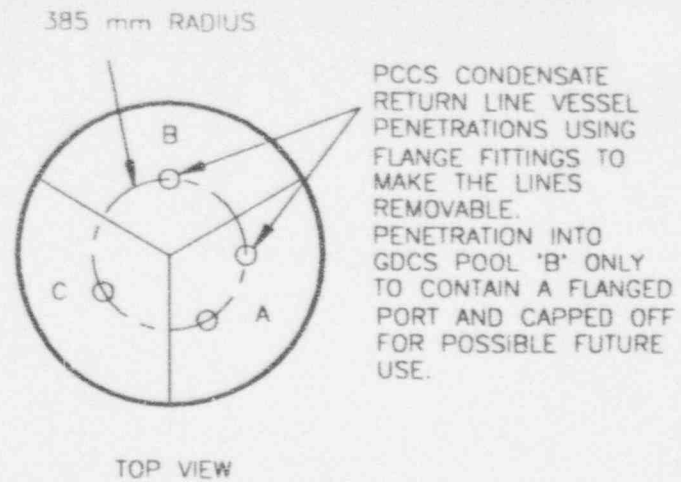
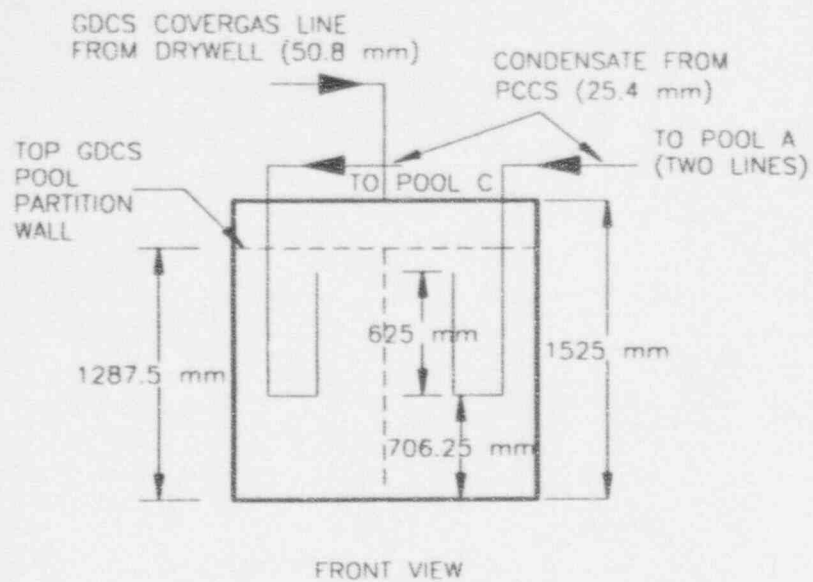


Figure 7.17 Gravity-driven cooling system (GDCS) design in PUMA



TOP VIEW OF GDCS TANK:

- THREE POOLS OF EQUAL VOLUME
- POOL "B" HAS NO PCCS DRAIN LINE
- ALL 3 POOLS COMMUNICATE AT TOP

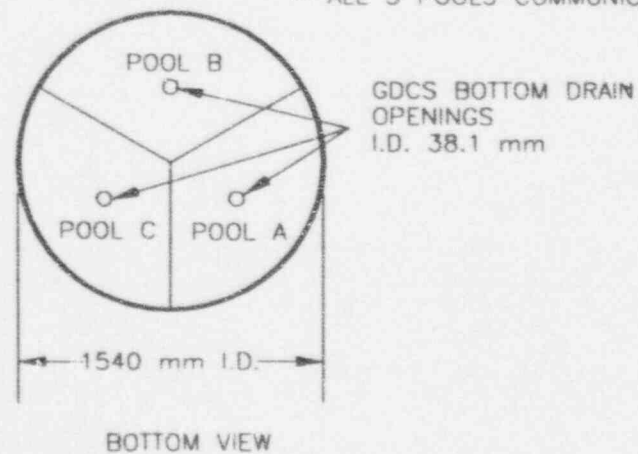


Figure 7-18 Design of GDCS pool

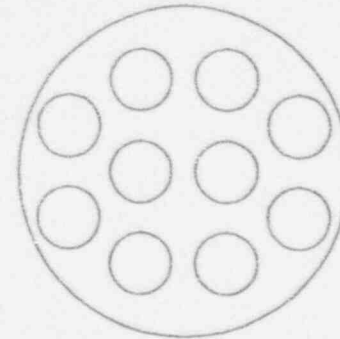
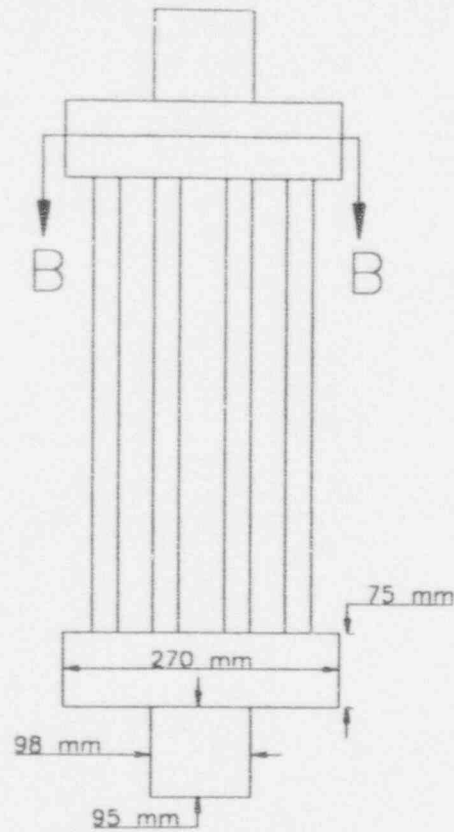
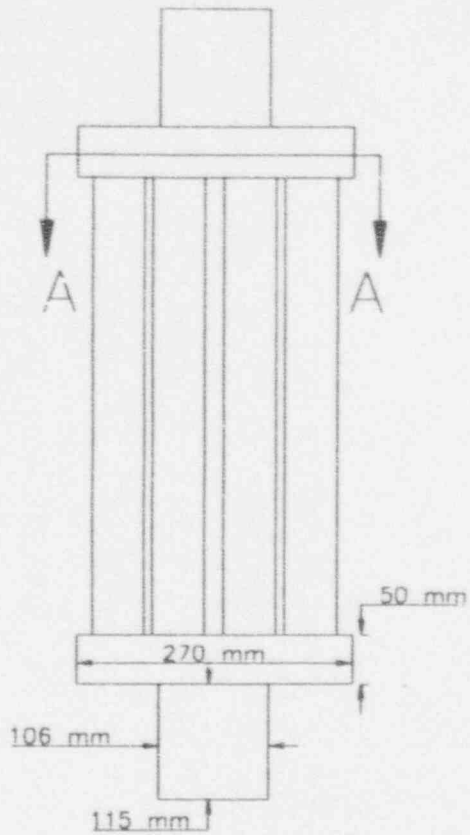
PCCS CONDENSER MODULE
 HEADER VOLUME 3894 cm³
 HEADER INSIDE HEIGHT 165 mm

ICS CONDENSER MODULE
 HEADER VOLUME 4977.8 cm³
 HEADER INSIDE HEIGHT 165 mm

PCCS CONDENSER
 MODULE
 10 TUBES PER MODULE

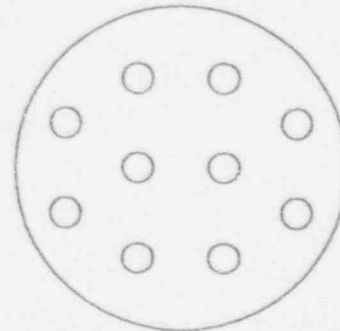
TUBE PARAMETERS:

- LENGTH 450 mm
- O.D. 50.8 mm
- I.D. 47.5 mm



SECTION A-A

ICS CONDENSER
 MODULE
 10 TUBES PER MODULE



SECTION B-B

TUBE PARAMETERS:

- LENGTH 450 mm
- O.D. 25.4 mm
- I.D. 23.3 mm

(NOTE: ALL DIMENSIONS ARE MEASURED INTERNALLY)

Figure 7.19 Design of ICS/PCCS condenser modules

PCCS CONDENSER MODULE

ICS CONDENSER MODULE

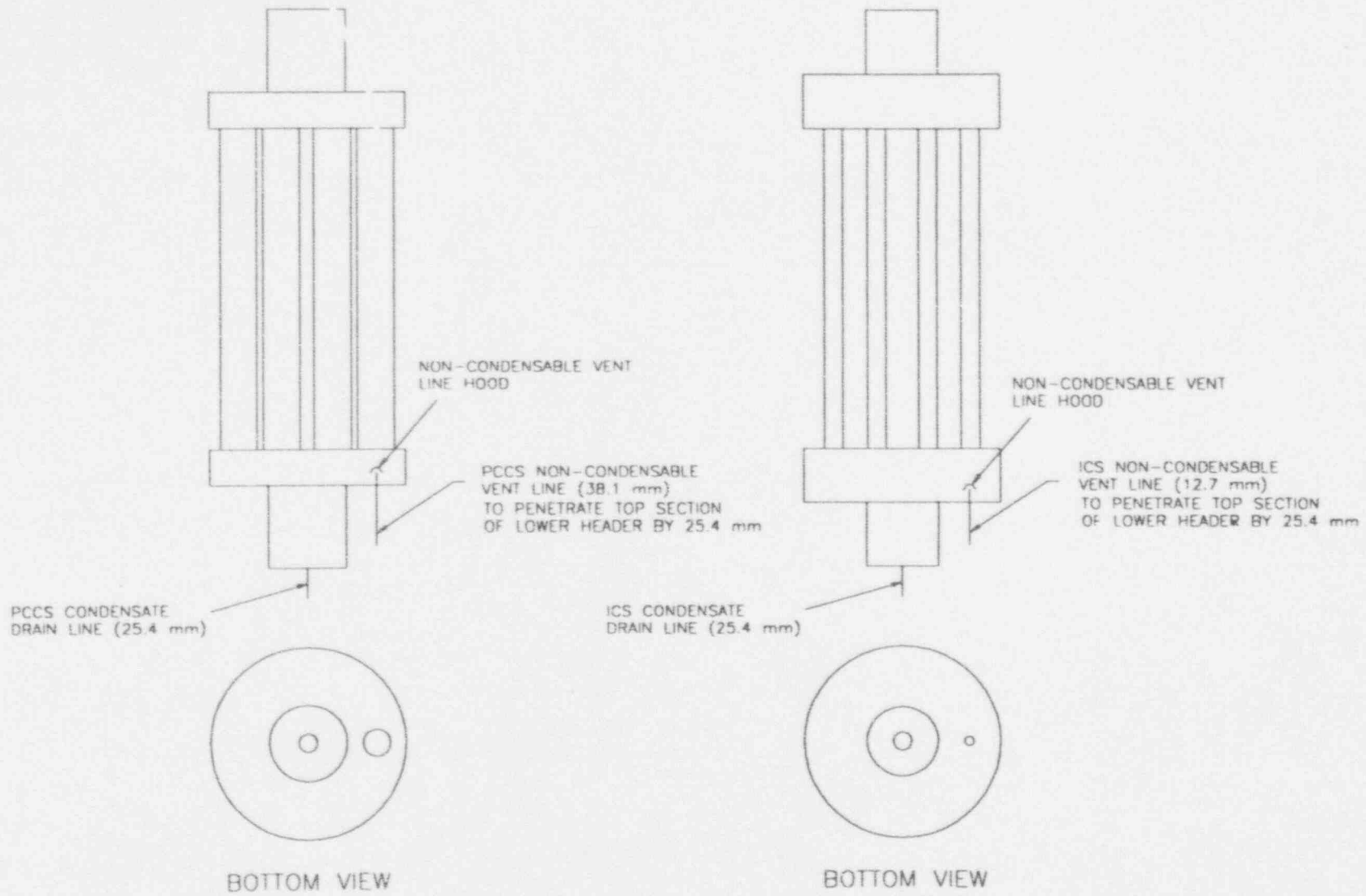
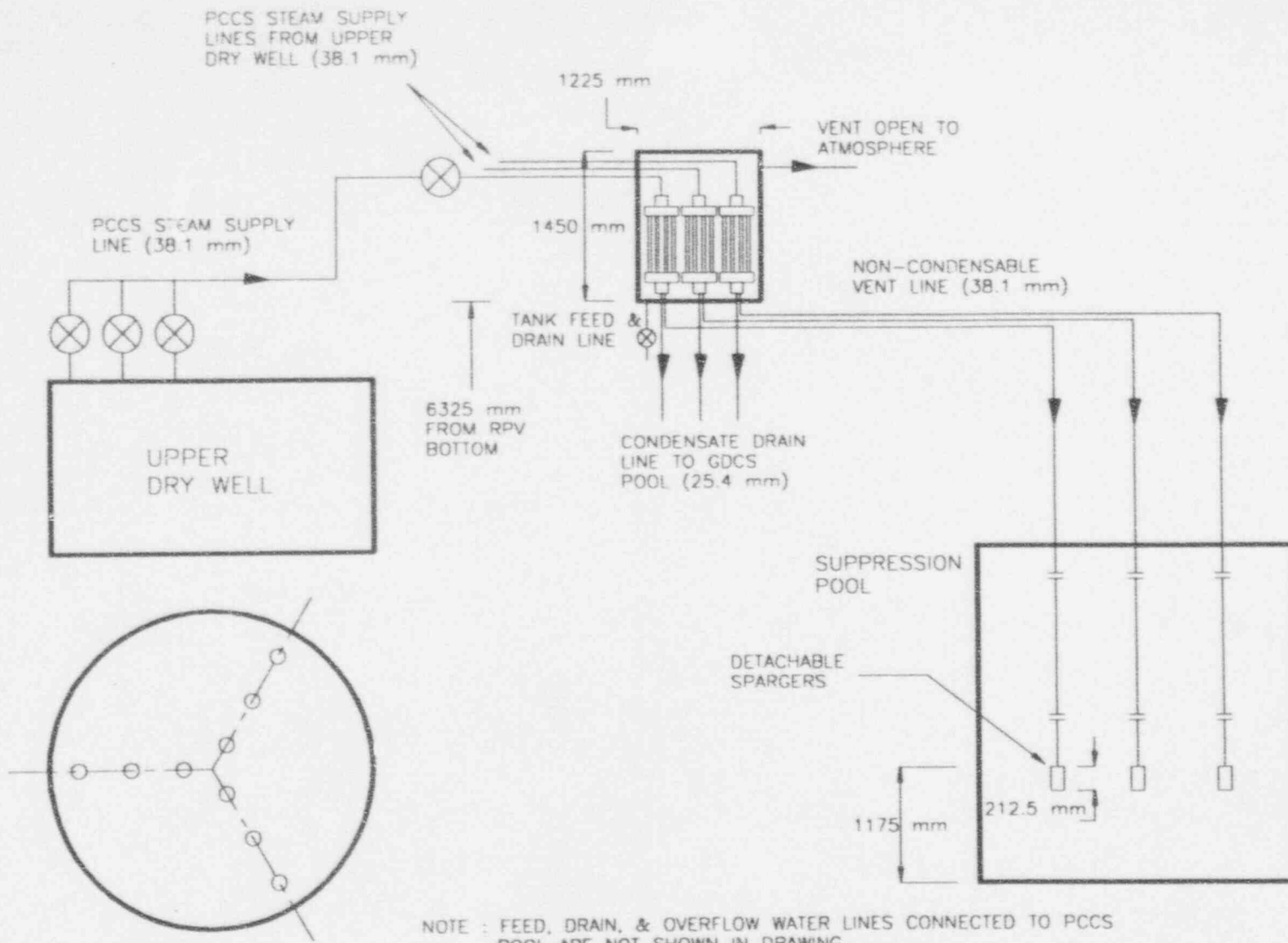


Figure 7.20 Lower header penetrations of the ICS/PCCS condenser modules in PUMA



TOP VIEW OF CONTAINMENT STEAM FEED LINE TO PCCS

Figure 7.21 Design of PUMA passive containment cooling system (PCCS)

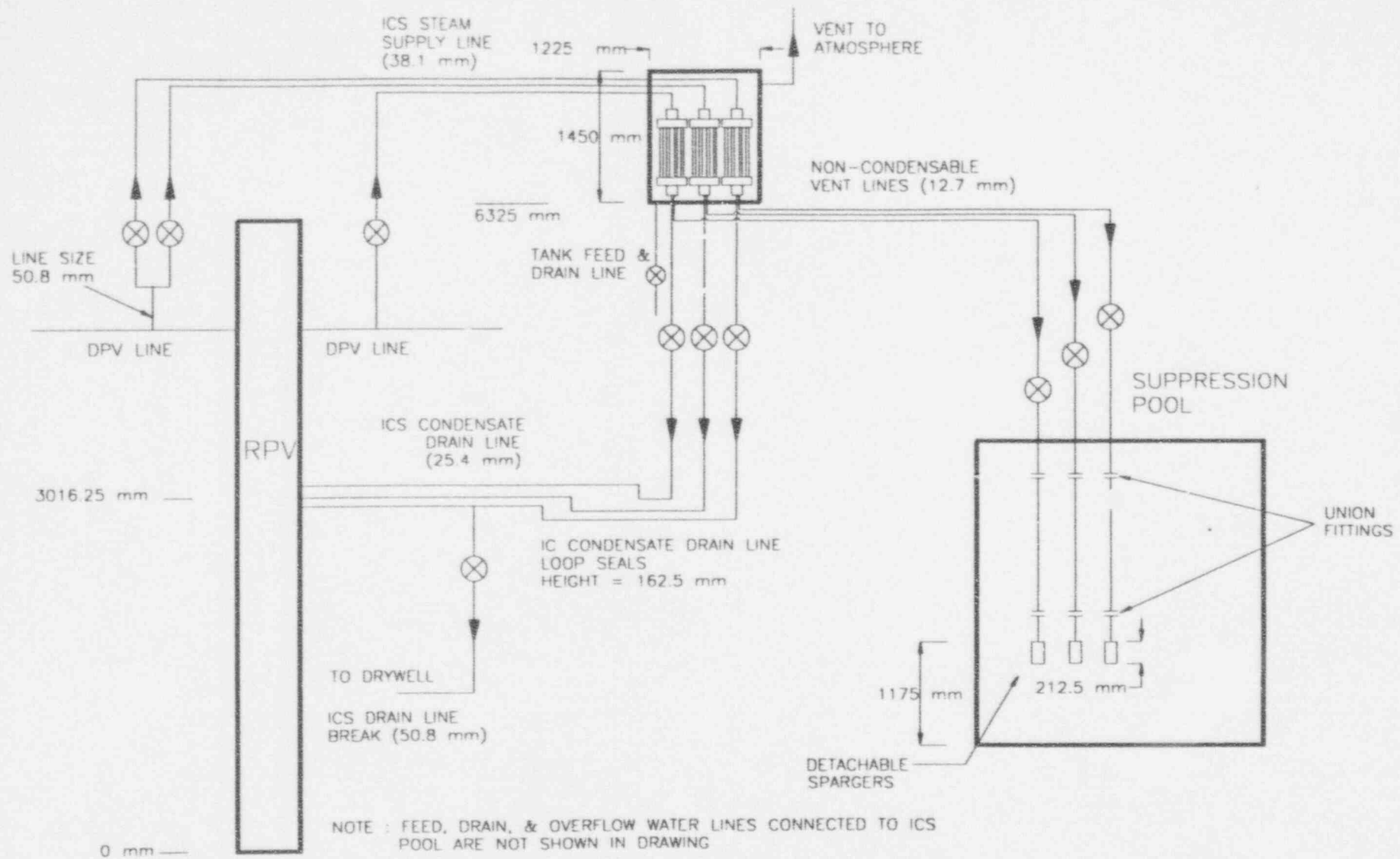
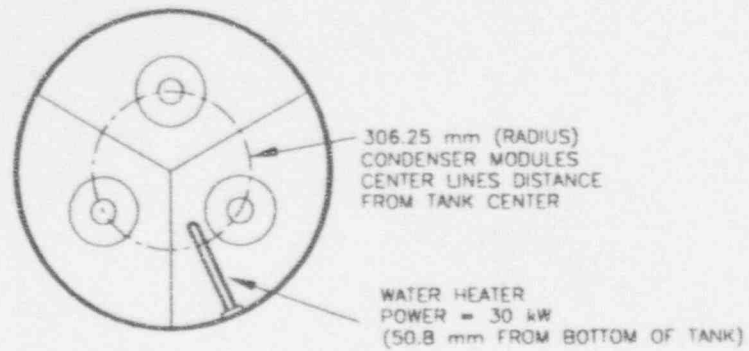
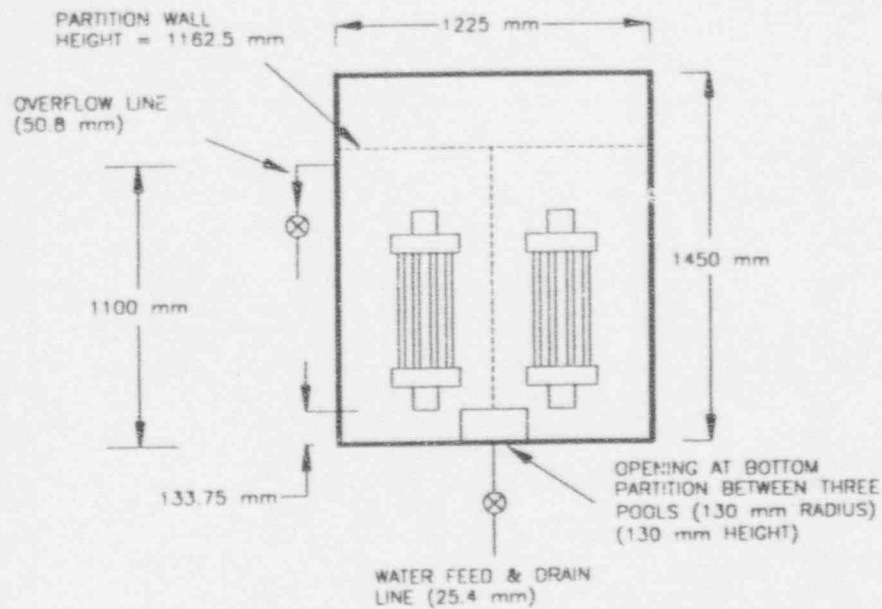
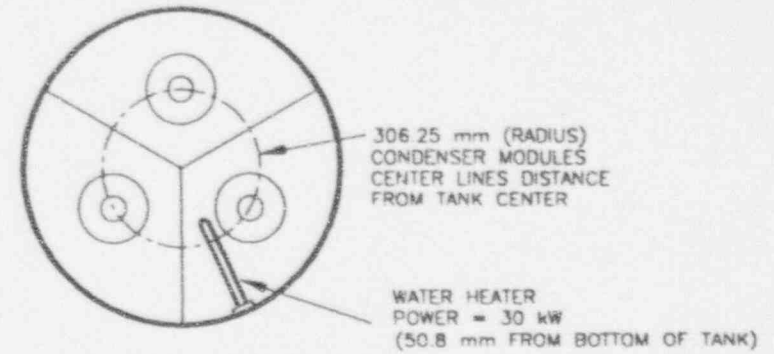


Figure 7.22 Design of PUMA isolation condenser system (ICS)

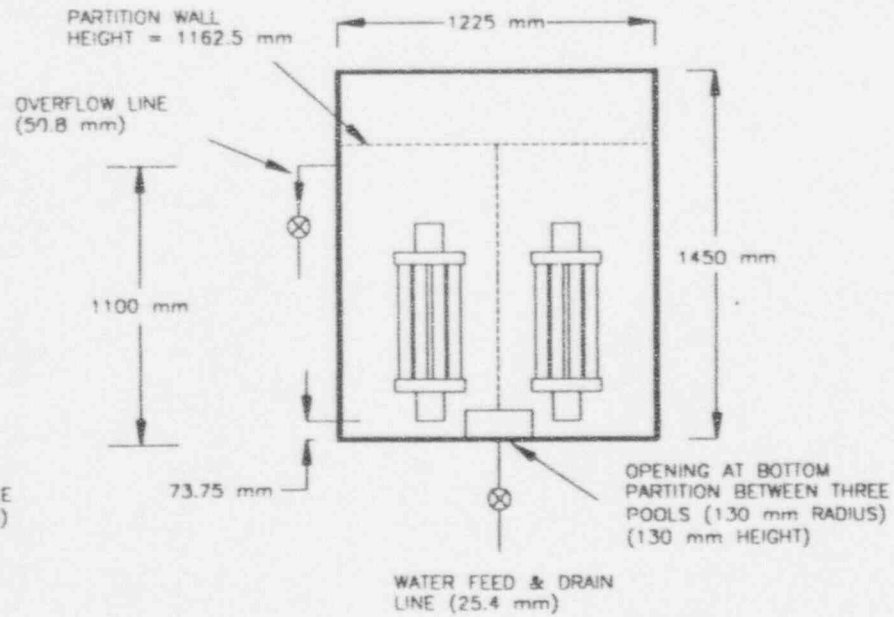
TOP VIEW OF ICS CONDENSERS TANK



TOP VIEW OF PCCS CONDENSERS TANK



FRONT VIEW OF ICS CONDENSERS TANK



FRONT VIEW OF PCCS CONDENSERS TANK

Figure 7.23 Design ICS/PCCS pools

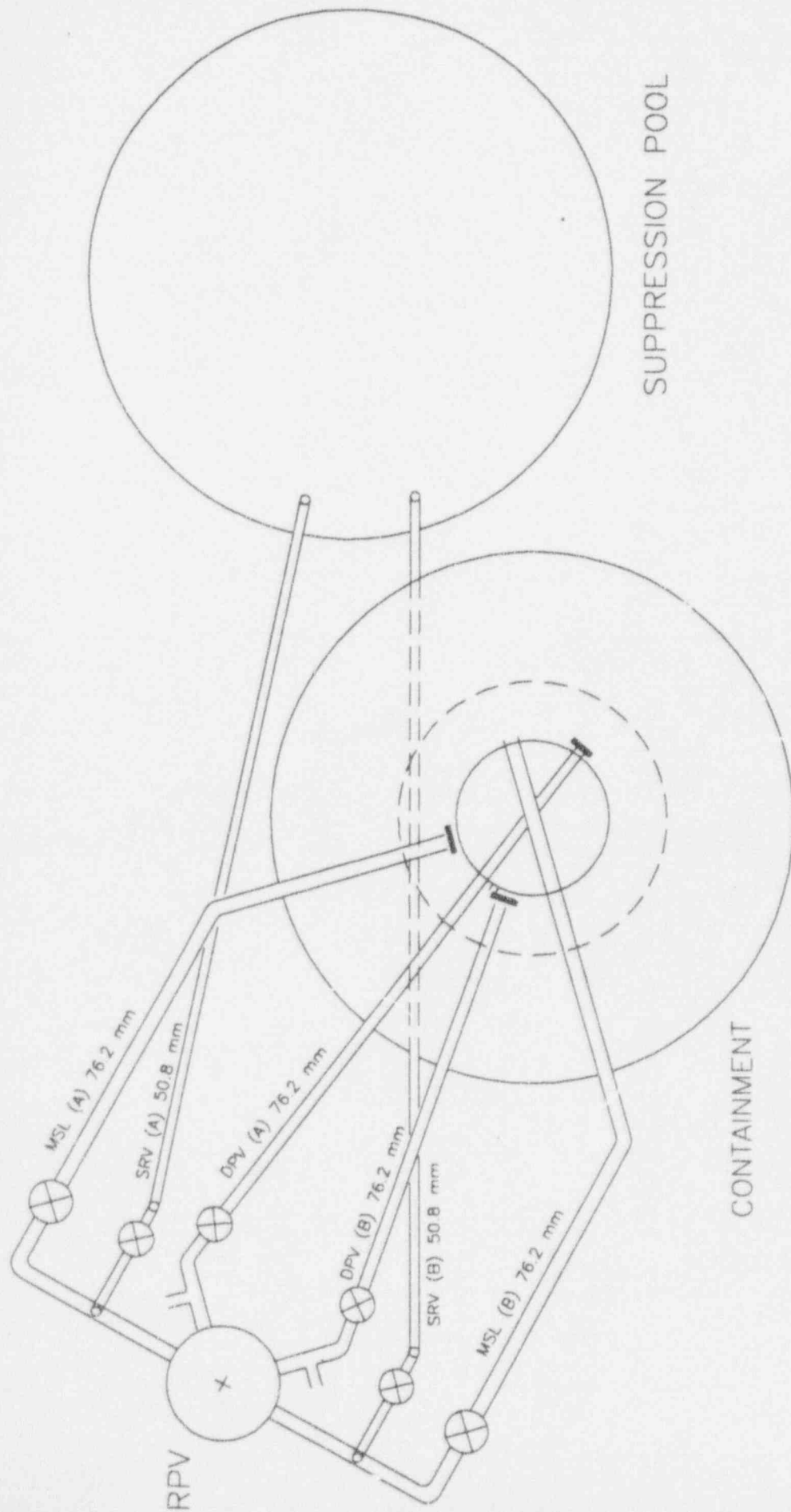


Figure 7.24 Plan view of ADS and MSL

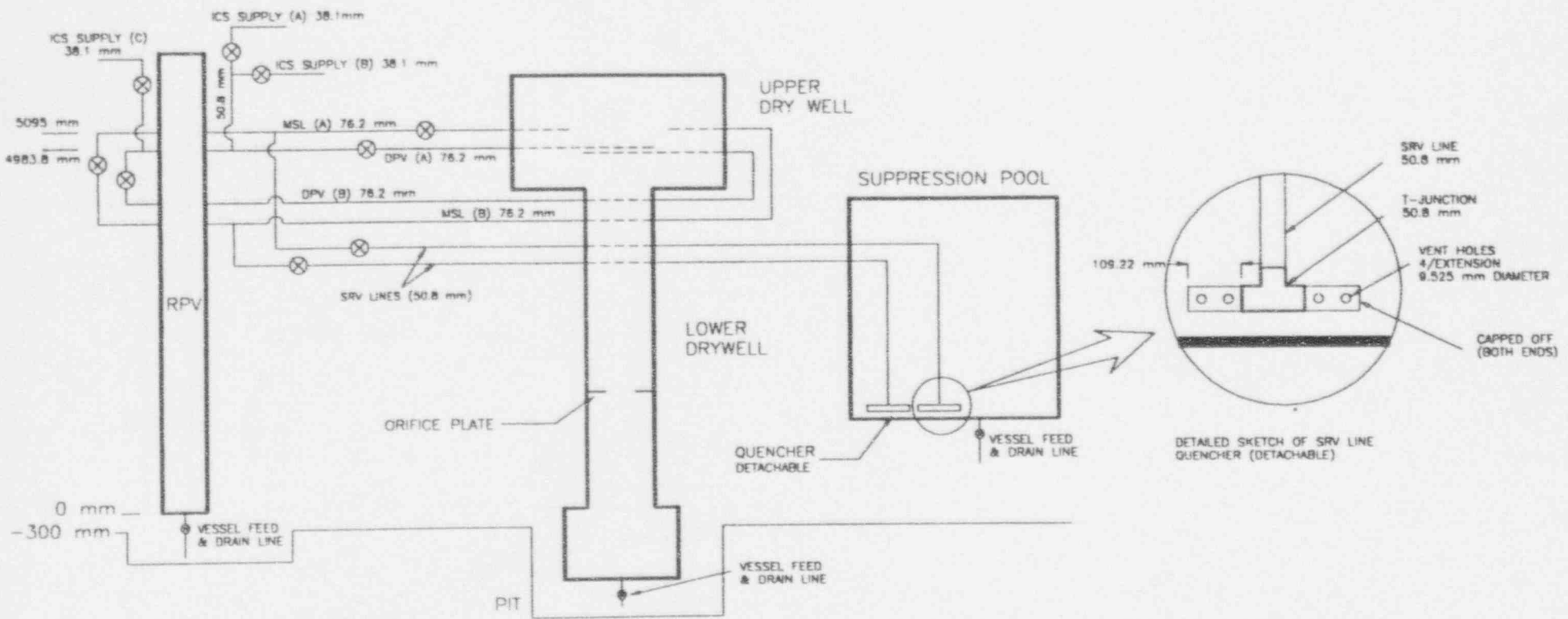


Figure 7.25 Automatic depressurization system (ADS) and main steam lines (MSL) schematic

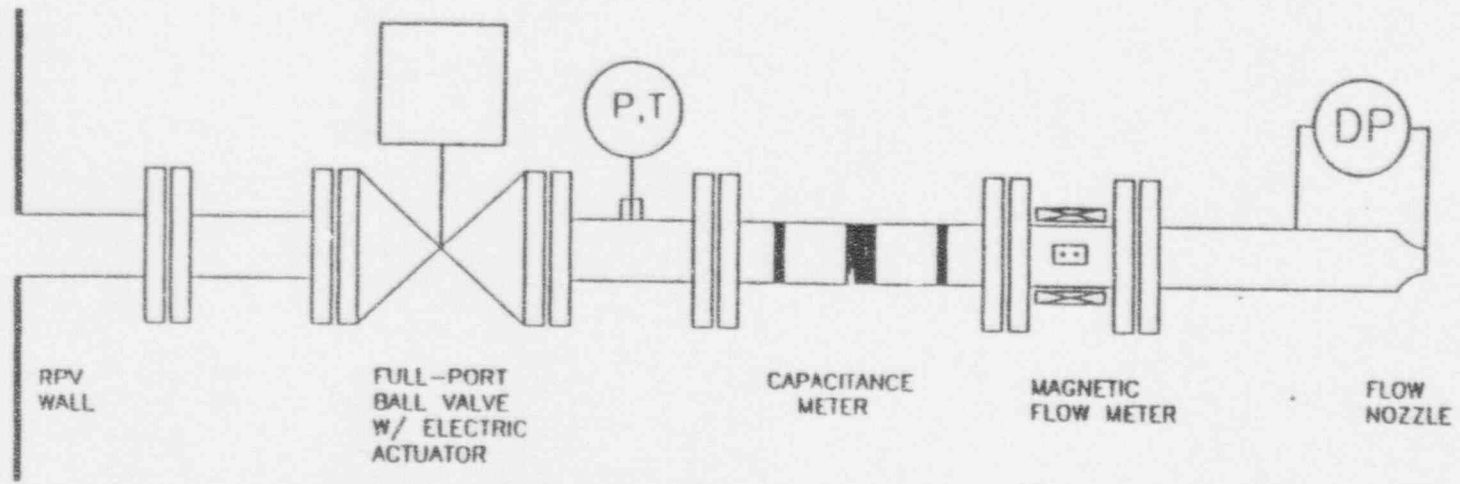


Figure 7.26 Typical instrumented ADS line

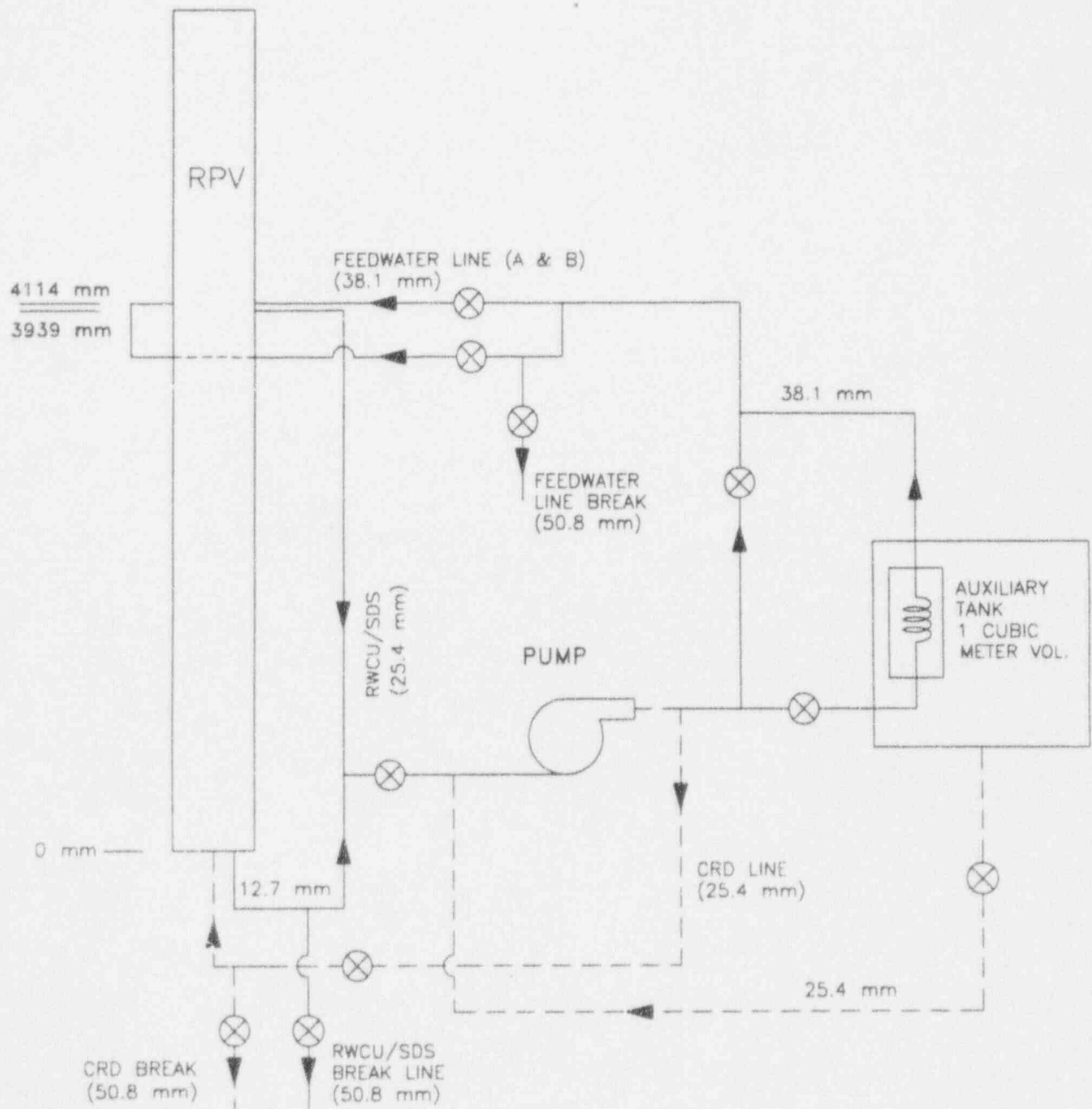


Figure 7.27 Reactor water clean-up/shutdown cooling (RWCU/SDC) system and control rod drive (CRD) system design in PUMA

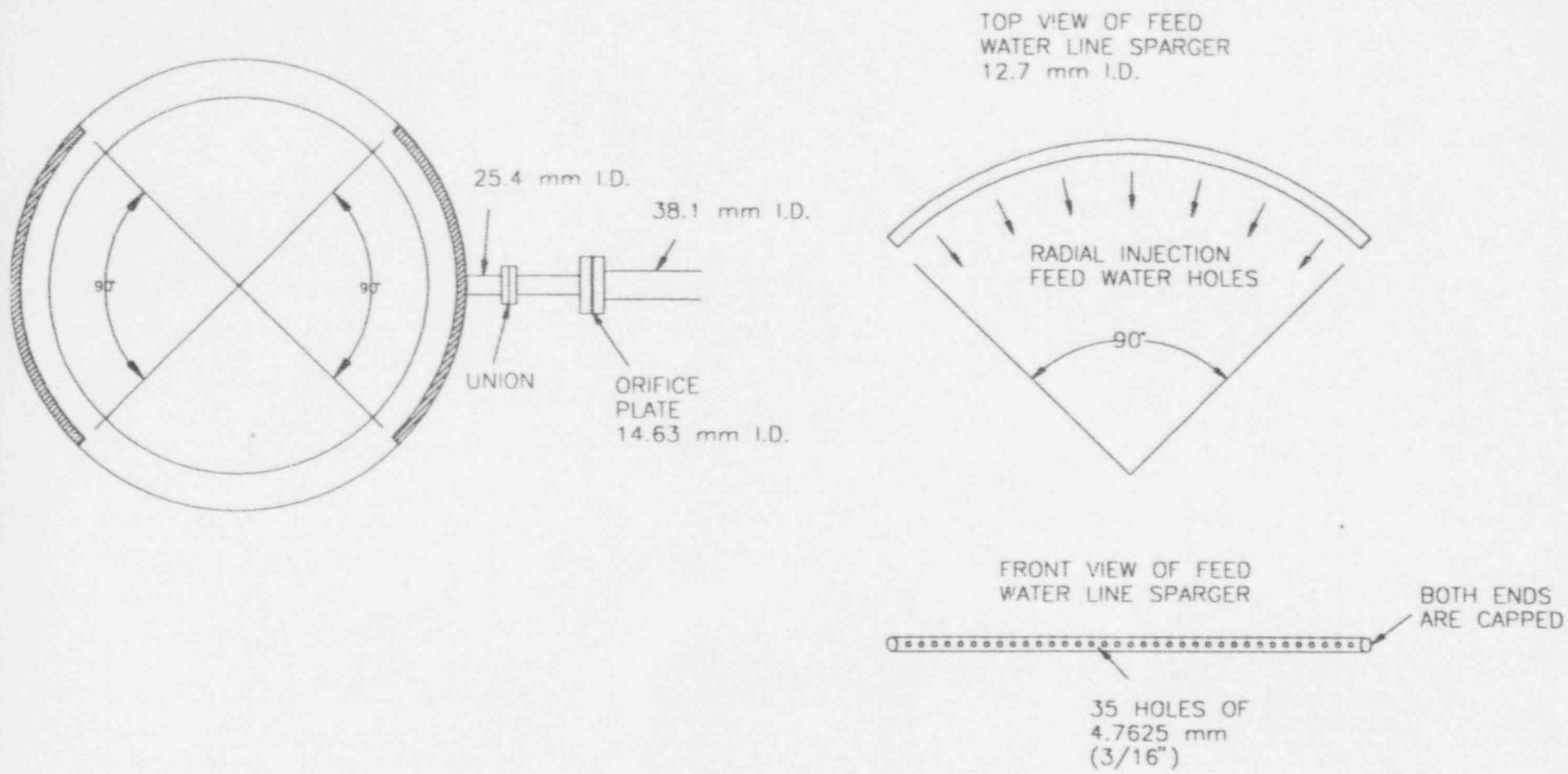


Figure 7.28 Feed water line and sparger in PUMA

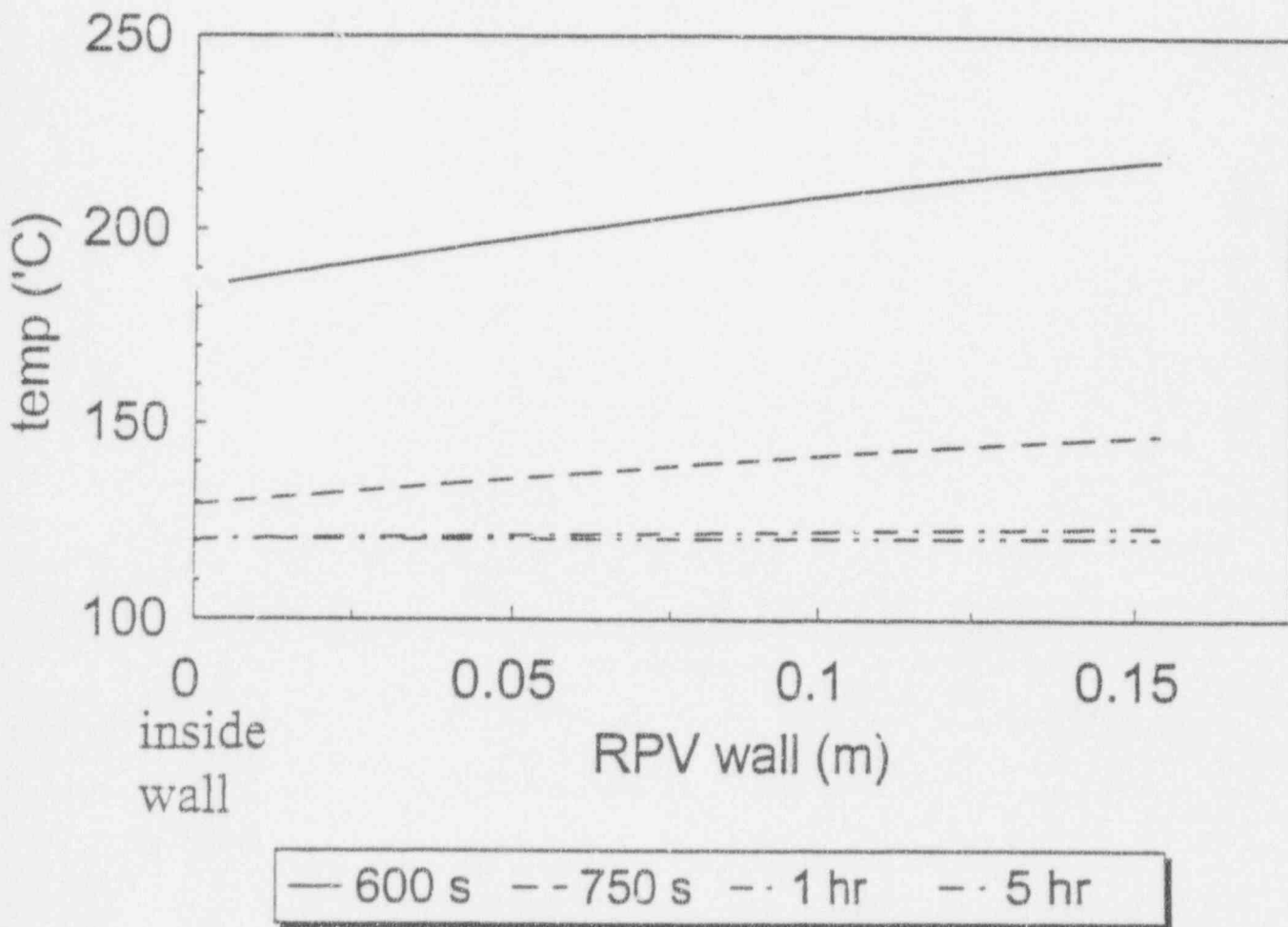


Figure 7.29 RPV wall temperature profile with time elapsed from blowdown

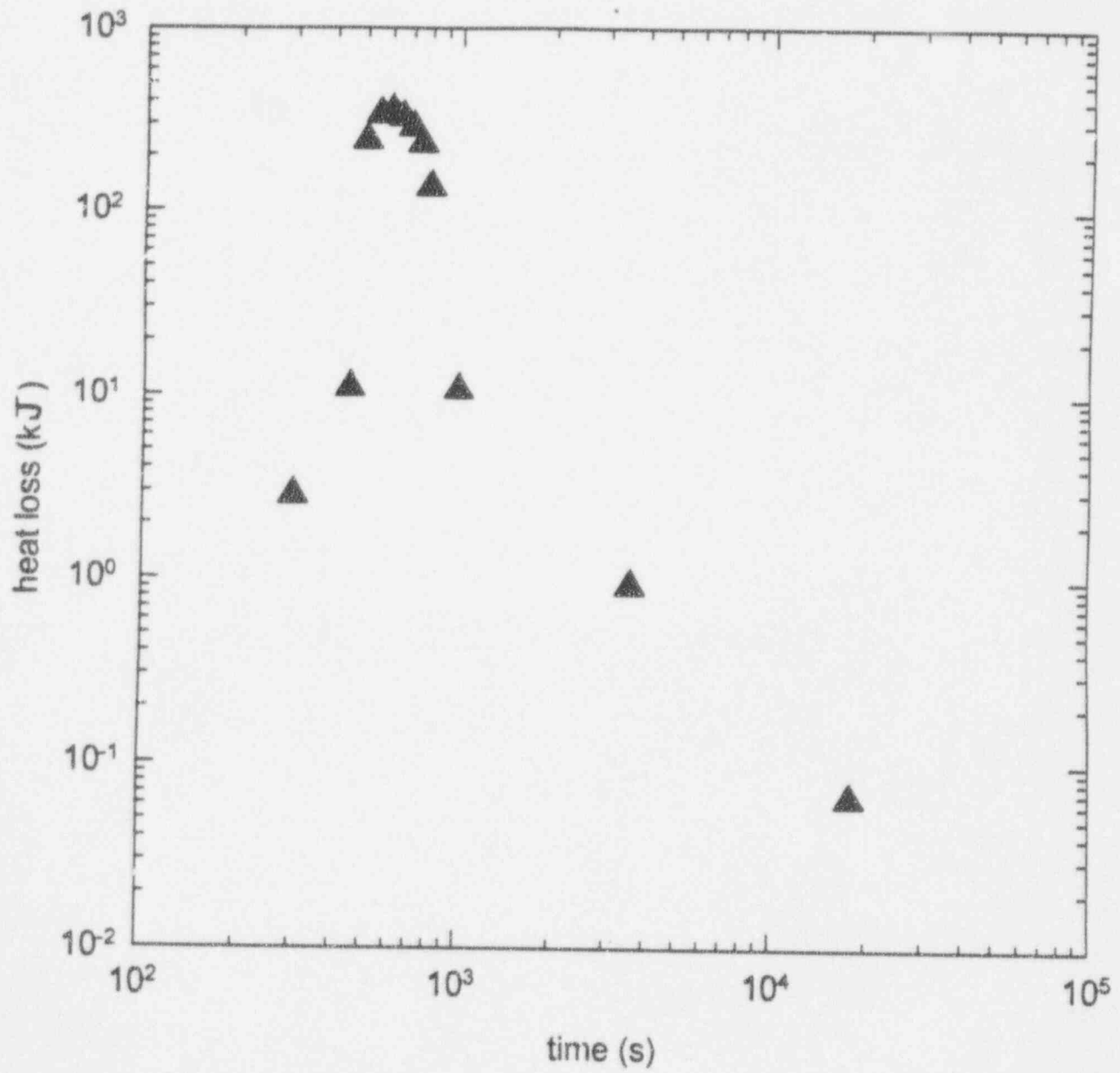


Figure 7.30 Estimated RPV wall heat loss with blowdown for SBWR

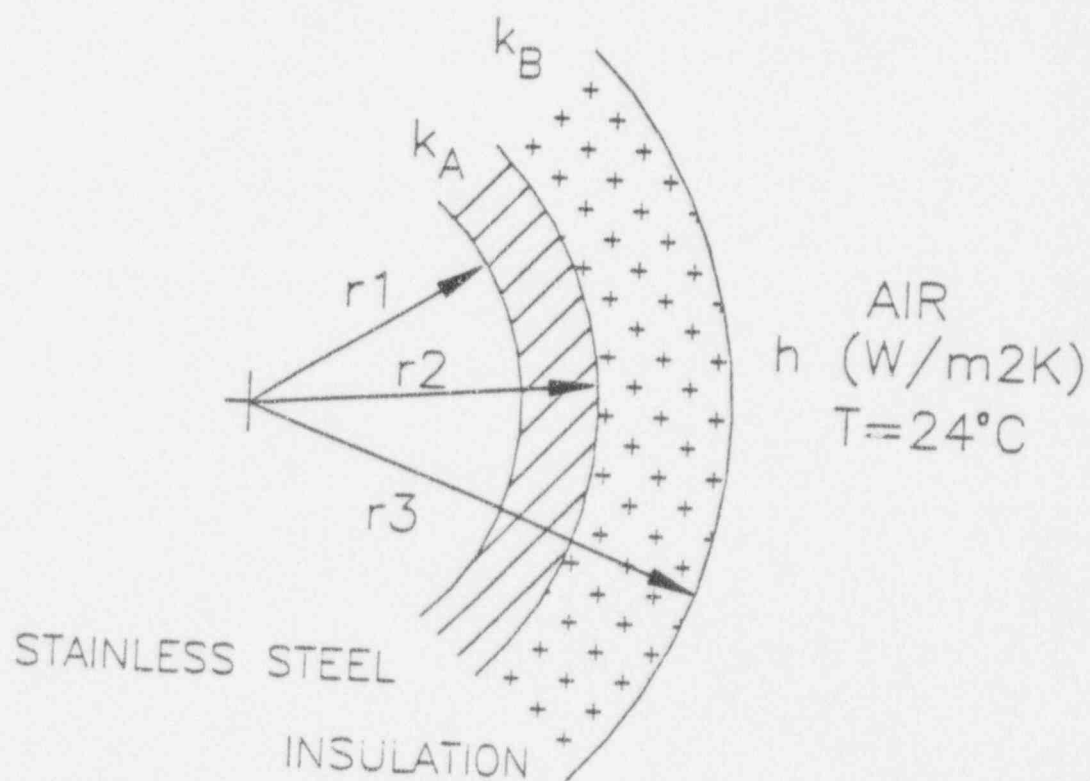


Figure 7.31 Cross-sectional view of insulation on typical vessel wall

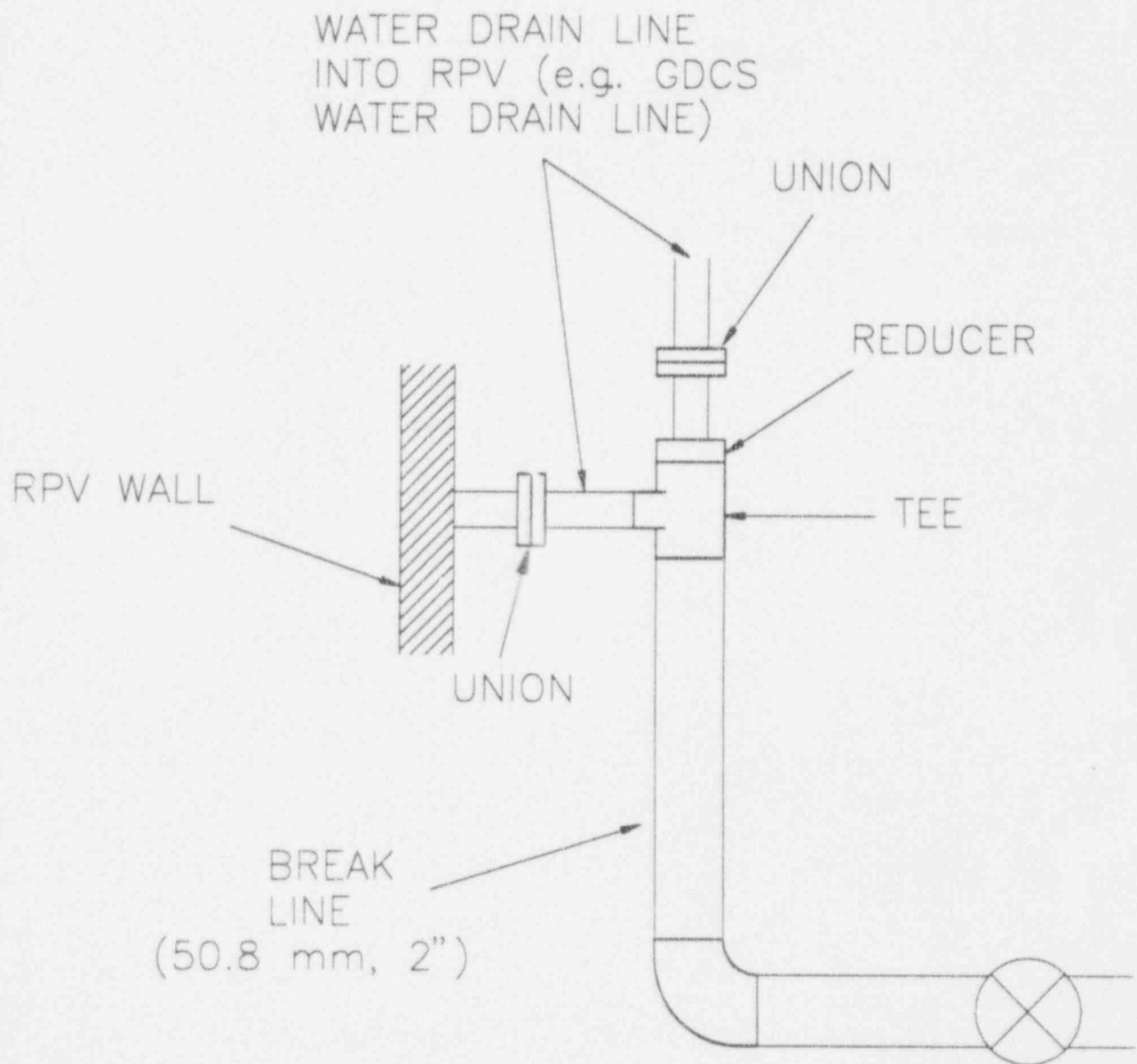


Figure 7.32 Typical break design in PUMA to simulate double-ended pipe break

Reference

- 7.1 Kocamustafaogullari, G., Ishii, M., "Scaling Criteria for Two-Phase Flow Natural and Forced Convection Loop and Their Application to Conceptual 2x4 Simulation Loop Design", ANL-83-61, NUREC/CR-3420 (1983).
- 7.2 G.E. Nuclear Energy, MFN. No. 170-93, October (1993).
- 7.3 G.E. Nuclear Energy, "SBWR Standard Safety Analysis Report", 25A5113 Rev. A, August (1992).
- 7.4 Kataoka, I. and Ishii, M., "Drift Flux Model for Large Diameter Pipe and New Correlation for Pool Void Fraction", *Intl. J. Heat Mass Transfer*, vol. 30, 1927-1939 (1987).
- 7.5 G.E. Nuclear Energy, MFN. No. 077-94, May (1994).
- 7.6 U.S. Nuclear Regulatory Commission Request for Proposal, No.RS-RES- 93-049, November (1992).
- 7.7 Rodi, W. "Turbulent Buoyant Jets and Plumes", HMT Volume 6, Pergamon Press, London, (1982).
- 7.8 Peterson, P.F., Schrock, V.E. and Greif, R., "Scaling for Integral Simulation of Mixing in large, Stratified Volumes", NURETH-6, October 508, Grenoble, France (1993).
- 7.9 Collier, J. G., *Convective Boiling and Condensation*, 2nd ed., McGraw-Hill, New York, (1981).
- 7.10 Private Communication with Brookhaven National Laboratory (BNL) Staff, April (1994).
- 7.11 G.E. Nuclear Energy, MFN. No.167-93, October (1993).
- 7.12 Churchill, S.W. and H.H.S. Chu, "Correlating Equations for Laminar and Turbulent Free Convection from a Vertical Plate," *Intl. J. Heat Mass Transfer*, 18, 1323 (1975).
- 7.13 Churchill, S.W. and H.H.S. Chu, "Correlating Equations for Laminar and Turbulent Free Convection from a Horizontal Cylinder," *Intl. J. Heat Mass Transfer*, 18, 1049 (1975).

8. INSTRUMENTATION SYSTEM

8.1 Overview of PUMA Instrumentation

The PUMA instrumentation consists of over 340 measurements that will provide a detailed picture of the mass and energy content in each vessel as well as pressures and liquid levels.

The steam and air mass inventory for component j in terms of the measurements is given by

$$m_{gj} = \sum_i \rho(T_{ij}, p_{ij}, x_{ij}) \Delta v_{ij} \quad (8.1)$$

where i is the subscript for measurement i , ρ is density, T and p are temperature and pressure, x is the concentration of steam and Δv is the volume corresponding to measurement i . Therefore, temperature, pressure and concentration are key measurements.

For the case of a liquid or two-phase mixture, the liquid mass inventory is simple to measure if the hydrostatic assumption is made and if $\rho_g \ll \rho_l$. Then the mass is given by

$$m_{lj} = \sum_i \frac{\Delta p_{ij} A_{ij}}{g} \quad (8.2)$$

where Δp_{ij} is the pressure across volume i and A_{ij} is the cross-sectional area. Therefore, Δp measurements are essential for the liquid inventory. Furthermore, these Δp measurements can be used to determine the liquid levels. In the case of the two-phase level in the reactor chimney, which is one of the most important variables in these tests, a number of Δp measurements will be performed in series. Assuming that the void fraction within the chimney is uniform, the two phase level is given by

$$\frac{l_i}{\Delta z_{i-1}} = \frac{\Delta p_i}{\Delta p_{i-1}} \quad (8.3)$$

where l_i is the level above pressure tap i , Δz_{i-1} is the distance between pressure taps i and $i-1$, Δp_i is the pressure drop between taps i and $i+1$ and Δp_{i-1} is the pressure drop between taps i and $i-1$.

The measurement of the energy inventory for component j is given by

$$m_j h_j = \sum_i \rho(T_{ij}, p_{ij}, x_{ij}) h(T_{ij}, p_{ij}, x_{ij}) \Delta v_{ij} \quad (8.4)$$

so the measurements required are basically the same as those for the mass inventory.

Table 8.1 is a list of the instrumentation associated with the mass and energy inventories for each component. This table is a subset of Tables 8.2 to 8.7, which list the complete measurements. Table 8.8 is a list of the instruments. A more detailed discussion of the specific measurements follows.

Table 8.1 Mass and energy measurements

Component	Pressure	Steam Concentration	Temperature	Water Level
Reactor vessel	p1 - p2, p 72	cnc 11	T1 - T66	p3 - p17
Drywell	p58 - p59	cnc5 - cnc9	T136 - %141 T157 - T161	p60 - p61
Pressure suppression pool	p66 - p67	cnc10	T146 - T153 T162 - T164	p63 - p64
GDCS	p58 - p59	cnc12	T82 - T90	p36 - p41
PCCS + ICS pools	--	--	T112 - T123	p62 - p63

Boundary flows between the vessels will also be measured. In addition, high frequency conductivity probes will be used for the first time in an integral test facility to determine the local value of the void fraction and the flow regime.

8.2 Reactor Pressure Vessel Instrumentation

The reactor vessel is the component that contains the majority of the instruments. Table 8.2 gives a summary of the technical specifications. The instrumentation layout for the reactor vessel is shown in Figures 8.1, 8.2 and 8.4.

The most important measurement is the two-phase level over the reactor. This measurement will be performed with sets of dp-cells and conductivity probes approximately 0.60 m apart in the axial direction. The conductivity probes will provide a check on the local density. This,

combined with the average density obtained by the dp-cells, will allow an accurate estimate of the two-phase mixture level, assuming that the void fraction in the chimney is uniform. Since the experimental transients are expected to be slow, this assumption should be valid except at the initial instants of the blowdown.

8 Temperatures

Temperatures are measured with K-type thermocouples (Omega Engineering, Inc., Stanford, CT). The range of measurements is 20°C to 180°C. The estimated uncertainty is 2°C.

The most important temperature measurement is at the steam dome. Therefore, a redundant measurement is performed (i.e., two thermocouples). A large number of thermocouples are used throughout the vessel to obtain a multidimensional picture of the temperature distribution. The downcomer has twenty-four thermocouples at six elevations and four azimuthal locations. Combined with the pressure measurements, they provide a detailed picture of the overall energy inventory. Furthermore, coolant bypass in case of a GDCS line break may be detected with these thermocouples. The temperature of the GDCS water is 20° C whereas the reactor vessel temperature will be greater than 100°C at the time of GDCS injection.

The lower plenum has twelve thermocouples at four elevations and three radial positions. The reactor core has eight thermocouples to measure flow temperatures and twelve thermocouples to measure heater surface temperatures. These are arranged at four elevations: 25%, 50%, 75% and 100% of the core height. The chimney has eight thermocouples at four elevations and two radial positions: the central duct and one peripheral duct.

Figure 8.1 also shows three wall heat flux sensors for measuring the heat loss from the reactor vessel. These are performed with ITI-TFM thermopile heat flux sensors (ITI Co., Delmar, CA). The uncertainty of these sensors is 1% of full scale. However, the uncertainty due to the intrusiveness of these probes needs to be determined.

8.2.2 Pressures

Figure 8.2.2 shows the locations of the pressure taps. Pressures will be measured with STD924, STD930 and STD974 pressure sensors (Honeywell, Inc., Phoenix, AZ). The uncertainty in these sensors is 0.1% of full scale. In case of the STD924 this is 10 mm of water. For practical considerations, a minimum resolution of 25 mm water head has been selected to account for various sources of experimental error such as noise, condensation in the pressure lines, etc. Therefore, the minimum uncertainty in the measurement of the liquid level will be approximately 25 mm.

Aside from the dome pressure and the bottom of core pressure, all other pressures are differential measurements. There are twelve differential pressure transmitters in the core-chimney

section to obtain a detailed picture of the two-phase levels. One of these dp-cells measures the pressure drop across the separators standpipes and the top separator plate. There are five dp cells in the downcomer. These have been arranged in the same way as in the SBWR design (see Figure 8.9).

8.2.3 Conductivity Probes

A dozen conductivity probes will be installed in the reactor and the chimney. A schematic probe is shown in Figure 8.3. These probes have been developed at Purdue over the past ten years and they provide reliable measurements of the indicator function [8.2]. They are sampled at 10 kHz and this signal is then integrated to obtain the void fraction. PUMA is the first integral test where this fundamental measurement will be performed. The accuracy of this measurement for bubbly and slug flows is approximately 10% of measurement. However, this is only a local measurement so the uncertainty in terms of the volume-averaged void fraction must be greater. The conductivity probes provide additional information on the local flow regime which may be valuable in case of two phase flow instabilities. Moreover, they provide a check on the two phase level measurements.

These twelve probes are located at six elevations and two radial locations to obtain a multidimensional set of data. Half of the probes are located in the core and the other half are located in the chimney.

The probes located in the chimney are inserted from the side of the vessel through special instrumentation ports that also hold pressure taps and thermocouples. The probes located in the reactor core together with the thermocouples are inserted from the bottom plate. These probes have the electrodes facing downward so they only detect bubbles that are moving up.

8.2.4 Additional Measurements

There are four view ports with two video cameras. One in the lower plenum and three in the chimney. The view ports in the chimney will consist of double windows to view the flow within the chimney.

Figure 8.4 shows the vessel and boundary flow measurements. Three flow measurements are performed at the same elevation and three azimuthal locations in the downcomer: two pitot tubes and an EGG-TSA-12-C-D turbine meter (EGG Flow Technology, Phoenix AZ). This last probe can measure flow velocities with an uncertainty of 0.1 m/s. It has 2 R.F. pickups so it can sense the flow direction as well.

8.2.5 Boundary Measurements

The objective of these measurements is to obtain the mass and energy flow rates flowing out of the reactor vessel under single-phase and two-phase conditions. The accuracy of these measurements in the two phase regime has not yet been determined.

All the boundary lines shown in Figure 8.4 are instrumented equally except for one: the feedwater flow. The reason is that the SRVs, the DPVs, the steam line break, the feedwater break and the small break all represent blowdown outflows. The schematic of the instrumentation in one of these lines is shown in Figure 8.5.

There are six measurements in each line. The first two are pressure and temperature to determine the single phase thermodynamic state. For two-phase flow, there is a capacitance probe that measures void fraction. The capacitance void meter was chosen over the gamma densitometer because of the cost and lengthy permit procedures required with gamma ray sources. Capacitance void meters have already been used by other researchers in two-phase flow [8.3-8.5]. We intend to calibrate these sensors in an air-water loop.

The capacitance probe presently under development is shown in Figure 8.6. It is driven by a 1 MHz signal. At this frequency the impedance is capacitive. The flow is expected to be homogeneous during the blowdown stage of the accident. This is important because the output of the capacitance probe is strongly dependent on the flow regime.

The boundary measurements also include three flow probes: a magnetic flow meter, a flow nozzle and a vortex flow meter. The magnetic flow meters are Honeywell MagneW-3000 models. Magnetic flow meters may be used also to measure the liquid velocity for two-phase flows if the void fraction is lower than 40% [8.1].

The flow nozzle provides a measurement of the kinetic energy of the flow. For homogeneous two-phase flow, this and the void fraction measurements obtained by the capacitance meter may be combined to obtain the flow rate. However, for separated flows with different phase velocities, the number of measurements is not sufficient to uniquely determine the flow. Fortunately, during blowdown the flow is homogeneous and after blowdown the flow is expected to be single-phase vapor or single-phase liquid.

For low steam flow rates during decay heat removal, J-TEC vortex flow meters have been chosen (J-Tec Associates, Inc., Cedar Rapids, IA). They are composed of an ultrasonic vortex sensor that can detect very low steam flows. These flow meters include a flow computer that accounts for temperature and pressure variations. With the aid of this computer the manufacturer claims an uncertainty of 1% of measurement across the full range.

8.3 Containment Instrumentation

The schematic of the containment measurements in the drywell, pressure suppression pool and other tanks is given in Figure 8.7. The boundary flows are shown in Figure 8.8.

8.3.1 Temperatures

Temperatures will be measured at four elevations in each partition of the PCCS tank as well as of the ICS tank. On one ICS condenser tube and on one PCCS condenser tube, detailed temperature measurements will be made: three center line temperatures and five surface temperatures of the tube. Three temperatures will be measured in each of the GDCS tanks. Six temperatures at six elevations will be measured within the drywell and four at the wall. Six temperatures at three elevations will be measured within the pressure suppression pool and two more in the gas volume.

8.3.2 Pressures

The PCCS/ICS tanks will have two differential pressure transducers for level, as will each GDCS tank, the drywell and the pressure suppression pool. The drywell and the pressure suppression chamber will also have two pressure probes each to measure absolute pressure. Additionally, there will be a differential pressure cell in the drywell vent to the pressure suppression pool.

8.3.3 Oxygen Concentrations

A Siemens Oxymat 5e oxygen sensor (Siemens Industrial Automation, Inc., Alpharetta, GA) will be used to measure all the oxygen concentrations. This instrument can produce fast and reliable concentration measurements. The error in these measurements is 1/2% of full scale. 10 points will be sampled: five in the drywell, one in the pressure suppression chamber and four in the PCCS/ICS lines. These measurements will provide data on the distribution of non-condensibles. In order to sample the locations systematically, an automatic array of solenoid valves will be cycled periodically by the data acquisition system. The tubing will be heated to prevent condensation.

The bleed time for each concentration measurement will be approximately 10 s, and the measurement time will be 5 s so each measurement will take approximately 15 s. Concentrations that vary over periods of time shorter than that cannot be measured accurately. This is not expected to be a problem during decay heat removal. Each measurement will bleed 300 c.c. from the system. This corresponds to 1 liter/min approximately and represents a very small perturbation of the containment systems.

8.3.4 Additional Measurements

The only additional measurement in the containment is a viewport to be installed in the pressure suppression pool.

8.3.5 Containment Boundary Measurements

Figure 8.8 is a schematic of the boundary measurements. Containment boundary measurements are simpler than the reactor vessel measurements because there are no two-phase flows. However, there are non-condensibles.

For the PCCS and ICS extraction lines, the flows are a mixture of steam and air. Concentrations and temperatures will be measured for thermodynamic state. The flows will be measured with vortex flow meters. Additionally, one venturi will be located in one PCCS line and another in one ICS line.

For the PCCS and ICS condensate lines, as well as the GDCS lines and the equalization line, the flows are single-phase water only. Temperatures will be measured for thermodynamic state. Liquid flows will be measured with magnetic flow meters.

The PCCS and ICS non-condensable bleed lines represent a more difficult problem since the flows are so low that they are hard to measure. Therefore, these flows will not be measured. Instead, differential pressure transducers will be used to determine the level within the drains into the suppression pool. This will indicate the times at which noncondensibles are being discharged. Thermodynamic state will be obtained by measuring temperature and concentration in these lines.

Finally, differential pressure transducers located across the valves will be used as vacuum breaker flow indicators.

8.4 Data Acquisition System

The data acquisition and control system will be based on a network of 5 PCs. To increase the capability of the DAS in the future, all that is needed is to add more PCs to the network. Since a sampling rate of 1 Hz is sufficient for this experiment, the total data collection rate is only 340 Hz which is substantially below the transfer rate of an Ethernet network. The server PC is a 66 MHz 486 machine. The other PCs are 486 machines of various clock speeds. The PC server will send a signal to all the DAS software across the network to launch the programs simultaneously. After that, no further synchronization is necessary, given the accuracy of the PC clocks.

A maximum data collection time of eight hours and a sampling rate of 1 Hz imply a total number of 9,792,200 data samples or approximately 20 MBytes (1 datum equals 2 Bytes). This

is well below the hard disk storage capability. All data will be stored in the server and each PC will store its own data for redundancy. The sampling rate of 1 Hz is sufficiently short with respect to all transients. For example, the blowdown stage of the main steam line break transient lasts approximately 400 s.

Keithley-Metabyte A/D and D/A converter boards will be used throughout the data acquisition system. The software for data acquisition and control will be Labtech Notebook. The software for communications will be Microsoft Windows for Workgroups. The bottleneck in the DAS is Labtech Notebook for Windows. At present it can only sample 300 channels per second on a 66 MHz PC, which nevertheless satisfies our requirements.

The central PC will collect all the data and send the necessary information to the control PC. It will communicate with the four PCs through the Ethernet local area network.

PC #1 will be fully dedicated to acquire the 156 temperatures and nine heat fluxes. Two DAS-801 boards and eleven EXP-16 terminal boards will be used.

PC #2 will be used to acquire the seventy-six pressures, twenty magnetic flow signals, eight capacitance probe signals and data from the concentration probe. Hardware is the same as PC #1.

PC #3 will be fully dedicated to the twelve conductivity probes. These are the only probes that need to be sampled at a rate higher than 1 Hz: 10 kHz. two DAS-58 data acquisition boards and two STA-U terminal boards will be used for this task.

PC #4 will be dedicated to monitor and control the valves and the heaters. Two PIO-24 parallel Digital I/O boards will be connected to two SSIO-24 relay boards with forty-eight SM-OAC5A relays and two PIO-HV boards will monitor the signals from the valves.

Table B.2: Vessel Measurement

MEASUREMENT	TYPE	LABEL	MAX RANGE	MIN RANGE	CATALOG #
STEAM DOME PRESSURE	P	P2	0-1 MPa	0-0.4 MPa	STD 974
LOWER PLENUM PRESSURE	P	P72	0-1 MPa	0-0.4 MPa	STD 974
STEAM DOME TEMP	T	T1	20-180°C	N/A	K-TYPE
STEAM DOME TEMP	T	T2	20-180°C	N/A	K-TYPE
CORE & CHIMNEY TEMP	T	T3	20-180°C	N/A	K-TYPE
CORE & CHIMNEY TEMP	T	T4	20-180°C	N/A	K-TYPE
CORE & CHIMNEY TEMP	T	T5	20-180°C	N/A	K-TYPE
CORE & CHIMNEY TEMP	T	T6	20-180°C	N/A	K-TYPE
CORE & CHIMNEY TEMP	T	T7	20-180°C	N/A	K-TYPE
CORE & CHIMNEY TEMP	T	T8	20-180°C	N/A	K-TYPE
CORE & CHIMNEY TEMP	T	T9	20-180°C	N/A	K-TYPE
CORE & CHIMNEY TEMP	T	T10	20-180°C	N/A	K-TYPE
CORE & CHIMNEY TEMP	T	T11	20-180°C	N/A	K-TYPE
CORE & CHIMNEY TEMP	T	T12	20-180°C	N/A	K-TYPE
CORE & CHIMNEY TEMP	T	T13	20-180°C	N/A	K-TYPE
CORE & CHIMNEY TEMP	T	T14	20-180°C	N/A	K-TYPE
CORE & CHIMNEY TEMP	T	T15	20-180°C	N/A	K-TYPE
CORE & CHIMNEY TEMP	T	T16	20-180°C	N/A	K-TYPE
CORE & CHIMNEY TEMP	T	T17	20-180°C	N/A	K-TYPE
CORE & CHIMNEY TEMP	T	T18	20-180°C	N/A	K-TYPE
CORE VOID FRACTION	CND	CND1	0-1	N/A	PURDUE
CORE VOID FRACTION	CND	CND2	0-1	N/A	PURDUE
CORE VOID FRACTION	CND	CND3	0-1	N/A	PURDUE
CORE VOID FRACTION	CND	CND4	0-1	N/A	PURDUE
CORE VOID FRACTION	CND	CND5	0-1	N/A	PURDUE
CORE VOID FRACTION	CND	CND6	0-1	N/A	PURDUE
CHIMNEY VOID FRACTION	CND	CND7	0-1	N/A	PURDUE
CHIMNEY VOID FRACTION	CND	CND8	0-1	N/A	PURDUE
CHIMNEY VOID FRACTION	CND	CND9	0-1	N/A	PURDUE
CHIMNEY VOID FRACTION	CND	CND10	0-1	N/A	PURDUE
CHIMNEY VOID FRACTION	CND	CND11	0-1	N/A	PURDUE
CHIMNEY VOID FRACTION	CND	CND12	0-1	N/A	PURDUE
CORE & CHIMNEY LEVEL	DP	P3	0-30 KPa	N/A	STD 924
CORE & CHIMNEY LEVEL	DP	P4	0-30 KPa	N/A	STD 924
CORE & CHIMNEY LEVEL	DP	P5	0-30 KPa	N/A	STD 924
CORE & CHIMNEY LEVEL	DP	P6	0-30 KPa	N/A	STD 924
CORE & CHIMNEY LEVEL	DP	P7	0-30 KPa	N/A	STD 924
CORE & CHIMNEY LEVEL	DP	P8	0-30 KPa	N/A	STD 924

Table 8.2: Vessel Measurement

MEASUREMENT	TYPE	LABEL	MAX RANGE	MIN RANGE	CATALOG #
SEPARATOR DP	DP	P9	0-30 KPa	N/A	STD 924
DOWNCOMER LEVEL	DP	P12	0-30 KPa	N/A	STD 924
DOWNCOMER LEVEL	DP	P13	0-30 KPa	N/A	STD 924
DOWNCOMER LEVEL	DP	P14	0-30 KPa	N/A	STD 924
DOWNCOMER LEVEL	DP	P15	0-30 KPa	N/A	STD 924
DOWNCOMER LEVEL	DP	P16	0-30 KPa	N/A	STD 924
DOWNCOMER LEVEL	DP	P17	0-30 KPa	N/A	STD 924
DOWNCOMER FLOW	DP	P10	0-5 KPa	N/A	STD 924
DOWNCOMER FLOW	DP	P11	0-5 KPa	N/A	STD 924
DOWNCOMER FLOW	TURBINE	TU1	0-3 m/s	N/A	EGG-TSA-12-C-D
VIDEO PORTS	VP				
VIDEO PORTS	VP				
VIDEO PORTS	VP				
VIDEO PORTS					
VIDEO CAMERA	CCD				
VIDEO CAMERA	CCD				
VIDEO CAMERA	CCD				
INSTRUMENT PORT	DOUBLE-PORT				
INSTRUMENT PORT	DOUBLE-PORT				
INSTRUMENT PORT	DOUBLE-PORT				
INSTRUMENT PORT	DOUBLE-PORT				
HEATER TEMP	T	T19	20-180°C	N/A	K-TYPE
HEATER TEMP	T	T20	20-180°C	N/A	K-TYPE
HEATER TEMP	T	T21	20-180°C	N/A	K-TYPE
HEATER TEMP	T	T22	20-180°C	N/A	K-TYPE
HEATER TEMP	T	T23	20-180°C	N/A	K-TYPE
HEATER TEMP	T	T24	20-180°C	N/A	K-TYPE
HEATER TEMP	T	T25	20-180°C	N/A	K-TYPE
HEATER TEMP	T	T26	20-180°C	N/A	K-TYPE
HEATER TEMP	T	T27	20-180°C	N/A	K-TYPE
HEATER TEMP	T	T28	20-180°C	N/A	K-TYPE
HEATER TEMP	T	T29	20-180°C	N/A	K-TYPE
HEATER TEMP	T	T30	20-180°C	N/A	K-TYPE
TEMP CONTROLLER	T-CONTROLLER				
TEMP CONTROLLER	T-CONTROLLER				
TEMP CONTROLLER	T-CONTROLLER				
POWER CONTROLLER	PWR-CONTROLLER		0-60 KW	N/A	
POWER CONTROLLER	PWR-CONTROLLER		0-60 KW	N/A	
POWER CONTROLLER	PWR-CONTROLLER		0-60 KW	N/A	

Table 8.2: Vessel Measurement

MEASUREMENT	TYPE	LABEL	MAX RANGE	MIN RANGE	CATALOG #
POWER CONTROLLER	PWR-CONTROLLER		0-60 KW	N/A	
POWER CONTROLLER	PWR-CONTROLLER		0-60 KW	N/A	
POWER CONTROLLER	PWR-CONTROLLER		0-60 KW	N/A	
POWER CONTROLLER	PWR-CONTROLLER		0-60 KW	N/A	
POWER CONTROLLER	PWR-CONTROLLER		0-60 KW	N/A	
POWER METER	PWR-METER		0-300 A	N/A	
POWER METER	PWR-METER		0-300 A	N/A	
POWER METER	PWR-METER				
POWER METER	PWR-METER				
POWER METER	PWR-METER				
POWER METER	PWR-METER				
POWER METER	PWR-METER				
DOWNCOMER TEMP	T	T31	20-180°C	N/A	K-TYPE
DOWNCOMER TEMP	T	T32	20-180°C	N/A	K-TYPE
DOWNCOMER TEMP	T	T33	20-180°C	N/A	K-TYPE
DOWNCOMER TEMP	T	T34	20-180°C	N/A	K-TYPE
DOWNCOMER TEMP	T	T35	20-180°C	N/A	K-TYPE
DOWNCOMER TEMP	T	T36	20-180°C	N/A	K-TYPE
DOWNCOMER TEMP	T	T37	20-180°C	N/A	K-TYPE
DOWNCOMER TEMP	T	T38	20-180°C	N/A	K-TYPE
DOWNCOMER TEMP	T	T39	20-180°C	N/A	K-TYPE
DOWNCOMER TEMP	T	T40	20-180°C	N/A	K-TYPE
DOWNCOMER TEMP	T	T41	20-180°C	N/A	K-TYPE
DOWNCOMER TEMP	T	T42	20-180°C	N/A	K-TYPE
DOWNCOMER TEMP	T	T43	20-180°C	N/A	K-TYPE
DOWNCOMER TEMP	T	T44	20-180°C	N/A	K-TYPE
DOWNCOMER TEMP	T	T45	20-180°C	N/A	K-TYPE
DOWNCOMER TEMP	T	T46	20-180°C	N/A	K-TYPE
DOWNCOMER TEMP	T	T47	20-180°C	N/A	K-TYPE
DOWNCOMER TEMP	T	T48	20-180°C	N/A	K-TYPE
DOWNCOMER TEMP	T	T49	20-180°C	N/A	K-TYPE
DOWNCOMER TEMP	T	T50	20-180°C	N/A	K-TYPE
DOWNCOMER TEMP	T	T51	20-180°C	N/A	K-TYPE
DOWNCOMER TEMP	T	T52	20-180°C	N/A	K-TYPE
DOWNCOMER TEMP	T	T53	20-180°C	N/A	K-TYPE
DOWNCOMER TEMP	T	T54	20-180°C	N/A	K-TYPE
LOWER PLENUM TEMP	T	T55	20-180°C	N/A	K-TYPE
LOWER PLENUM TEMP	T	T56	20-180°C	N/A	K-TYPE

Table 8.2: Vessel Measurement

MEASUREMENT	TYPE	LABEL	MAX RANGE	MIN RANGE	CATALOG #
LOWER PLENUM TEMP	T	T57	20-180°C	N/A	K-TYPE
LOWER PLENUM TEMP	T	T58	20-180°C	N/A	K-TYPE
LOWER PLENUM TEMP	T	T59	20-180°C	N/A	K-TYPE
LOWER PLENUM TEMP	T	T60	20-180°C	N/A	K-TYPE
LOWER PLENUM TEMP	T	T61	20-180°C	N/A	K-TYPE
LOWER PLENUM TEMP	T	T62	20-180°C	N/A	K-TYPE
LOWER PLENUM TEMP	T	T63	20-180°C	N/A	K-TYPE
LOWER PLENUM TEMP	T	T64	20-180°C	N/A	K-TYPE
LOWER PLENUM TEMP	T	T65	20-180°C	N/A	K-TYPE
LOWER PLENUM TEMP	T	T66	20-180°C	N/A	K-TYPE
VESSEL OUTSIDE TEMP	T	T70	20-180°C	N/A	K-TYPE
VESSEL OUTSIDE TEMP	T	T71	20-180°C	N/A	K-TYPE
VESSEL OUTSIDE TEMP	T	T72	20-180°C	N/A	K-TYPE
WALL HEAT FLUX	Q	Q1	0-100W/m ²	N/A	ITI-TFM
WALL HEAT FLUX	Q	Q2	0-100W/m ²	N/A	ITI-TFM
WALL HEAT FLUX	Q	Q3	0-100W/m ²	N/A	ITI-TFM
INLET CONCENTRATION	CNC	CNC11	0-20 %	N/A	OXYMAT 5E

Table 8.3: Drywell Measurement

MEASUREMENT	TYPE	LABEL	MAX RANGE	MIN RANGE	CATALOG #
PRESSURE	P	P58	0-0.5 MPa	0-0.1 MPa	STD 930
PRESSURE	P	P59	0-0.5 MPa	0-0.1 MPa	STD 930
TEMPERATURE	T	T136	20-180°C		K-TYPE
TEMPERATURE	T	T137	20-180°C		K-TYPE
TEMPERATURE	T	T138	20-180°C		K-TYPE
TEMPERATURE	T	T139	20-180°C		K-TYPE
TEMPERATURE	T	T140	20-180°C		K-TYPE
TEMPERATURE	T	T141	20-180°C		K-TYPE
TEMPERATURE	T	T157	20-180°C		K-TYPE
TEMPERATURE	T	T158	20-180°C		K-TYPE
TEMPERATURE	T	T159	20-180°C		K-TYPE
TEMPERATURE	T	T160	20-180°C		K-TYPE
TEMPERATURE	T	T161	20-180°C		K-TYPE
SUMP LEVEL	DP	P60	0-30 KPa	N/A	STD 924
SUMP LEVEL	DP	P61	0-30 KPa	N/A	STD 924
CONCENTRATION	CNC	CNC5	0-20 %	N/A	OXYMAT 5E
CONCENTRATION	CNC	CNC6	0-20 %	N/A	OXYMAT 5E
CONCENTRATION	CNC	CNC7	0-20 %	N/A	OXYMAT 5E
CONCENTRATION	CNC	CNC8	0-20 %	N/A	OXYMAT 5E
CONCENTRATION	CNC	CNC9	0-20 %	N/A	OXYMAT 5E
WALL TEMP	T	T142	20-180°C	N/A	K-TYPE
WALL TEMP	T	T143	20-180°C	N/A	K-TYPE
WALL TEMP	T	T144	20-180°C	N/A	K-TYPE
WALL TEMP	T	T145	20-180°C	N/A	K-TYPE
HEAT FLUX	Q	Q4	0-100W/m ²	N/A	ITI-TFM
HEAT FLUX	Q	Q5	0-100W/m ²	N/A	ITI-TFM
HEAT FLUX	Q	Q6	0-100W/m ²	N/A	ITI-TFM
HEAT FLUX	Q	Q7	0-100W/m ²	N/A	ITI-TFM
RPV-DRYWELL DP	P	P62	0-10 KPa		STD 924

Table 8.4: Suppression Pool Measurement

MEASUREMENT	TYPE	LABEL	MAX RANGE	MIN RANGE	CATALOG #
WATER TEMP	T	T146	20-180°C	N/A	K-TYPE
WATER TEMP	T	T147	20-180°C	N/A	K-TYPE
WATER TEMP	T	T148	20-180°C	N/A	K-TYPE
WATER TEMP	T	T149	20-180°C	N/A	K-TYPE
WATER TEMP	T	T150	20-180°C	N/A	K-TYPE
WATER TEMP	T	T151	20-180°C	N/A	K-TYPE
TEMPERATURE	T	T162	20-180°C	N/A	K-TYPE
TEMPERATURE	T	T163	20-180°C	N/A	K-TYPE
TEMPERATURE	T	T164	20-180°C	N/A	K-TYPE
LEVEL	DP	P63	0-14 KPa	0-10 KPa	STD 924
LEVEL	DP	P64	0-14 KPa	0-10 KPa	STD 924
VENT LEVEL	DP	P65	0-14 KPa	0-10 KPa	STD 924
PRESSURE	P	P66	0-0.5 MPa	0-0.1 MPa	STD 930
PRESSURE	P	P67	0-0.5 MPa	0-0.1 MPa	STD 930
GAS CONCENTRATION	CNC	CNC10	0-20 %	N/A	OXYMAT 5E
GAS TEMPERATURE	T	T152	20-180°C	N/A	K-TYPE
GAS TEMPERATURE	T	T153	20-180°C	N/A	K-TYPE
VIDEO PORT	VP				
VIDEO PORT	VP				
VIDEO PORT	VP				
HEAT FLUX	Q	Q8	0-100W/m ²	N/A	ITI-TFM
HEAT FLUX	Q	Q9	0-100W/m ²	N/A	ITI-TFM
CAMERA	CCD				

Table 8 5. PCCS and ICS Measurement

MEASUREMENT	LABEL	TYPE	MAX RANGE	MIN RANGE	CATALOG #
INLET CONCENTRATION	CNC01	CNC	0-21%	0-21%	OXYMAT 5E
INLET CONCENTRATION	CNC02	CNC	0-21%	0-21%	OXYMAT 5E
NONCONDENSABLE VENT CONC	CNC03	CNC	0-21%	0-21%	OXYMAT 5E
NONCONDENSABLE VENT CONC	CNC04	CNC	0-21%	0-21%	OXYMAT 5E
CONDENSER PRESSURE DROP	P44	DP			STD 924
CONDENSER PRESSURE DROP	P45	DP			STD 924
CONDENSER PRESSURE DROP	P46	DP			STD 924
CONDENSER PRESSURE DROP	P47	DP			STD 924
CONDENSER PRESSURE DROP	P48	DP			STD 924
CONDENSER PRESSURE DROP	P49	DP			STD 924
INLET FLOW	P42	DP	0-3 KPa	0-3 KPa	STD 924
INLET FLOW	P43	DP	0-3 KPa	0-3 KPa	STD 924
NONCONDENSABLE VENT PRESS	P50	DP	-1KPa-5KPa	-1KPa-5KPa	STD 924
NONCONDENSABLE VENT PRESS	P51	DP	-1KPa-5KPa	-1KPa-5KPa	STD 924
NONCONDENSABLE VENT PRESS	P52	DP	-1KPa-5KPa	-1KPa-5KPa	
NONCONDENSABLE VENT PRESS	P53	DP	-1KPa-5KPa	-1KPa-5KPa	
NONCONDENSABLE VENT PRESS	P54	DP	-1KPa-5KPa	-1KPa-5KPa	
NONCONDENSABLE VENT PRESS	P55	DP	-1KPa-5KPa	-1KPa-5KPa	
POOL LEVEL	P56	DP	110 cm	110 cm	STD 924
POOL LEVEL	P57	DP	110 cm	110 cm	STD 924
CONDENSATE FLOW	MAG12	MAG	N/A	0-0.1 m/s	MagneW 3000
CONDENSATE FLOW	MAG13	MAG	N/A	0-0.1 m/s	MagneW 3000
CONDENSATE FLOW	MAG14	MAG	N/A	0-0.1 m/s	MagneW 3000
CONDENSATE FLOW	MAG15	MAG	N/A	0-0.1 m/s	MagneW 3000
CONDENSATE FLOW	MAG16	MAG	N/A	0-0.1 m/s	MagneW 3000
CONDENSATE FLOW	MAG17	MAG	N/A	0-0.1 m/s	MagneW 3000
INLET FLOW	N10	VENTURI	N/A	4.7-14.1 m/s	
INLET FLOW	N11	VENTURI	N/A	4.7-14.1 m/s	
CONDENSATE TEMP	T100	T	20-180°C	20-140°C	K-TYPE
CONDENSATE TEMP	T101	T	20-180°C	20-140°C	K-TYPE
CONDENSATE TEMP	T102	T	20-180°C	20-140°C	K-TYPE
CONDENSATE TEMP	T103	T	20-180°C	20-140°C	K-TYPE
CONDENSATE TEMP	T104	T	20-180°C	20-140°C	K-TYPE
CONDENSATE TEMP	T105	T	20-180°C	20-140°C	K-TYPE
CONDENSER TUBE TEMP	T124	T	20-180°C	20-140°C	K-TYPE
CONDENSER TUBE TEMP	T125	T	20-180°C	20-140°C	K-TYPE
CONDENSER TUBE TEMP	T126	T	20-180°C	20-140°C	K-TYPE
CONDENSER TUBE TEMP	T127	T	20-180°C	20-140°C	K-TYPE
CONDENSER TUBE TEMP	T128	T	20-180°C	20-140°C	K-TYPE

Table 8.5 PCCS and ICS Measurement

MEASUREMENT	LABEL	TYPE	MAX RANGE	MIN RANGE	CATALOG #
CONDENSER TUBE TEMP	T129	T	20-180°C	20-140°C	K-TYPE
CONDENSER TUBE TEMP	T130	T	20-180°C	20-140°C	K-TYPE
CONDENSER TUBE TEMP	T131	T	20-180°C	20-140°C	K-TYPE
CONDENSER TUBE TEMP	T132	T	20-180°C	20-140°C	K-TYPE
CONDENSER TUBE TEMP	T133	T	20-180°C	20-140°C	K-TYPE
CONDENSER TUBE TEMP	T134	T	20-180°C	20-140°C	K-TYPE
CONDENSER TUBE TEMP	T135	T	20-180°C	20-140°C	K-TYPE
CONDENSER TUBE TEMP	T165	T	20-180°C	20-140°C	K-TYPE
CONDENSER TUBE TEMP	T166	T	20-180°C	20-140°C	K-TYPE
CONDENSER TUBE TEMP	T167	T	20-180°C	20-140°C	K-TYPE
CONDENSER TUBE TEMP	T168	T	20-180°C	20-140°C	K-TYPE
CONDENSER TUBE TEMP	T169	T	20-180°C	20-140°C	K-TYPE
CONDENSER TUBE TEMP	T170	T	20-180°C	20-140°C	K-TYPE
CONDENSER TUBE TEMP	T171	T	20-180°C	20-140°C	K-TYPE
CONDENSER TUBE TEMP	T172	T	20-180°C	20-140°C	K-TYPE
CONDENSER TUBE TEMP	T173	T	20-180°C	20-140°C	K-TYPE
CONDENSER TUBE TEMP	T174	T	20-180°C	20-140°C	K-TYPE
CONDENSER TUBE TEMP	T175	T	20-180°C	20-140°C	K-TYPE
CONDENSER TUBE TEMP	T176	T	20-180°C	20-140°C	K-TYPE
INLET TEMP	T94	T	20-180°C	20-140°C	K-TYPE
INLET TEMP	T95	T	20-180°C	20-140°C	K-TYPE
INLET TEMP	T96	T	20-180°C	20-140°C	K-TYPE
INLET TEMP	T97	T	20-180°C	20-140°C	K-TYPE
INLET TEMP	T98	T	20-180°C	20-140°C	K-TYPE
INLET TEMP	T99	T	20-180°C	20-140°C	K-TYPE
NONCONDENSABLE VENT TEMP	T106	T	20-180°C	20-140°C	
NONCONDENSABLE VENT TEMP	T107	T	20-180°C	20-140°C	
NONCONDENSABLE VENT TEMP	T108	T	20-180°C	20-140°C	K-TYPE
NONCONDENSABLE VENT TEMP	T109	T	20-180°C	20-140°C	K-TYPE
NONCONDENSABLE VENT TEMP	T110	T	20-180°C	20-140°C	K-TYPE
NONCONDENSABLE VENT TEMP	T111	T	20-180°C	20-140°C	K-TYPE
POOL TEMPERATURE	T112	T	20-180°C	20-140°C	K-TYPE
POOL TEMPERATURE	T113	T	20-180°C	20-140°C	K-TYPE
POOL TEMPERATURE	T114	T	20-180°C	20-140°C	K-TYPE
POOL TEMPERATURE	T115	T	20-180°C	20-140°C	K-TYPE
POOL TEMPERATURE	T116	T	20-180°C	20-140°C	K-TYPE
POOL TEMPERATURE	T117	T	20-180°C	20-140°C	K-TYPE
POOL TEMPERATURE	T118	T	20-180°C	20-140°C	K-TYPE
POOL TEMPERATURE	T119	T	20-180°C	20-140°C	K-TYPE

Table 8.5: PCCS and ICS Measurement

MEASUREMENT	LABEL	TYPE	MAX RANGE	MIN RANGE	CATALOG #
POOL TEMPERATURE	T120	T	20-180°C	20-140°C	K-TYPE
POOL TEMPERATURE	T121	T	20-180°C	20-140°C	K-TYPE
POOL TEMPERATURE	T122	T	20-180°C	20-140°C	K-TYPE
POOL TEMPERATURE	T123	T	20-180°C	20-140°C	K-TYPE
POOL TEMPERATURE	T177	T	20-180°C	20-140°C	K-TYPE
POOL TEMPERATURE	T178	T	20-180°C	20-140°C	K-TYPE
POOL TEMPERATURE	T179	T	20-180°C	20-140°C	K-TYPE
POOL TEMPERATURE	T180	T	20-180°C	20-140°C	K-TYPE
POOL TEMPERATURE	T181	T	20-180°C	20-140°C	K-TYPE
POOL TEMPERATURE	T182	T	20-180°C	20-140°C	K-TYPE
POOL TEMPERATURE	T183	T	20-180°C	20-140°C	K-TYPE
POOL TEMPERATURE	T184	T	20-180°C	20-140°C	K-TYPE
POOL TEMPERATURE	T185	T	20-180°C	20-140°C	K-TYPE
POOL TEMPERATURE	T186	T	20-180°C	20-140°C	K-TYPE
POOL TEMPERATURE	T187	T	20-180°C	20-140°C	K-TYPE
POOL TEMPERATURE	T188	T	20-180°C	20-140°C	K-TYPE
FLOW RATE	V07	VORTEX	0.0267kg/s	0.0089 kg/s	VP715TS
FLOW RATE	V08	VORTEX	0.0267kg/s	0.0089 kg/s	VP715TS
FLOW RATE	V09	VORTEX	0.0267kg/s	0.0089 kg/s	VP715TS
FLOW RATE	V10	VORTEX	0.0267kg/s	0.0089 kg/s	VP715TS
FLOW RATE	V11	VORTEX	0.0267kg/s	0.0089 kg/s	VP715TS
FLOW RATE	V12	VORTEX	0.0267kg/s	0.0089 kg/s	VP715TS

Table 8.6: GDCS Measurement

MEASUREMENT	TYPE	LABEL	MAX RANGE	MIN RANGE	CATALOG #
LEVEL	DP	P36	0-14 KPa	N/A	STD 924
LEVEL	DP	P37	0-14 KPa	N/A	STD 924
LEVEL	DP	P38	0-14 KPa	N/A	STD 924
LEVEL	DP	P39	0-14 KPa	N/A	STD 924
LEVEL	DP	P40	0-14 KPa	N/A	STD 924
LEVEL	DP	P41	0-14 KPa	N/A	STD 924
TEMPERATURE	T	T82	20-180°C	N/A	K-TYPE
TEMPERATURE	T	T83	20-180°C	N/A	K-TYPE
TEMPERATURE	T	T84	20-180°C	N/A	K-TYPE
TEMPERATURE	T	T85	20-180°C	N/A	K-TYPE
TEMPERATURE	T	T86	20-180°C	N/A	K-TYPE
TEMPERATURE	T	T87	20-180°C	N/A	K-TYPE
TEMPERATURE	T	T88	20-180°C	N/A	K-TYPE
TEMPERATURE	T	T89	20-180°C	N/A	K-TYPE
TEMPERATURE	T	T90	20-180°C	N/A	K-TYPE
OUTLET FLOW	MAG	MAG9	0-1 m/s	N/A	MagneW 3000
OUTLET FLOW	MAG	MAG10	0-1 m/s	N/A	MagneW 3000
OUTLET FLOW	MAG	MAG11	0-1 m/s	N/A	MagneW 3000
OUTLET TEMP	T	T91	20-180°C	N/A	K-TYPE
OUTLET TEMP	T	T92	20-180°C	N/A	K-TYPE
OUTLET TEMP	T	T93	20-180°C	N/A	K-TYPE
COVER GAS CONCENTRATION	CNC	CNC12	0-20%	N/A	OXYMAT 5E

Table 8.7: Boundary Flow Measurement

COMPONENT	MEASUREMENT	TYPE	LABEL	MAX RANGE	MIN RANGE	CATALOG #
STEAM LINE BREAK	FLOW RATE	DP	P18	0-8 KPa		STD 924
STEAM LINE BREAK	FLOW RATE	VORTEX	V1	0.022 m/s	0.66 m/s	VP702TS
STEAM LINE BREAK	FLOW RATE	NOZZLE	N1	0.022 m/s	0.66 m/s	
STEAM LINE BREAK	FLOW RATE (LIQUID)	MAG	MAG1	0-5 m/s	N/A	MagneW 3000
STEAM LINE BREAK	VOID FRACTION	CAP	CAP1	0-1	N/A	PURDUE
STEAM LINE BREAK	PRESSURE	P	P19	0-1 MPa	0-0.01 MPa	STD 974
STEAM LINE BREAK	TEMPERATURE	T	T73	20-180°C	N/A	K-TYPE
VESSEL DPV	FLOW RATE	DP	P20	0-0.5 MPa		STD 930
VESSEL DPV	FLOW RATE	DP	P22	0-0.5 MPa		STD 930
VESSEL DPV	FLOW RATE	VORTEX	V2	0.0082 m/s	1.11 m/s	VP715TS
VESSEL DPV	FLOW RATE	VORTEX	V3	0.0082 m/s	1.11 m/s	VP715TS
VESSEL DPV	FLOW RATE	NOZZLE	N2	0.0082 m/s	1.11 m/s	
VESSEL DPV	FLOW RATE	NOZZLE	N3	0.0082 m/s	1.11 m/s	
VESSEL DPV	FLOW RATE (LIQUID)	MAG	MAG2	0-7 m/s	N/A	MagneW 3000
VESSEL DPV	FLOW RATE (LIQUID)	MAG	MAG3	0-7 m/s	N/A	MagneW 3000
VESSEL DPV	VOID FRACTION	CAP	CAP2	0-1	N/A	PURDUE
VESSEL DPV	VOID FRACTION	CAP	CAP3	0-1	N/A	PURDUE
VESSEL DPV	PRESSURE	P	P21	0-1 MPa	0-0.04 MPa	STD 974
VESSEL DPV	PRESSURE	P	P23	0-1 MPa	0-0.04 MPa	STD 974
VESSEL DPV	TEMPERATURE	T	T74	20-180°C	N/A	K-TYPE
VESSEL DPV	TEMPERATURE	T	T75	20-180°C	N/A	K-TYPE
MSL DPV	FLOW RATE	DP	P24	0-0.5 MPa	0-8 kPa	STD 930
MSL DPV	FLOW RATE	VORTEX	V4	0.0012 m/s	0.19 m/s	VP700TS
MSL DPV	FLOW RATE	NOZZLE	N4	0.0012 m/s	0.19 m/s	
MSL DPV	FLOW RATE (LIQUID)	MAG	MAG4	0-1.2 m/s	N/A	MagneW 3000
MSL DPV	VOID FRACTION	CAP	CAP4	0-1	N/A	PURDUE
MSL DPV	PRESSURE	P	P25	0-1 MPa	0-0.01 MPa	STD 974
MSL DPV	TEMPERATURE	T	T76	20-180°C	N/A	K-TYPE
MSL DPV	TEMPERATURE	T	T76-1	20-180°C	N/A	K-TYPE
SRV	FLOW RATE	DP	P26	0-0.5 MPa	0-8 KPa	STD 930
SRV	FLOW RATE	DP	P28	0-0.5 MPa	0-8 KPa	STD 930
SRV	FLOW RATE	NOZZLE	N5			
SRV	FLOW RATE	NOZZLE	N6			
SRV	FLOW RATE (LIQUID)	MAG	MAG5	0-2.9 m/s	N/A	MagneW 3000
SRV	FLOW RATE (LIQUID)	MAG	MAG6	0-2.9 m/s	N/A	MagneW 3000
SRV	VOID FRACTION	CAP	CAP5	0-1	N/A	PURDUE
SRV	VOID FRACTION	CAP	CAP6	0-1	N/A	PURDUE
SRV	PRESSURE	P	P27	0-1 MPa	0-1 MPa	STD 974
SRV	PRESSURE	P	P29	0-1 MPa	0-1 MPa	STD 974

Table 8.7: Boundary Flow Measurement

COMPONENT	MEASUREMENT	TYPE	LABEL	MAX RANGE	MIN RANGE	CATALOG #
SRV	TEMPERATURE	T	T77	20-180°C	N/A	K-TYPE
SRV	TEMPERATURE	T	T78	20-180°C	N/A	K-TYPE
FEED WATER BREAK	FLOW RATE	DP	P30	0-1 MPa		STD 930
FEED WATER BREAK	FLOW RATE	VORTEX	V5	0.0051 kg/s	0.0153 kg/s	VP701TS
FEED WATER BREAK	FLOW RATE	NOZZLE	N7	0.0051 kg/s	0.80 kg/s	
FEED WATER BREAK	FLOW RATE (LIQUID)	MAG	MAG7	0-1 m/s	N/A	MagneW 3000
FEED WATER BREAK	VOID FRACTION	CAP	CAP7	0-1	N/A	PURDUE
FEED WATER BREAK	PRESSURE	P	P31	0-1 MPa	0-0.4 MPa	STD 974
FEED WATER BREAK	TEMPERATURE	T	T80	20-180°C	N/A	K-TYPE
SMALL BREAKS	FLOW RATE	DP	P32			STD 924
SMALL BREAKS	FLOW RATE	VORTEX	V6			VP700TS
SMALL BREAKS	FLOW RATE	NOZZLE	N8			
SMALL BREAKS	FLOW RATE (LIQUID)	MAG	MAG8			MagneW 3000
SMALL BREAKS	VOID FRACTION	CAP	CAP8	0-1	N/A	PURDUE
SMALL BREAKS	PRESSURE	P	P33	0-1 MPa	0-0.4 MPa	STD 974
SMALL BREAKS	TEMPERATURE	T	T81	20-180°C	N/A	K-TYPE
FEED WATER	FLOW RATE	DP	P34			
FEED WATER	FLOW RATE	ORIF	N9			
FEED WATER	PRESSURE	P	P35	0-1 MPa	0-0.01 MPa	STD 974
FEED WATER	TEMPERATURE	T	T79	20-180°C	N/A	K-TYPE
FEED WATER	FLOW CONTROLLER	FLW - CONTROL				
VACUUM BREAKER	VACUUM BREAKER FLOW	DP	P68	0-20 KPa	N/A	STD 924
VACUUM BREAKER	VACUUM BREAKER FLOW	DP	P69	0-20 KPa	N/A	STD 924
VACUUM BREAKER	VACUUM BREAKER FLOW	DP	P70	0-20 KPa	N/A	STD 924
VACUUM BREAKER	VACUUM BREAKER LEAK	DP	P71	0-20 KPa	N/A	STD 924
EQUALIZATION LINE	FLOW	MAG	MAG18	0-0.5 m/s	N/A	MagneW 3000
EQUALIZATION LINE	FLOW	MAG	MAG19	0-0.5 m/s	N/A	MagneW 3000
EQUALIZATION LINE	FLOW	MAG	MAG20	0-0.5 m/s	N/A	MagneW 3000
EQUALIZATION LINE	TEMP	T	T154	20-180°C	N/A	K-TYPE
EQUALIZATION LINE	TEMP	T	T155	20-180°C	N/A	K-TYPE
EQUALIZATION LINE	TEMP	T	T156	20-180°C	N/A	K-TYPE

Table 8.8: Instruments

CATALOG #	TYPE	MIN RANGE	MAX RANGE	SENSITIVITY
VP702TS	VORTEX	0.0056-0.181 kg/s		1% reading
VP715TS	VORTEX	0.0028-0.113 kg/s		1% reading
VP701TS	VORTEX	0.0014-0.0396 kg/s		1% reading
VP700TS	VORTEX	0.00048-0.0112 kg/s		1% reading
MAGNEW 3000	MAGNETIC	0.1-1 m/s	1-10 m/s	2% reading at 10%, 1/2% reading at 40%
STD 924	PRESSURE	0-0.0062 MPa	0-0.1 MPa	250 Pa or 1/4% range
STD 930	PRESSURE	0-0.035 MPa	0-0.7 MPa	250 Pa or 1/4% range
STD 974	PRESSURE	0-0.7 MPa	0-21 MPa	1/4% RANGE
OMEGA K-TYPE	TEMPERATURE	-200'-1250'C		2.2'C
PURDUE	CONDUCTIVITY	0-100%		10% reading
EGG-TSA-12-CA-HG-43-dL	TURBINE	0.07-0.76 m/s	0.07-6.1 m/s	2% reading
FLOW SYSTEMS	VENTURI+NOZZLE			1.25% reading
ITI-TFM	HEAT FLUX	0-200 w/m		2w/m
SIEMENS OXYMAT SE	CONCENTRATION	0.1-20%		1/2% reading
PURDUE	CAPACITANCE	0-100%		

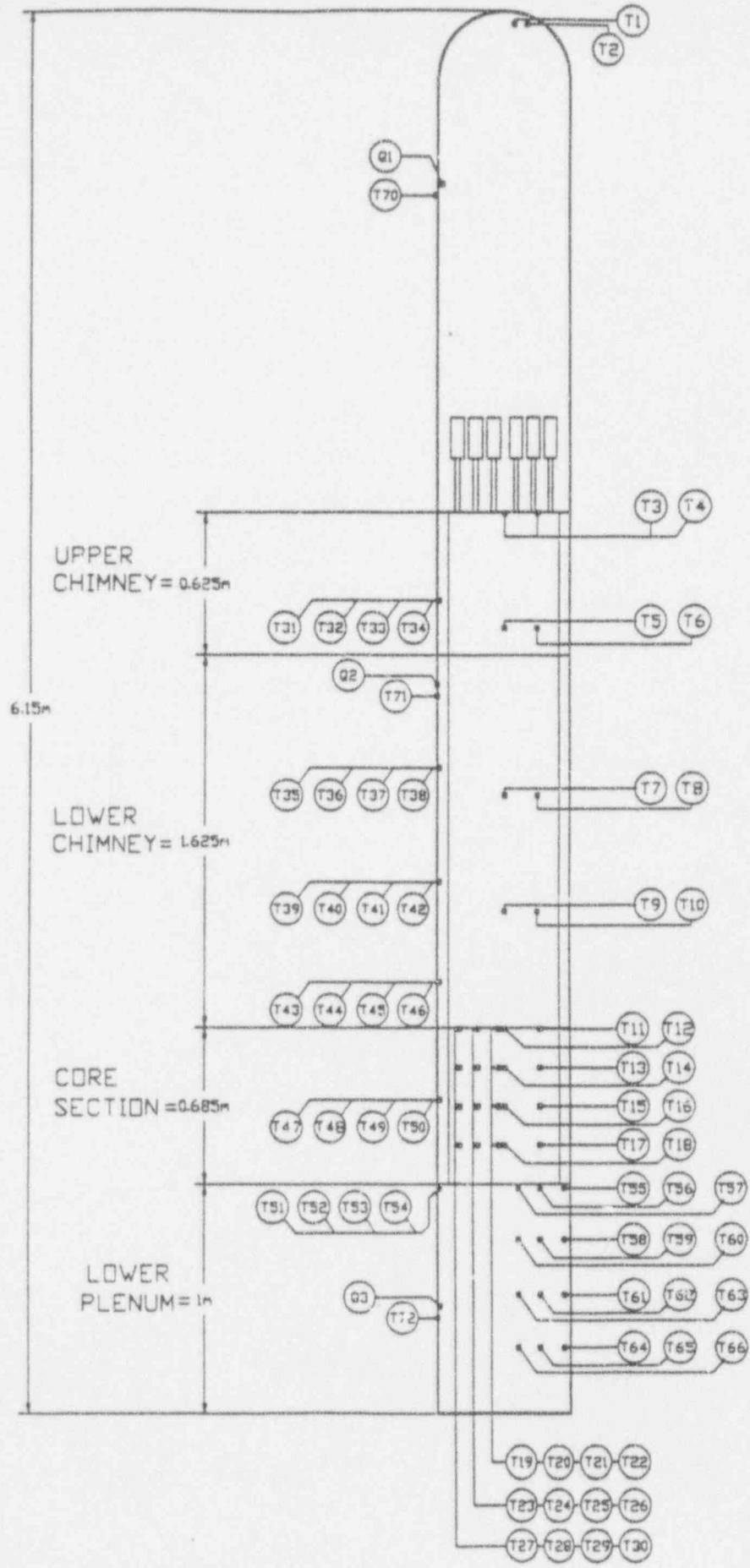


Figure 8.1 PUMA RPV temperature instrumentation

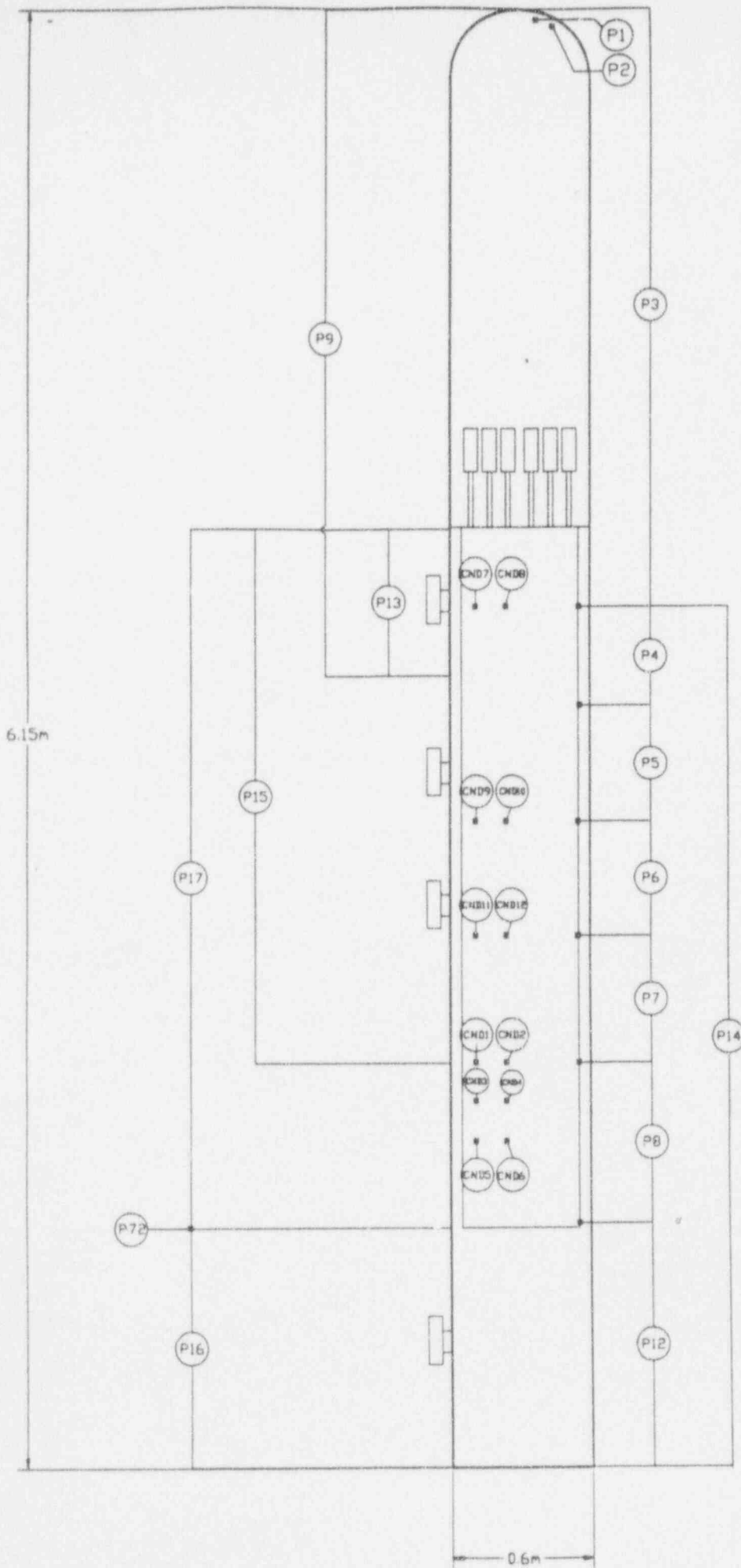


Figure 8.2 PUMA RPV pressure and void fraction instrumentation

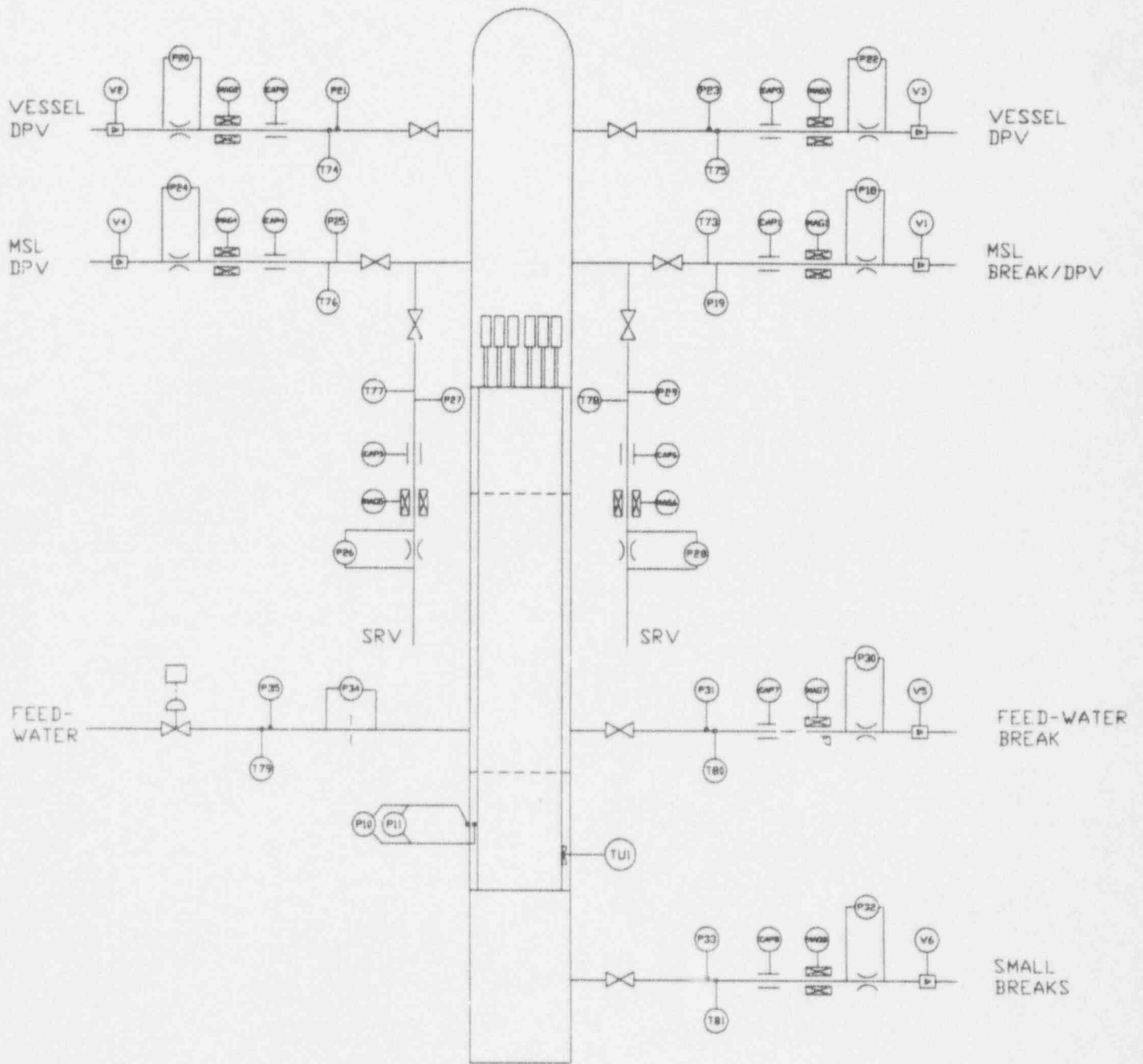


Figure 8.4 PUMA RPV boundary measurements

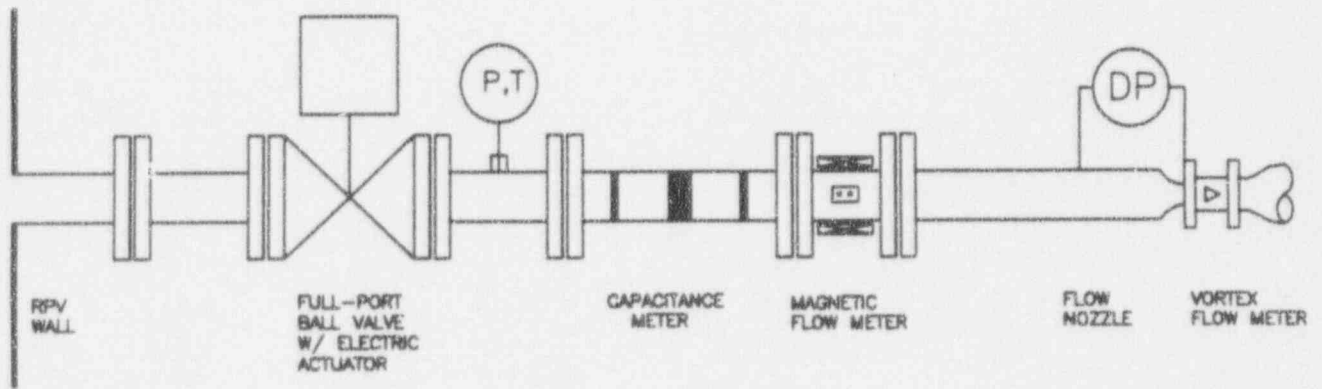


Figure 8.5 Typical instrumented ADS line

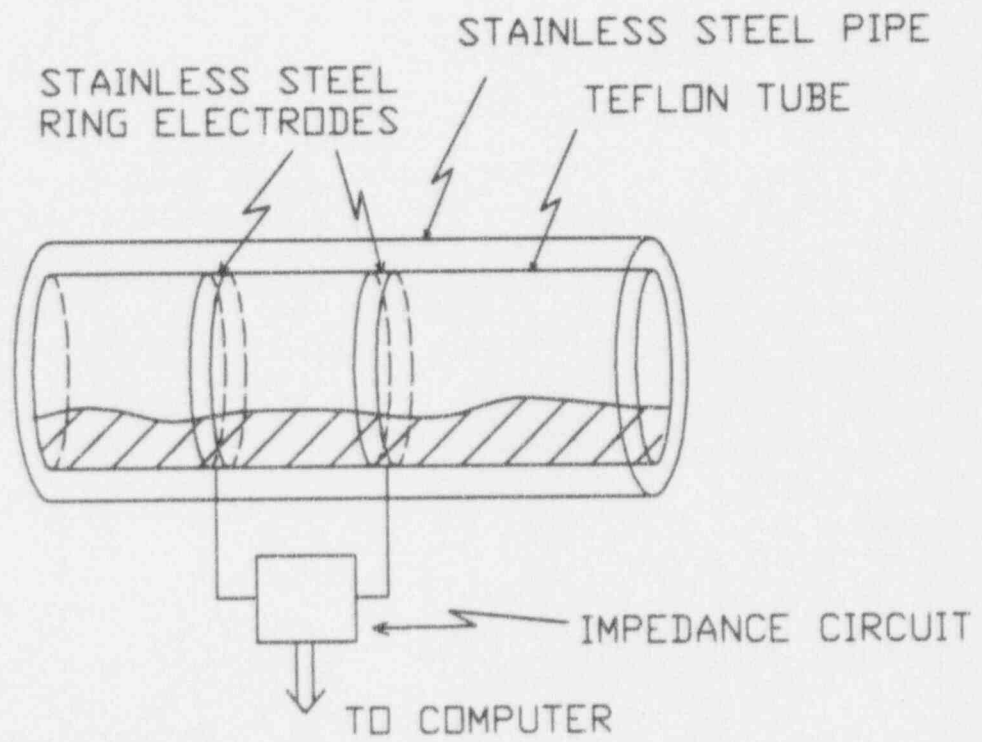


Figure 8.6 Capacitance probe schematic

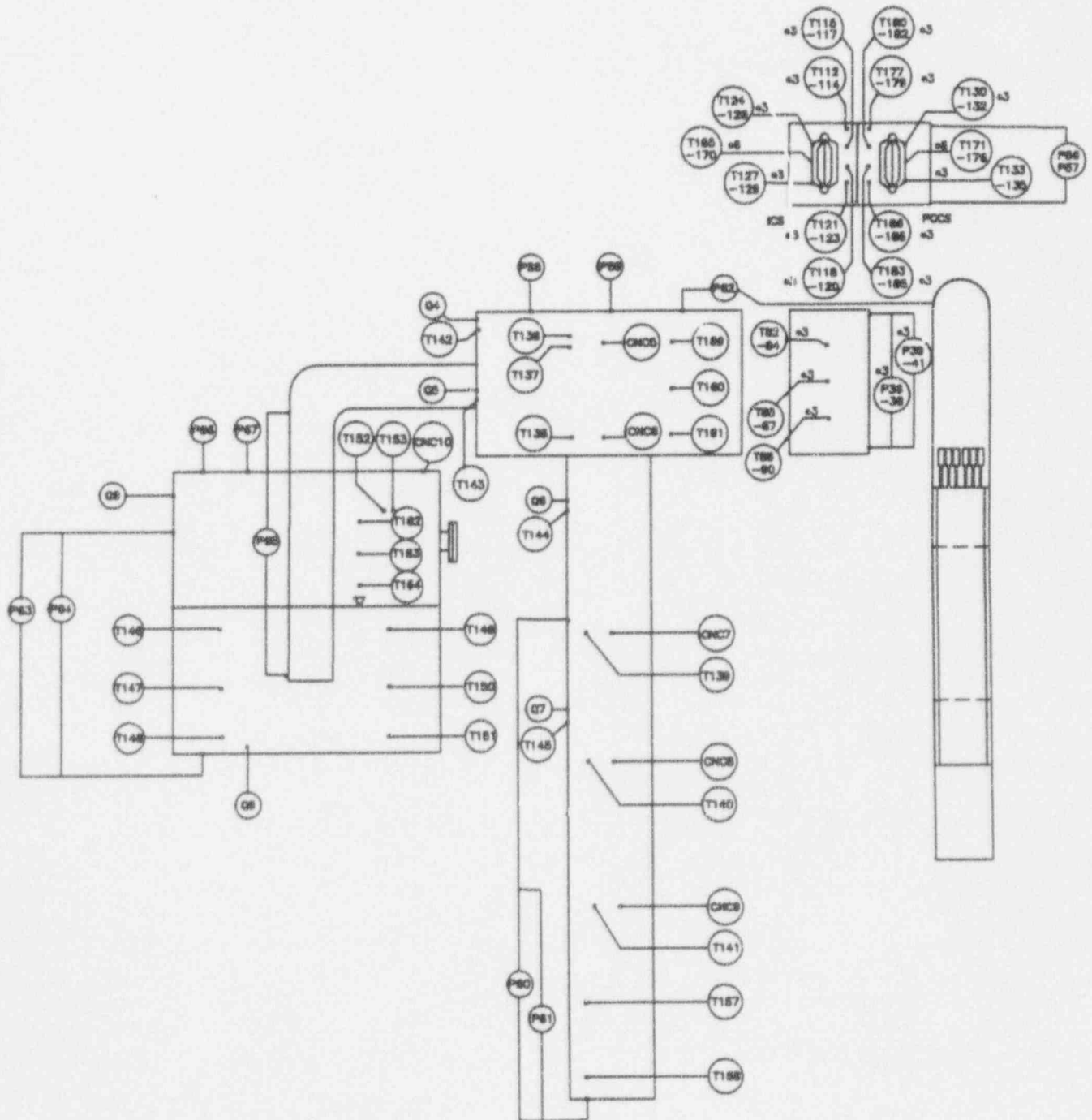


Figure 8.7 PUMA containment temperatures and pressures

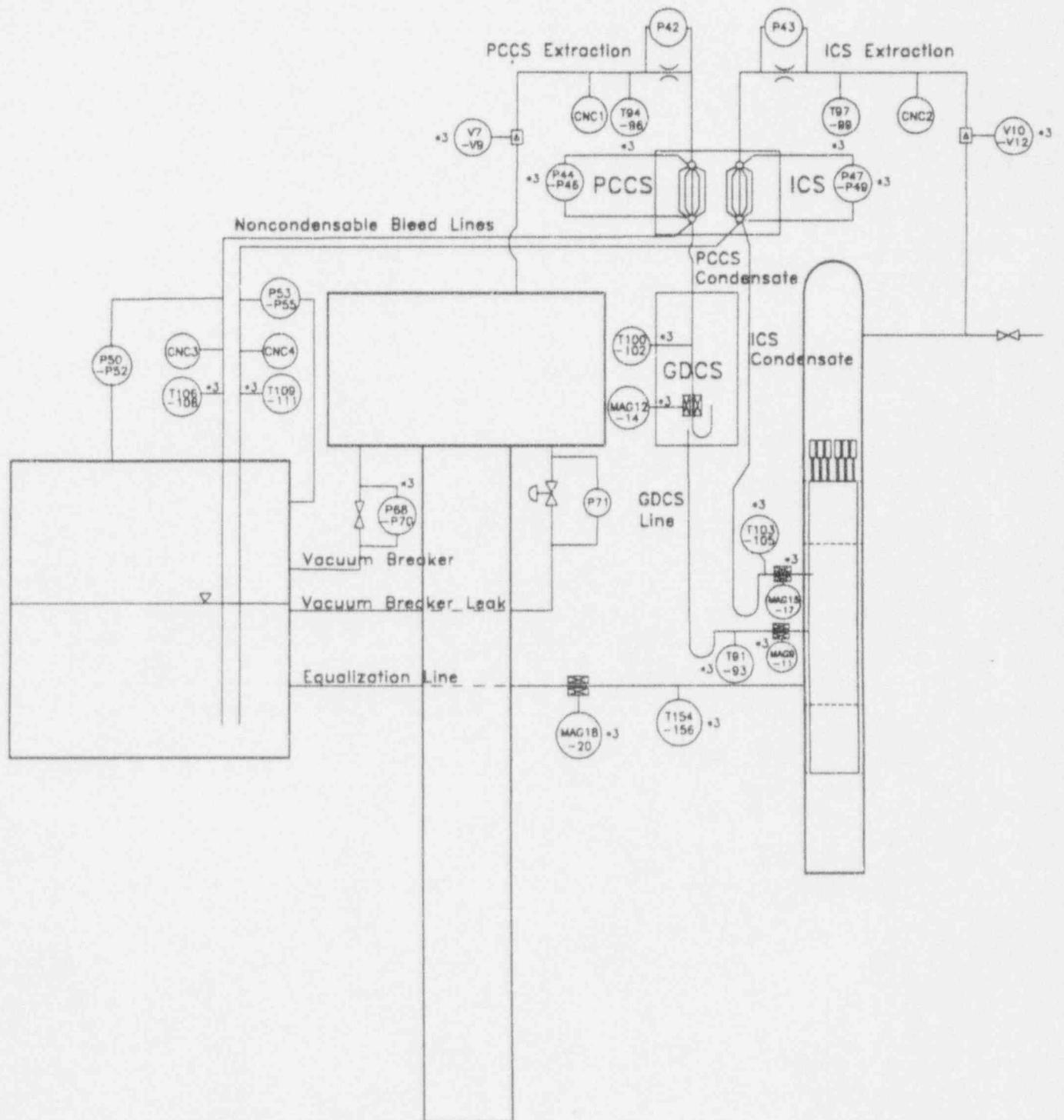


Figure 8.8 PUMA containment boundary flow measurement

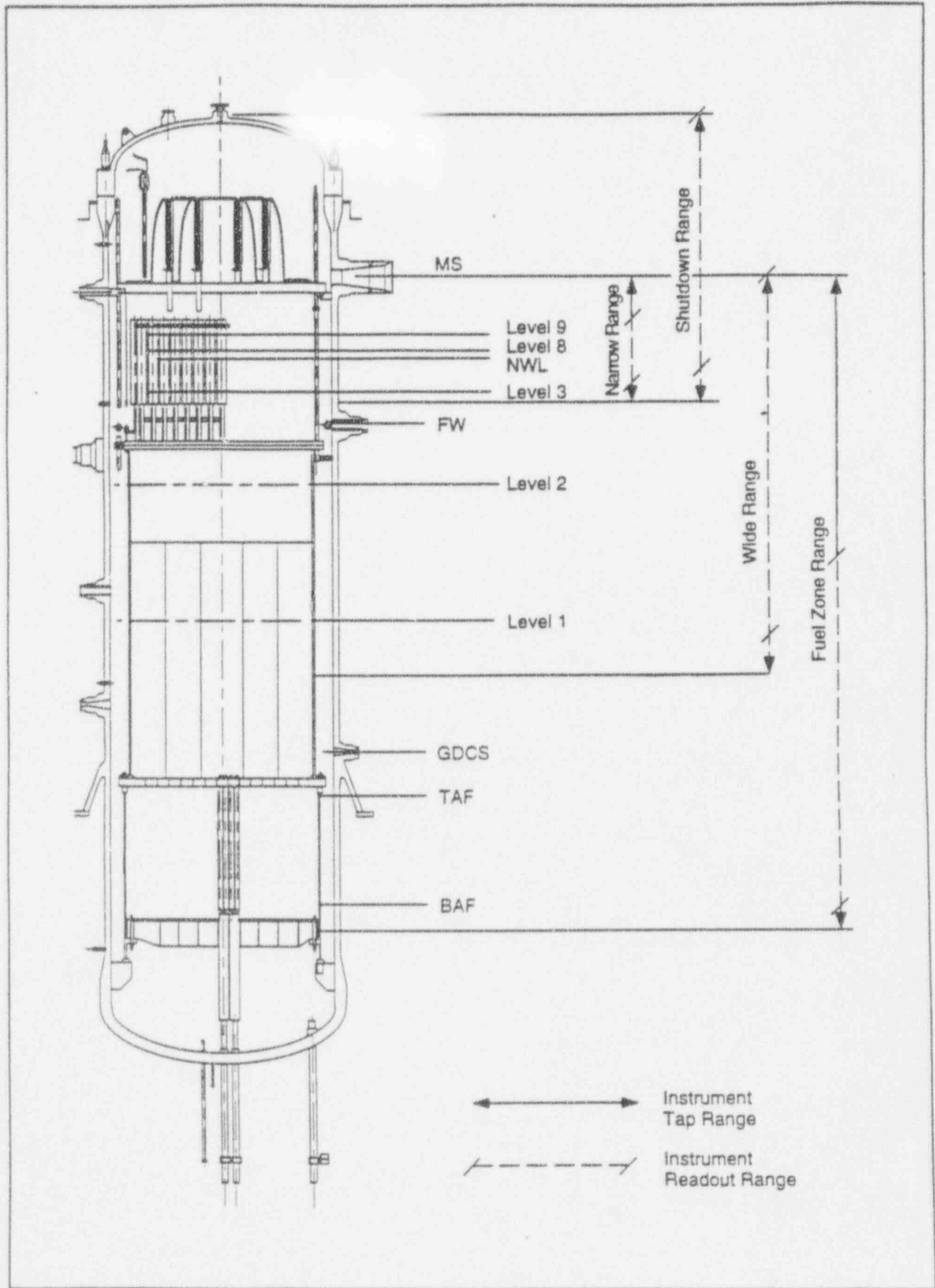


Figure 8.9 Water level ranges in the SBWR

References

- 8.1 Knoll, K. E., "Investigation of an Electromagnetic Flow Meter for Gas-Liquid Two-Phase Flow Measurement," ANS Winter Meeting, San Francisco, CA, November 11, 1991.
- 8.2 Revankar, S.T., Ishii, M., "Local Interfacial Area Measurement in Bubbly Flow," *Intl. J. Heat Mass Transfer*, Vol. 35, 913-925 (1992).
- 8.3 Andreussi, P., D.I. Donfrancesco, A. and Messia, M., "An Impedance Method for the Measurement of Liquid Hold-up in Two-phase Flow," *Intl. J. Multiphase Flow*, Vol 16, No. 6, 777-785 (1988).
- 8.4 Merilo, M., Dechene, R.L., and Ciconlas, W.M., "Void Fraction Measurement with a Rotating Electric Field Conductance Gauge," *J. Heat Transfer*, Vol. 99, 330-332 (1977).
- 8.5 Cimorelli, L. Evangelisti, R., "The Application of the Capacitance Method for Void Fraction Measurement in Bulk Boiling Conditions," *Intl. J. Heat & Mass Transfer*, Vol. 10, 277-288 (1967).

9. PUMA SYSTEM DESIGN

9.1. Scaling of PUMA Facility

The scaling approach for PUMA is based on three levels of scaling: integral system scaling; mass and energy inventory and boundary flow scaling; and local phenomena scaling. In the integral system scaling, the fluid continuity, integral momentum and energy equations in one-dimensional, area-averaged forms are used with the appropriate boundary conditions and the solid energy equation. From the non-dimensional form of the integral response functions under small perturbations, important dimensionless groups characterizing geometric, kinematic, dynamic, and energetic similarity parameters are derived. These are the geometrical non-dimensional groups, friction number, Richardson number, characteristic time constant ratio, Biot number and heat source number. For a two-phase system, the non-dimensional numbers are the phase change number, subcooling number, Froude number, drift-flux number, thermal inertia ratio number, two-phase friction number and orifice number.

In the mass and energy inventory and boundary flow scaling, the overall control volume balance equations for mass and energy are used. The scaling criteria give the similarity for flow area, velocity of fluid and enthalpy flow in the channel.

In the local phenomena scaling, the dominant phenomena are examined individually and appropriate similarity parameters are derived. The local phenomena considered are flow instabilities, choked flow, un-choked flow, flow regime and relative velocity, critical heat flux, natural circulation, flashing, condensation, heat source and sink, and mixing and stratification.

The scaling factors chosen for the confirmatory integral test facility (PUMA) are, of course, a compromise between several factors. For example, there is the requirement of keeping the facility within manageable size and cost, while at the same time constructing as large a facility as possible in order to provide a meaningful basis for extrapolation to the full-scale nuclear reactor. The plan to construct a facility scaled by 1/4 in height and 1/400 in volume was such a compromise.

The overall cost of the facility is mainly determined by the facility volume scale, and the number of instrumentations, and in lesser degree is affected by the total height of the facility. The proposed 1/400 volume scale is determined by the overall cost constraint, scale relation to the existing facility, and simulation capability of key phenomena.

The advantages of the present scale model are summarized below.

1. Well-balanced simulation of the frictional resistance and the hydrostatic driving head. This balance is essential in preserving the thermal-hydraulic characteristics of the loop.

2. Small aspect ratio similar to the prototype system. The value of l_R/d_R is only 2.5 relative to the linear scale of 1. This value of 2.5 is closer to unity than any facility which has been built or is under construction. Hence, the 2-D and 3-D phenomena are best simulated.
3. Relatively small heat loss to the structure by using the reduced-height model. For a fixed-volume scale model, the heat loss distortion is smaller for a shorter facility. The reduction of height by 1/4 gives considerable advantage over a full-height facility.
4. Accurate simulation of flow rates in interconnecting lines driven by hydrostatic head. By using the scaling method presented here, the flow rates in PCCS, GDCS and other connecting lines are well-scaled to simulate the prototype conditions. The scaling study indicates that it is not necessary to have the full height. This is contrary to the common belief that full-height simulation is necessary for the best simulation.
5. Preservation of flashing phenomena due to hydrostatic head decrease as the liquid rises in the RPV. A detailed study of the flashing phenomena indicates that reduction of the height beyond 1/4 scale may start to decrease the liquid flashing phenomena significantly. Since the mixture level is one of the most important parameters in terms of safety, the choice of the 1/4-height appears to be optimum.

9.2 Preliminary Design

Based on the above system scale of $l_R = 1/4$ and $a_R = 1/100$, a preliminary design of the prototypic pressure, reduced-height integral test facility has been developed at Purdue. The facility is designed to simulate the low-pressure phenomena of SBWR. The basic dimensions and parameters are given in Table 9.1. The overall configuration of the facility is shown in Figures 9.1 and 9.2. These figures show the relative locations and components.

It is clear from these drawings that the reactor vessel, containment and suppression pool are installed as independent pressure vessels with interconnecting piping systems. This option has been chosen over the integrated component system for increased accessibility to each component, simplified instrumentation systems, including flow visualization capability, and flexibility of the system. Any later modifications by GE to the SBWR prototype design can be easily accommodated by this separate component design.

The reactor vessel itself is geometrically scaled and the vessel internals are simulated. This insures that important 2-D and 3-D voiding phenomena and natural circulation instability phenomena can be well-preserved. It has an annulus downcomer with cylindrical core and chimney sections. Since the reactor vessel is outside of the containment, the vessel and all the connecting lines for ADS, GDCS and suppression pool are accessible from the outside.

9.3 Overall Instrumentation

The instrumentation consists of approximately 340 measurement points. The main objective is to measure the mass and energy content in each vessel as well as the two-phase level in the reactor vessel. High-frequency conductivity probes will be used for the first time in an integral test facility to determine the local value of the void fraction and the flow regime in the reactor vessel.

Approximately 200 measurements will be made in the reactor vessel. The most important quantity is the two-phase level in the core-chimney section. For this purpose, pressure taps are located approximately every 600 mm axially and at two radial locations corresponding to the central and peripheral sections of the chimney. These, combined with the conductivity probe measurements at the same locations, will provide the position of the two-phase level within the resolution of the pressure sensors (i.e., 25 mm of water) assuming a uniform void fraction above the measurement point closest to the surface. Another set of differential pressure transducers will be used to measure the downcomer level and a redundant measurement at the steam dome provides the vessel pressure. Seventy-two thermocouples will be used for detailed temperature distributions in the downcomer, lower plenum, reactor and chimney.

Measurements in the containment include single-phase levels, pressures, temperatures and non-condensable concentrations. Temperatures at six elevations will be measured in the suppression pool to determine the level of stratification. For drywell stratification, ten temperatures and five concentrations will be measured.

Boundary flows between the vessel and the containment will be measured as well. The measurement in the blowdown lines represent a very challenging task because the flow may be either single-phase liquid or vapor or two-phase flow. Moreover, these measurements must be non-intrusive since the vessel and containment are strongly coupled during decay heat removal. Capacitance probes will be used to determine the density. The flow will be measured by a variety of instruments.

Magnetic flow meters will be used to measure the velocity of single-phase liquid and bubbly two-phase flows. These measurements are effective up to 40% void fraction.

Nozzles will be used to measure the inertia of two-phase flows and high-speed vapor flows during blowdown. If it is assumed that these flows are homogeneous, the flow can be calculated from the flow nozzle pressure drop and the capacitance meter measurements combined.

Vortex flow meters and RTDs will be used to measure low-speed vapor flows during decay heat removal. These can measure very low steam velocities because of a unique ultrasonic sensing technique.

9.4 Initialization of Test

The design of the PUMA facility includes the necessary provisions to establish initial conditions for the proposed set of experiments. The PUMA facility is designed to study transient phenomena at and below 1.03 MPa (150 psia). Hence, the initial conditions for each test should correspond to the conditions at 1.03 MPa (150 psia). It is proposed to use results of RELAP5/CONTAIN computer code calculations to determine initial conditions. A team from Brookhaven National Laboratory (BNL) will conduct analysis using RELAP5/CONTAIN code, for each break simulation. The computer code calculations are performed for the prototype SBWR from the initiation of an accident (Break-LOCA) and progress through blowdown to the long term cooling scenario. The results of the code calculations are the basis for the initial test conditions on the PUMA facility. Purdue will determine the initial condition for PUMA testing at 1.03 MPa (150 psia) from the initial blowdown phase predicted by the code. It should be noted that the code predictions for the blowdown phase have been validated against experimental data.

The RELAP5/CONTAIN code involves models for RPV, core, vessel wall heat structures, PCCS/ICS condensers, containment, suppression pool, connecting piping, etc. The transient calculations provide the following parameters in all components of the facility modeled:

- Pressure
- Liquid levels in RPV, SP, DW, etc.
- Reactor decay power
- Mass inventory in each component
- Temperature of both phases
- Heat structure temperature (walls of RPV, DW, condenser, etc.)
- Heat flux in the heat transfer components
- Non-condensable concentration
- Void fraction
- Mass flow rate
- Liquid and gas velocity

Thus, all necessary initial conditions are obtained from RELAP5/CONTAIN code calculations at 1.03 MPa (150 psia) pressure. In order to establish these initial conditions in the experiments, the RPV, DW, SP and other vessels and piping have adequate provisions. All components in the facility have fill and drain lines to establish the mass inventory. Components with thermalhydraulic phenomena, such as RPV, SP and PCCS/ICS pools, have independent electrical heaters. Using these heaters, the required temperature in these units are established. To set the steam/air

concentration in DW and SP, an independent steam generator is used. The RPV, SP and DW have independent purge and pressure relief lines. These purge and relief lines each contain two sets of lines, one for coarse setting and the other for fine tuning. Using these lines, the required void fraction in the RPV can be established. Pressure conditions in all vessels can be established using the purge and relief lines. The reactor power level is controlled electronically through the computer.

A number of shakedown tests will be conducted to study the characteristics of heating and cooling, steam and liquid flow from component to component, fluid motion within each component, pressure response and stability of the thermodynamic condition. These characterization tests guide the nature of establishment of initial conditions required for each test. Once the loop is characterized for both adiabatic and heated cases, the actual test will be conducted. Table 9.2 summarizes the provisions and controls associated with each component for establishing the initial conditions for a test.

9.5 Preliminary Test Matrix

The preliminary test matrix consists of a total of approximately 50 tests which cover a broad spectrum of LOCAs and transients [9.6]. The preliminary test matrix is divided into two phases.

Phase 1 of the preliminary test matrix consists of 17 tests - 5 base case tests (Tests 1, 4, 7, 10, and 12), 8 GE counterpart tests (Tests, 2, 5, 8, 11, and 14-17), and 4 complementary tests (Tests, 3, 6, 9, and 13). In Table 9.3, Phase 1 of the preliminary test matrix is listed. Four types of LOCAs and transient tests will be investigated in this phase: bottom drain line break (BDLB), main steam line break (MSLB), GDCS line break (GDLB), feed water line break (FWLB), and loss of feed water (LOFW). Note that Tests 12 and 13 for FWLB have no counterpart tests in GIST, GIRAFFE, or PANDA. The numbers of operational components for Tests 14-17 are left in blank due to current lack of information. Few repeatability tests will be carried out as a part of the Phase 1 tests.

In Table 9.4, Phase 2 of the preliminary test matrix is listed. These tests include sensitivity study tests and beyond design-basis accident (DBA) tests. In Table 9.4, Tests 25-50 are not listed as they have yet to be selected and are reserved to accommodate future NRC needs. Tests 18-22 are for BDLB concurrent with a single component failure. Test 23 has multiple component failure - all three vacuum breakers failed in open position. Test 24 is a station blackout test (namely, loss of all AC power) cocurrent with a PCCS unit not available for operation.

9.6 Scaling Distortion and Potential Impact on Integral Test

The present scaled model cannot represent all detailed geometrical features of the SBWR. The model design was based on number of considerations. First, the requirements of global scaling were met. Then, important phenomena were identified and scaled for local scaling. In some cases, both global and local scaling cannot be satisfied simultaneously. In such cases, the requirement on global scaling was kept intact and certain compromises on local scaling were made. In addition to scaling considerations, hardware components were evaluated for ease of construction, operation and cost. Certain geometrical features in the model for some components were thus distorted. The most relevant distortion of components and their impact on the phenomena are discussed here.

9.6.1 RPV Core

The geometry of the RPV core is not modeled exactly as in the prototype. In Table 9.5, the major geometric distortions in the core and lower plenum are shown. The impact of these distortions is that the flow distribution in the heated section and in the by-pass flow section will be different from the prototype. The inventory of the fluid is also distorted in the core. This will distort the flow regime and void fraction in the core, which will impact the RPV thermal hydraulics in cases where the RPV water level is near or below the top of the core. The core behaves as the void generating section. Total height of the core is about 30% that of chimney length. In the chimney, the fluid flashes as it rises. The chimney provides the largest buoyancy head to the natural circulation flow in the RPV. Hence, the distortion of the model core geometry on the natural circulation flow is negligible. Distortion of liquid inventory in the core amounts to only about 3% of the total RPV liquid inventory. Moreover, during transients, the core has at least 30% void fraction. Hence, the impact of the distorted liquid inventory in the core on RPV thermal hydraulics is insignificant.

In the present facility (PUMA), the four SRVs on each MSL are replaced by the one SRV equivalent to the scaled flow area of four SRVs. Also, four stub tube DPVs from RPV are replaced by two DPV lines. However, for one of the ADS stages, four SRVs open simultaneously and for a later stage, two stub tube DPVs open simultaneously. Hence, combining these lines does not affect the blowdown phenomena.

9.6.2 GDCS Lines

The six GDCS lines are combined into three main injection lines in the present model facility. One of the main injection lines is branched into two lines at the RPV, so that a single line

break can be simulated. The important phenomena to be considered are the plume spread and mixing in the downcomer. The distortion introduced by reducing the number of injection lines on the plume spread and mixing in the downcomer needs to be investigated. The present facility has a l/d ratio of 2.5 compared to that of the prototype. This means that the effect of plume spread is almost 2.5 times larger in the model facility. Hence, reducing the number of injection lines by half compensates for the excess plume spread effect. Thus, in the present model facility, the reduction of six GDCS injection lines to three main injection lines has little distortion on the mixing phenomena in the downcomer region.

9.6.3 PCCS Condensation

In the present 1/4-height scale facility, the PCCS condenser heat transfer rates are higher. This distortion in PCCS condenser heat transfer will have an impact on a number of phenomena. The PCCS condensate supply to the GDCS tank increases which, in turn, provides cooling water to the RPV. This will accelerate the RPV coolant supply. The increased condensation rate will increase PCCS venting frequency into the suppression pool. Higher condensation in PCCS decreases the drywell pressure faster. The opening of the vacuum breaker is also accelerated. Hence, the transient may diverge from the ideal case. This distortion can be eliminated by reducing the condensation area of the PCCS condenser. This is implemented in the present facility by wrapping the required outside surface area of the PCCS condenser tubes (tentatively 30% of the tubes - to be confirmed by separate effect tests) with insulating sheets of material such as Teflon™, after the initial facility characterization and shakedown tests.

9.6.4 Drywell

The drywell design is simplified in the present model facility. The geometric distortion in the lower and upper drywell will have an impact on phenomena such as mixing, concentration and thermal stratification, natural circulation and heat transfer to the wall. Distortion of the wall material and area of the drywell affects the heat transfer characteristic. This can be corrected by using a material determined by thermal penetration scaling methodology. The drywell is covered by this material to simulate the concrete. The excess surface area of the drywell can be thermally insulated to avoid excess heat loss. The mixing and stratification phenomena in the drywell was found to depend on the jet Froude number, as presented in Chapters 5 and 7. However, the boundary flow of mass and energy is correctly scaled in the drywell. Thus, the global phenomena are preserved. The distortion of local phenomena, mixing and stratification, is not expected to significantly affect the overall integral response of the facility.

9.6.5 Suppression Pool

In the suppression pool, a single vent line is drawn from the drywell. This vent line has eight openings corresponding to the eight vent lines of the prototype. This distortion in design does not impact the discharge phenomena from the horizontal vents during the initial blowdown. However, at later stages of blowdown when the discharge is in the form of bubbles, the bubble vent phenomena may be distorted, as discussed in the scaling analysis of Chapter 5. Discharge phenomena from the sparger of the SRV have similar distortions. Also, due to the 1/4-height scale, the bubble residence time is smaller. This may have some impact on the condensation of vapor containing non-condensable gases. However, a recent study of condensation of steam bubbles containing non-condensable gases [9.7] indicates that the bubbles condense within a short distance of the discharge nozzle. Thus, the effect of 1/4-height scale is not expected to be significant. The thermal stratification of the pool water may introduce significant scaling distortions. Rising bubbles (non-condensable) purged from the PCCS condensers induce plume, which will raise the hot water to the pool surface. The heat from the pool surface may not quickly diffuse to the pool bottom. Hence, thermal stratification may occur. Due to 1/4-height scaling and 1/10 diameter scaling, plume dimensions are different in the present model. This will impact the degree of thermal stratification, which will have an impact on the suppression pool pressure. Scaling considerations on this phenomena are presented in the scaling analysis (Chapter 5).

9.6.6 Helium Gas Distribution

The simulation of hydrogen gas release into the drywell is carried out by injecting helium gas into the upper drywell through the bottom wall of the upper drywell. This is a distortion of initial hydrogen source location. However, present tests do not make any local measurement of helium concentration. The impact of the total helium injection on the PCCS condensation is studied by observing the response of the integral loop.

Table 9.1 Comparison of components dimensions between SBWR and PUMA.

<u>COMPONENT</u>	<u>SBWR</u>	<u>SOURCE OF ORIGIN</u>	<u>PUMA</u>
<u>RPV</u>			
Total height (mm)	*		6126.3
I.D. (mm)	6000	Ref. 9.1, p. 1.3-5	600
Total volume (m ³)	669	Ref. 9.4	1.732
Free volume (m ³)	607.3	Ref. 9.1, p. 5.1-5	1.5706
Wall material	Low alloy steel	Ref. 9.1, p. 1.3-5	S.S
Top of separator tubes	19364	Ref. 9.4	4841
Bottom of dryer skirt(mm)	*		4267.8
Top of dryer skirt(mm)	*		5316.8
Elevation of penetrations (mm)			
- GDCS equalization line	7493	Ref. 9.4	1873.3
- GDCS drain line	9493	Ref. 9.4	2373.3
- IC drain line	12065	Ref. 9.4	3016.3
- SDCS line			3938.8
- FW line	16455	Ref. 9.4	3999
- DPV line	19935	Ref. 9.4	4983.8
- MSL line	20380	Ref. 9.4	5095
<u>CORE</u>			
No. of rods	43920	Ref. 9.1, p. 1.3-3	38
Rod dia. (mm)	12.27	Ref. 9.1, p. 1.3-3	25.4
Rod clad material	Zr clad	Ref. 9.1, p. 1.3-3	S.S alloy clad
Hydraulic dia. (mm)	19.73	Calculated	63.2
Flow area (m ²)	7.4	Ref. 9.1, p. 4.4-6	0.153
	(inside channel)		
	5.6	Ref. 9.4	
	(outside channel)		
Core pressure drop (MPa)	0.048	Ref. 9.1, p. 4.4-6	0.012
Core height (mm)	3830	Ref. 9.1 p. 4.4-8	957.5
Active fuel length (mm)	2743	Table 1.3-1	685.8
Total power (at 2% power level) (MW)	40	Ref. 9.1, p. 1.3-2	0.2
Power per rod (at 2% power level) (kW)	0.91	Ref. 9.1, p. 1.3-2,3	5.26

Table 9.1 Continued ...

<u>COMPONENT</u>	<u>SBWR</u>	<u>SOURCE OF ORIGIN</u>	<u>PUMA</u>
Power density (at 2% power level) (kW/m ²)	8.61	Ref. 9.1, p. 1.3-2	96.13
Core shroud I.D. (mm)	5150	Ref. 9.2, p. 2.1-9	520
TAF elevation (mm)	6493	Table 21.5-5-5 Sheet 7	1623.3
BAF elevation (mm)	3750	Calculated (6493-2743)	937.5
Total fuel length + control rod (mm)	6934	Table 4.4-2	1733.5
Top of core plate elevation (mm)	*		880.8
Bottom of core shroud elevation (mm)	2146	Table 4.4-2	536.5
Core shroud O.D. (mm)	5250	Table 2.1.1-2 (Tier1)	525
Core Shroud wall thickness (mm)	50	Table 2.1.1- 2 (Tier 1)	2.5
Core downcomer width (mm)	375	Calculated (6000-5250)/2	37.5
Core downcomer annular area (m ²)	6.627	Calculated $\pi/4(6.0^2-5.25^2)$	0.0663
Core downcomer hydraulic diameter (mm)	750	Calculated	75
<u>CHIMNEY SECTION</u>			
Chimney shroud I.D. (mm)	4955	Ref. 9.4	502
Chimney shroud O.D. (mm)	5055	Ref. 9.4, p. 3 of 7	508
Top of chimney partition (mm)			3375.3
Chimney partition height (mm)	6500	Ref. 9.4	1625
Top of chimney (mm)	15996	Ref. 9.4	3999
Gap between TAF & bottom of chimney (mm)	*		110.75

Table 9.1 Continued ...

<u>COMPONENT</u>	<u>SBWR</u>	<u>SOURCE OF ORIGIN</u>	<u>PUMA</u>
Chimney wall thickness (mm)	50	Ref. 9.4	3
Chimney downcomer width (mm)	472.5	Calculated	46
Chimney downcomer area (m ²)	8.205	Calculated	0.0801
Chimney downcomer hydraulic diameter (mm)	945	Calculated	92
# of divided areas	25	Ref. 9.4	9
Dimension of divided areas		Ref. 9.4	five 165 (mm) dia. pipes
Water levels inside RPV measured from inside bottom (mm)			
- Normal water level (NWL)	18260	Ref. 9.4, Table 21.5-1-1, SH. 7	4565
- Level 9	19355.5	Ref. 9.1, Table 15.0-1	4838.9
- Level 8	18713	Ref. 9.4, Table 21.5-1-1, SH. 7	4678.3
- Level 3	17333	Ref. 9.4, Table 21.5-1-1, SH. 7	4333.3
- Level 2	14423	Ref. 9.4, Table 21.5-1-1, SH. 7	3605.8
- Level 1	10423	Ref. 9.4, Table 21.5-1-1, SH. 7	2605.8
- Level 0.5	7493	Ref. 9.4, Table 21.5-1-1, SH. 7	1873.3
Water level ΔP lines:			
- Fuel zone range: bottom sense port (mm)	2600	Ref. 9.4, Table 21.5-1-1, SH 7	650
- Fuel zone range: top sense port (mm)	20600	Ref. 9.4, Table 21.5-1-1, SH 7	5100
- Wide range: bottom sense port level (mm)	9600	Ref. 9.4, Table 21.5-1-1, SH 7	2400

Table 9.1 Continued ...

<u>COMPONENT</u>	<u>SBWR</u>	<u>SOURCE OF ORIGIN</u>	<u>PUMA</u>
- Wide range: top sense port level (mm)	20600	Ref. 9.4. Table 21.5-1-1, SH 7	5100
- Shutdown range: bottom sense line level (mm)	17060	Ref. 9.4. Table 21.5-1-1, SH 7	4265
- Shutdown range: top sense line level (mm)	24612	Ref. 9.4. Table 21.5-1-1, SH 7	6150
- Narrow range: bottom sense port level (mm)	17060	Ref. 9.4. Table 21.5-1-1, SH 7	4265
- Narrow range: top sense port level (mm)	20600	Ref. 9.4. Table 21.5-1-1, SH 7	5100
<u>CONTAINMENT</u>			
Wall material	Reinforced concrete with steel liner	Ref. 9.1, p. 1.3-9	S.S
Upper dry well free volume (above RPV skirt level) (m ³)	*		10.99
Lower dry well free volume (below RPV skirt level) (m ³)	*		2.56
Total volume (m ³)	*		13.55
Orifice plate elevation (RPV skirt) (mm)	*		1525
Top elevation (central section) (mm)	*		5825
Bottom elevation (central section) (mm)	*		-2250
Elevation of penetrations			
MSL break line (mm)	20380	Ref. 9.4	5095
DPV break line (mm)	19935	Ref. 9.4	4983.8
SRVs (mm)	20380	Ref. 9.4	5095
Suppression pool vent (mm)	17200	Ref. 9.1, p. 6.2-115	4300
Vacuum breakers (mm)	17200	Ref. 9.1, p. 21-3	4300
PCCS supply line (mm)	23300	Ref. 9.1, p. 6.2-113	5825
GDCS opening (mm)	23300	Ref. 9.1, p. 6.2-113	5825
FWL break (mm)	15996	Ref. 9.4	3699

Table 9.1 Continued ...

<u>COMPONENT</u>	<u>SBWR</u>	<u>SOURCE OF ORIGIN</u>	<u>PUMA</u>
GDCS drain line break (mm)	9493	Ref. 9.4	2073.25
GDCS equalization line break (mm)	7493	Ref. 9.4	1573.25
ICS condensate drain line break (mm)	12065	Ref. 9.4	2716.25
CRD line break (mm)	0	Ref. 9.4	0
RWCU/SDS line break (mm)	0	Ref. 9.4	0
Vacuum line leak (mm)	17200	Ref. 9.1, p. 21-3	4300
<u>SUPPRESSION POOL</u>			
Initial water volume (m ³)	3255	Ref. 9.1, p. 6.2-60	8.492
Initial gas space volume (m ³)	3819	Ref. 9.1, p. 6.2-60	9.193
Top elevation (mm)	16000	Ref. 9.1, 6.2-113	4000
Height (mm)	11350	Ref. 9.1, p. 6.2-113	2837.5
Pool surface area (m ²)	588	Ref. 9.1, p. 6.2-60	6.133
Pool equivalent diameter (mm)	27450	Ref. 9.1, p. 6.2-60	2817
Water level height (mm)	5450	Calculated	1362.5
Vertical vent area (m ²)	9	Ref. 9.1, p. 6.2-60	0.0993
Vertical channel diameter (mm)	1200 (total 8)	Ref. 9.1, p. 6.2-61	356 (one channel only)
# of horizontal vents	24	Ref. 9.1, p. 6.2-61	12
Diameter of horizontal vents (mm)	700	Ref. 9.1, p. 6.2-61	175x200
# of vacuum breakers	3	Ref. 9.1, p. 21-9	3
Diameter of vacuum breaker (mm)	508	Ref. 9.1, p. 6.2-15	50.8
Elevation of penetrations w.r.t. RPV inside bottom			
Dry well vent (mm)	16000	Ref. 9.1, p. 6.2-117	4000
Vacuum breakers (mm)	16000	Ref. 9.1, p. 21-3	4000

Table 9.1 Continued ...

<u>COMPONENT</u>	<u>SBWR</u>	<u>SOURCE OF ORIGIN</u>	<u>PUMA</u>
SRVs (mm)	16000	Ref. 9.1, p. 21-3	3562.8
GDCS equalization lines (mm)	7493	Ref. 9.4	1872.8
Non-condensable return line	16000	Ref. 9.4	4000
Non-condensable sparger height (mm)	860	Ref. 9.4	212.5
<u>ICS/PCCS Pools</u>			
Initial water height (mm)	*		1100
Pool height (mm)	*		1450
Bottom elevation (mm)	25300	Ref. 9.1, p. 6.2-113	6325
Top elevation (mm)	*		7775
Initial total water volume (m ³)	*		2.158
Initial gas volume (m ³)	*		0.825
Total volume of IC/PCC pools (m ³)	*		3.42
Boiloff height above PCC tubes (mm)	*		377.5
IC (or PCC) pool diameter (mm)	Not circular		1225
<u>ISOLATION CONDENSER (1 0.F 3)</u>			
Number of units	3	Ref. 9.1, p. 21-5	3
Modules per unit	2	Ref. 9.1, p. 21-5	1
Tubes per Module	*		10
Total heat transfer area (m ²)			
- Inside	*		0.988
- Outside	*		1.077
Total flow area (m ²)	*		0.0128
Condenser tubes			
- length (mm)	*		450
- OD (mm)	*		25.4
- ID (mm)	*		23.3
- Material	*		SS

Table 9.1 Continued ...

<u>COMPONENT</u>	<u>SBWR</u>	<u>SOURCE OF ORIGIN</u>	<u>PUMA</u>
Headers per module:			
- I.D. (height of liquid space) (mm)	*		170
Volume (m ³)	*		0.0024889
Vent nozzle size (mm)	*		4.949 (critical flow) 7 (non-critical flow)
centerline elevation of lower header from bottom of IC pool (mm)	*		230
<u>PCCS CONDENSER (1 OF 3)</u>			
Number of units	3	Ref. 9.1, p. 5.4-9	3
Modules per unit	2	Ref. 9.1, p. 5.4-9	1
Tubes per Module	*		10
Total heat transfer area (m ²)			
- Inside	*		2.012
- Outside	*		2.155
Total flow area (m ²)			0.0532
Condenser tubes			
- length (mm)	*		450
- OD (mm)	*		50.8
- ID (mm)	*		47.5
- Material	*		SS
Headers			
- I.D. (height of liquid space) (mm)	*		165
Volume (m ³)	*		0.001947
Centerline elevation of lower header from bottom of IC pool (mm)	*		167.5
<u>GDCS POOL</u>			
Water volume (m ³)	*		2.608

Table 9.1 Continued ...

<u>COMPONENT</u>	<u>SBWR</u>	<u>SOURCE OF ORIGIN</u>	<u>PUMA</u>
Normal water height (mm)	*		1400
Gas space volume (m ³)	*		0.233
Gas space height (mm)	*		125
Total volume (m ³)	*		2.841
Non-drainable water volume (m ³)	*		0.14
Non-drainable water height (mm)	*		75
Total height (mm)	6100	Ref. 9.1, p. 6.2-115	1525
Diameter (mm)	Not circular	Ref. 9.1, p. 6.2-115	1540
<u>ADS & MSL</u>			
MSL length (mm)	22865	Ref. 9.4	4431
MSL diameter (mm)	711.2	Ref. 9.1, p. 6.2-118	76.2
MSL nozzle (mm)	353.822	Ref. 9.1, p. 6.2-118	25.019
MSL break size (mm)	711.2	Ref. 9.1, p. 6.3-20,21	50.289
Minor loss	6.90	Calculated	36.37
SRV line length (mm)	20320	Calculated	8000
SRV line (mm)	203.2 (4 each)	Ref. 9.1, p. 21-39	50.8
SRV nozzle (mm)	92.202 (4 each)	Ref. 9.4	13.056
Minor loss	7.17	Calculated	70.04
DPV (MSL) line length (mm)	4712	Ref. 9.4	4431
DPV (MSL) line diameter (mm)	304.8	Ref. 9.1, p. 21-39	76.2 (connected to MSL)
DPV (MSL) nozzle (mm)	177.876	Ref. 9.4	12.573
Minor loss	101.95	Calculated	537.50
DPV (RPV) line length (mm)	2300	Ref. 9.4	3686
DPV (RPV) line diameter (mm)	457.2 (4 each)	Ref. 9.1, p. 21-39	76.2 (2 each)
DPV nozzle (mm)	304.8 (4 each)	Ref. 9.4	30.48 (2 each)
Minor loss	14.71	Calculated	113.43

Table 9.1 Continued ...

<u>COMPONENT</u>	<u>SBWR</u>	<u>SOURCE OF ORIGIN</u>	<u>PUMA</u>
<u>IC SUPPLY LINE (1 OF 3)</u>			
Length (mm)	18118	Ref. 9.4	11000
Diameter (mm)	254	Ref. 9.1, p. 21-45	38.1
Elevation change (mm)	9765	Ref. 9.4	2441.25
Minor loss	7.51	Calculated	152.08
<u>IC CONDENSATE LINE (1 OF 3)</u>			
Length (mm)	27560	Ref. 9.4	11000
Diameter (mm)	152.4	Ref. 9.1, p. 21-45	25.4
Elevation change (mm)	17635	Ref. 9.4	4408.75
Break size (mm)	146.2	Ref. 9.1, p. 6.3-20,21	50.8
Minor loss	4.8	Calculated	37.04
<u>IC VENT LINE (1 OF 3)</u>			
Length (mm)	*		4000
Diameter (mm)	*		12.7
Elevation change (mm)	*		5055
Minor loss	43.08	Calculated	85096.3
<u>PCCS SUPPLY LINE (1 OF 3)</u>			
Length (mm)	7960	Ref. 9.4	7000
Diameter (mm)	254 & 203.2	Ref. 9.1, p. 21-53	38.1
Elevation change (mm)	6400	Ref. 9.4	1600
Minor loss	5.08	Calculated	25.72
<u>PCCS VENT LINE (1 OF 3)</u>			
Length (mm)	24039	Ref. 9.4	4000
Diameter (mm)	203.2 & 254	Ref. 9.1, p. 21-53	38.1
Elevation change (mm)	16620	Ref. 9.4	4155
Minor loss	4.6	Calculated	23.29

Table 9.1 Continued ...

<u>COMPONENT</u>	<u>SBWR</u>	<u>SOURCE OF ORIGIN</u>	<u>PUMA</u>
<u>PCCS CONDENSATE LINE</u>			
<i>(1 OF 3)</i>			
Length (mm)	8661	Ref. 9.4	10000
Diameter (mm)	101.6 & 152.4	Ref. 9.1, p. 21-53	25.4
Elevation change (mm)	490	Ref. 9.4	122.5
Minor loss	6.68	Calculated	51.54
<u>GDCS EQUALIZATION LINE</u>			
<i>(1 OF 3)</i>			
Length (mm)	11432	Ref. 9.4	5500
Diameter (mm)	152.4	Ref. 9.1, p. 21-54	12.7
Elevation change (mm)	1840	Ref. 9.4	460
Nozzle size (mm)	50.8	Ref. 9.1, p. 6.3-6	3.59
Line break size (mm)	152.4	Ref. 9.1, p.6.3-20,21	50.8
Minor loss	41.67	Calculated	20.1
<u>GDCS DRAIN LINE (1 OF 3)</u>			
Length (mm)	25766	Ref. 9.4	6000
Diameter (mm)	203.2 & 152.4	Ref. 9.1, p. 21-54	38.1
Elevation change (mm)	8107	Ref. 9.4	2026.75
Line nozzle size (mm)	76.2	Ref. 9.1, p. 6.3-6	5.385
Line break size (mm)	152.4	Ref. 9.1, p. 6.3-20,21	50.8
Minor loss	13.59	Calculated	132.72
<u>FEEDWATER LINE</u>			
<i>(1 OF 2)</i>			
Length (mm)	*		4000
Diameter (mm)	355.6	Ref. 9.1, p. 21-41	38.1
Line break size (mm)	227.7	Ref. 9.1, p. 6.3-20,21	50.8
sparger reducing tee (mm)	127	Ref. 9.5, p. 3	12.7
Sparger nozzles I.D. (mm)	7.37	Ref. 9.5, p. 3	4.763
Minor loss	7.37	Calculated	9.71
<u>AUXILIARY LINES</u>			
CRD line (mm)	31.75	Ref. 9.1, p. 21-35	25.4
Bottom break line (mm)	50.8	Ref. 9.1, p. 21-34	50.8

Table 9.1 Continued ...

<u>COMPONENT</u>	<u>SBWR</u>	<u>SOURCE OF ORIGIN</u>	<u>PUMA</u>
RWCU/SDC line (mm)	76.2	Ref. 9.1, p. 21-46	12.7
RWCU/SDC line (side of RPV) (mm)	203.2	Ref. 9.1, p. 21-46	25.4
Line break size (mm)	193.6	Ref. 9.1, p.6.3-20,21	50.8

* Information available from GE Nuclear Energy

Table 9.2 Controls and Provisions on Various Components of PUMA

Control/Provision	Component
Liquid Injection and Drain Line	RPV, Drywell, SP, GDSCS, PCCS and ICS pools
Steam Injection and Relief Valve Systems	RPV, Drywell, SP
Liquid Level Measurement	RPV, Drywell, SP, GDSCS, PCCS/ICS pools
Temperature and Pressure Measurement at Different Height	RPV, Drywell, SP, GDSCS, PCCS/ICS pools
Non-Condensable Concentration Measurement	Drywell, SP, ICS/PCCS Condensers
Void Fraction Measurement	RPV
Heater Power	RPV Core 400 kW, SP 50 kW, ICS/PCCS pools - 30 kW each
Timer Controlled by Computer	ADS (SRVs and DFVs)

Table 9.3 Phase 1 of the Preliminary Test Matrix - Base Case and GE Counterpart Tests

Test	Event	Operational Components					EQLN	DWS	WWS
		PCCS	ICS	GDCS Lines	DPV	VB			
1 (Base)	MSLB	3	3	6	6	3	3	0	0
2*	MSLB (GIST B01)	0	0	4	6	3	3	0	0
3	MSLB	3	3	4	6	3	3	0	0
4 (Base)	BDLB	3	3	6	6	3	3	0	0
5*	BDLB (GIST A07)	0	0	4	6	3	3	0	0
6	BDLB	3	3	4	6	3	3	0	0
7 (Base)	GDLB	3	3	5	3	3	0	0	0
8*	GDLB (GIST C01A)	0	0	4	6	3	3	0	0
9	GDLB	3	3	4	6	3	3	0	0
10 (Base)	LOFW	3	3	6	6	3	3	0	0
11*	LOFW (GIST D03A)	0	0	4	6	3	3	0	0
12 (Base)	FWLB	3	3	6	6	3	3	0	0
13*	FWLB	0	0	4	6	3	3	0	0
14	MSLB (GIRAFFE/PANDA)								
15	BDLB (GIRAFFE)								
16	GDLB (GIRAFFE/PANDA)								
17	ICRLB								

* Test will be terminated when a temperature or pressure set point is reached to prevent damage. VB = vacuum breaker between drywell and wetwell, EQLN = equalization line connecting suppression pool to the vessel (e.g., 3 means all three equalization lines will be open if actuated automatically or manually), DWS = drywell spray, WWS = wetwell spray, MSLB = main steam line break, BDLB = bottom drain line break, GDLB = GDCS line break, LOFW = loss of feed water, FWLB = feedwater line break, ICRLB = isolation condenser condensate return line break. No information is currently available regarding the number of operational components in the GIRAFFE and PANDA tests

Table 9.4 Phase 2 of the Preliminary Test Matrix - Sensitivity Study and Beyond DBA Tests

Test	Event	Operational Components					EOLN	DWS	WWS
		PCCS	ICS	GDCS Lines	DPV	VB			
18	BDLB	3	3	6	5	3	3	0	0
19	BDLB	3	3	5	6	3	3	0	0
20	BDLB	3	3	6	6	3	2	0	0
21	BDLB (1 VB failed in open position)	3	3	6	6	2	3	0	0
22	BDLB (1 VB failed in open position)	3	3	6	6	2	3	0	0
23	BDLB (all 3 VBs failed in open position)	3	3	6	6	0	3	0	0
24	Blackout	2	3	4	6	3	3	0	0

In addition to the above tests, the following tests will be selected:

1. Several additional tests with multiple component failure.
2. A few tests to assess the impact of non-safety systems upon GDCS and PCCS (e.g., control rod drive flow or RWCU/SDCS flow on GDCS performance, drywell spray on PCCS and GDCS performance, wetwell spray on suppression pool flow to the vessel via equalization line).
3. A few tests at different break sizes (e.g., 50% of BDLB).
4. A few tests to assess natural circulation flow characterization by measuring core flow as a function of power, downcomer water level, and vessel pressure (including the determination of any flow oscillation or instability).
5. Several sensitivity tests by varying core power or other PIRT-identified important parameters.
6. A few helium tests to investigate the presence of hydrogen on PCCS performance.
7. A few repeatability tests.

Table 9.5 Geometric Distortion in RPV

Item	SBWR	Ideal Scale Model	PUMA	Distortion
Lower Plenum Free Volume (m ³)	71.4	0.1785	0.2077	+16.4%
Lower Plenum Average Flow Area (m ²)	16.51	0.1651	0.1972	+19.5%
Core Free Volume (m ³)	39.7	0.0992	0.1209	+21.8%
Core Flow Area (m ²)	13	0.13	0.1584	+21.8%
Chimney Free Volume (m ³)	171.46	0.4367	0.4370	0%
Downcomer Volume (m ³)	73.85	0.1846	0.1846	0%
Core and Chimney Free Volume (m ³)	211.16	0.5279	0.5579	+5.7%
Downcomer and Lower Plenum Free Volume (m ³)	145.25	0.3631	0.3923	+7.4%

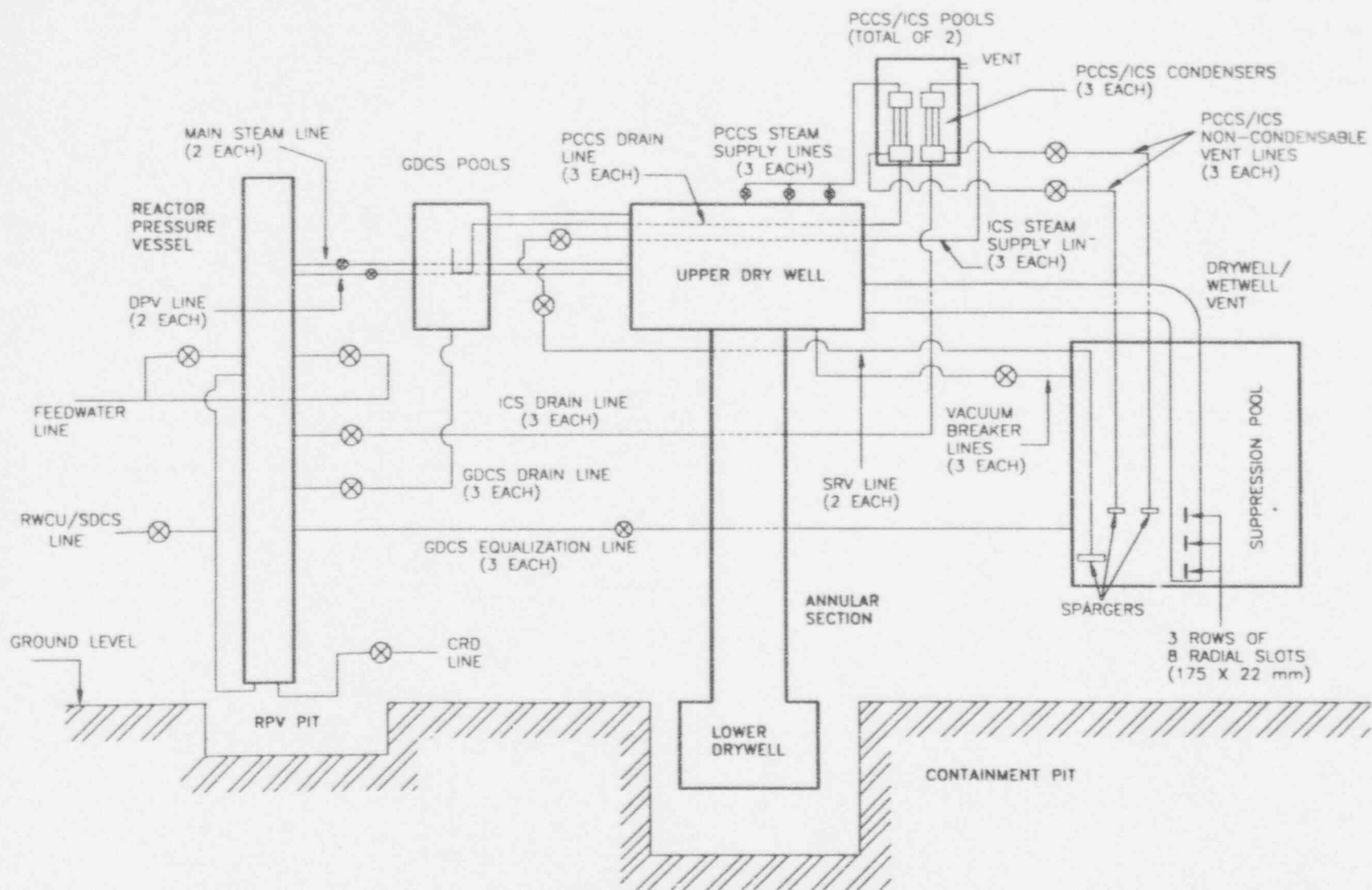


Figure 9.1 Overall schematic of PUMA facility

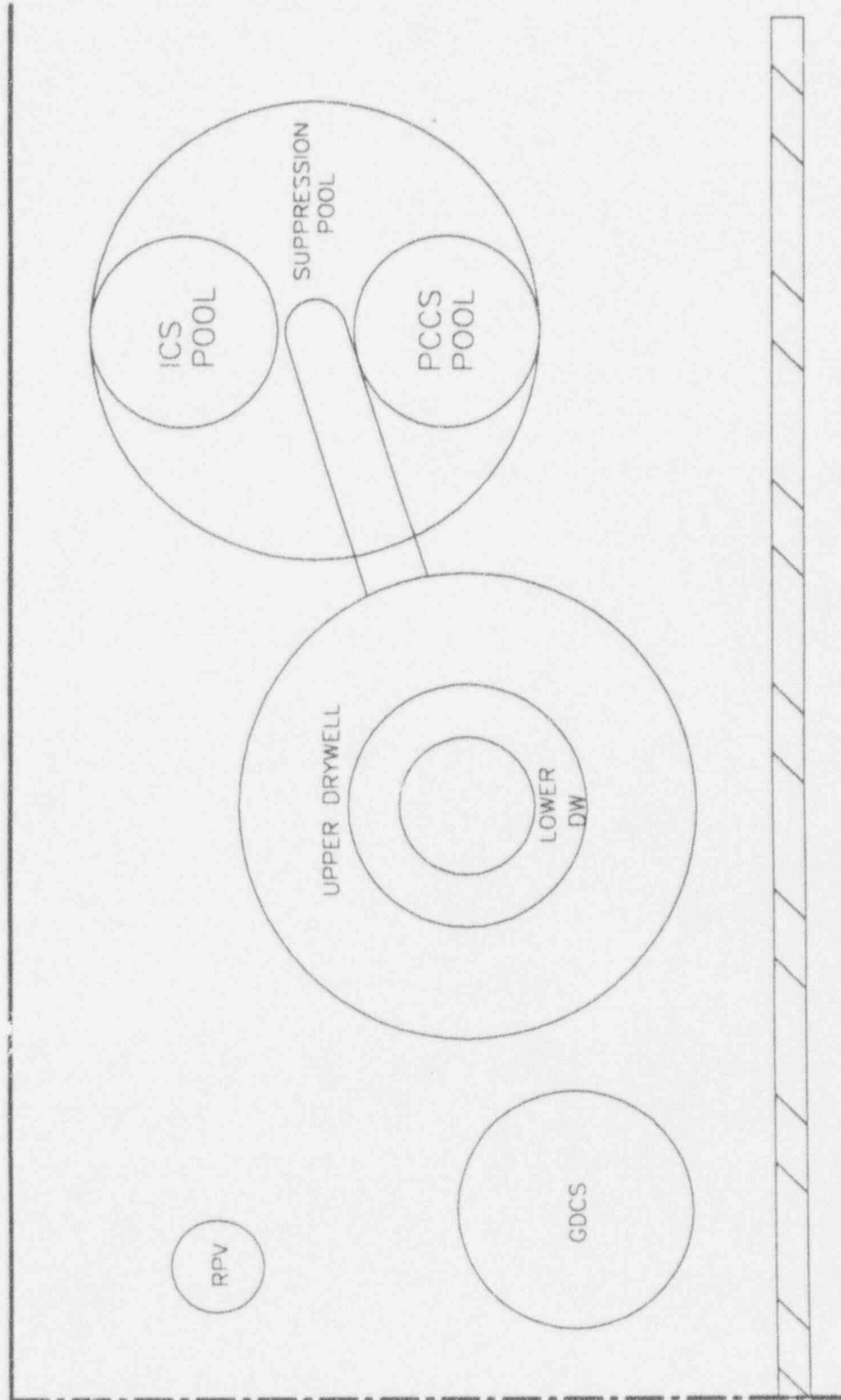


Figure 9.2 Plan view of main vessels in PUMA

References

- 9.1 SBWR Standard Safety Analysis Report (SSAR), GE Nuclear Energy, 25A5113 Rev. A, August 1992.
- 9.2 SBWR Tier 1 Design Certification Document, GE Nuclear Energy, 25A5354 Rev. A, February 1993.
- 9.3 Private Communication with Brookhaven National Laboratory (BNL) Staff, January 1994.
- 9.4 U.S. Nuclear Regulatory Commission Request for Proposal No. RS-RES-93-049, November 25, 1992.
- 9.5 GE Nuclear Energy Report: MFN No. 170-93, Attachment B.
- 9.6 Han, J. T., Bessett, D. E., Shotkin, L. M., "NRC Confirmatory Testing Program for SBWR," Proceedings of the Twenty-first Water Reactor Safety Information Meeting, October 25-27, Bethesda, Maryland (1993).
- 9.7 Liang, K-S, "Experimental and Analytical Study of Direct Contact Condensation of Steam in Water," Ph.D. Thesis, MIT (1994).

10. SUMMARY AND CONCLUSIONS

The U.S. NRC requires independent confirmatory data for the General Electric Nuclear Energy (GE) Simplified Boiling Water Reactor (SBWR) which can be used to assess the uncertainties associated with the use of the RELAP5/CONTAIN code for simulation of SBWR safety system performance under accident and operational transient modes. In order to satisfy this requirement, the NRC has awarded a contract to the Purdue University School of Nuclear Engineering to obtain this data through the design, construction, and operation of a scaled integral test facility named the Purdue University Multi-dimensional Integral Test Assembly (PUMA).

The major objectives of the confirmatory research program are to:

- provide integral data to NRC for the assessment of the RELAP5/CONTAIN code for SBWR application
- assess the integral performance of the GDCS and PCCS
- assess SBWR phenomena important to LOCAs and other transients

These objectives are being accomplished by the following sequence of tasks:

- develop a well balanced and justifiable scaling approach for use in design of the PUMA facility,
- identify important SBWR phenomena associated with LOCAs and applicable operational transients and, based on the identified phenomena, establish a test matrix
- design the scaled integral test facility, including necessary and sufficient instrumentation
- construct the scaled integral facility
- develop boundary and initial conditions and procedures for conducting the integral tests based on the scaling methods and by using computer code calculations (RELAP5/CONTAIN)
- perform the required integral system tests under strict quality control procedures and provide associated documentation

The scaling methods that have been developed for the purposes of the PUMA facility design and the results of the scientific design analyses are documented in this report.

The necessary scaling relationships for design of a full pressure, but less than full height scaled facility have been developed. The criteria that have been used for scaling are to maintain similarity of: integral system response (loops), interaction between components, and preservation of local phenomena. The results of this development show that all of the objectives of the

program can be achieved by use of a full pressure but reduced-height scaled facility.

Parametric preliminary design studies show that a 1/4 height scaled facility could best meet all the program objectives without compromising either geometric similarity or preservation of the important two-phase phenomena. The 1/4 height scaled facility is easily constructable and satisfies the geometrical requirements in order to preserve important thermal-hydraulic phenomena.

The details of the PUMA scientific design, and the supporting analysis are documented herein. The basic design features 1/4 height and 1/400 volume scales which result in a 1/2 time scale. The facility has a reactor pressure vessel height of 6 m and 0.6 m diameter. The system contains all the important safety and non-safety systems of the SBWR. The facility is designed to simulate the phenomena at and below 1.03 MPa (150 psi) following SBWR scram. The pressure is scaled 1:1 and the power is scaled by 1/200 of prototype. The facility is designed with 340 instrumentation devices to measure pressure, temperature, flow rate, local void fraction, two-phase flow void fraction and non-condensable gas concentration. The site for the facility has been identified and the preliminary layout of the facility is completed. Purdue has contracted the mechanical design and construction of the PUMA facility to an engineering firm (Phoenix Solutions Company, Minneapolis, MN).

In conclusion, all program objectives can be achieved using a 1/4 height scaled facility. The resulting design fits nicely within the range of scaled national and international SBWR experimental facilities that either exist or are in the construction phase. This will provide the ability to cross check the system behavior for important thermal hydraulic phenomena. These characteristics will help increase the accuracy of uncertainty assessments that will be based on data from this facility.